Mechanistic Studies on Aldehyde Decarbonylase from Cyanobacteria: A New Enzyme for Alkane Biosynthesis

by

Debasis Das

A dissertation submitted in partial fulfillment
of the requirements for the degree of
Doctor of Philosophy
(Chemistry)
in The University of Michigan
2014

Doctoral Committee:

Professor E. Neil G. Marsh, Chair
Professor Carol A. Fierke
Associate Professor Nicolai Lehnert
Associate Professor Bruce A. Palfey
Professor Stephen W. Ragsdale

@Debasis Das
2014

Dedication

To my parents – for their love, support and encouragement

Acknowledgements

I would like to take this opportunity to convey my deep gratitude to my research advisor, Prof. Neil Marsh, for his endless patience, encouragements, guidance and valuable suggestions throughout the design and accomplishment of the research described in this thesis. I would also like to express my great appreciation to Prof. Stephen Ragsdale and Prof. Carol Fierke for being extremely supportive with their guidance and for letting me use their lab facilities. I also thank Prof. Bruce Palfey, Prof. Nicolai Lehnert and Prof. Vincent Pecoraro for their valuable suggestions and guidance on my research. I would like to convey my special thanks to former Marsh lab members Dr. Dustin Patterson and Dr. Bekir Eser for being my mentors and teaching me all the necessary skills required for doing research in a biochemistry lab. I also thank the present and past Marsh group members Dr. Ben Buer, Dr. Bishwajit Paul, Dr. Fengming Lin, Dr. Yuta Suzuki, Dr. Jaehong Han, Dr. Roberto de la Saud Bea, Dr. Lei Li, Gabriel Roman, Matt Waugh, Ben Ellington, Matthew Demars, Tad Ogorzalek, Aaron Sciore, McKenna Schroeder, Dorota Marchael, Ben Levin and Umair Daimee for their productive collaborations, suggestions, friendship and for maintaining a fun-full atmosphere in the lab. I would like to extend my special thanks to Dr. Amelie Bernerd for her expert advices and help on expression of membrane proteins, Jim Windak for his great assistance with mass spectroscopy, Dr. Venky Basrur for his expertise and guidance on ES-MS/MS spectroscopy and Dr. Naresh Theddu for his valuable support on organic synthesis. I wish to acknowledge the encouragements provided by

all my Ann Arbor friends especially Dr. Bishwajit Paul, Dr. Pralay Mitra, Dr. Susanta Ghosh, Dr. Trisha Sain and Dr. Saumen Chakraborty, Krishna and Riddhiman.

Table of Contents

List of Figures

List of Appendices

List of Abbreviations

CoA	Coenzyme A
AD	Aldehyde decarbonylase
cAD	Cyanobacterial aldehyde decarbonylase
ACR	Acyl-CoA reductase
cACR	Cyanobacterial acyl-CoA reductase
orf	Open reading frame
ACP	Acyl carrier protein
E. coli	*Escherichia coli*
SOC	Super Optimal Broth
IPTG	Isoprpyl-β-D-galactopyranoside
PMSF	Phenylmethylsulfonyl fluoride
OD	Optical density
HEPES	4-(2-hydroxyethyl)-1-piperazineethanesulfonic acid
SDS-PAGE	Sodium dodecyl sulfate polyacrylamide gel electrophoresis
APS	Ammonium persulfate
TEMED	Tetramethylethelenediamine
EDTA	Ethylenediaminetetraacetic acid
NTA	Nitrilotriacetic acid
His	Histidine
Fd	Ferredoxin
FdR	Ferredoxin reductase
PMS	Phenazine methosulphate
NADPH	Nicotinamide adenine dinucleotide phosphate, reduced
NADH	Nicotinamide adenine dinucleotide, reduced
FeAS	Ferrous ammonium sulfate
Pm	*Prochlorococcus marinus*
Np	*Nostoc punctiforme*
Ss	*Synechococcus sp.*
Syn. Sp.	*Synechocystis sp.*
GC	Gas chromatography
GC-MS	Gas chromatography-mass spectrometry
FID	Flame ionization detector
2-NPH	2-Nitrophenylhydrazine
EDC	1-Ethyl-3-(3-dimethylaminopropyl)carbodiimide
Py	Pyridine
ICP-MS	Inductively coupled plasma-mass spectrometry

LC-MS	Liquid chromatography-mass spectrometry
TOF	Time of flight
PDC	Pyridinium dichromate
BSA	Bovine serum albumin
CO	Carbon monoxide
2, 4-DNPH	2, 4-Dinitrophenylhydrazine
ES	Electrospray
TEV	Tobacco etch virus
CytC	Cytochrome C
PBN	α-Phenyl-N-tert-butyl-nitrone
MALDI	Matrix-assisted laser desorption/ionization
DTT	Dithiothreitol
CHCA	α-Cyano-4-hydroxycinnamic acid
TPP	Trans-proteomic pipeline
HppE	(S)-2-Hydroxypropylphosphonic acid epoxidase
TIC	Total ion chromatogram

Abstract

The challenge posed by global warming has sparked great interest in the development of new, green biofuels. Existing biofuels such as ethanol and biodiesel suffer from fundamental disadvantages associated with their bulk properties, energy densities and resources needed for their production. Hence, there is significant interest in developing a new generation of superior alkane/hydrocarbon-based 'drop-in' biofuels that could be direct substitutes for gasoline. For this purpose, microbial biosynthesis of hydrocarbons has recently gained tremendous attention. In Nature, alkanes are biosynthesized from fatty aldehyde precursors by enzymes collectively known as aldehyde decarbonylases (ADs). Conversion of aldehydes to alkanes is an unusual and chemically challenging reaction. As a consequence the mechanisms of these enzymes are very poorly understood. One such enzyme, aldehyde decarbonylase from cyanobacteria (cAD, also known as aldehyde deformylating oxygenase, cADO) is the subject of this dissertation.

Cyanobacterial aldehyde decarbonylase was over-expressed and purified from *E. coli*. Spectroscopic characterization established that the enzyme is a metallo-protein and requires only iron for activity. The enzyme converted octadecanal to heptadecane in the presence of a reducing system comprising spinach ferredoxin/spinach ferredoxin reductase/NADPH. However, the activity was extremely sluggish (~1 turnover/overnight). Therefore, a superior cyanobacterial ferredoxin reducing system was developed that improved the activity of cAD ~

60 fold. Furthermore, an alternate reducing system made of phenazine methosulphate (PMS)/NADH was employed that resulted in ~100 fold improvement in activity. It was found that the enzyme has broad substrate range and converts aldehydes of chain lengths C18-C7 to corresponding alkanes. The kinetic properties of the enzyme were investigated using octadecanal as well as a relatively soluble substrate heptanal. Unlike plant AD that produces CO and insect AD that produces CO_2 as the co-product, formate was identified as the co-product of the cAD-catalyzed reaction. Although initial investigation in the reaction suggested cAD may catalyze the reaction in an oxygen-independent manner, further experiments led to the conclusion that oxygen is involved as a co-substrate in the reaction.

The nature of the C1-C2 bond cleavage of aldehydes by cAD has also been investigated. A preliminary investigation using EPR spectroscopy suggested that a radical intermediate might be involved in the cAD-catalyzed reaction. To further probe the mechanism of the cleavage, a 'radical clock' cyclopropyl analog of octadecanal was investigated as a substrate for cAD. This substrate exhibited only one turnover and underwent rearrangement to a terminal alkene during the reaction implying homolytic cleavage of the C1-C2 bond of the aldehyde. The cyclopropyl aldehyde also inactivated the enzyme by covalent modification that was characterized using LC-ES-MS and LC-ES-MS/MS. Further evidence of involvement of radical intermediates came from studies using α-oxiranyl aldehydes. These aldehydes underwent rearrangement resulting in an unusual tandem deformylation to form C_{n-2} alkanes.

These observations provide a framework to design further experiments to understand other crucial steps in the reaction mechanism. Once the mechanism is understood, engineering

of the enzyme may be possible to improve the activity of the enzyme towards its applications in biofuel production.

Chapter 1

Introduction

1.1 Biofuels

1.1.1 Requirement for Biofuels

The ever-deepening global warming crisis due to increasing levels of greenhouse gases in the atmosphere by burning fossil fuels and the depleting level of petroleum fuels have sparked intense interest in the development of renewable eco-friendly fuels, known as biofuels. Although known for many decades, biofuels did not receive much attention due to the discovery of huge deposits of fossil fuels that are inexpensive. Fossil fuels (primarily known as gasoline) are derived from biomass of plants and animals that were buried beneath Earth's surface for millions of years. Use of fossil fuels generates carbon dioxide, a main greenhouse gas that creates pollution and results in an increase in the global temperature. In contrast, biofuels are produced mostly from living or recently dead plants that capture sunlight and CO_2 from the atmosphere and store them as biomass. Thus the use of biofuels does not increase the net level of CO_2 in the atmosphere, making the process carbon neutral (Figure 1.1). Biofuels are also renewable as plants can be grown fairly quickly to obtain biomass that can subsequently be converted to biofuels. The increase in energy demand associated with the population explosion created an urgent need for a sustainable biofuel that would fit the current economic infrastructure.

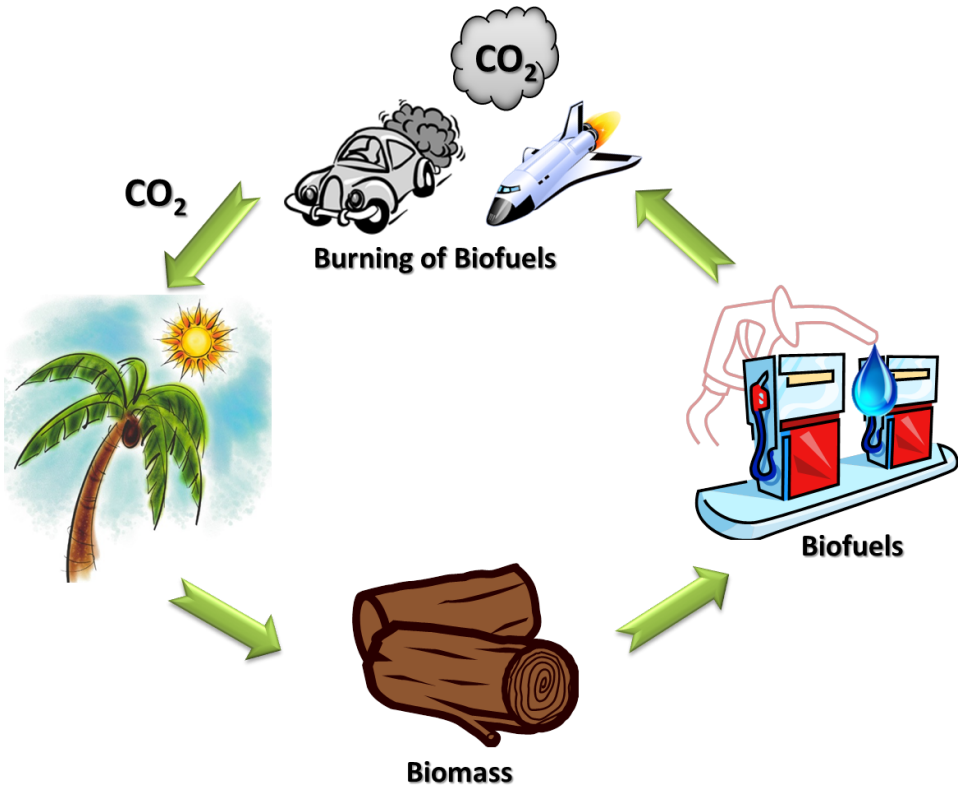

Figure 1.1. Carbon neutral pathway of biofuels

1.1.2 Different Types of Biofuels

Over the years, different types of biofuels have emerged based on the availability and sustainability of the resources. Biofuels can be categorized in four different generations as follows.

First-generation of biofuels. These types of biofuels are derived from food crops such as wheat and corn. These resources are enriched with starch and sugar that are processed for ethanol production by fermentation. Ethanol is the major biofuel used in the current fuel infrastructure and accounts for ~2% of the total transportation fuel usage worldwide.[1] Another type of biofuel

in this category is biodiesel (accounts for 0.01% of the transportation fuel usage[2]) that is derived from rapeseed, soybean, sunflower seeds and several other food crops. Chemical transesterification of vegetable oil (triglyceride) extracted from the resources produce biodiesel that is compatible with various car engines.

Second-generation of biofuels. These types of biofuels are derived from cellulosic non-food crops such as woods, leaves, stalks of wheat, etc.[3] Different high-energy crops such as switchgrass and miscanthus that are rich in carbohydrates are also used for generating biofuels. Not only ethanol can be produced from these resources, the left-over biomass could also be utilized for production of heat.

Third-generation of biofuels. These types of biofuels are derived from green algae that are energy-rich and can be grown on unused lands and waste water. Although algae can produce and deposit substantial amount of oil (~55% of dry wt),[4] cultivation of algae and extraction of fuels from algae is expensive.

Next-generation of hydrocarbon-based advanced biofuels. Petroleum fuels are mostly comprised of hydrocarbons that are energy-rich molecules. Therefore, it would be ideal to develop hydrocarbon-based biofuels that could serve as 'drop-in' replacements for the existing fuels.[5] Although hydrocarbons are amongst the simplest molecules, their biosynthesis is exceedingly challenging.[6] Many organisms such as plants,[7] insects[8,9] and animals[10] are known to synthesize hydrocarbons; however, the process is very poorly understood. Recently, the alkane biosynthesis pathway was explored in cyanobacteria and efforts for microbial production of alkanes are currently in progress.[11]

1.1.3 Challenges Associated with Biofuel Production

There are several fundamental challenges associated with existing biofuels. Ethanol and biodiesel are the two most commonly used biofuels that are developed for industrial production.[1,2] However, there is a controversial 'food *vs.* fuel' debate as the resources to produce these two biofuels could alternatively be used for food production. Furthermore, ethanol is corrosive and miscible with water, which restricts its transportation using conventional pipelines. In addition, ethanol has only 67% of the energy density compared to gasoline. Although the energy density of biodiesel is closer to gasoline, the resources for the production of biodiesel are limited. In that respect, second generation cellulosic biofuels are quite attractive; however, extraction of sugars from non-food crops suffers from challenges associated with the recalcitrant nature of the biomass and inefficiency of the enzymes used for cellulosic biomass digestion to release sugars.[12] Significant technological advances are required to ensure efficient sugar extraction from biomass. Third generation algae fuel is very promising as it could produce significantly higher energy compared to land crops; however, commercial level fuel production from algae would need technical improvements as extraction of fuels from algae is challenging. Finally, a new generation of advanced hydrocarbon-based biofuels could be ideal replacements for gasoline; however, currently the process of efficient production of hydrocarbons is in the preliminary stage of development and would require substantial optimization before commercial applications would be feasible.

1.2 Biosynthetic Pathways for Biofuels

1.2.1 Alcohol-Derived Biofuels

At present, ethanol is the most commonly used biofuel. Propanol and butanol are also used in the existing fuel infrastructure.[12,13] Most of the alcohol-derived biofuels are used as additives to gasoline to improve fuel properties of gasoline by increasing its octane number.[5] Nevertheless, butanol can work as a direct replacement for gasoline as its energy density is close to that of gasoline and it doesn't suffer from miscibility with water or corrosiveness.[5]

Ethanol is produced from sugars through fermentation by yeast and other microorganisms. The process is well developed for commercial purposes. Briefly, glycolysis converts glucose to pyruvate that undergoes decarboxylation under anoxic conditions catalyzed by pyruvate decarboxylase to produce acetaldehyde. Ethanol production from acetaldehyde in the following step is catalyzed by the enzyme alcohol dehydrogenase (Scheme 1.1).[14]

Scheme 1.1. Pathway of conversion of glucose to ethanol

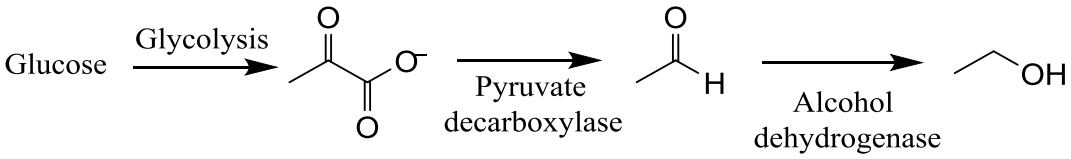

Alcohols, including ethanol and butanol, could also be produced in an alternative non-fermentive route known as the Ehrlich Pathway.[15] The process involves conversion of amino acids to the corresponding keto acids by the enzyme amino transferases. The keto acids undergo decarboxylation by decarboxylases to yield aldehydes that further undergo reduction by an alcohol dehydrogenase to furnish alcohols (Scheme 1.2).

Scheme 1.2. Ehrlich pathway depicting conversion of amino acids to alcohols through keto acid intermediate

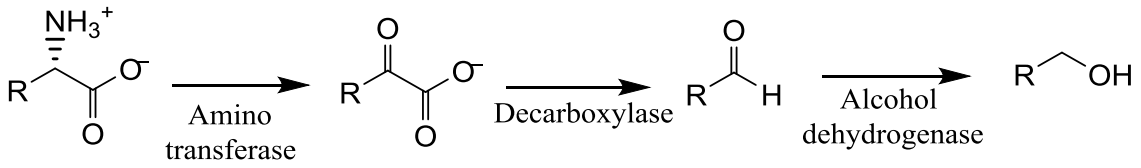

Synthesis of higher alcohols with lengths up to 6-carbons could also be achieved using this pathway by recombinant expression of the engineered enzymes. It has been shown that the keto acid intermediates produced from valine, leucine, isoleucine and phenylalanine can be converted to the corresponding aldehydes using a keto acid decarboxylase from *Lactococcus lactis*. In the next step, these aldehydes are converted to the corresponding alcohols by yeast alcohol dehydrogenase.[13,16,17] By deleting genes competing for different substrates of this pathway, alcohol production was optimized. It was possible to produce alcohols with C7 and C8 chain lengths by further engineering the binding pocket of the keto acid decarboxylase.[18]

Ethanol and butanol can also be produced using an alternative pathway known as ABE (Acetone-Butanol-Ethanol) pathway.[19] This is an acetyl-CoA-dependent pathway in *Clostridia*. For butanol production, two molecules of acetyl-CoA produce acetoacetyl-CoA that undergoes reduction to 3-hydroxybutyryl-CoA. Following dehydration and reduction, butyryl-CoA is produced that further undergoes reduction to butanol (Scheme 1.3).[19,20,21] Using a heterologous ketothiolase, the butyryl-CoA can be further elongated by two carbon atoms to produce 3-ketohexanoyl-CoA, which can undergo the subsequent transformations to produce hexanol.[22]

Scheme 1.3. Butanol production through ABE pathway

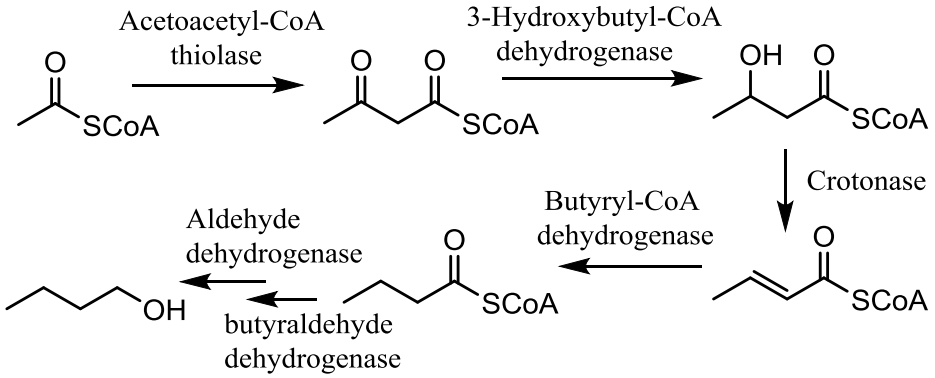

1.2.2 Isoprenoid-Derived Biofuels

Isoprenoids are naturally occurring hydrocarbons that are widely used in pharmaceuticals, perfumes, pesticides and can effectively be used for the next generation of hydrocarbon biofuels.[5,23] Isoprenoids have branched hydrocarbon backbones, which make them excellent candidates for 'drop-in' replacements for gasoline and jet fuels as branching enhances the octane number of the fuel. Isoprenoid biosynthesis is widely distributed in Nature. There are two major biosynthetic pathways for isoprenoid. The mevalonic acid (MVA) pathway is used by bacteria, plant and animals,[24,25] whereas the methylerythritol phosphate (MEP) pathway is used primarily by green algae.[26,27] The MVA pathway starts with acetyl-CoA. In a multistep enzymatic process it undergoes conversion to 3-isopentenyl pyrophosphate (IPP) that is isomerized to dimethylallyl pyrophosphate (DMAPP). The MEP pathway starts with the reaction of pyruvate with glyceraldehyde-3-phosphate. Through a series of enzymatic reactions, IPP is produced that is further isomerized to DMAPP similar to the MVA pathway. The DMAPP serves as the precursor for the synthesis of various isoprenoids such as isoprene, farnesene,

bisabolene and limonene.[5,13] These conversions are catalyzed by various enzymes as shown in the Scheme 1.4. These isoprenoid molecules could be effectively used as future biofuels, e.g. isoprene could be used as liquid fuel, whereas farnesene and bisabolene could serve as petroleum replacements and limonene could be utilized as a fuel additive.

Scheme 1.4. Isoprenoid pathway depicting synthesis of different isoprenoid molecules from a common precursor 3-isopentenyl pyrophosphate (IPP)

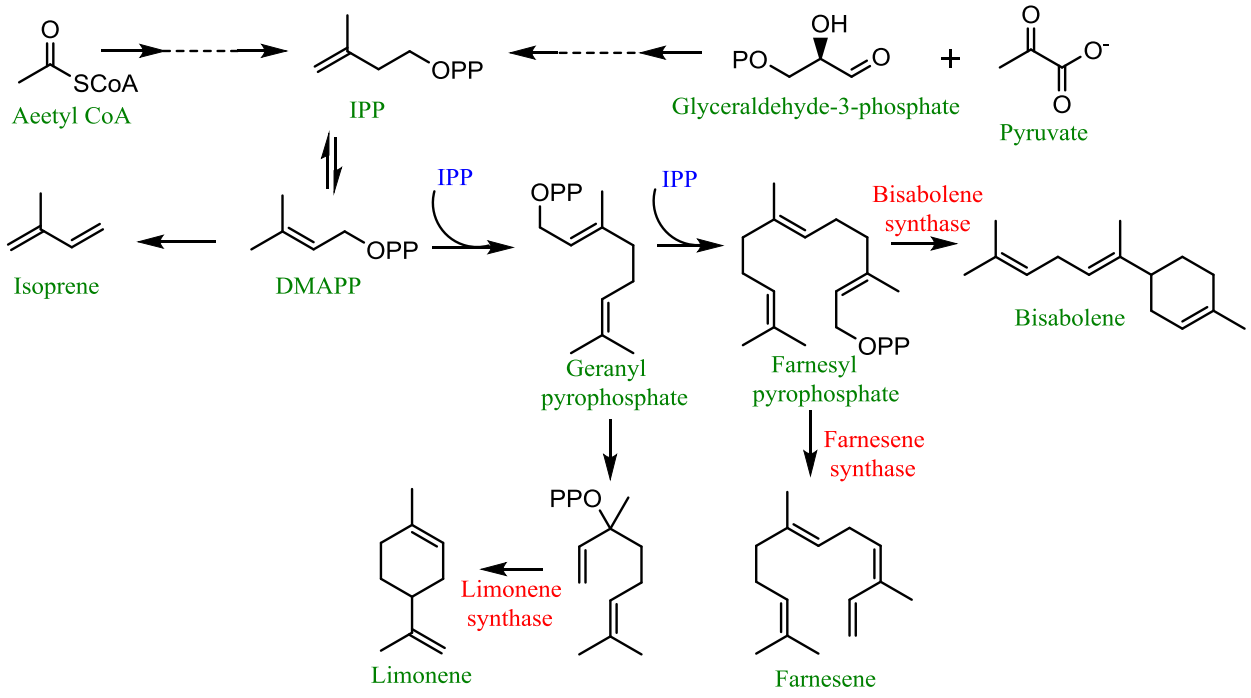

1.2.3 Fatty Acid-Derived Biofuels

Fatty acids are the major components of lipids that serve as energy storage molecules in many organisms. Fatty acid biosynthesis is ubiquitous in Nature.[28,29] Fatty acids are synthesized from acetyl-CoA by the action of the enzyme complex fatty acid synthase (FAS) that is comprised of four different enzymes as shown in the Scheme 1.5. Fatty acids with chain lengths of C16-C18 are synthesized by this process.

Scheme 1.5. Fatty acid biosynthesis catalyzed by fatty acid synthase (FAS) complex

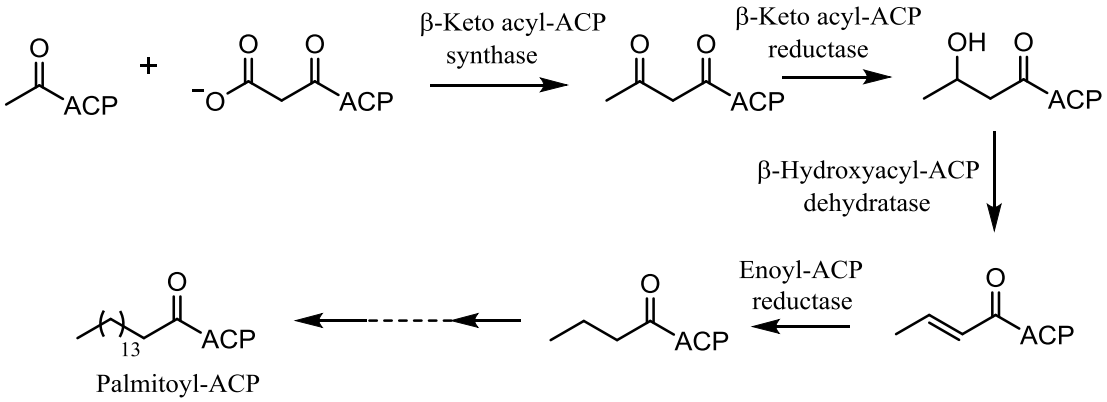

Fatty acids shorter than palmitic acid could be generated by release of fatty acyl-ACPs in the intermediate steps. Production of fatty acids as short as C8 can be achieved by employing a truncated thioesterase.[5] Improvements in the yield of fatty acid biosynthesis can be made by deleting the genes responsible for fatty acid degradation. Fatty acids longer than C16/C18 carbon chain are produced in mitrochondria or through the endoplasmic reticulum-mediated elongation of long-chain fatty acids.[30] This process is catalyzed by an enzyme complex known as fatty acid elongase (FAE), which is a membrane-associated complex and is believed to work in a similar fashion as the soluble FAS complex. These very long-chain fatty acids with chain lengths up to C34 carbon play essential roles in the biology of plants, insects and other organisms.

Both short-chain and long-chain (up to C23) fatty acids could be utilized as biofuels. Direct use of fatty acids as biofuels is not feasible due to the ionic character of the carboxyl head group;[5] instead, fatty acids can be converted to fatty acid methyl esters (FAMEs) and fatty acid ethyl esters (FAEEs) that are used as biodiesel.

Fatty acids can also be converted to alcohols and alka(e)nes that can serve as high-energy density biofuels.[31] Free fatty acids are converted to fatty acyl-CoAs using an acyl-CoA synthase. A fatty acyl-CoA reductase then reduces the fatty acyl-CoAs to the corresponding alcohols. Conversion of fatty acyl-CoA to alka(e)nes is a poorly understood process that involves an acyl-CoA reductase that produces aldehydes from fatty acyl-CoAs and an aldehyde decarbonylase that produces alka(e)nes from aldehydes.[32,33] Conversion of aldehydes to alka(e)nes is amongst the most unusal chemical reactions in both chemical and biological realms.

1.3 Chemical Decarbonylation Reactions

Decarbonylation involves the formal removal of carbon monoxide from a compound. The reaction is quite challenging as it involves cleavage of a C-C bond and delivery of hydrogen at the same site. The bond possesses a high energy (85 kcal/mol) and both the carbon atoms are attached to other atoms that makes the environment around the C1-C2 bond sterically difficult to access.[34,35] Decarbonylations have gained significant attention over decades because of the unusual nature of the reaction as well as its use for synthetic chemistry purposes.[36,37] Recently, chemical decarbonylation gained renewed interest because the product alkanes/alkenes are valuable molecules for biofuel applications.

Decarbonylation without transition metal catalysts. Although chemical decarbonylation usually requires transition metal catalysts, photochemical and radical mediated decarbonylation have been known for decades.[38] It has been shown that

cyclohexanecarbaldehyde undergoes peroxide-mediated radical-induced decarbonylation at ~130 °C to furnish cyclohexane and CO. Aliphatic aldehydes and ketones also undergo photochemical decarbonylation to produce alkanes and CO (Scheme 1.6).[38]

Scheme 1.6. Radical-mediated (A) and photochemical (B) decarbonylation of aldehydes and ketones

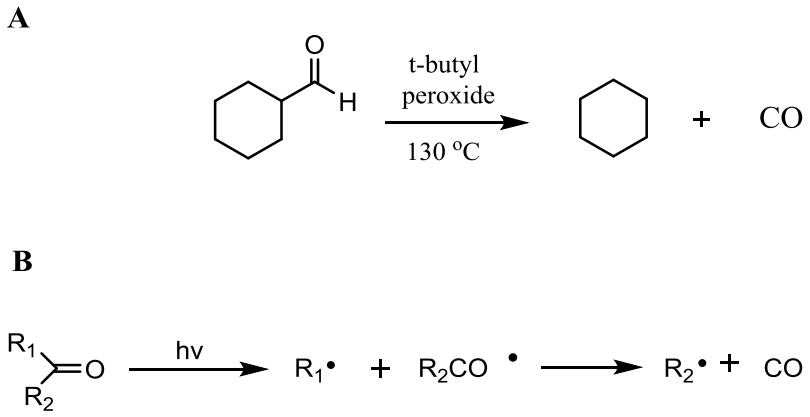

Transition-metal-mediated decarbonylation. Metal-mediated decarbonylation is well known in the realm of organometallic chemistry. Many transition metal catalysts, derived from Rh, Pd, Ru and Ir, have been used to decarbonylate various aldehydes, although these reactions suffer from sluggish rates and the reactions require very high temperature (180-280 °C).[37] A classic transition metal catalyst used for the conversion of aldehydes to alkanes (and to some extent alkenes) is Wilkinson's catalyst ($[Rh(Cl)(PPh_3)_3]$).[39] The mechanism of this reaction involves four steps: (i) coordination of aldehydes, (ii) oxidative addition, (iii) migratory extrusion and (iv) reductive elimination as shown in Figure 1.2.[36] Migratory extrusion (step iv) is the slowest step of the reaction sequence.

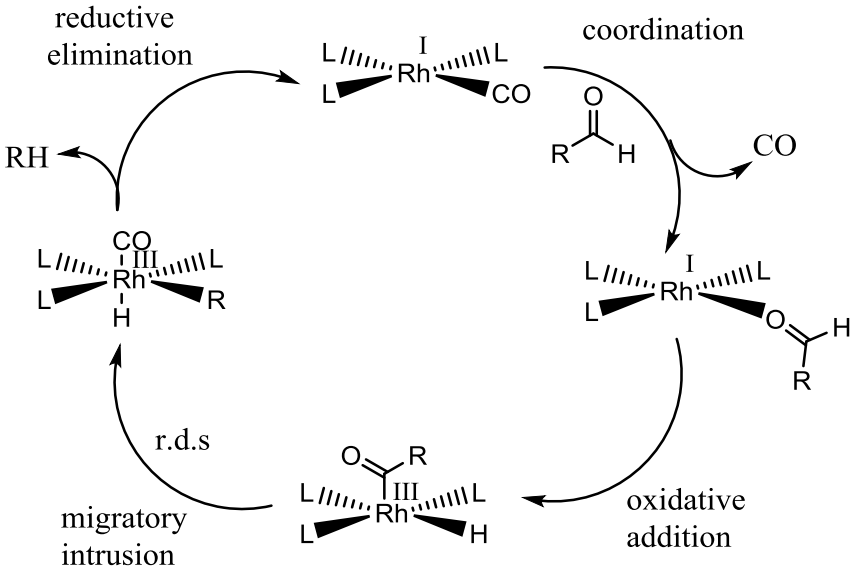

Figure 1.2. Rhodium complex-catalyzed decarbonylation of aldehydes to alkanes.

Palladium-catalyzed decarbonylation is also well studied. A few decades ago, Pd-catalysts were shown to decarbonylate aldehydes to alkenes (as major products) and alkanes (as minor products).[40] Recently, a catalytic amount of palladium acetate in presence of molecular sieves was shown to decarbonylate various aldehydes to produce the corresponding alkanes at lower temperatures (100 – 140 °C) with good yields (Scheme 1.7),[37] however, the reactions usually take ~24 h. This method was effective for various aldehydes including linear aliphatic, aromatic, polycyclic and heterocyclic aldehydes.[37]

Scheme 1.7. Palladium acetate-catalyzed decarbonylation of aldehydes to alkanes

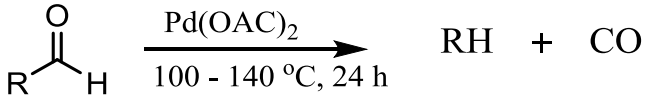

In spite of the recent advances in metal-catalyzed decarbonylation, the process is not cost-effective as the catalysts are expensive and the reaction requires high temperature for over 24 h to obtain significant yield.

1.4 Biological Decarbonylation Reactions

Decarbonylation reactions in biological systems are quite widespread. alkanes produced, due to this reaction, play significant roles for survival of many organisms such as plants,[7] animals[10] and insects.[9,41] In plant leaves and stems, alkanes are the major components of the cuticular wax that protects the plant from desiccation in dry conditions, produce a barrier against invading pathogens and UV-radiation and help protect against dust and pollutant deposition from the environment.[30] In waterfowl, alkanes are secreted from uropygial gland to make a waterproofing barrier on the birds' feathers, which prevents waterlogging.[10] In insects, alkanes are important components of cuticle and protect the organism from desiccation, especially in the larval form. Furthermore, alkanes play important roles as insect pheromones for insect:insect recognition.[9,41] In green algae, alkane accumulation can be as high as ~55% of dry weight[4] and serve as a source of cellular energy when photosynthesis is not possible. Recently, photoautotrophic cyanobacteria were also shown to produce alkanes[11] however, the extent of alkane production and purpose served by alkanes in this microorganism remains unknown.

Although alkanes are simple molecules that lack any functionality and are made of only hydrogen and carbon atoms, the mechanism by which they are produced are amongst the most

enigmatic of biological reactions. Hydrocarbons (alkanes/alkenes) are produced from fatty acids. Long chain fatty acyl-CoAs (or acyl-ACPs), produced from this pathway, are reduced by a reductase enzyme to produce aldehydes that subsequently undergoe decarbonylation by the enzyme known as aldehyde decarbonylase to furnish alka(e)nes (Scheme 1.8).

Scheme 1.8. Two step conversion of long chain fatty acyl-CoA/ACP to alka(e)ne, which involves a fatty acyl-CoA/ACP reductase and an aldehyde decarbonylase

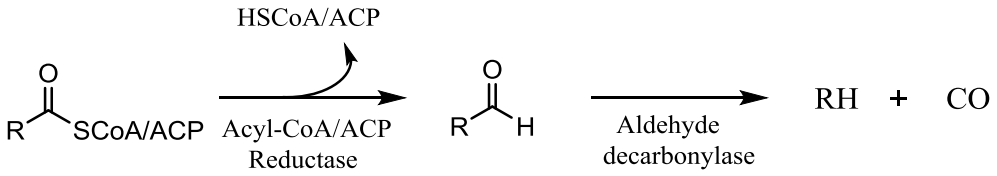

1.4.1 Acyl-CoA Reductase

Fatty acyl-CoA reductase enzymes play a crucial role in wax biosynthesis in plants and animals. In fact, it became apparent that, in plants, there are two different acyl-CoA reductase enzymes that work on the same acyl-CoA substrate to catalyze two different reactions to produce alcohols or aldehyde.[32] Wax is comprised of wax esters and alkanes.[30] Wax esters are formed by the condensation of long-chain alcohols with long-chain acids whereas alkanes are derived from decarbonylation of long-chain aldehydes. Although it has been proposed that the conversion of acyl-CoA to alcohol involves an aldehyde intermediate, the aldehyde has never been identified. This is probably because the reaction is tightly coupled to the next step of reduction to alcohol. In green algae that do not produce significant amount of wax esters, the enzyme has been found to be a membrane-associated, NADH-dependent protein[42] (molecular wt 35 kDa). In organisms that produce wax esters and do not produce alkanes, the enzyme is

also membrane-associated, but is an NADPH-dependent protein of molecular wt ~60 kDa.[43] In higher organisms such as *Pisum sativam* that produce both wax esters and alkanes, two reductase enzymes have been identified. The smaller protein (28 kDa) is responsible for aldehyde formation and the larger protein (58 kDa) is responsible for alcohol formation (Scheme 1.9).[32]

Scheme 1.9. An aldehyde forming and an alcohol forming acyl-CoA reductase are responsible for the production of long chain aldehydes and long-chain alcohols from long-chain fatty acyl-CoA

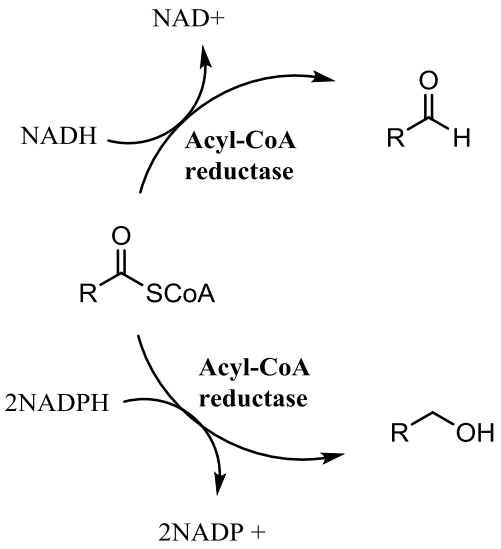

Although partially characterized, a great deal of the mechanistic aspects of these enzymes remains to be explored. The challenge derives from their insolubility as both these enzymes are membrane-associated proteins that have proven hard to purify.

Recently, genome analyses of cyanobacteria have successfully identified a soluble acyl-CoA reductase (cACR) that produces long chain aldehydes from the corresponding acyl-CoAs. The enzyme was shown to be active both *in vivo* and *in vitro*.[11] The enzyme was also shown to be more selective for acyl-ACP compared to acyl-CoA. A detailed mechanistic investigation of

this enzyme has recently been carried out using acyl-CoA as substrates.[44] The enzyme from cyanobacterium *Synechococcus elongates* was heterologously expressed in *E. coli*. The enzyme was found to be active only with NADPH; NADH did not support activity. It has been shown that stearoyl-CoA serves as a better substrate for the enzyme compared to both longer and shorter chain CoAs. A 10-fold improvement in enzyme activity was achieved by optimizing the assay conditions.[44] Steady state kinetic parameters were also established. The enzyme incorporates a conserved active site cysteine residue that participates in catalysis and undergoes reaction with stearoyl-CoA to form a covalent intermediate that was detected by LC-ES-MS. In the presence of NADPH, the enzyme undergoes a 'ping-pong' mechanism to furnish aldehyde (Scheme 1.10).[44] Although soluble and purified in good yield from *E. coli*, no more than ~20 turnovers/h could be obtained. This activity is ~20000-fold slower compared to the archaeal malonyl-CoA reductase.[45] This most likely indicates the inherently slow nature of the cyanobacterial enzyme. It might also be possible that acyl-CoAs do not serve as substrates for the enzyme.

Scheme 1.10. Mechanism for the cyanobacterial acyl-CoA reductase-catalyzed conversion of fatty acyl-CoA to fatty aldehyde

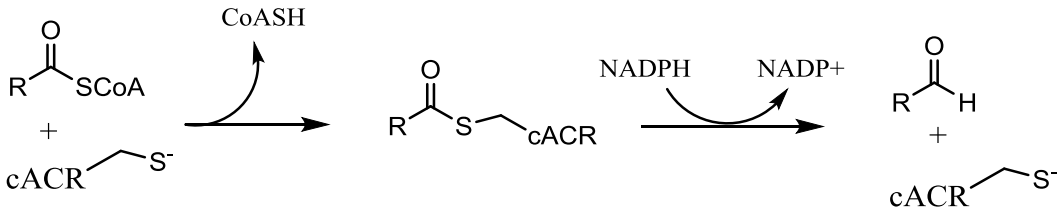

1.4.2 Aldehyde Decarbonylase

The second step of the pathway is catalyzed by aldehyde decarbonylase (AD). Although aldehyde decarbonylase catalyzes an apparently simple conversion of aldehyde to a very simple molecule (alka(e)ne) the mechanism that underlies this reaction is very poorly understood. Recently, it has become apparent that the family of aldehyde decarbonylase enzymes catalyze the conversion of aldehydes to alka(e)nes in three mechanistically distinct ways. The reactions catalyzed by ADs from insects, plants and cyanobacteria differ in the fate of the aldehyde carbon. Researchers have spent decades exploring the mechanism of aldehyde decarbonylase from plants and insects, however, very little advancement could be made due to the recalcitrant nature of these membrane-associated (most likely transmembrane) proteins. However, recent interest in renewable hydrocarbon-based biofuels initiated a search for easily tractable enzymes directly involved in hydrocarbon biosynthesis, which led to the discovery of cyanobacterial aldehyde decarbonylase (cAD).[11]

Insect aldehyde decarbonylase. Alkane biosynthesis in insects is a known phenomenon. Different insects such as the house fly *Musca domestica*, fruit fly *Drosophila melanogaster* and cockroach *Periplaneta americana* have been investigated for the presence of AD enzymes.[9,46,47] Insect cuticle is mostly composed of a mixture of hydrocarbons including alkanes, alkenes and branched components.[8] An important house fly pheromone is (Z)-9-tricosene. Insect AD was found to be a cytochrome P450 enzyme. Antibodies used against both the house fly CytP450 (CYP6A1) and the CytP450 reductase inhibited hydrocarbon biosynthesis.[46] Insect ADs require cofactors such as NADPH and molecular oxygen for activity. When microsomal preparations of house fly *Musca domestica* were treated with (Z)-15-tetracosenoyl-CoA in the presence of

NADPH and O_2, both C24:1 aldehyde and C23:1 alkane were detected suggesting the formation of aldehyde as the most likely intermediate for alkane formation.[9] Later, it was shown that treatment of aldehyde (Z)-15-tetracosenal with the same microsomal preparations resulted in the formation of tricosene. From the labeling experiments, it was confirmed that the aldehyde carbon was converted to CO_2 that formed in a 1:1 ratio with alkane.[9] The aldehyde hydrogen was found to be retained in the alkane (Scheme 1.11). The presence of NADPH and molecular oxygen were absolutely necessary for the catalysis.[9] It was also found that oxidizing agents such as hydrogen peroxide, cumene peroxide or iodosobenzene could effectively substitute for NADPH and O_2 suggesting to activate the enzyme the formation of an iron-peroxo intermediate during the catalysis.[46] Recently, wax associated CytP450s and the corresponding reductase from both house fly and fruit fly were heterologously expressed in *Saccharomyces cerevisiae*.[48] *In vitro* activity studies were able to verify the role of the CytP450 as an insect AD. Microsomal preparations from yeast engineered for the coexpression of CytP450 and the corresponding reductase were able to convert octadecanal to heptadecane and removed the C1 carbon of aldehyde as CO_2.[48] The mechanism of the reaction can be best described by Scheme 1.11.[46,49] Molecular oxygen reacts with the reduced form of the CytP450 to produce an iron-peroxo intermediate that undergoes heterolytic cleavage to produce high-valent iron-oxo species (It's currently not known whether this species is Compound I or II). This is followed by abstraction of an electron from the aldehyde carbonyl group by the iron-oxo species to produce a hemi-acetal radical that most likely undergoes fragmentation to produce iron-bound formyl radical and an alkyl radical. In the final step, the alkyl radical abstracts the formyl hydrogen to generate the alkane and CO_2 is released.[46,49]

Scheme 1.11. Proposed mechanism for oxidative aldehyde decarbonylation catalyzed by insect aldehyde decarbonylase

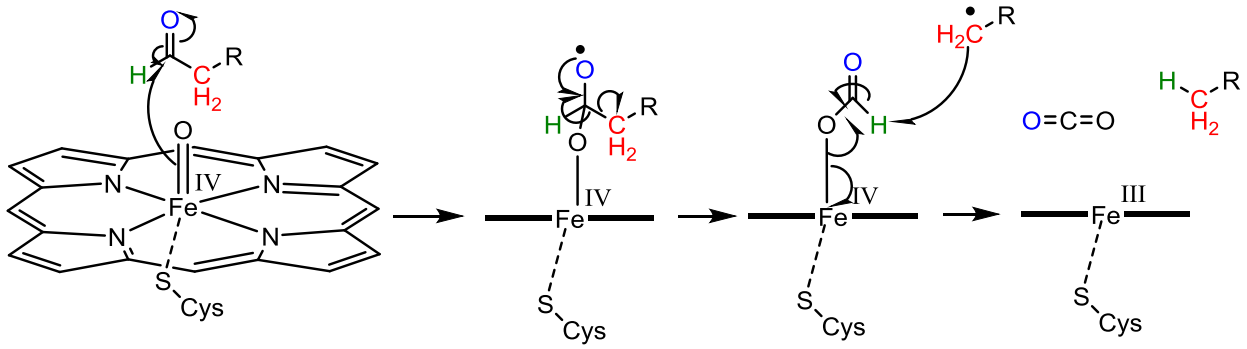

Plant and algal aldehyde decarbonylases. Although extensive attempts were made to characterize aldehyde decarbonylase from plants that produce significant amounts of alkanes in their young leaves and stems and from green algae that are known to produce substantial amount of alkanes,[33,50,51] very little success was achieved and this class of aldehyde decarbonylase is probably the least well-understood. Kolattukudy and co-workers initiated investigations on these enzymes in the early 1970s when no genetic information on these enzymes was available. Taking the advantage of relatively fast-growing pea leaves and green algae, the researchers attempted isolation of these enzymes using standard biochemical techniques. Decarbonylation was found to be associated with the membrane fraction that was isolated using different detergents and lipids as well as various chromatographic techniques. Both the plant and algal proteins were found to have MW ~66 kDa.[33,52] It was found that the partially purified enzymes were capable of converting octadecanal to heptadecane. The aldehyde carbon was converted to carbon monoxide (CO) that was trapped by the complex $Rh(Cl)(PPh_3)_3$. The ratio of alkane and CO formation was ~1:1. From radiolabeling experiments it was concluded that the aldehyde hydrogen was retained in the alkane for the plant enzyme[51]

whereas, for the algal enzyme, most of the aldehyde hydrogen was lost to water.[52] These enzymes did not require any cofactors for activity and were inhibited by NADPH, molecular oxygen and metal chelators. The plant enzyme was identified as a Cu^{2+} containing enzyme. The activity of the de-metallated plant enzyme could be reconstituted by Cu^{2+}. From UV-Visible spectroscopic analysis, the algal enzyme was reported to be a Co-porphyrin enzyme. However, recent identification of the aldehyde decarbonylase gene (*cer1*) from the model organism *Arabidopsis thaliana*[7] suggests that the enzyme is a member of stearoyl-CoA desaturase/hydroxylase family of enzymes that contain a conserved '8-His motif'.[53] This enzyme is an integral membrane protein and harbors a non-heme di-iron active site. Heterologous expression of Cer1 was also carried out; however, all attempts to detect activity were unsuccessful.[54] With the assumption that partner protein(s) might be necessary for the activity of Cer1, an extensive search was carried out and it was found that a wax associated protein Cer3 (a similar protein to Cer1 with 35% sequence identity and containing the '8-His' motif) and endoplasmic reticulum (ER) associated Cytb5-isoform proteins physically interact with Cer1.[55] Co-expression of Cer1 and Cer3 in *Saccharomyces cerevisiae* engineered to produce very long chain fatty acyl-CoA resulted in production of nonacosane, the major alkane in plant wax albeit in very small amounts. Expression of Cer1 and Cer3 alone did not support alkane formation. Furthermore, expression of Cytb5-isoforms along with Cer1 and Cer3 enhanced the activity, suggesting the redox dependent nature of the Cer1/Cer3 complex.[55] Evidence for involvement of metal (most likely iron) derived from mutation studies. When three 'His' from the Cer1 '8-His' motif were mutated together, no activity was found. In contrast, the similar mutations on Cer3 did not have any effect on the activity. This suggested that the '8-His' motif of Cer1 forms

the catalytic core that is responsible for alkane formation.[55] This also indicated that Cytb5-isoforms possibly interact with Cer1 rather than Cer3. These observations suggested that formation of very long chain alkanes from very long chain fatty acyl-CoA in plants (Arabidopsis) depends on the presence of both Cer1 and Cer3. Cer1 plays the role of aldehyde decarbonylase whereas Cer3 is possibly an acyl-CoA reductase that provides the aldehyde intermediate by reducing long chain-CoAs, although no free aldehyde was detected. The summary of these findings are shown in Figure 1.3.

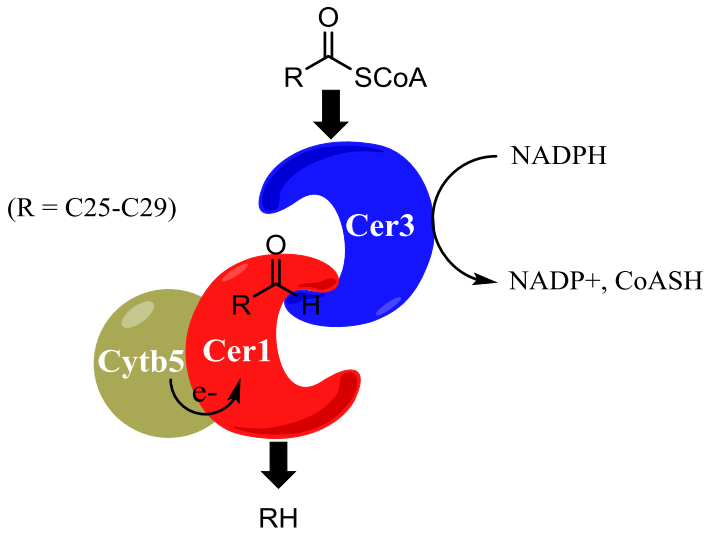

Figure 1.3. Proposed model for alkane biosynthesis in *Arabidopsis thaliana.* The catalysis involves three poteins namely Cer1, Cer3 and Ctyb5 in which Cer1 and Cer3 interact with each other and Cytb5 interacts with Cer1.

1.5 Aims of This Work

Investigations on aldehyde decarbonylase were originally initiated with the aim of understanding the biosynthesis of alkanes in Nature. The research was intriguing as alkanes play crucial roles for the survival of many organisms including plants, insects and animals. However, the studies encountered significant challenges as alkane biosynthesis takes places in the epidermal cells and the enzymes associated with this pathway are membrane proteins.[7] Although molecular biology and enzymology techniques have made enormous advances, our ability to study membrane proteins is still quite limited as the biochemical tools to support membrane protein purification and characterization have not made significant improvements. In the 1970s', when investigations on alkane biosynthesis pathway were initiated, systematic studies were exceedingly challenging. Because of this, the enzymes involved in this pathway could only be partially characterized. In particular, aldehyde decarbonylase still remains as a very puzzling enzyme.

With the aim of developing a new generation of alkane-based biofuels, renewed interest in alkane biosynthetic enzymes has recently been kindled. It was considered that microorganisms would be suitable hosts for the biosynthesis of alkanes as microorganisms grow quickly and can be manipulated. Although common laboratory-microorganisms such as bacteria or yeast do not produce alkanes, some photosynthetic cyanobacteria were found to produce alkanes.[11] Furthermore, genomic analysis was able to identify the enzyme capable of converting aldehydes to alkanes. Cyanobacterial aldehyde decarbonylase (cAD) is a small soluble protein unlike all other ADs that are membrane associated enzymes. cAD was found to be active both *in vivo* and *in vitro*; however, activity was extremely low. A reducing system made of ferredoxin

(Fd), ferredoxin reductase (FdR) and NADPH was found to be absolutely required for *in vitro* activity. Serendipitously, before this discovery, a crystal structure of a cyanobacterial aldehyde decarbonylase was already deposited in the protein data bank without having any function assigned.[56] The structure indicates that cAD is a member of non-heme di-iron family of oxygenase containing ferretin, methane monoxygenase and R2 subunit of ribonucleotide redeructase.[57,58,59,60] In all these structures, the di-metal center is contained within 4-α helical bundle.

Taking the advantage of soluble nature of cyanobacterial aldehyde decarbonylase, my first goal was to characterize this novel enzyme. Heterologous expression of this enzyme was carried out in *Escherichia coli.* The enzyme was then purified and studied by UV-Vis spectroscopy to examine the presence of any bound cofactor(s). In addition, different preparations of the enzyme were studied by ICP-MS (Inductively Coupled Plasma Mass Spectrometry) to determine the metal content.

As there was uncertainty about the metal content, my next goal was to improve the activity of cAD. This approach significantly facilitated the determination of active metal(s) for the enzyme. The activity of cAD was reported to be absolutely dependent on a biological reducing system Fd/FdR/NADPH.[11] Notably, spinach Fd and FdR was used for this purpose and conversion of octadecanal to heptadecane was detected. I initiated my investigations by verifying the reported activity following the literature procedures. Once the reported activity was established, various other reducing systems were tested for activity. I investigated the ability of known chemical reductants such as dithionite, ascorbate, methyl viologen, phenazine

methosulphate (PMS) for activity. I also investigated the cognate cyanobacterial physiological reducing system (Fd/FdR/NADPH) for improved activity. Once enhanced activity was obtained, unambiguous assessment of metal requirement was possible as the enzyme could be loaded with biologically relevant metal(s) and the activity could be reliably tested.

cAD was shown to convert octadecanal to heptadecane, however, no kinetic parameters had been measured. To obtain these parameters, which are essential to judge the efficiency of an enzyme, I used octadecanal as well as various other shorter-chain aldehydes as substrates for cAD. This allowed me to measure the substrate range of cAD as well as the kinetic parameters k_{cat} and K_M. It was predicted that similar to plant AD, the C1-carbon of aldehydes would be converted to CO in the cAD-catalyzed reaction, however, no evidence was provided. To establish the nature of C1, as well as the fate of aldehyde hydrogen, isotopically labeled substrates were synthesized and employed as substrates for cAD.

Most of my studies were aimed to explore the mechanism of unusual conversion of aldehyde to alkane by cAD. To explore the mechanism of energetically challenging C1-C2 bond cleavage of aldehyde, an analog of octadecanal was synthesized as molecular probe. In particular, to determine the nature of C1-C2 bond cleavage, a 'radical clock' cyclopropyl analog of octadecanal was synthesized. If the reaction goes through a radical mechanism, depending on the lifetime of the radical, the cyclopropyl group could undergo ring opening. Oxiranyl analogs of the aldehydes that are known to work as slow 'radical clocks' were also investigated. Utilization of these chemical probes provided information on the mechanism of the C1-C2 bond cleavage as well allowed the lifetime of the intermediate(s) to be determined.

These experiments provided better understanding of the properties, activity and the mechanism of cyanobacterial aldehyde decarbonylase, In addition, detailed mechanistic knowledge of various steps in catalysis may allow the protein to be engineered in an informed way for future biofuel applications.

1.6 References

1. Farrell, A. E., Plevin, R. J., Turner, B. T., Jones, A. D., O'Hare, M., and Kammen, D. M. (2006) Ethanol can contribute to energy and environmental goals, *Science 311*, 506-508.
2. Somerville, C. (2007) Biofuels, *Curr. Biol. 17*, R115-R119.
3. Kumar, R., Singh, S., and Singh, O. V. J. (2008) Bioconversion of lignocellulosic biomass: biochemical and molecular perspectives, *J. Ind. Microbiol. Biotechnol. 35*, 377-391.
4. Rosenberg, J. N., Oyler, G. A., Wilkinson, L., and Betenbaugh, M. J. (2008) A green light for engineered algae: redirecting metabolism to fuel a biotechnology revolution, *Curr. Opin. Biotechnol. 19*, 430-436.
5. Peralta-Yahya, P. P., Zhang, F., del Cardayre, S. B., and Keasling, J. D. (2012) Microbial engineering for the production of advanced biofuels, *Nature 488*, 320-328.
6. Buist, P. H., and Adeney, R. A. (1991) Synthesis of a new family of chiral fluorinated synthons - (R)-4-fluoro-1-alkynes and (S)-4-fluoro-1-alkynes, *J. Org. Chem. 56*, 3449-3452.
7. Aarts, M. G. M., Keijzer, C. J., Stiekema, W. J., and Pereira, A. (1995) Molecular characterization of the CER1 gene of arabidopsis involved in epicuticular wax biosynthesis and pollen fertility, *Plant Cell 7*, 2115–2127.
8. Howard, R. W., and Blomquist, G. J. (2005) Ecological, behavioral, and biochemical aspects of insect hydrocarbons, *Annu. Rev. Entomol. 50*, 371-393.
9. Reed, J. R., Vanderwel, D., Choi, S. W., Pomonis, J. G., Reitz, R. C., and Blomquist, G. J. (1994) Unusual mechanism of hydrocarbon formation in the housefly: cytochrome-P450 converts aldehyde to the sex-pheromone component (Z)-9-tricosene and CO_2, *Proc. Natl. Acad. Sci. USA. 91*, 10000–10004.
10. Cheesbrough, T. M., and Kolattukudy, P. E. (1988) Microsomal preparation from an animal tissue catalyzes release of carbon monoxide from a fatty aldehyde to generate an alkane, *J. Biol. Chem. 263*, 2738–2743.
11. Schirmer, A., Rude, M. A., Li, X. Z., Popova, E., and del Cardayre, S. B. (2010) Microbial biosynthesis of alkanes, *Science 329*, 559–562.
12. Bokinsky, G., Peralta-Yahya, P. P., George, A., Holmes, B. M., Steen, E. J., Dietrich, J., Lee, T. S., Tullman-Ercek, D., Voigt, C. A., Simmons, B. A., and Keasling, J. D. (2011) Synthesis

of three advanced biofuels from ionic liquid-pretreated switchgrass using engineered Escherichia coli, *Proc. Natl. Acad. Sci. USA. 108*, 19949-19954.
13. Rabinovitch-Deere, C. A., Oliver, J. W., Rodriguez, G. M., and Atsumi, S. (2013) Synthetic biology and metabolic engineering approaches to produce biofuels, *Chem. Rev. 113*, 4611-4632.
14. Nelson, D. L., and Cox, M. M. (2008) *Lehninger Principles of Biochemistry*, W. H. Freeman and Company, New York.
15. Yan, Y., and Liao, J. (2009) Engineering metabolic systems for production of advanced fuels, *J. Ind. Microbiol. Biotechnol. 36*, 471-479.
16. Atsumi, S., Hanai, T., and Liao, J. C. (2008) Non-fermentative pathways for synthesis of branched-chain higher alcohols as biofuels, *Nature 451*, 86-89.
17. Russell, D. W., Smith, M., Williamson, V. M., and Young, E. T. (1983) Nucleotide sequence of the yeast alcohol dehydrogenase II gene, *J. Biol. Chem. 258*, 2674-2682.
18. Zhang, K., Sawaya, M. R., Eisenberg, D. S., and Liao, J. C. (2008) Expanding metabolism for biosynthesis of nonnatural alcohols, *Proc. Natl. Acad. Sci. USA. 105*, 20653-20658.
19. Jones, D. T., and Woods, D. R. (1986) Acetone-butanol fermentation revisited, *Microbiol. Rev. 50*, 484-524.
20. Lee, S. Y., Park, J. H., Jang, S. H., Nielsen, L. K., Kim, J., and Jung, K. S. (2008) Fermentative butanol production by Clostridia, *Biotechnol. Bioeng. 101*, 209-228.
21. Waterson, R. M., Castellino, F. J., Hass, G. M., and Hill, R. L. (1972) Purification and characterization of cortonase from Clostridium acetobutylicum, *J. Biol. Chem. 247*, 5266-5671.
22. Dekishima, Y., Lan, E. I., Shen, C. R., Cho, K. M., and Liao, J. C. (2011) Extending carbon chain length of 1-butanol pathway for 1-hexanol synthesis from glucose by engineered Escherichia coli, *J. Am. Chem. Soc. 133*, 11399-11401.
23. Kirby, J., and Keasling, J. D. (2009) Biosynthesis of plant isoprenoids: perspectives for microbial engineering, *Annu. Rev. Plant. Biol. 60*, 335-355.
24. Chaykin, S., Law, J., Phillips, A. H., Tchen, T. T., and Bloch, K. (1958) Phosphorylated Intermediates in the Synthesis of Squalene, *Proc. Natl. Acad. Sci. USA. 44*, 998-1004.
25. Goldstein, J. L., and Brown, M. S. (1990) Regulation of the mevalonate pathway, *Nature 343*, 425-430.
26. Lichtenthaler, H. K. (1999) The 1-Deoxy-D-Xylulose-5-Phosphate Pathway of Isoprenoid Biosynthesis in Plants, *Annu. Rev. Plant. Physiol. Plant. Mol. Biol. 50*, 47-65.
27. Eisenreich, W., Bacher, A., Arigoni, D., and Rohdich, F. (2004) Biosynthesis of isoprenoids via the non-mevalonate pathway, *Cell. Mol. Life Sci. 61*, 1401-1426.
28. Fujita, Y., Matsuoka, H., and Hirooka, K. (2007) Regulation of fatty acid metabolism in bacteria, *Mol. Microbiol. 66*, 829-839.
29. Magnuson, K., Jackowski, S., Rock, C. O., and Cronan, J. E., Jr. (1993) Regulation of fatty acid biosynthesis in Escherichia coli, *Microbiol. Rev. 57*, 522-542.
30. Kunst, L., and Samuels, A. L. (2003) Biosynthesis and secretion of plant cuticular wax, *Prog. Lipid Res. 42*, 51-80.
31. Steen, E. J., Kang, Y. S., Bokinsky, G., Hu, Z. H., Schirmer, A., McClure, A., del Cardayre, S. B., and Keasling, J. D. (2010) Microbial production of fatty-acid-derived fuels and chemicals from plant biomass, *Nature 463*, 559-562.

32. Vioque, J., and Kolattukudy, P. E. (1997) Resolution and purification of an aldehyde-generating and an alcohol-generating fatty acyl-CoA reductase from pea leaves (Pisum sativum L), *Arch. Biochem. Biophys. 340*, 64-72.
33. Schneider-Belhaddad, F., and Kolattukudy, P. (2000) Solubilization, partial purification, and characterization of a fatty aldehyde decarbonylase from a higher plant, Pisum sativum, *Arch. Biochem. Biophys. 377*, 341-349.
34. Ito, Y., and Murakami, M. (1999) Cleavage of Carbon–Carbon Single Bonds by Transition Metals, *Top. Organomet. Chem. 3*, 97-129.
35. Jun, C. H. (2004) Transition metal-catalyzed carbon-carbon bond activation, *Chem. Soc. Rev. 33*, 610-618.
36. Fristrup, P., Kreis, M., Palmelund, A., Norrby, P. O., and Madsen, R. (2008) The mechanism for the rhodium-catalyzed decarbonylation of aldehydes: a combined experimental and theoretical study, *J. Am. Chem. Soc. 130*, 5206-5215.
37. Modak, A., Deb, A., Patra, T., Rana, S., Maity, S., and Maiti, D. (2012) A general and efficient aldehyde decarbonylation reaction by using a palladium catalyst, *Chem. Commun. (Camb) 48*, 4253-4255.
38. Tsuji, J., and Kiyotaka, O. (1969) Decarbonylation Reactions Using Transition Metal Compounds, *Synthesis 4*, 157-169.
39. Doughty, D. H., and Pignolet, L. H. (1978) Catalytic Decarbonylation of Aldehydes, *J. Am. Chem. Soc. 100*, 7083-7085.
40. Tsuji, J., and Kiyotaka, O. (1968) Organic Syntheses by Means of Noble Metal Compounds. XXXIV. Carbonylation and Decarbonylation Reactions Catalyzed by Palladium, *J. Am. Chem. Soc. 1*, 94-98.
41. Yoder, J. A., Denlinger, D. L., Dennis, M. W., and Kolattukudy, P. E. (1992) Enhancement of diapausing flesh fly puparia with additional hydrocarbons and evidence for alkane biosynthesis by a decarbonylation mechanism, *Insect Biochem. Mol. Biol. 22*, 237–243.
42. Wang, X., and Kolattukudy, P. E. (1995) Solubilization and purification of aldehyde-generating fatty acyl-CoA reductase from green alga *Botryococcus braunii*, *FEBS Lett. 370*, 15–18.
43. Wang, X., and Kolattukudy, P. E. (1995) Solubilization, Purification and Characterization of Fatty Acyl-Coa Reductase from Duck Uropygial Gland, *Biochem. Biophys. Res. Commun. 208*, 210-215.
44. Lin, F., Das, D., Lin, X. N., and Marsh, E. N. G. (2013) Aldehyde-forming fatty acyl-CoA reductase from cyanobacteria: expression, purification and characterization of the recombinant enzyme, *FEBS J. 280*, 4773–4781.
45. Kockelkorn, D., and Fuchs, G. (2009) Malonic semialdehyde reductase, succinic semialdehyde reductase, and succinyl-coenzyme A reductase from Metallosphaera sedula: enzymes of the autotrophic 3-hydroxypropionate/4 hydroxybutyrate cycle in Sulfolobales., *J. Bacteriol. 191*, 6352-6362.
46. Reed, J. R., Quilici, D. R., Blomquist, G. J., and Reitz, R. C. (1995) Proposed mechanism for the cytochrome P450-catalyzed conversion of aldehydes to hydrocarbons in the house fly, Musca domestica, *Biochemistry 34*, 16221–16227.
47. Mpuru, S., Blomquist, G. J., Schal, C., Roux, M., Kuenzli, M., Dusticier, G., Clement, J. L., and Bagneres, A. G. (2001) Effect of age and sex on the production of internal and

external hydrocarbons and pheromones in the housefly, Musca domestica, *Insect Biochem. Mol. Biol. 31*, 139-155.

48. Qui, Y., Tittiger, C., Wicker-Thomas, C., Le Goff, G., Young, S., Wajnberg, E., Fricaux, T., Taquet, N., Blomquist, G. J., and Feyereisen, R. (2012) An insect-specific P450 oxidative decarbonylase for cuticular hydrocarbon biosynthesis, *Proc. Natl. Acad. Sci. USA. 109*, 14858–14863.
49. Marsh, E. N. G., and Waugh, M. (2013) Aldehyde decarbonylases: enigmatic enzymes of hydrocarbon biosynthesis, *ACS catal. 3*, 2515–2521.
50. Dennis, M. W., and Kolattukudy, P. E. (1991) Alkane biosynthesis by decarbonylation of aldehyde catalyzed by a microsomal preparation from *Botryococcus braunii*, *Arch. Biochem. Biophys. 287*, 268–275.
51. Cheesbrough, T. M., and Kolattukudy, P. E. (1984) Alkane biosynthesis by decarbonylation of aldehydes catalyzed by a particulate preparation from *Pisum sativum*, *Proc. Natl. Acad. Sci. USA. 81*, 6613–6617.
52. Dennis, M., and Kolattukudy, P. E. (1992) A cobalt-porphyrin enzyme converts a fatty aldehyde to a hydrocarbon and CO, *Proc. Natl. Acad. Sci. USA. 89*, 5306–5310.
53. Shanklin, J., Whittle, E., and Fox, B. G. (1994) 8 Histidine-Residues Are Catalytically Essential in a Membrane-Associated Iron Enzyme, Stearoyl-Coa Desaturase, and Are Conserved in Alkane Hydroxylase and Xylene Monooxygenase, *Biochemistry 33*, 12787-12794.
54. Bourdenx, B., Bernard, A., Domergue, F., Pascal, S., Leger, A., Roby, D., Pervent, M., Vile, D., Haslam, R. P., Napier, J. A., Lessire, R., and Joubes, J. (2011) Overexpression of Arabidopsis ECERIFERUM1 promotes wax very-long-chain alkane biosynthesis and influences plant response to biotic and abiotic stresses, *Plant Physiol. 156*, 29–45.
55. Bernard, A., Domergue, F., Pascal, S., Jetter, R., Renne, C., Faure, J. D., Haslam, R. P., Napier, J. A., Lessire, R., and Joubes, J. (2012) Reconstitution of plant alkane biosynthesis in yeast demonstrates that Arabidopsis ECERIFERUM1 and ECERIFERUM3 are core components of a very-long-chain alkane synthesis complex, *Plant Cell 24*, 3106-3118.
56. Unpublished, structure solved by Joint Center of Structural Genomics (protein database entry PDB|2OC5|A).
57. Baik, M. H., Newcomb, M., Friesner, R. A., and Lippard, S. J. (2003) Mechanistic studies on the hydroxylation of methane by methane monooxygenase, *Chem. Rev. 103*, 2385-2419.
58. Stubbe, J., Nocera, D. G., Yee, C. S., and Chang, M. C. Y. (2003) Radical initiation in the class I ribonucleotide reductase: Long-range proton-coupled electron transfer?, *Chem. Rev. 103*, 2167-2201.
59. Feig, A. L., and Lippard, S. J. (1994) Reactions of non-heme iron(II) centers with dioxygen in biology and chemistry, *Chem. Rev. 94*, 759-805.
60. Lange, S. J., and Que, L. (1998) Oxygen activating nonheme iron enzymes, *Curr. Opin. Chem. Biol. 2*, 159-172.

Chapter 2

Conversion of Aldehydes to Alkanes by Cyanobacterial Aldehyde Decarbonylase

2.1 Introduction

Microbial biosynthesis of alkanes has recently gained tremendous attention .[1,2,3] A two-step conversion of long chain fatty acyl esters, derived from fatty acid biosynthesis pathway, to the corresponding alkanes has recently been discovered in cyanobacteria.[4] Schirmer and co-workers, from LS9, Inc. California, for the first time described the existence of two soluble proteins that play crucial role for the alkane production in cyanobacteria. The authors compared the genomes of ten cyanobacteria that produce alkanes with the one that doesn't produce them. Using a subtractive genomic analysis, the authors identified 17 proteins that were present in alkane-producing cyanobacteria and were absent in the non-producing cyanobacterium. Most of the identified proteins were assigned functions based on sequence analogs except a few that were previously not characterized. Finally, two hypothetical proteins in cyanobacterium *S elongates* PCC7942 with open reading frames orf1594 and orf1593 stood out as the most likely candidates to catalyze the last two steps of alkane biosynthesis pathway in cyanobacteria. The protein encoding orf1594 belongs to the dehydrogenase/reductase family of enzymes and the protein encoding orf1593 belongs to the methane monooxygenas/ribonucleotide reductase family of enzymes that contain a non-heme di-iron active site. Involvement of these two proteins in cyanobacterial alkane biosynthesis was

confirmed by heterologous 'knock in' and 'knock out' experiments in *E*. *coli*. Over-expression of orf1594 alone showed *in vivo* production of long-chain aldehydes and alcohols in *E*. *coli,* whereas over-expression of orf1593 alone did not show any aldehyde or alkane production. Over-expression of both the reading frames simultaneously showed production of long-chain alkanes along with long-chain aldehydes that were shown to be the intermediates of conversion of long-chain fatty acyl esters to long-chain alkanes. Thus, orf1594 was attributed to be a reductase that reduces long-chain acyl-ACPs (ACP: Acyl Carrier Protein)/acyl-CoAs (CoA: Coenzyme A) to the corresponding aldehydes. Orf1593 was attributed to be an aldehyde decarbonylase (AD) that decarbonylates long-chain aldehydes to the corresponding alkanes. The identity of these two proteins was further established by their *in vitro* expression in *E. coli* followed by activity studies. Recombinantly over-expressed reductase protein showed esterase activity with greater affinity for acyl-ACP (K_M = 8 μM for oleoyl-ACP) than acyl-CoA (K_M = 130 μM for oleoyl-CoA) in the presence of NADPH as the cofactor and thus attributed as acyl-ACP reductase. The decarbonylase enzyme was shown to convert octadecanal to heptadecane in presence of ferredoxin (Fd)/ferredoxin reductase (FdR)/NADPH as cofactors. Serendipitously, there was a structure (Figure 2.1) of an ortholog of orf1593 from cyanobacteria *Prochlorococcus marinus* MIT9313 already deposited in the Protein Data Bank (PDB ID 2OC5) that was solved by the Joint Center of Structural Genomics, without having any function assigned.[5] The structure revealed that the enzyme is a member of non-heme dinuclear iron oxygenase family of enzymes such as methane monooxygenase, class I ribonucleotide reductase and ferritin. In the α-helical structure, a di-metal core is contained within four anti-parallel α-helices in which two

histidines and four glutamates serve as the metal ligands. The structure also shows a co-crystalized long chain fatty acid that coordinates to the metal center by replacing a glutamate.

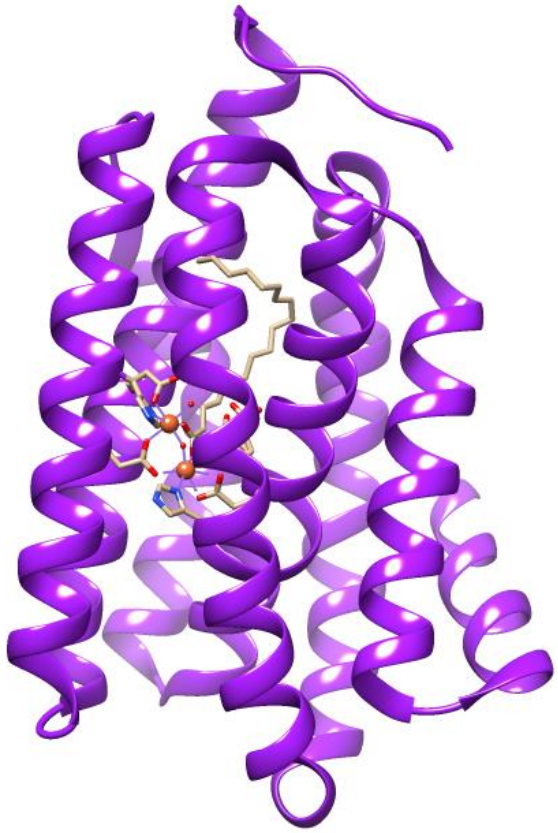

Figure 2.1. X-ray structure of cAD from *P. marinus* MIT9313 (PDB ID 2OC5), illustrating the position of the di-metal center and fatty acid bound at the active site of α-helical structure.

The pioneering work by Schirmer and co-workers revealed identity of the proteins involved in the two-step biosynthesis of alkanes in cyanobacteria and thus opened a new direction for the scientific community seeking to develop the next generation of advanced 'drop in' biofuels made of hydrocarbons from microorganism. The enzyme not only holds potential for future biofuel application but also attracts significant attention because it catalyzes a very unusual conversion of an aldehydes to alkanes. Reactions that produce completely un-functionalized

compounds are rare and their mechanisms are very poorly understood. Although aldehyde decarbonylase enzymes (ADs) from higher organisms (e.g. plant, algae, insect) have been studied for the last three decades,[6,7,8] not much is known about the substrate specificity, kinetics and mechanisms of these enzymes. This is partly because the eukaryotic aldehyde decarbonylase enzymes are all membrane associated proteins and none of them could be purified in good quantity to homogeneity for extensive mechanistic investigations. With this premise, I sought to investigate the cyanobacterial aldehyde decarbonylase (cAD) with the objective to heterologously over-express and purify significant amount of active protein for extensive characterization and activity studies.

Enzyme purification, characterization, isotope studies, formate detection and kinetic studies were carried out in collaboration with Dr. Bekir Eser. Mr. Aaron Sciore assisted with metal requirement determination. The work has been published in part in *Angewandte Chemie International Edition,* **2011**, *50* (31), 7148-7152 and *Biochemistry* **2011**, *50* (49), 10743-10750.

2.2 Materials and Methods

E. coli BL21 (DE3) competent cells were obtained from Novagen. Cells were made electro-competent according to the procedure of high efficiency electro-transformation of *E. coli* from Bio-Rad. The cells were stored at -80 °C up to 6 months without any noticeable loss in competency. The 2x-YT media (Fisher Bioreagent) was used for bacterial growth. Electro-competent *E. Coli* cells were transformed with the pET-28b(+) construct, carrying the aldehyde decarbonylase gene, following the protocol of bacterial electroporation of Bio-Rad. An *E. coli*

pulser apparatus (Bio-Rad) and electroporation cuvettes plus (Fisherband) were used for this purpose. The SOC (Super Optimal Broth) media for recovery growth was obtained from Novagen. Agar plates were made using bacto peptone, yeast extracts, NaCl and bacto agar. Kanamycin was used as the antibiotic selection. Isoprpyl-β-D-galactopyranoside (IPTG) was used for protein expression. All these reagents were purchased from Fisher Bioreagents. A New Burnswick Scientific Excella E25 Incubator Shaker was used for cell culture.

For cell lysis and purification, HEPES, imidazole, glycerol were purchased from Fisher Bioreagents, lysozyme from Sigma-Aldrich, EDTA-free protease inhibitor tablet from Roche and DNAse from Novagen. A Fisher Scientific 550 Sonic Dismembrator was used for sonication using a microtip. A Sorvall Legend XTR and a Beckman Coutler Microfuge 18 centrifuge were used for centrifugation purpose.

Protein purification was carried out using Fast Protein Liquid Chromatography (FPLC, ActaPure UPC10, GE Healthcare) coupled to a UPC-900 UV/pH/conductivity detector. HisTrap, HP columns (5 mL, GE Healthcare) pre-packed with Ni-Sepharose was employed for the purification purpose. Eluted proteins were monitored at 280 nm and collected by a frac-920 automatic fraction collector. Purified protein was dialyzed using 10-12 kDa molecular wt. cutoff dialysis tubing (Fisherband). After dialysis, the protein was concentrated using Amicon Ultra-15 centrifugal filters (Millipore). SDS-PAGE gels for protein analysis, the buffers for running the gels, stain and destain solutions were all made according to the protocol of U. K. Laemmli.[9] The reagents used for this purpose were acrylamide (40% aqueous solution), Bis-acrylamide, sodium dodecyl sulphate (SDS), Tris-HCl buffer, ammonium persulfate (APS),

tetramethylethelenediamine (TEMED), coomassie blue, methanol and glacial acetic acid. All the reagents were obtained from Fisher Bioreagents. The BenchMark protein ladder (Invitrogen) was used as molecular weight standard. A HP 8453 UV-Vis spectrophotometer was used for regular determination of protein concentration. LC-MS analysis was carried out using Agilent 6520 LC - accurate-mass Q-TOF MS system.

For metal dependence studies, Ferrous ammonium sulphate, manganous chloride, cobalt(II) chloride, copper (II) sulphate, zinc (II) chloride of their best analytical standards were purchased from Sigma-Aldrich. Ferrozine, nitriloacetic acid (NTA), ethylenediaminetetraaceticacid (EDTA) was also obtained from the same vendor.

For activity and kinetic studies, spinach ferredoxin (Fd), spinach ferredoxin reductase (FdR), phenazine methosulphate (PMS), heptanal, octanal, nonanal, decanal, dodecanal, trans-2-dodecanal, trans-2,4-dodecadienal, trans-2-decanal, hexane, heptane, octane, nonane, decane, undecane were obtained from Sigma-Aldrich. NADPH and NADH were obtained fron Acros organics. All other chemicals were of purest grade commercially available.

Heterologous expression of Prochlorococcus marinus* MIT9313 *aldehyde decarbonylase (Pm cAD) in E. coli. A synthetic gene, *Pm cAD*, (741 bp), encoding aldehyde decarbonylase from cyanobacterial species *Prochlorococcus marinus* MIT9313*,* was purchased from GenScript USA Inc. (Piscataway, NJ, USA). The expression vector pET-28b(+) was obtained from Novagen. The gene was cloned into pET-28b(+) using the restriction sites NdeI and BamHI (New England Biolabs). The molecular cloning work was carried out according to the protocol of J. R. D.

Sambrook.[10] After cloning, the identity of the gene was confirmed by DNA sequencing by the DNA sequencing core facility at the University of Michigan.

The gene was cloned in such a way that allows expression of an N-terminus His-tag along with the expected protein. After transformation of electro-competent *E.coli* BL21 (DE3) cells with this construct, cells were grown overnight on agar plates with kanamycin antibiotics resistance to obtain single colonies. To express the protein, a single colony was grown overnight at 37 °C in 5 mL 2x-YT media supplemented with 50 µg/mL of kanamycin, transferred to 1 L of the same medium and grown at 37 °C to an optical density of 0.6 at 600 nm. IPTG was added to a final concentration of 1 mM to induce protein expression. Cells were further grown for 8 h at the same temperature and then harvested by centrifugation at 4000 *g* at 4 °C for 25 min.

Purification of recombinant cAD. 15 g (damp weight) of cells were resuspended in 120 mL 50 mM Tris-HCl buffer, pH 8.0, containing 100 mM NaCl, 10 mM imidazole, 5% glycerol, 0.5 mg/mL of lysozyme, 1/ 50 mL EDTA-free protease inhibitor tablet and 2 µl of DNAse for 1 h on ice and lysed by sonication using a 550 Sonic Dismembrator with a micro-tip at maximum power using 2s pulses separated by 8s to prevent overheating for a total time of 30 min. The supernatant was separated from cell pellet by centrifugation at 15000 *g* at 4 °C for 30 min.

Purification of cAD was achieved using FPLC by affinity chromatography using a Ni-affinity column (5 mL, HisTrap HP) and taking the advantage of expressed N-terminal His-tag. The column was equilibrated with buffer A: 20 mM HEPES, pH 7.4, 500 mM NaCl, 20 mM imidazole, 5% glycerol. The supernatant from cell lysis was loaded onto the column using a 50 mL super-loop at a flow rate of 1 mL/min and the column was washed with 25 mL of the same

buffer at a flow rate of 2 mL/min. Non-specifically bound proteins were washed out of the column with 20 mL of buffer containing 20 mM HEPES, pH 7.4, 500 mM NaCl, 50 mM imidazole, 5% glycerol at the same flow rate. Finally, cAD was eluted from the column with 10 mL of buffer B: 20 mM HEPES, pH 7.4, 500 mM NaCl, 500 mM imidazole, 5% glycerol at a flow rate of 2 mL/min. The fractions were judged by SDS-PAGE gel for purity. The fractions containing pure protein were pooled and dialyzed using 10-12 kDa molecular wt. cutoff dialysis tubing at 4 °C against the final assay buffer: 100 mM HEPES, pH 7.2 containing 100 mM KCl and 10% glycerol. After dialysis, the protein was concentrated using Amicon Ultra-15 centrifugal filters to a concentration >500 μM.

The genes encoding cyanobacterial aldehyde decarbonylase proteins from other cyanobacterial species *N. punctiformes* PCC73102, *Synechococcus sp.* RS9917, and *Synechocystis sp.*PCC6803 were generous gifts from Prof. Patick Jones, University of Turku, Finland. The genes were cloned in pET-28b(+) expression vector. The proteins were expressed and purified following the same procedure as described for the expression and purification of *Pm* cAD.

Protein concentration determination. In order to measure the protein concentration, the extinction coefficient of cAD was determined using both Bradford assay[11] and the method of Gill and von Hippe.[12] To determine the extinction coefficient by the second method, absorbance of as-isolated cAD ($A_{as\text{-}isolated}$) was measured by UV-Vis spectroscopy at 280 nm cAD was then denatured in 6M guanidine hydrochloride and the absorbance was measured

($A_{denatured}$). A theoretical extinction coefficient ($\varepsilon_{denatured}$) was also calculated based on the number of tyrosine, tryptophan and cysteine residues using the following formula:

$$\varepsilon_{M,Gdn.HCl} = a\varepsilon_{M,tyr} + b\varepsilon_{M,trp} + c\varepsilon_{M,cys}$$

where, $\varepsilon_{M,tyr}$, $\varepsilon_{M,trp}$ and $\varepsilon_{M,cys}$ are the molar extinction coefficient of tyrosine (1280 M^{-1} cm^{-1}), tryptophan (5690 M^{-1} cm^{-1}) and cysteine (120 M^{-1} cm^{-1}) respectively at 280 nm and a, b, c are the numbers of the corresponding residues.

Finally using the formula:

$\varepsilon_{as\text{-}isolated}$ cAD/$\varepsilon_{denatured}$ cAD = $A_{as\text{-}isolated}$ cAD/$A_{denatured}$ cAD,

the molar extinction coefficient of as-isolated cAD ($\varepsilon_{as\text{-}isolated}$) was measured.

Both methods were in good agreement and gave an extinction coefficient ($\varepsilon_{280\ nm}$) 19.9 $mM^{-1}cm^{-1}$ at 280 nm. cAD concentration reported in this study were determined based on this extinction coefficient.

Preparation of apo-cAD. De-metallation of a metallo-enzyme allows exploration of the apo-enzyme as well as reconstitution of the apo-enzyme with other biologically relevant metals and their properties to be studied. As-isolated cAD was de-metallated by rigorous treatment with various metal chelating agents. Endogenously bound transition metals were removed from cAD by incubating the protein at 4 °C overnight in 100 mM HEPES, pH 7.2 containing 100 mM KCl, and 10% glycerol, to which sodium dithionite (5 mM) and ferrozine (10 mM) were added,[13] followed by desalting to remove ferrozine and dithionite on a column made of Sephadex G-25 fine resin at 4 °C. The protein from this step was then dialyzed against the same HEPES buffer with/without the metal chelators EDTA (ethelenediaminetetraacetic acid, 10 mM) and NTA

(nitriloacetic acid, 10 mM) at 4 °C overnight. Finally, the protein was dialyzed at 4 °C against several changes of the HEPES buffer without metal chelators and concentrated using Amicon-15 concentrator to a concentration > 500 μM.

Synthesis of 1-octadecanyl aldehyde and n -octadecyl-1-d aldehyde. Synthesis 1-octadecanal was carried out by pyridinium dichromate oxidation of 1-octadecanol as described below. n-octadecyl-1-d aldehyde was also synthesized in a very similar way in order to pursue isotope labeling experiments, which will be described later. Synthetic route to these compounds are outlined in Scheme 2.1.

Octadecanal and 1-d-octadecanal were prepared by oxidation of 1-octadecanol and n-octadecyl-1,1-d_2 alcohol respectively with pyridinium dichromate. To a solution of pyridinium dichromate (4.22 g, 11.23 mmol) in 250 mL dichloromethane, 1-octadecanol (Acros) (1.98 g, 7.29 mmol)/n-octadecyl-1,1-d_2 alcohol (CDN isotopes, 1.98 g, 7.26 mmol) was added and stirred overnight at room temperature.[14] 250 mL hexane was added and the resulting mixture was filtered. The dark brown filtrate was collected and evaporated to dryness. The expected product 1-octadecanal/n-octadecyl-1-d aldehyde was obtained as a white powder from the dried filtrate upon purification by silica column chromatography using hexane: ethyl acetate (9:1) as eluting solvent. For n-octadecyl aldehyde, Yield: 0.82 g (41.8 %). For n-octadecyl-1-d aldehyde Yield: 0.79 g (40.3 %).

Enzyme assays with octadecanal. Typically, assays were performed in 100 mM HEPES or potassium phosphate buffer, pH 7.2 containing 100 mM KCl and 10% glycerol. Assays were performed microaerobically in an anaerobic chamber (Coy Laboratory Product Inc., Grass Lake,

MI) with oxygen percentage ~10-20 ppm unless otherwise specified. Aldehyde substrates were made up as stock solutions in DMSO by heating at 60 °C and vortexing. In general, enzymatic reactions contained 5 µM cAD, 10 µM ferrous ammonium sulfate, 300 µM octadecanal in a total volume of 500 µL. The reducing system comprised either 30 µg/mL ferredoxin, 0.04 U/mL ferredoxin reductase and 800 µM NADPH ("biological" reducing system) or 75 µM phenazine methosulfate (PMS) and 750 µM NADH ("chemical" reducing system). When using the biological reducing system, the reaction mixtures were incubated at 37 °C for 30 min with intermittent shaking (necessary because of the poor solubility of the substrate). The biological reducing system appeared to become inactivated by prolonged shaking, presumably due to denaturation of the enzymes. When using the chemical reducing system, the reaction mixtures were shaken continuously at 37°C for 30 min at 200 rpm. Reactions were quenched by addition of 500 µL ethyl acetate and vortexed well to extract alkane product and un-reacted substrate. A 10 µL sample of the ethyl acetate layer was injected into either a GC or GC-MS for analysis. Enzymatic conversion of octadecanal to heptadecane was quantified using a calibration plot of heptadecane.

Enzyme assays with heptanal. Assays in which heptanal was used as the substrate were performed under microaerobic environment in 1.5 mL gastight vials with a total assay volume of 500 µL. O_2 concentration was ~10-20 ppm in the glove box. This corresponds to ~ 0.025 µM of dissolved oxygen. However, the assays were continuously shaken and the vials used for these assays appear to be not completely gas-tight, which allows slow diffusion of molecular oxygen into the reaction mixture. A typical reaction contained 10 µM cAD, 20 µM ferrous ammonium sulfate, 75 µM PMS, 1 mM NADH, 2 mM heptanal in 100 mM HEPES buffer, pH 7.2 containing

100 mM KCl and 10% glycerol and 3% DMSO. Heptanal stock solutions were freshly made in DMSO. After addition of all the components, reactions were shaken at 200 rpm at 37 °C. To determine the amount of hexane produced, a sample of the headspace was collected using a gastight sample lock Hamilton syringe and analyzed by GC-MS or GC. The amount of hexane produced was quantified by a standard curve constructed from aqueous buffer equilibrated with known concentrations of hexane.

Gas Chromatography-Mass Spectrometry (GC-MS). Detection and quantification of alkanes were performed using a Shimadzu QP5000 GC-MS system equipped with GC 17A and quadrupole mass detector. A DB-5 column (Restek, 30 m x 0.25 mm x 0.25 μm) was employed for elution. For analysis of heptadecane, the flow rate of the helium carrier gas was 1.5 mL/min and the inlet temperature was maintained at 160 °C. Injections were made in split mode with a split ratio of 20:1 and a total flow of 34.4 mL/min. The interface temperature was maintained at 250 °C. The oven temperature was held at 70 °C for 2 min and then increased to 250 °C at 20 °C/min and finally maintained at 250 °C for 5 min. For analysis of hexane, injections were made in a splitless mode. The flow rate of helium carrier gas was 1.0 mL/min and the injection temperature was 200 °C. The oven temperature was held at 40 °C for 2 min and then increased to 150 °C at 20 °C/min and finally maintained at that temperature for 2 min. Chromatographic data were analyzed using the associated PostRun analysis software.

Gas Chromatography. For GC analysis, Agilent 6850 GC equipped with a flame ionization detector (FID) was used to detect and quantify alkaness formed in enzyme reactions. The column employed for alkane analysis was a Restek Rtx-5 capillary column (30 m × 0.25 mm × 0.25 μm). For the detection of heptadecane, the flow rate of the helium carrier gas was 1.1

mL/min and the inlet temperature was maintained at 320 °C. Injections were made in split mode with a split ratio of 5:1 and a total flow of 5.7 mL/min. The oven temperature was held at 70°C for 2 min and then increased to 280 °C at 20 °C/min and finally maintained at 280 °C for 5 min. For the detection of hexane, injections were made in split mode with a split ratio 2:1 and a total flow 2.2 mL/min. The oven temperature was held at 40 °C for 2 min and then increased to 150 °C at 20 °C/min and finally maintained at that temperature for 2 min. The FID detector was at 260°C with a continuous flow of H_2 at 40 mL/min and air at 400 mL/min. Chromatographic data were analyzed using HP ChemStation software.

Formate assays. To detect formate as the co-product of cAD-catalyzed reaction, enzyme reactions were performed in 10 mM HEPES, pH 7.2. Assays were carried out with octadecanal as substrate and in the end of an assay, 500 μL of the reaction mixture was mixed with 40 μL of 40 mM 2-NPH (2-nitrophenylhydrazine) solution (aqueous solution with 0.2 M HCl and 50% ethanol) and 100 μL of EDC (1-ethyl-3-(3-dimethylaminopropyl)carbodiimide) working solution (125 mM EDC with 1.5% pyridine in 50% ethanol). After vortexing for ~30 s, the reaction mixtures were incubated at 65 °C for 30 min. The samples were then centrifuged to remove precipitated protein and insoluble reaction products. 500 μL of the clear supernatant were subjected to chromatography on a Nucleosil C18 RP HPLC column (250 mm x 4 mm, 5 μM, 120 Å). The column was equilibrated in 90 % water, pH 4.5 (acidified with HCl) and 10 % acetonitrile and compounds were eluted isocratically at 1 mL/min using the same solvent.

2.3 Results and Discussion

2.3.1 Characterization and Properties of cAD

Pm cAD appeared to be a reasonably stable protein. No precipitation was detected during and after the purification by FPLC. Room temperature purification yielded similar amounts of protein as purification at 4 °C. Very little precipitation was observed during dialysis at 4 °C for 24 h. The protein was purified in a very high yield of ~ 150 mg/L of culture.

SDS-PAGE and LC-MS analysis. The purified protein was judged to be more than 95 % pure as determined by SDS-PAGE (Figure 2.2). The identity of the protein was verified by electrospray mass-spectrometry using Agilent 6510 quadrupole time-of-flight mass spectrometer: expected average mass: 29342.19 Da, experimentally determined mass: 29211.23 Da (Figure 2.3) (N-terminus methionine was cleaved during mass analysis).

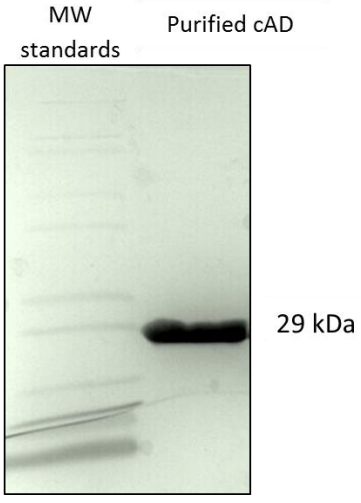

Figure 2.2. SDS-PAGE analysis of cAD depicting molecular wt. standards and purified cAD.

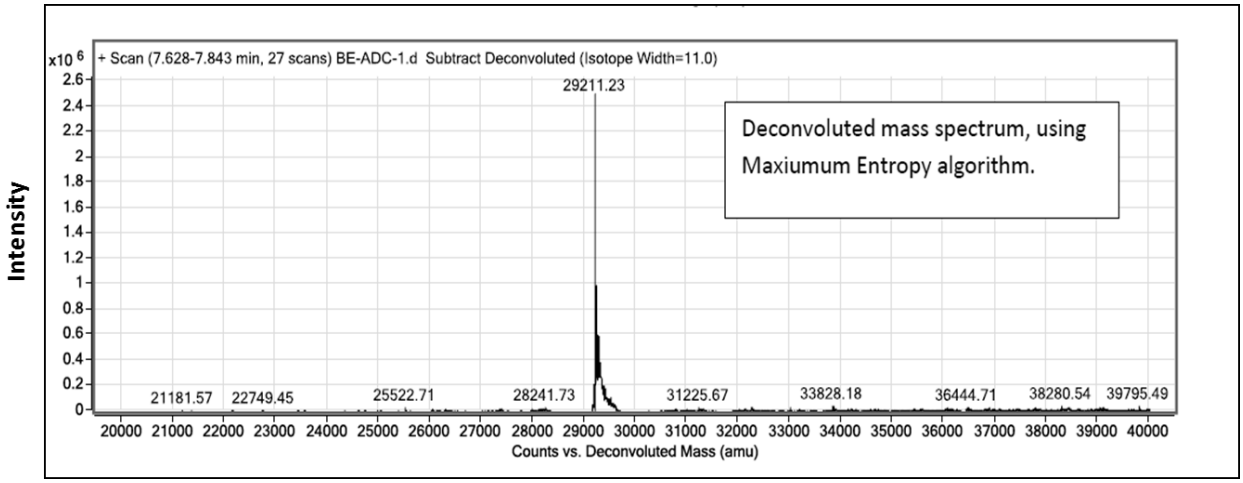

Figure 2.3. Mass spectrum of purified recombinant cAD depicting the deconvoluted average mass.

UV-Visible spectrum of cAD. The enzyme as-purified from *E. coli* was pale brown in color. The absorption spectrum of the enzyme (Figure 2.4) had a broad peak at around ~350 nm ($\varepsilon_{350\ nm}$ ~ 5 $mM^{-1}cm^{-1}$), which is typical of non-heme di-iron enzymes, due to the presence of Fe(III)-oxo charge transfer band.[15,16]

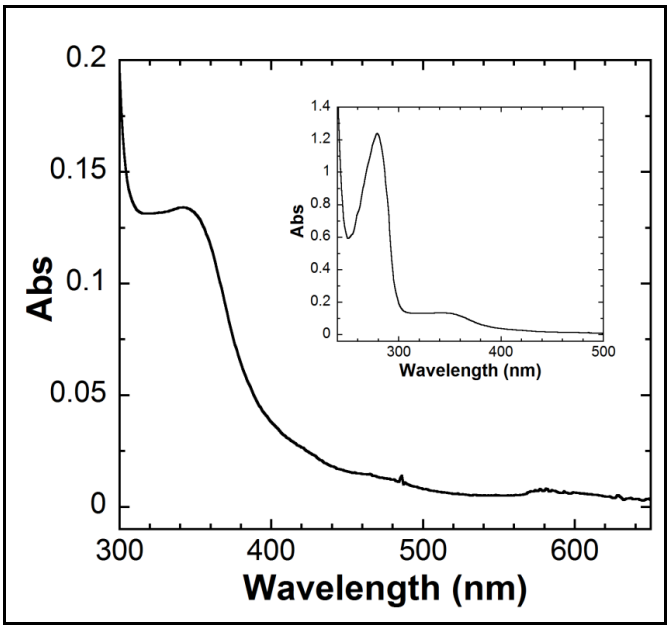

Figure 2.4. The absorption spectrum of as-isolated cAD from *E. coli* showing charge transfer bands at ~350 nm; *inset* is the full UV-Visible absorption spectrum of cAD showing absorbance at 280 nm as well as at 350 nm.

Metal content of cAD. The metal content of the enzyme was determined by inductively coupled plasma-mass spectrometry (ICP-MS) at the University of Michigan, Department of Geological Sciences facility. Samples for ICP-MS analysis were prepared in collaboration with Dr. Bekir Eser in 10 mM HEPES buffer, pH 7.2 containing 1% glycerol. 200 μL of sample of concentration 20-50 μM was submitted to the facility. Metal analysis indicated that a typical cAD preparation contain only ~ 30-35% of total metals (assuming two metals per cAD) with Fe 17.8%, Zn 9.6%, Ni 5.1%, Mn 3%, Cu <0.2%, Co < 0.01% (Table 2.1). For routine determination of the iron content of protein preparations, the well-established assay based on chelation of Fe(II) by ferrozine was utilized.[17] The protein was denatured by addition of HCl (0.2 M final) and the precipitated protein was removed by centrifugation. The supernatant was diluted to 500 μL with MilliQ water and ascorbic acid (2.3 mM final), ferrozine (0.3 mM final) and 120 μL saturated

ammonium acetate were added. After incubation for ~30 min, the iron content was calculated from the absorbance at 562 nm, using the extinction coefficient of 26.4 $mM^{-1}cm^{-1}$.[13] The iron content in a typical cAD preparation was found to be ~20%, which was good agreement with the results from ICP-MS data.

Properties of apo-cAD. Apo-cAD was prepared in collaboration with Dr. Bekir Eser. As-isolated cAD was incubated with different metal chelating agents as described in the materials and methods section. The UV-Vis spectrum of apo-cAD did not show the broad peak at 350 nm that was present in the spectrum of as-isolated cAD. ICP-MS data of ferrozine treated cAD indicated significant depletion in the percentage of bound iron but the percentage of zinc increased to some extent which indicated strong affinity of the apo-enzyme to bind to zinc. More rigorous treatment of the enzyme with other metal chelators: EDTA and NTA sufficiently depleted the metal content to a trace level with 1.4% iron, 0.1% manganese and 2.4% zinc. When this preparation of cAD was incubated with 3 equivalent of iron (assuming cAD binds to 2 iron atoms) and excess free iron was removed by dialysis , the reconstituted enzyme showed ~ 90% iron occupancy along with ~ 7% zinc (Table 2.1).

Table 2.1. ICP-MS data of different preparations of cAD

Protein samples	% Fe	% Mn	% Cu	% Ni	% Co	% Zn
As-isolated	17.8	3	< 0.2	5.1	< 0.01	9.6
Ferrozine treated	1.4	6.1	0.7	0.3	< 0.01	24.2
Ferrozine/NTA/EDTA treated	1.4	0.1	< 0.1	< 0.5	< 0.01	2.4
Fe(II) reconstituted*	89	1.6	0.5	1.8	< 0.01	6.9

* cAD was treated with 3 eq. ferrous ammonium sulfate and the excess unbound iron was removed by dialysis.

2.3.2 Activity and Kinetics of cAD

Characterization of 1-octadecanyl aldehyde and n -octadecyl-1-d aldehyde. In the original discovery, 1-octadecanyl aldehyde was shown to be a substrate for cAD.[4] Synthesis of octadecanal and deuterated 1-d-octadecanal were carried out as described in the material and method section and as outlined in Scheme 2.1. Both the compounds were characterized by mass spectroscopy. LC-MS *m/z* (TOF) of n-octadecyl aldehyde ($C_{18}H_{36}O$) $[M + Na]^+$: 291.2 (Figure 2.5). LC-MS *m/z* (TOF) ($C_{18}H_{35}DO$) $[M + Na]^+$: 292.2 (Figure 2.6). The products were also characterized by GC-MS.

Scheme 2.1. Synthetic route to octadecanal and 1-d-octadecanal

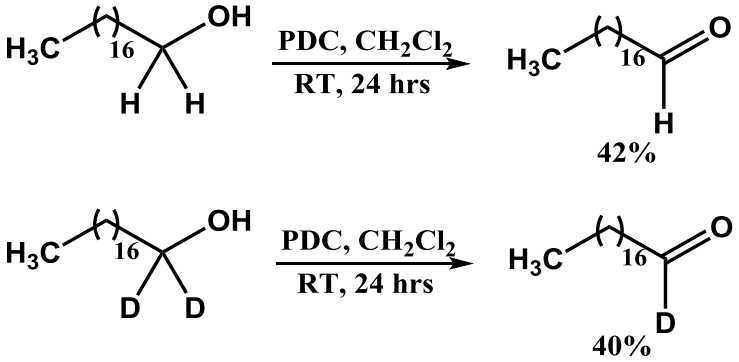

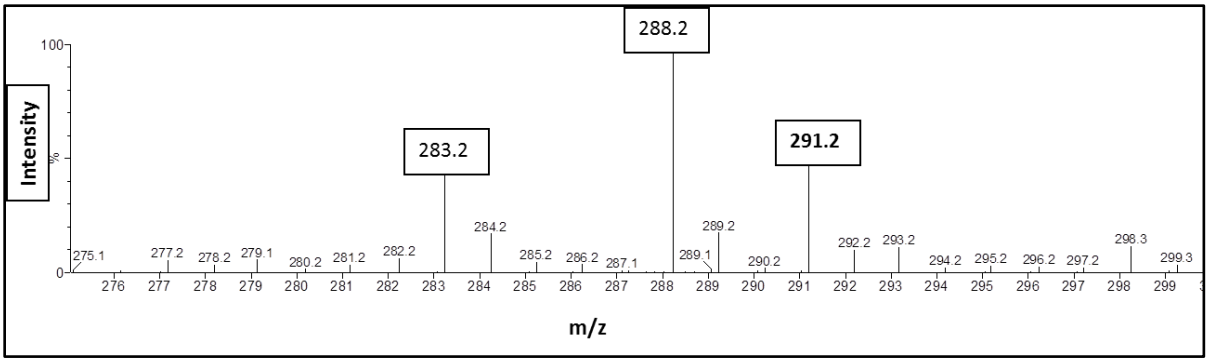

Figure 2.5. Mass spectrum of n-octadecyl aldehyde.

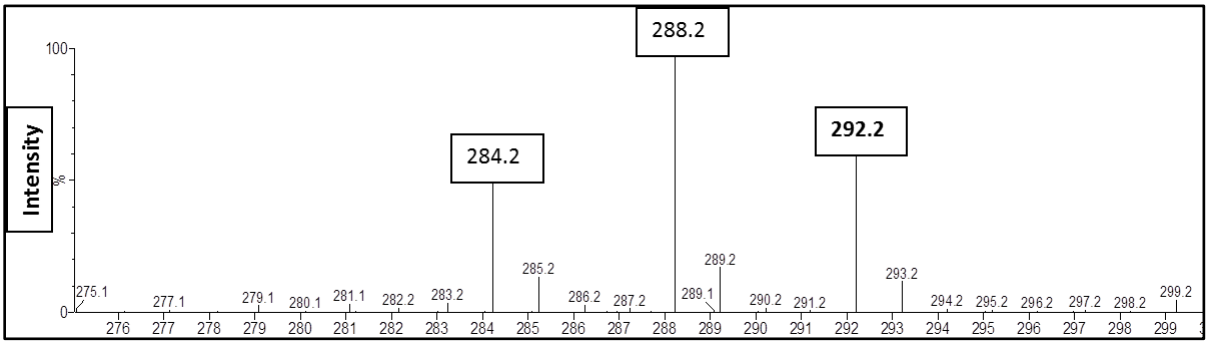

Figure 2.6. Mass spectrum of n-octadecyl-1-d-aldehyde.

Requirement of auxiliary reducing system for activity. *In vivo*, different cyanobacterial ADs were shown to produce alka(e)nes with the highest titer of alka(e)nes produced by *Nostoc punctiforme* PCC73102.[4] This particular cAD was further heterologously expressed in *E.coli* and its *in vitro* activity was established. Using octadecanal as a substrate, the enzyme was shown to produce heptadecane.[4] The *in vitro* activity was also reported to be exclusively dependent on cofactors ferredoxin (Fd)/ferredoxin reductase (FdR)/NADPH in accord with expectations from other non-heme iron enzymes.[18,19,20] Omission of one of these components from assay mixture completely abolished activity. Using commercially available spinach Fd, spinach FdR and NADPH, the reaction proceeded extremely slowly and produced ~1 turnover product in overnight.[21] This very sluggish activity raised questions about whether the correct cofactor metal(s) were present in the assay.

The reported activity of cAD in presence of spinach Fd/FdR and NADPH was first verified according to the literature procedure.[4] However, based on the assay conditions by Schirmer et. al, i.e. 5 μM cAD, 10 μM ferrous ammonium sulfate, 300 μM octadecanal, 30 μgmL^{-1} spinach ferredoxin and 0.04 UmL^{-1} spinach ferredoxin reductase and 800 μM NADPH, only ~1 turnover of the product was obtained in 1 h. Because of this very sluggish activity using physiological reducing system, other possible chemical reducing systems were investigated. It was found that a chemical reducing system comprising of N-methylphenazinium methylsulfate (PMS, Scheme 2.2) and NADH could effectively replace for the ferredoxin reducing system (Scheme 2.3) and resulted in greatly improved activity. PMS is a widely used electron transfer catalyst and serve as an electron mediator in various enzyme system.[22,23,24] Replacing the ferredoxin system with

75 µM PMS and 750 µM NADH in the assay mixture resulted in multiple turnovers and the reaction rates could be determined from initial time points as described later.

Scheme 2.2. Chemical structure of N-methylphenazinium methylsulfate (PMS)

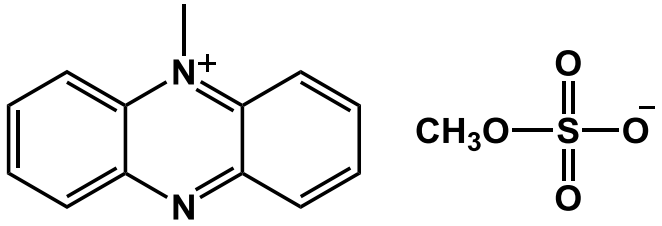

Scheme 2.3. Conversion of octadecanal to heptadecane by cAD in the presence of different reducing systems

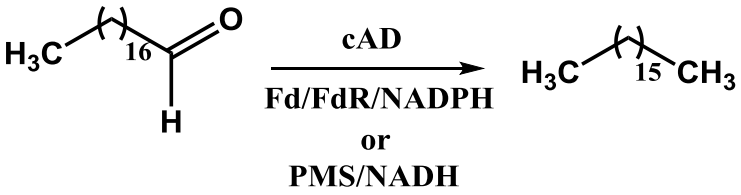

Gas chromatogram and mass spectrum of octadecanal to heptadecane conversion. A GC-MS chromatograph demonstrating conversion of octadecanal to heptadecane is shown in Figure 2.7A. Heptadecane eluted at 9.60 min, octadecanal eluted at 11.75 min and authentic standard of octadecane that was used as an internal standard eluted at 10.45 min. Heptadecane was characterized by co-elution of a standard heptadecane sample as well as by the molecular ion peak of 240 Da (Figure 2.7B).

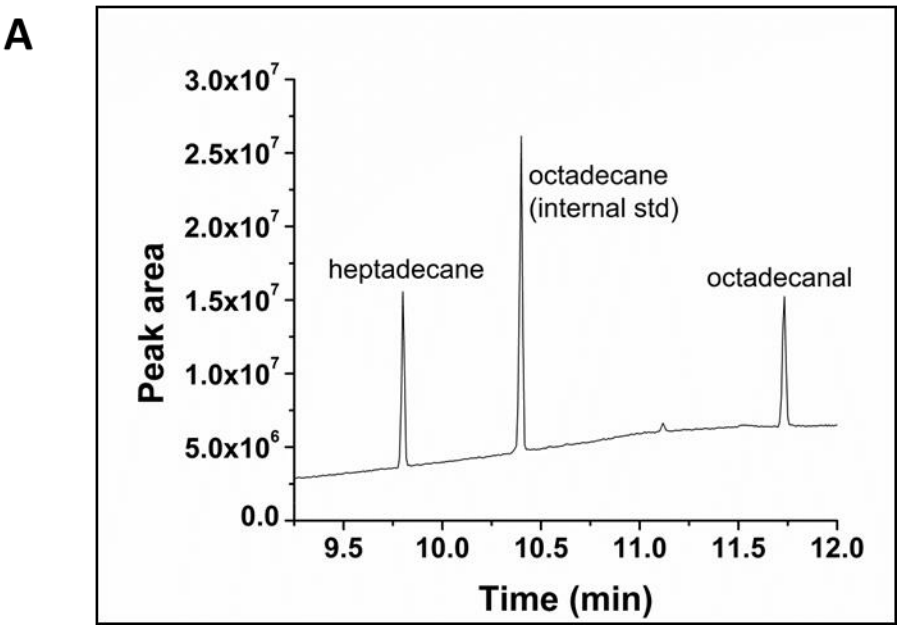

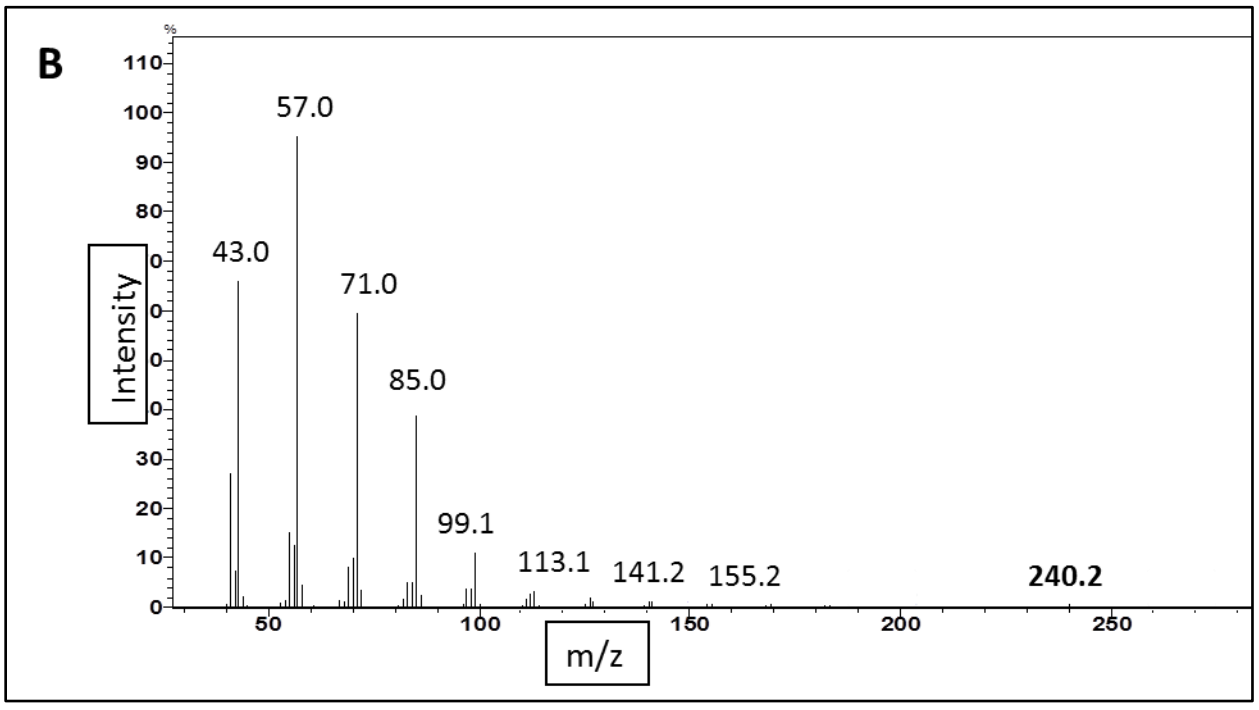

Figure 2.7. (A) GC-MS chromatograph demonstrating conversion of octadecanal to heptadecane. Octadecane was added as an internal standard in the assay mixture during extraction. (B) Mass spectrum of heptadecane showing fragmentation pattern of heptadecane as well as molecular ion peak 240 Da.

Metal dependence of cAD catalytic activity. These assays were carried out in collaboration with Dr. Bekir Eser and Mr. Aaron Sciore. To determine the identity of the active metal cofactor for cAD, assays were performed with apo-cAD using PMS/NADH reducing system as described above in the presence of Fe(II) and the most relevant biologically active divalent metals; Mn(II), Cu(II), Zn(II), Co(II) and Ni(II). Each of these metals were varied against Fe(II) at a total metal equivalency of 2 per cAD active site. Octadecanal was used as the substrate and heptadecane product was quantified using a calibration curve. Activity was plotted as a function of iron mole fraction. In all cases, highest activity was observed with 2 equivalents of Fe(II) and none of the other metals supported activity alone (Figure 2.8). Zinc was proven to be slightly inhibitory. In the presence of one equivalent of Fe(II) and one equivalent of each of the other metals per cAD active site (1:1 heterodinuclear composition), the activity was not higher than half of the activity of that obtained when 2 equivalents of Fe(II) are present, ruling out a heterodinuclear active site involved the enzyme, unlike R2 protein of class 1c of ribonucleotide reductases.[25] Thus cAD appeared to function as dinuclear iron enzyme.

Time-course and substrate concentration dependence. To determine the progress of the cAD-catalyzed reaction, assays were performed with octadecanal as described before. Reactions were quenched at different time points and the product heptadecane was quantified using GC-MS. The time course experiment allowed the rate of the reaction to be determined from initial time points with turnover number approaching 0.4 min^{-1} at 37 °C (Figure 2.9a). The reaction rate also increased with the increase in octadecanal concentration with no sign of saturation at concentration upto 500 µM (Figure 2.9b). An apparent k_{cat}/K_M of ~1 $M^{-1}min^{-1}$ may be calculated

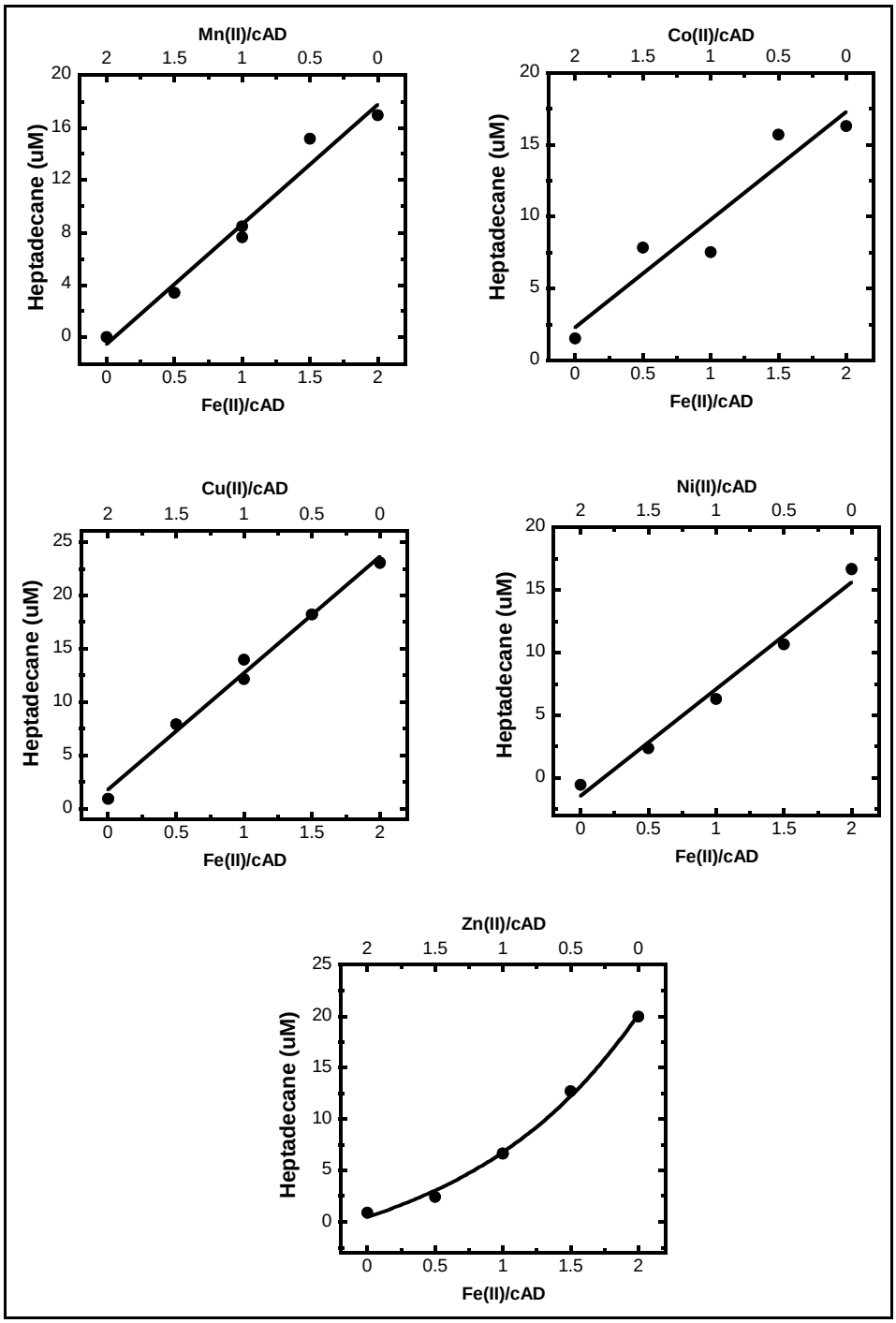

Figure 2.8. Dependence of heptadecane formation upon reconstitution of apo-cAD with Fe (II) and other most relevant biologically active metals at a total metal equivalency of 2 per cAD active site. Assay conditions: 20 μM apo cAD, 300 μM octadecanal, 100 μM PMS and 1 mM NADH were reacted at 37 °C for 1 hour as described above in assay procedures and heptadecane was quantified by GC. In all cases, highest activity was observed with 2

equivalents of Fe(II) and none of the other metals supported activity alone. Zinc was proven to be slightly inhibitory.

from these data but this might significantly underestimate the true value of k_{cat}/K_M. The low rate of catalysis undoubtedly derived in part from the very poor solubility of the substrate octadecanal. Addition of detergents such as triton did not improve activity. Assays had to be shaken vigorously to obtain consistent activity. Even at very low concentration, the substrate appears to be present as micelles in the solution and it is very likely that the reaction kinetics is dominated by the phase transfer of the substrate from the micelles to the solution.

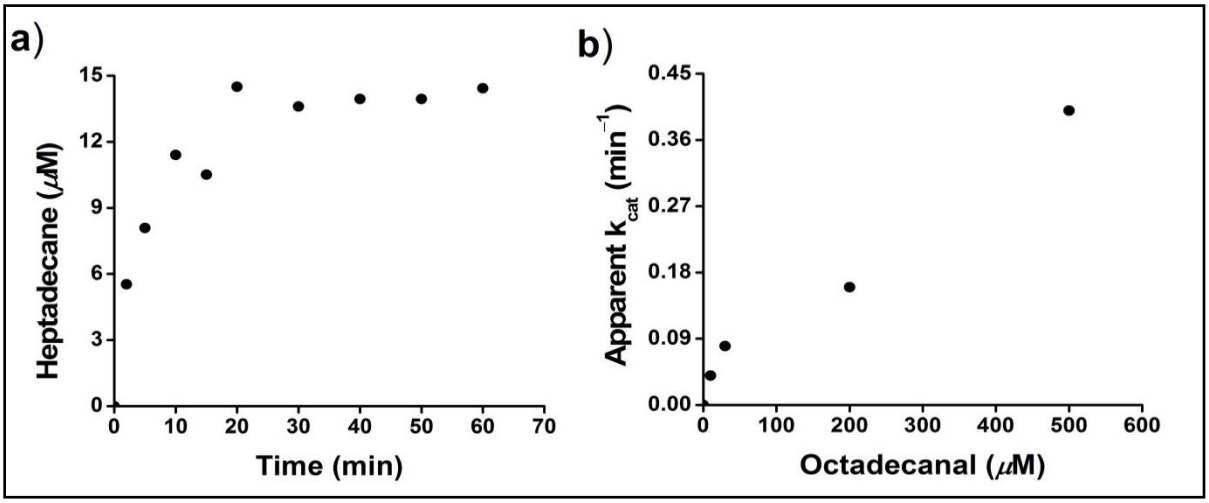

Figure 2.9. Kinetics of heptadecane formation by cAD. a) Time course of heptadecane formation (octadecanal conc. kept at 200 μM); b) rate of reaction as a function of octadecanal concentration.

Factors affecting the kinetics of alkane formation. Although multiple turnovers and improved activity of cAD was supported by PMS/NADH reducing system, the activity is still sluggish compared to other non-heme di-iron proteins.[15,16] The very low solubility of octadecanal might be a factor that likely contributes to the low activity of cAD. Although slightly inhibitory, the introduction of organic solvents such as 4 % DMSO/ethanol in the regular assay improved

solubility of the substrate, but significant light scattering was apparent at octadecanal concentrations higher than ~100 µM, indicating that the substrate forms micelles, and vigorous shaking was necessary to obtain consistent activity, suggesting that the reaction kinetics may be dominated by phase transfer of substrate molecules from micelles. The percentage of the organic solvent in the assay was not increased beyond 4% due to gradual loss of enzyme activity with increase in organic solvent concentration in the assay as shown in Figure 2.10.

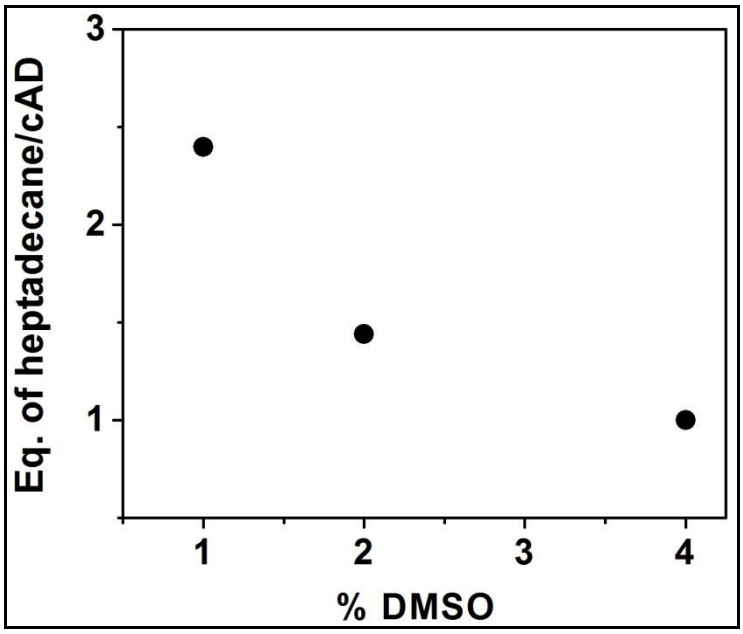

Figure 2.10. Effect of DMSO on heptadecane formation from octadecanal by cAD. Activity gradually decreases with increase in DMSO concentration in the assay. Assays were performed for 25 min.

In an attempt to improve substrate delivery to the enzyme, the effect of including bovine serum albumin (BSA) in the assay was examined. These assays were performed by Dr. Bekir Eser. BSA binds fatty acids and has been used to facilitate the assay of other enzymes that act on long chain aldehyde substrates.[26] Inclusion of 15 µM BSA (1 mg mL^{-1}) in an assay containing 150 µM octadecanal resulted in a ~ 5-fold increase in the steady state activity of cAD

and eliminated the need for shaking. Significantly, the reaction now exhibited an initial burst phase characteristic of product release being rate-determining (Figure 2.11). At 37 °C the apparent rate constant for heptadecane formation in the burst phase was 3.4 ± 0.5 min^{-1}. Although this is relatively slow, this was comparable with rates measured for other di-iron enzymes, such as fatty acyl-ACP desaturases, that catalyze chemically difficult reactions on similarly hydrophobic substrates.[27,28] Inclusion of BSA did not improve the activity of cAD with the ferredoxin-based reducing system.

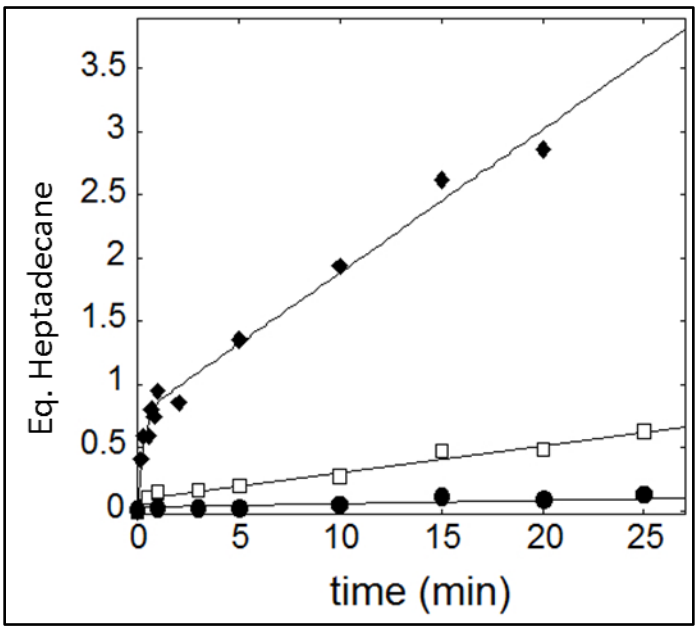

Figure 2.11. Changes to cAD activity dependent upon reducing system and BSA. (●) activity in the presence of 30 μg/ml ferredoxin, 0.04 units ferredoxin reductase and 1 mM NADPH, (□) activity in the presence of 150 μM PMS and 1 mM NADH, (♦) activity in the presence of 150 μM PMS, 1 mM NADH and 15 μM BSA w/o shaking; note activity now shows a burst phase indicative of product release being rate-limiting. All assays contained 10 μM *Pm* cAD, 500 μM octadecanal and were carried out under microanaerobic conditions at 37 ^{o}C.

An interesting observation was that excess BSA inhibited the reaction. Thus, when BSA was present in excess over the substrate (300 μM BSA, 150 μM octadecanal) the rate of

reaction was significantly lower and no burst phase was observed. This suggested a direct interaction between BSA and cAD rather than a general solubilizing effect of BSA. Apo-BSA presumably competed with aldehyde-loaded BSA for binding to cAD, thereby inhibiting the reaction. This observation also hinted at the possibility that, as yet unidentified, lipid binding proteins may be important for substrate delivery to cAD *in vivo*.

2.3.3 Co-Product of cAD-Catalyzed Reaction

Aldehyde decarbonylase (AD) enzymes are quite versatile in nature and vary from species to species. Although all AD enzymes produce alkanes; they differ in size, hydrophobicity, metal cofactor(s) and very interestingly the nature of co-product that they form after cleavage of C1-C2 bond of the aldehyde substrates. It has been shown that the plant and algal AD removes C1 carbon as carbon monoxide (CO) whereas the insect AD converts the C1 carbon to CO_2. It was interesting to investigate whether the co-product of cAD-catalyzed reaction is one of the above mentioned molecules or something else.

Attempts to detect CO. These assays were performed by Dr. Bekir Eser. To detect CO formation myoglobin was introduced in the enzyme assay.[29] Myoglobin has a high affinity for CO and exhibits characteristic changes in the heme spectrum. Myoglobin (5 μM final concentration) was reduced by sodium dithionite (10 μM final) and was incubated with the other components of the assay mixture; 5 μM cAD, 10 μM ferrous ammonium sulfate, 100 μM PMS and 800 μM NADH, before turnover was initiated by addition of 300 μM octadecanal. No change in the UV-Visible spectrum of myoglobin indicative of carbon monoxide binding was evident after one

hour of incubation (Figure 2.12). Analysis of the heptadecane produced in the reaction suggested that CO should have been readily detectable had it been formed in stoichiometric amounts. In a complementary experiment, high resolution mass spectroscopy was used to analyze the head space of samples in which ~ 250 μM heptadecane was produced by the action of cAD. Again no CO was detected, although it should have been easily observed if it had been formed in stoichiometric amounts with heptadecane.

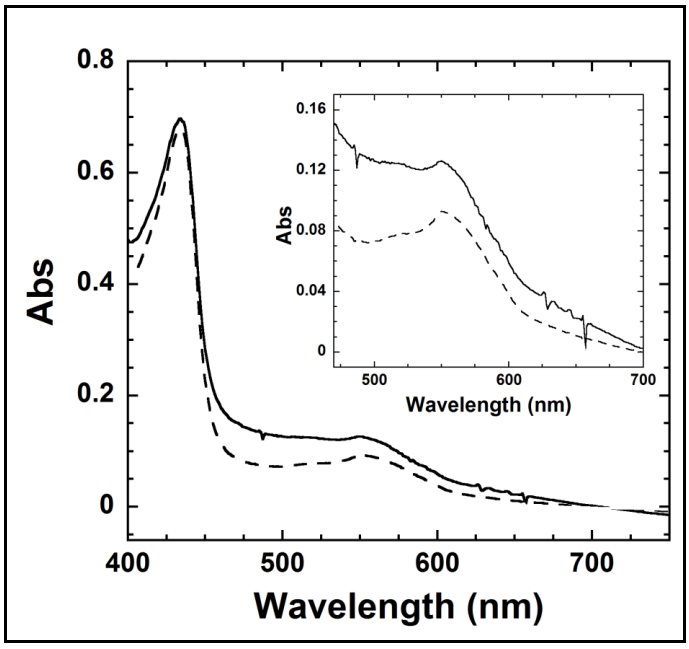

Figure 2.12. UV-Visible spectra of the no cAD (dashed line) and the enzymatic assay (solid line) with reduced myoglobin. The assays were incubated in micro-anaerobic environment at ~30 °C for one hour. *Inset* an expanded view of the 550 nm region of the main spectrum. Spectra show no difference between control and assay indicating absence of CO.

Attempts to detect formaldehyde. To check the possibility of formation of formaldehyde as the co-product, derivatizing agents; 2, 4-dinitrophenylhydrazine (2, 4-DNPH) and purpald/$NaIO_4$ were employed. 2,4-DNPH is well known to react with formaldehyde and the derivative is easily

detectable by LC-MS.[30] Purpald also readily reacts with formaldehyde and the derivative, upon oxidation with $NaIO_4$ exhibits strong absorption at 550 nm.[31] Both of these methods are sensitive enough to detect lower micro-molar concentration of formaldehyde but formaldehyde could not be detected from cAD-catalyzed assays using these methods. Thus formaldehyde was ruled out as the co-product. The remaining possibility was that formate is the co-product of the cAD-catalyzed reaction.

Detection of formate as the co-product. These assays were performed in collaboration with Dr. Bekir Eser. Detection of formate is quite tricky and there are not many well derived simple methods in the literature to detect lower micro-molar concentration of formate. Measurement becomes even more challenging by the sluggish activity of the enzyme and the contamination of assay buffer with the environmental formate. Direct detection of formate by mass spectroscopy of the assay mixture was proven to be difficult; however, formate could be reliably detected and quantified as its 2-nitrophenylhydrazide derivative by LC-MS. Therefore, the formation of formate by cAD was investigated by derivatizing the products of the enzyme reaction with 2-nitrophenylhydrazine (2-NPH) followed by reverse phase HPLC.[32] Higher buffer concentration and the presence of salt in the assay buffer appeared to be interfering with the formate derivatization. Therefore, assays were performed in 10 mM HEPES, pH 7.2 as described in the material and method section. The hydrazide derivative of formate (2-NPH formate, Scheme 2.4) was detected at 230 nm and eluted at ~16 min (Figure 2.13). The presence of formate in the derivatized assay samples was confirmed by comparison with the retention time of an authentic standard (Figure 2.13). Analysis of this peak by UV-visible spectroscopy and mass spectrometry in the ES- mode further confirmed the identity of the compound as the 2-

NPH derivative of formate. Observed *m/z* of formate-NPH in TOF-ES$^-$ = 180, which is in excellent agreement with the expected *m/z* = 180 (Figure 2.14).

Scheme 2.4. A. cAD-catalyzed conversion of aldehyde to alkane and formate; B. Derivatization of formate with 2-NPH to produce 2-NPH formate

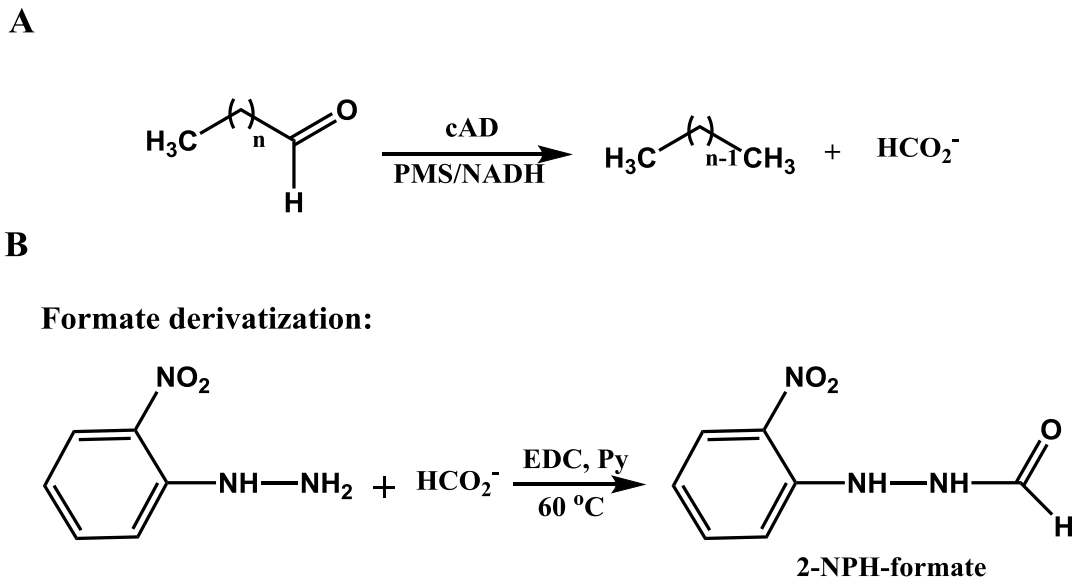

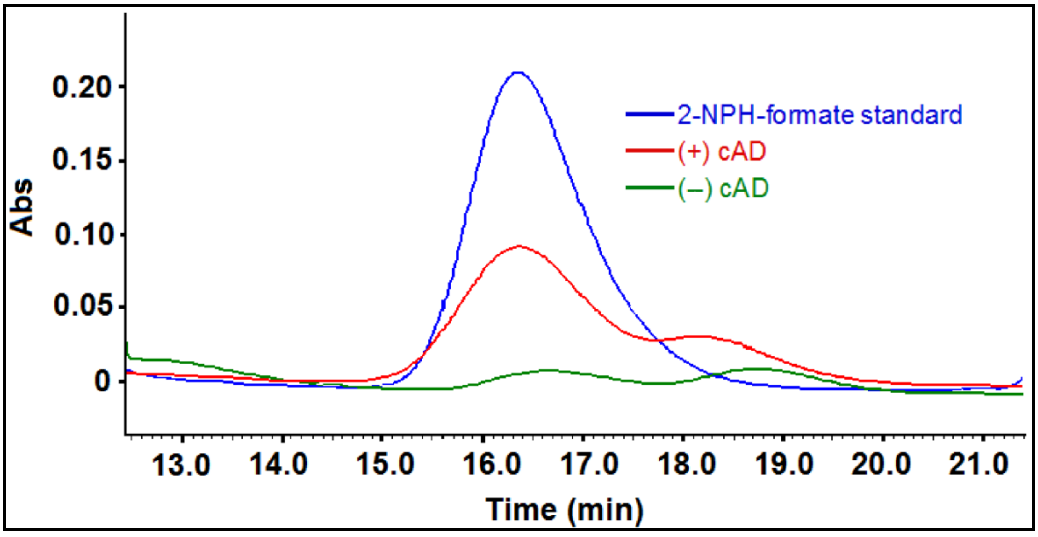

Figure 2.13. HPLC trace of 2-NPH-derivatized formate produced from octadecanal by reaction with cAD. (a minor peak with retention time ~ 18.5 min is present in both cAD and control reactions indicating it does not arise by the action of the enzyme).

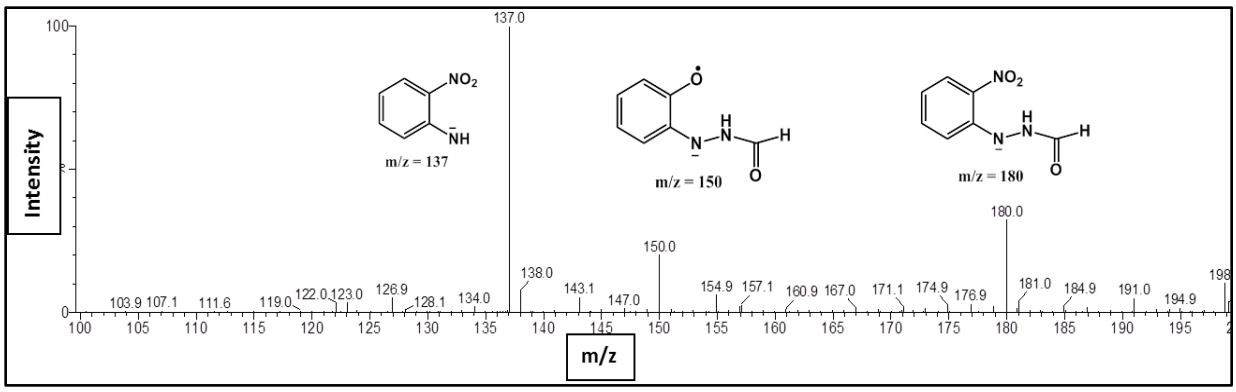

Figure 2.14. Mass spectrum of 2-NPH-formate derivative from the cAD-catalyzed reaction. The structures corresponding to the mass peaks are also depicted in Figure.

The amount of formate formed in the enzyme assay was quantified by HPLC using a calibration plot of standard 2-NPH-formate and the amount of heptadecane formed was quantified from a duplicate assay by GC. Formate and heptadecane were produced in nearly equal molar amounts (~100 μM of each of the products were detected in a ~30 min assay with 50 μM cAD and 500 μM octadecanal, in similar assay conditions as described above) as required by a mechanism in which both are derived from hydrolysis of octadecanal.

2.3.4 Nature of the Aldehyde Hydrogen and the New Hydrogen in Product Alkane.

Having established the activity and kinetics of octadecanal with cAD the nature of the proton in the newly formed methyl group of heptadecane as well as fate of the aldehyde hydrogen after C1-C2 bond cleavage was investigated. The aldehyde hydrogen was shown to be retained in the product alkane in the reaction catalyzed by membrane bound aldehyde decarbonylase from plant.[6] In contrast, the hydrogen was lost to water when the enzyme was

studied from animal tissues.[33] Given that the co-product of plant AD-catalyzed reaction and the animal tissue-catalyzed reaction was CO which is in contrast to the formate formed by cyanobacterial AD, the fate of aldehyde hydrogen in cAD-catalyzed reaction was investigated. When n-octadecyl-1-d aldehyde was used as a substrate for cAD and the reaction mixture was analyzed for formate, deuterium from the aldehyde was found to be retained in formate as evident from the 181 Da peak of formate-NPH derivative (Figure 2.15).

To determine the nature of the proton in the newly formed methyl group of the product heptadecane, the deuterated aldehyde was again employed as a substrate the mass spectrum of heptadecane product was analyzed and compared to that of heptadecane formed from regular 1-octadecanal. The molecular ion peaks heptadecane formed from these two assays were identical with mass 240 Da (Figure 2.16).

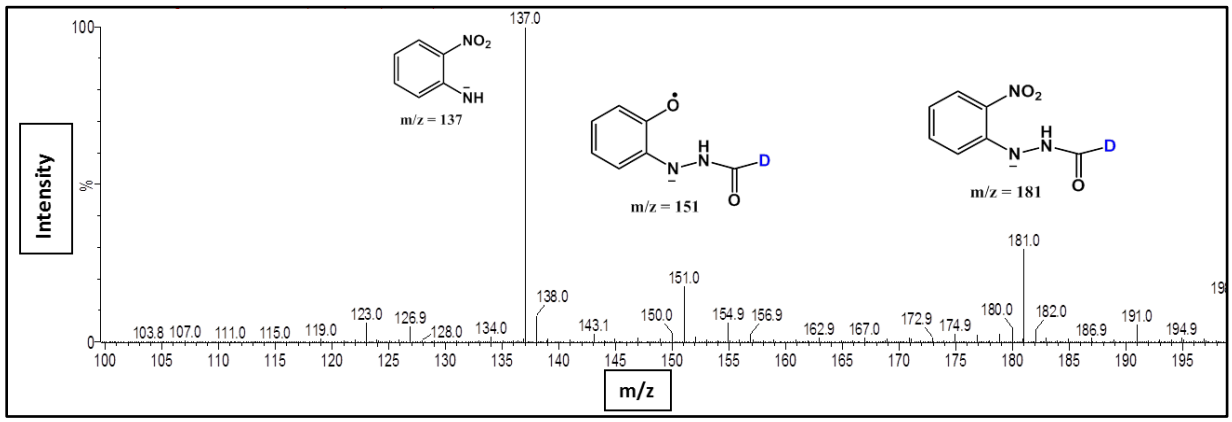

Figure 2.15. Mass spectrum of 2-NPH-formate derivative from the cAD-catalyzed reaction in D_2O buffer. The structures corresponding to the mass peaks are also depicted in Figure.

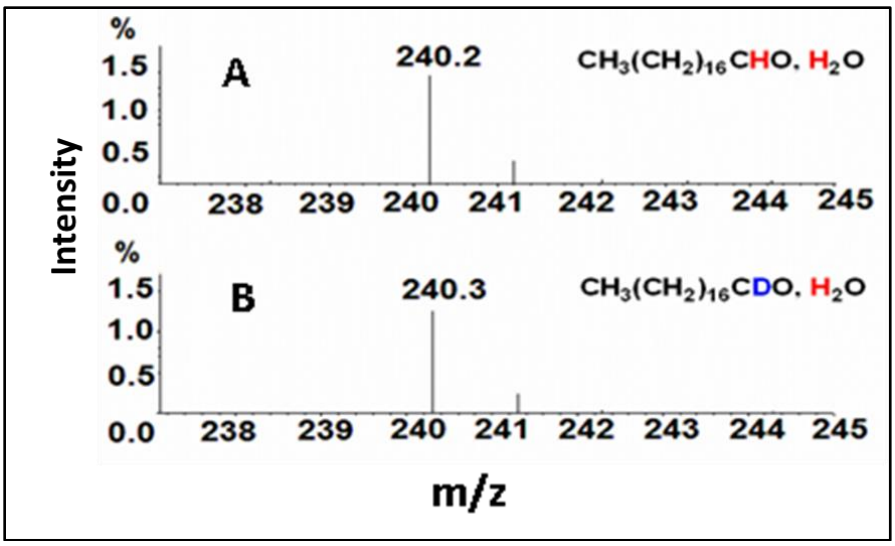

Figure 2.16. Comparison of molecular ion peak of heptadecane from 1-octadecanal (A) and from n-octadecanyl-1-d-aldehyde (B) in H_2O buffer. The molecular ion peaks for heptadecane (240 Da) were identical from both the experiments which indicate aldehyde hydrogen is not retained into the product.

These results indicated that the aldehyde hydrogen was not retained in the product alkane and possibly a solvent derived hydrogen was incorporated in the newly formed methyl group of heptadecane. To validate this hypothesis, unlabeled 1-octadecanal was treated with cAD in regular buffer as well as in buffer made in D_2O (99.9%) and the molecular ion peak of heptadecane was compared. Interestingly, when the assay was performed in D_2O buffer, heptadecane molecular ion peak increased to 241 Da (Figure 2.17), signifying incorporation of a deuterium from D_2O into the product. The labeling pattern was identical when deuterated substrate was treated with cAD in D_2O buffer. Some additional deuterium derives from the exchange of α-protons of the aldehyde with the solvent during the assay period but the control experiments established that this accounts for the less than half of the deuterium incorporation.

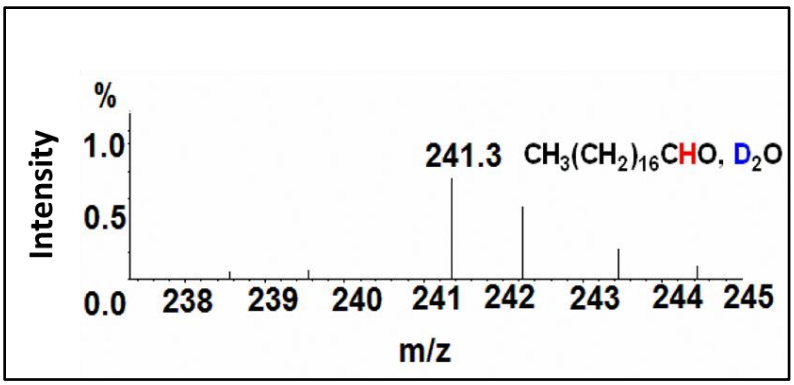

Figure 2.17. Molecular ion peak of heptadecane from 1-octadecanal in D_2O buffer. Incorporation of deuterium is shown by the increase of molecular ion peak to 241.

2.3.5 Shorter Chain Aldehydes as Substrate of cAD: Kinetics with Heptanal

To avoid the complications posed by the low solubility of long-chain aldehydes, the ability of shorter, more soluble, aliphatic aldehydes to act as substrate for cAD was examined. An initial screen of aldehydes of varying lengths identified dodecanal, decanal, nonanal, octanal and heptanal as substrates of cAD (Figure 2.18). While assaying octanal and heptanal, headspace samples were studied by GC-MS due to volatility of the product alkanes. Heptanal was quite soluble and relatively efficient substrate and could be assayed easily by GC. Therefore, heptanal kinetics was explored in more details.

Kinetics of cAD with heptanal. k_{cat} and K_M are useful steady state kinetic parameters that facilitate the comparison of enzyme reactions. They have not been previously determined for cAD, but measurement of these parameters was initiated using heptanal as the substrate. Assays were conducted at 37 °C under microaerobic conditions with 75 µM PMS and 1 mM

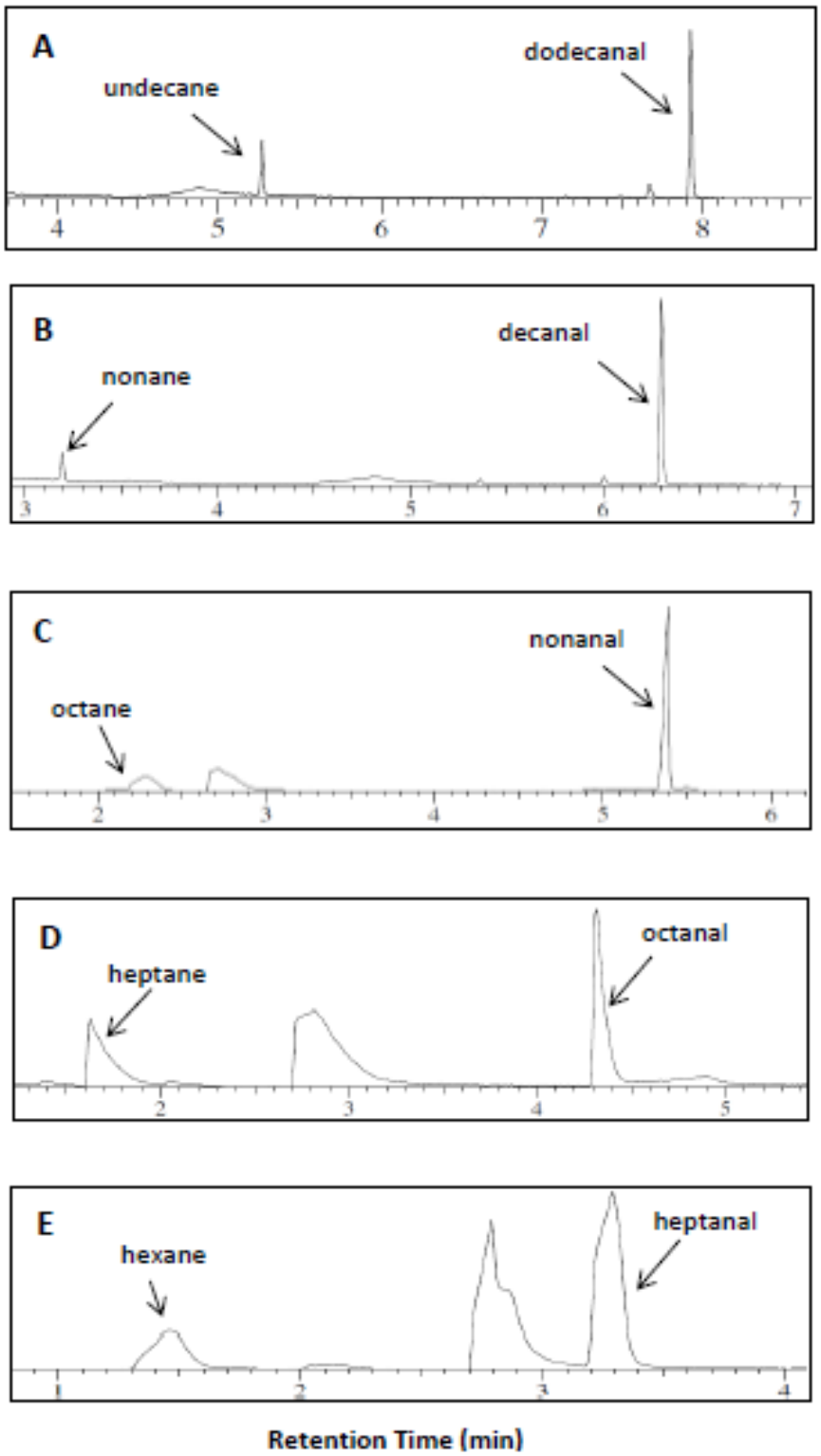

Figure 2.18. cAD-catalyzed conversion of dodecanal (A), decanal (B), nonanal (C), octanal (D) and heptanal (E) to the corresponding alkanes. The broad peak eluted just before 3 min in (C), (D) and (E) corresponds to DMSO.

NADH present – at these concentrations the components of the reducing system do not limit the activity of the enzyme, as discussed below. As shown in Figure 2.19, hexane formation increased linearly with time and the dependence of cAD activity on heptanal concentration could be well described by the Michaelis-Menten equation with K_M = 260 ± 40 µM and k_{cat} = 0.17 ± 0.01 min^{-1} (Figure 2.20). No burst phase was observed with this substrate (either with or without BSA), indicating that product release does not limit the rate of turnover. There might be an apparent lag phase at shorter time points, the reason of which is unknown.

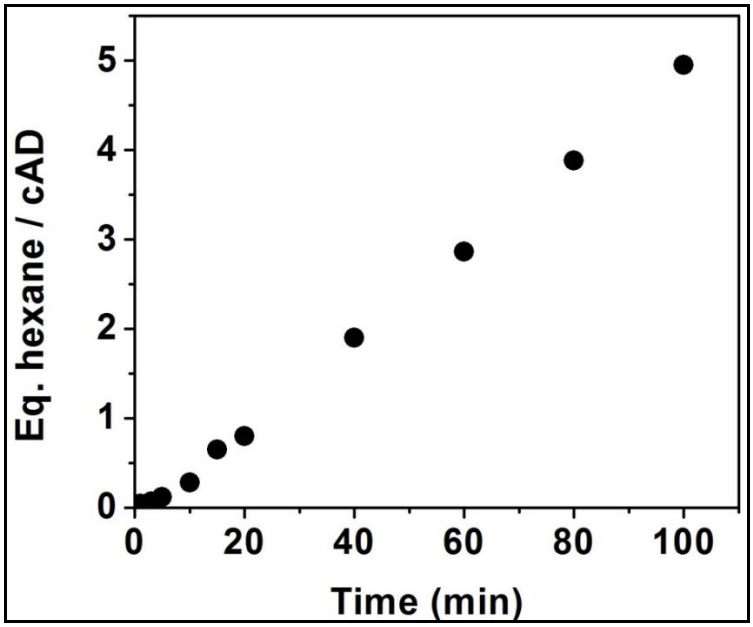

Figure 2.19. Time course of hexane formation from heptanal catalyzed by cAD.

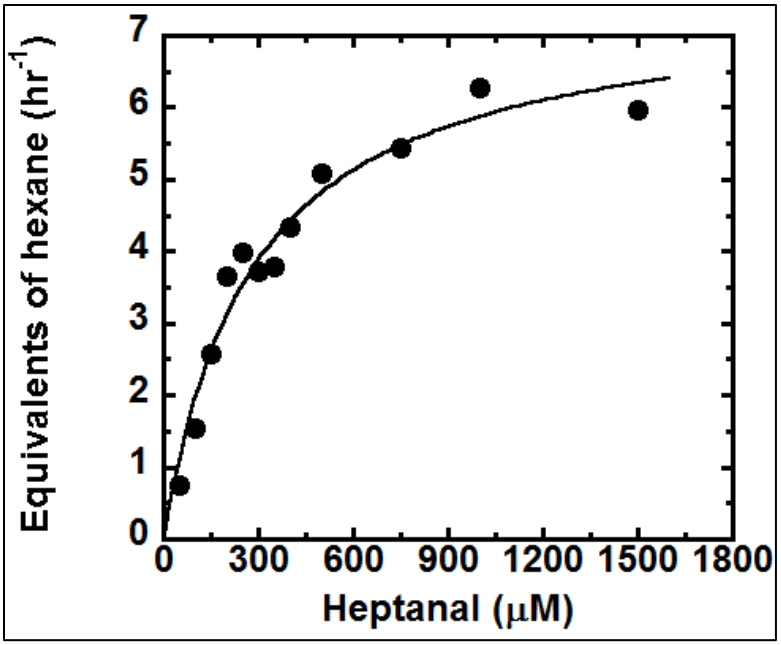

Figure 2.20. Kinetics of cAD with heptanal. Data were fit to the Michaelis–Menten equation with k_{cat} = 0.17 ± 0.01 min^{-1} and K_M =260 ± 40 μM.

2.3.6 α,β -Unsaturated Aldehydes as Reversible Competitive Inhibitors of cAD

After exploring the activity and kinetics of cAD with a relatively soluble aldehyde heptanal, it was of interest to learn whether α,β- and α,β,γ,δ-unsaturated aliphatic aldehydes would serve as substrates for cAD to produce the corresponding alkenes. On introducing a double bond in conjugation to the aldehyde carbonyl group, the C1-C2 bond of the aldehyde acquires some double bond character, which makes the bond more stable. Several commercially available unsaturated aldehydes (Figure 2.21) were tested against cAD. Assays were performed as described previously. When using C10 and C12 unsaturated aldehydes, the assay mixture was extracted with ethyl acetate and analyzed by GC-MS, whereas, for C7

unsaturated substrate, the reaction headspace was directly tested for product formation. None of these aldehydes were able to produce any alkane.

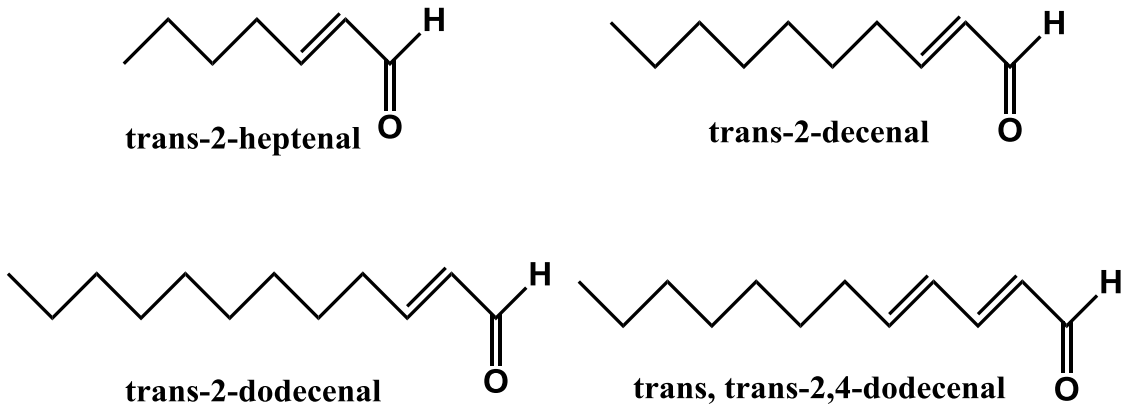

Figure 2.21. Unsaturated aldehydes tested as substrate for cAD. None of these aldehydes served as substrate for cAD.

Given that the structures of the unsaturated aldehydes are very similar to the true aldehyde substrates, it was important to examine whether they behave as inhibitors of the enzyme. Taking the advantage of already explored kinetics of heptanal with cAD, the ability trans-2-heptenal to act as an inhibitor of cAD was tested. When this unsaturated aldehyde was added to an assay of cAD with heptanal, depletion in activity of the enzyme was noticed. In particular, assays containing 10 µM cAD, 20 µM Fe(II), 50 µM PMS, 1 mM NADH, 500 µM heptanal and heptenal concentrations were varied from 0 to 1 mM. Hexane production from heptanal was quantified from headspace samples by GC. As shown in Figure 2.22, with increase in concentration of trans-2-heptenal from 0 to 1 mM, hexane production decreased from ~ 3 turnovers to ~0.4 turnovers/h.

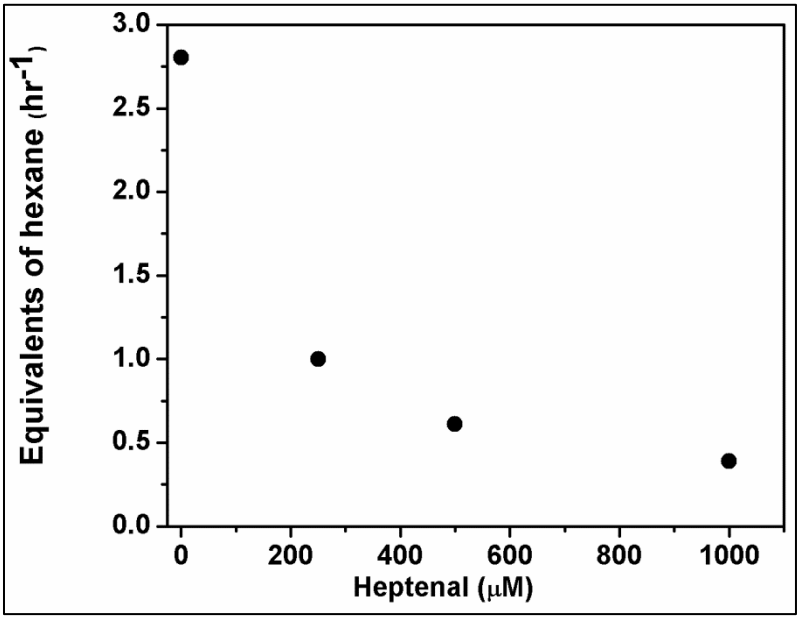

Figure 2.22. Trans-2-heptenal serves as an inhibitor of cAD. With increase in the concentration of heptenal, hexane formation gradually decreased.

To investigate the nature of inhibition, 10 μM cAD was incubated with varying concentration (100-200 μM) of trans-2-heptenal, and for each particular concentration of heptenal in the assay, heptanal concentration was varied from 50 μM to 2.5 mM and the reaction rates were measured. As shown in Figure 2.23, the dependence of cAD activity on heptanal concentration in the presence of heptenal could be well described by the Michaelis-Menten equation. The K_M for heptanal increased with increasing heptenal concentrations in the assay. Using 100 μM trans-2 heptenal as an inhibitor, K_M value for heptanal was 600 ± 91 μM and using 200 μM trans-2 heptenal as an inhibitor, the K_M value for heptanal was 1100 ± 360 μM (K_M for heptanal in the absence of heptenal is 260 ± 40 μM). The V_{max} for the reaction remained constant at 6.6 μM/h.

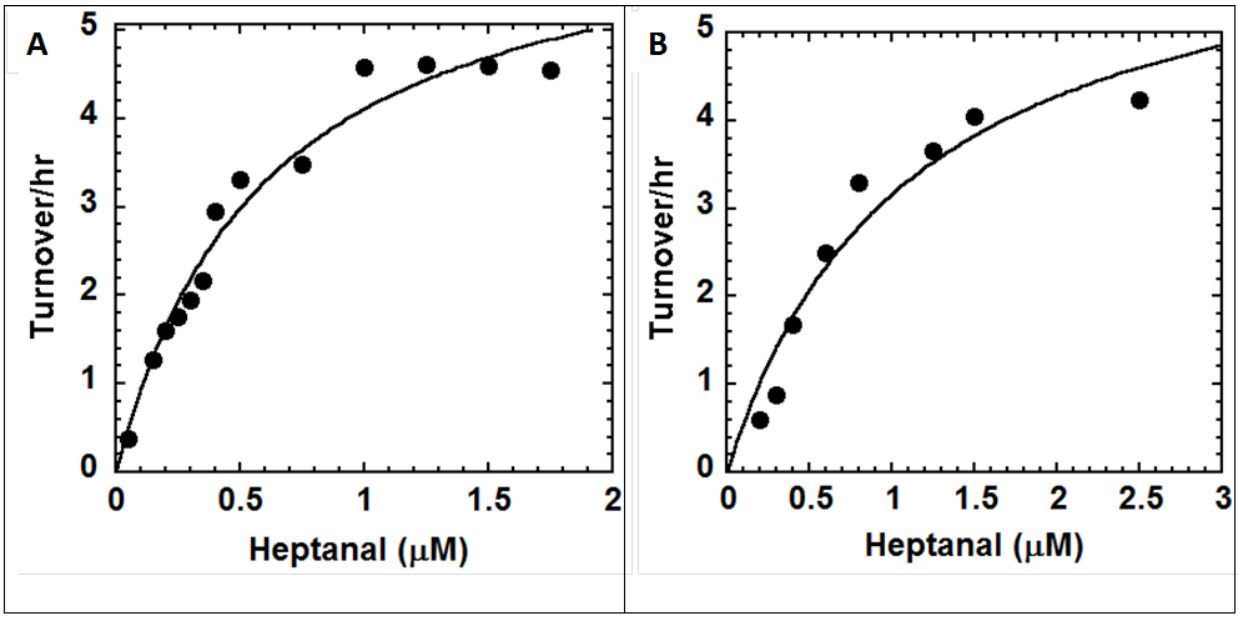

Figure 2.23. Kinetics of cAD with heptanal in presence of 100 μM (A) and 200 μM (B) trans-2-heptenal.

The data from all these sets of experiment could be well fitted on Lineweaver-Burk plot using the equation 1 as shown below where, V = the velocity of the reaction, V_{max} = the maximum velocity, K_M = Michaelis constant and [S] = substrate concentration.

$$1/V = 1/V_{max} + (K_M/V_{max} * 1/[S]) \qquad \text{Eq. 1}$$

From the fitting, it appears that the plots (w/o inhibitor, 100 μM inhibitor, 200 μM inhibitor) intersect almost at the same point on 1/V axis indicating the competitive nature of the inhibitor heptenal (Figure 2.24). The data were fitted globally to obtain a good estimate of inhibition constant (K_i) for trans-2-heptenal. The following equations were employed:

$$V = \frac{V_{max} * [S]}{[S] + K_M^{app}} \qquad \text{Eq. 2}$$

$$\text{Where, } K_M^{app} = (1 + [I]/K_i)K_M \qquad \text{Eq. 3}$$

The global fitting of these data gives a K_i = 40.3 ± 7.1 µM for trans-2-heptenal. Along with this, the measured values of K_M for heptanal = 260 ± 60 µM and V_{max} = 7.3 ± 0.6 µM/h were in good agreement with values measured before using heptanal as a substrate. I note that these K_i amd K_M values were derived from global fitting and not from the Lineweaver-Burk plot.

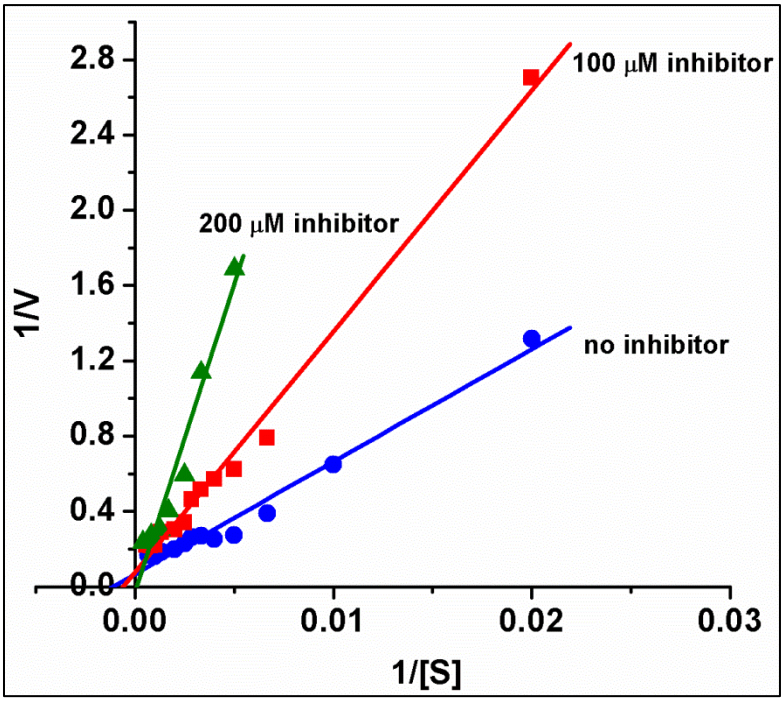

Figure 2.24. Lineweaver-Burk plots of cAD reaction with heptanal using various concentration of trans-2-heptenal as an inhibitor. It seems the plots intersect almost at a single point on 1/V axis indicating reversible competitive nature of the inhibitor.

2.3.7 Role of the Reducing System in cAD-Catalyzed Reaction

Most of the di-iron enzymes require an auxiliary reducing system to support multiple turnovers. The established role of the auxiliary ferredoxin/ferredoxin reductase/NADPH reducing system in di-iron oxygenases is to reduce the inactive di-ferric enzyme to the active di-ferrous form at the start of each turnover.[34,35] Usually, the di-ferrous form of an enzyme is capable of executing one turnover without the help of any auxiliary reducing system. Interestingly, unlike other di-iron enzymes, when the apo-cAD was reconstituted with Fe(II), no activity was obtained in the presence of O_2 in the absence of external reducing system. This observation was very intriguing as it departs from the conventional mechanistic route of two electron transfer from reduced metal centers to di-oxygen followed by chemistry by activated intermediates. Inactivity of the di-ferrous state of the enzyme confirms the requirement of auxiliary reducing system to yield any product.

The chemical reducing system made of PMS/NADH supported improved activity and multiple turnovers compared to the biological reducing system made of Fd/FdR/NADPH. So, the investigation on this chemical auxiliary system was initiated to gain more knowledge about this very intriguing catalytic process. Phenazine methosulfate (PMS), which is often used as an electron mediator, was found to be absolutely required for cAD activity. If PMS was omitted from the enzyme assay components no alkane formation was observed, either under microaerobic or aerobic conditions with either the reduced di-ferrous form of the enzyme or with the oxidized di-ferric form. Other common electron mediators such as methyl viologen did not support activity. Consistent with its proposed role as a transient electron donor during the

reaction, PMS functions catalytically. In the presence of stoichiometric amounts of PMS (10 µM PMS, 10 µM cAD) and excess NADH (1 mM) multiple turnovers were observed.

Although PMS functioned catalytically and resulted in multiple turnovers, to obtain the highest activity, concentration of PMS was optimized. Using heptanal as a substrate, assays were performed as described above for 1 h with varying PMS concentration from 5 µM to 100 µM. As shown in Figure 2.25, with increasing PMS concentrations up to 75 µM, activity increased gradually followed by slight decrease at 100 µM. Thereafter, 75 µM PMS was used in the assays unless otherwise stated.

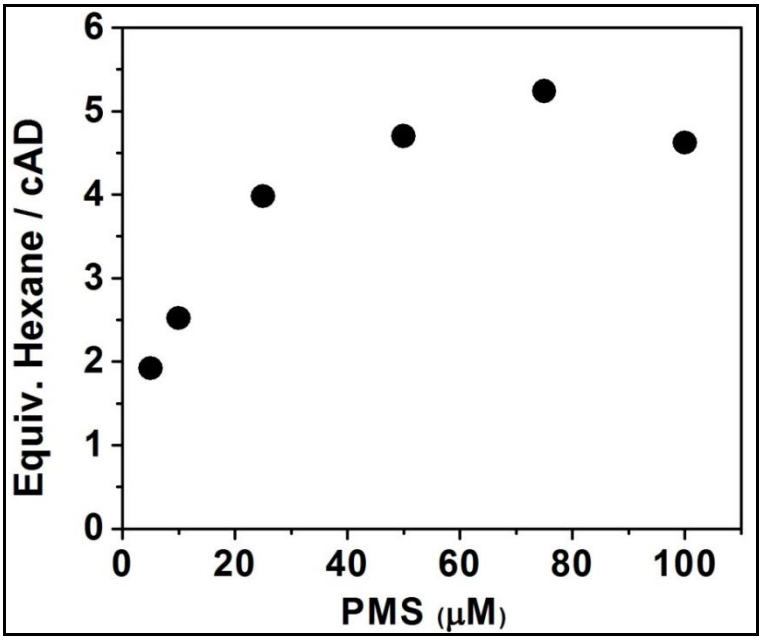

Figure 2.25. Rate of hexane formation from heptanal by cAD as a function of PMS concentrations.

PMS binding to cAD. Consistent with its role as an electron mediator, reduced PMS was found to bind stoichiometrically to the enzyme. Experiments were performed by Dr. Bekir Eser. Either

oxidized PMS or NADH-reduced PMS (300 μM) were incubated with either di-ferrous reconstituted-cAD or apo-cAD (100 μM) under anaerobic conditions overnight at 4 °C in dark. After the incubation period, the enzyme sample was applied to a spin desalting column to remove unbound PMS and NAD^+. To quantify the amount of PMS bound a sample of desalted enzyme was opened to the air to fully oxidize any PMS bound and the concentration of PMS was determined spectrophotometrically using the reported extinction coefficient of 26.4 $mM^{-1}cm^{-1}$ at 388 nm for oxidized PMS.[23] This resulted in ~1 equivalent of PMS/cAD being bound to the protein. Although quite tight, reduced PMS binding is reversible, as it could be removed from the enzyme by prolonged dialysis. The activity of the enzyme:PMS complex depended only upon the addition of substrate and NADH to the assay. The binding of reduced PMS was independent of the metal cluster, as apo-cAD was also able to bind stoichiometric amounts of reduced PMS. Oxidized PMS, which is positively charged, did not bind tightly to the enzyme.

The dependence of the rate of alkane formation on NADH concentration was examined in assays that contained 10 μM cAD, 20 μM ferrous ammonium sulfate, 10 μM PMS and 300 μM octadecanal. Under these conditions the rate of reaction exhibited saturation kinetics as shown in Figure 2.26A, with an apparent $K_{1/2}$ of ~100 μM for NADH. While using shorter chain substrate heptanal as substrate, a very similar trend is observed with an apparent $K_{1/2}$ of ~110 μM for NADH (Figure 2.26B). In this case the assay mixture contained 5 μM cAD, 10 μM ferrous ammonium sulfate, 50 μM PMS and 1 mM heptanal (heptanal is soluble at this concentration).

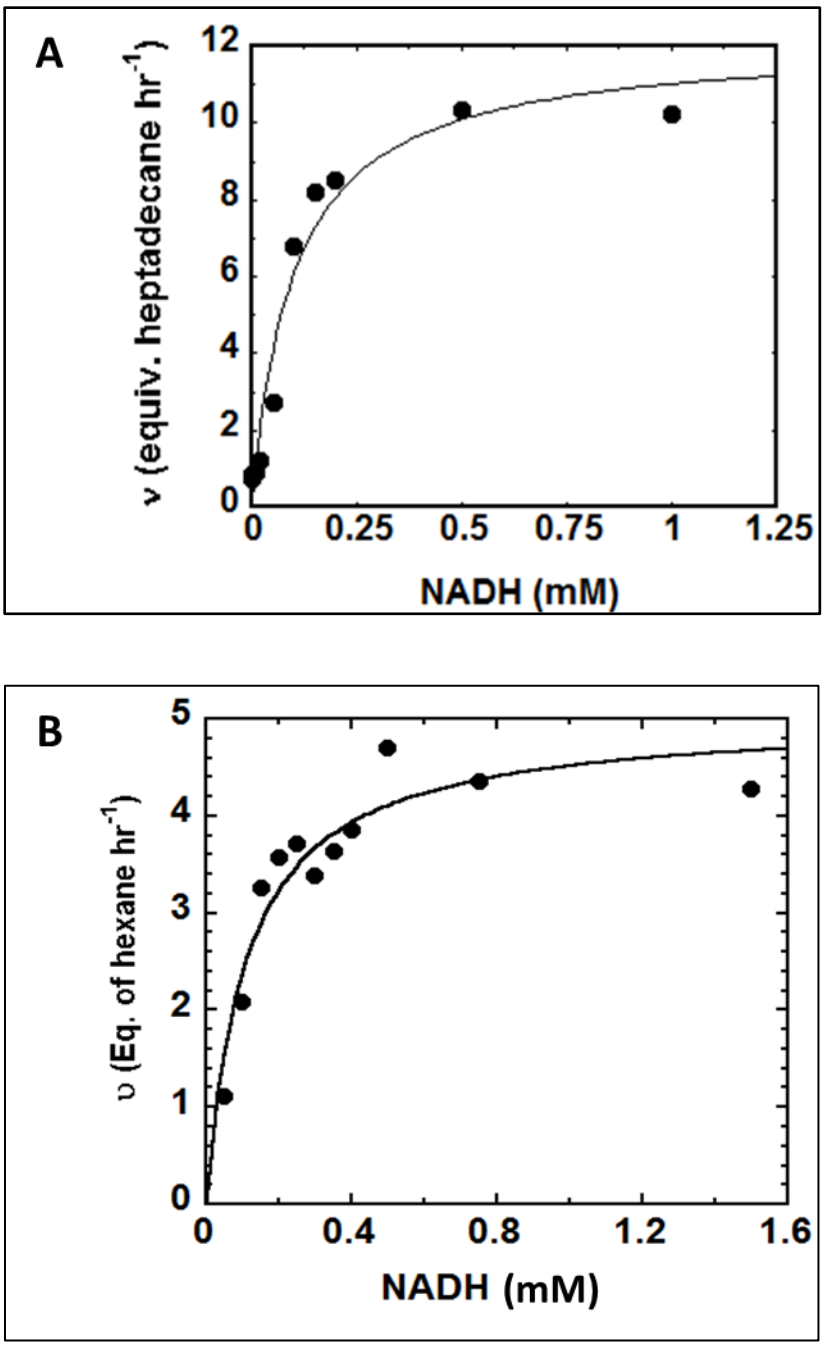

Figure 2.26. The dependence of the rate of heptadecane formation from octadecanal (A) and the rate of hexane formation from heptanal (B) on NADH.

The interpretation of this result is complicated by the fact that NADH directly reduces PMS in free solution, and probably also enzyme-bound PMS. Thus $K_{1/2}$ is also dependent on PMS concentration and reflects multiple kinetic steps, not all of which occur on the enzyme.

Surprisingly, it could be seen that in the presence of oxidized PMS, the di-ferrous form of cAD undergoes slow turn-over, even in the absence of a reducing agent. The rate of heptadecane formation from octadecanal is ~20-fold slower than in the presence of excess NADH. This NADH-independent activity may be due to reduction of PMS by the enzyme itself. One molecule of di-ferrous cAD may reduce a molecule of PMS, which can then diffuse to another molecule of di-ferrous cAD to catalyze the reaction at that enzyme active site. In support of this explanation it was found that high concentrations di-ferrous cAD rapidly reduces oxidided PMS with $t_{1/2}$ ~2 s, as determined by stopped flow measurements (Dr. Bekir E. Eser, unpublished data). It appears that PMS binds tightly to the protein. In the absence of additional reductants, oxidized PMS supports a low level of turn over with the di-ferrous form of cAD. Thus interactions between PMS and cAD appear to be crucial for the reaction to occur, implying that electron shuttling between PMS and the active site metal center must occur during turnover.

Effectiveness of other reductants. The effectiveness of other reducing agents to support cAD activity has also been tested. Reductants such as dithionite and ascorbate were found to be active in the assay, although none gave as high activity as NADH (Figure 2.27). For comparison, the kinetics of the reaction with ascorbate as reductant as a function of ascorbate

concentration have been examined. Enzyme activity exhibited saturation behavior similar to that observed with to NADH (data not shown).

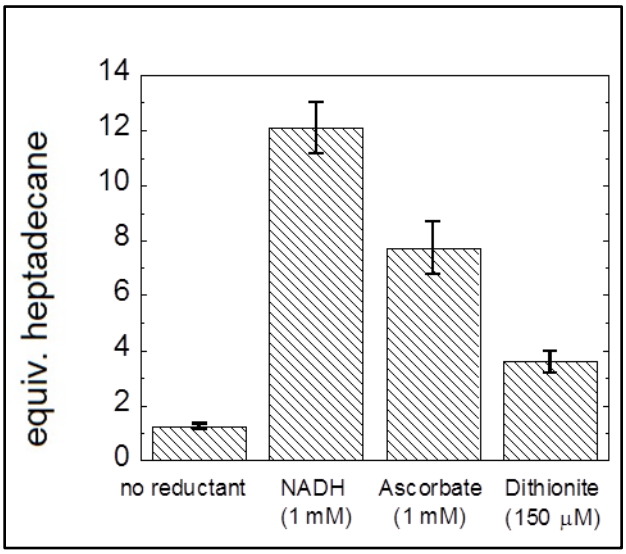

Figure 2.27. Activity of cAD with different reducing agents. The concentrations of reducing agents used in the comparison were those that gave maximum activity. Higher concentrations of dithionite proved inhibitory.

2.3.8 Aldehyde Decarbonylases from Different Classes of Cyanobacteria

During the discovery of cyanobacterial AD, different orthologs of this enzyme from different classes of cyanobacteria were shown to exhibit *in vivo* activity when co-expressed with the acyl-ACP reductase. But to demonstrate *in vitro* activity, only *N. punctiformes,* PCC73102 cAD was expressed. The *in vivo* activity of different cAD from different cyanobacteria varied up to ~ an order of magnitude with *Np* PCC73102 cAD being the most active, producing ~ 80 mg/L hydrocarbons and *Pm* MIT9313 and *Ss* RS9917-2 cAD being the least active, producing ~ 8 mg/L of hydrocarbon titer. To have an estimate of the relative activity of various cyanobacterial AD enzymes, 4 orthologs sequences of cAD were selected from the broad phylum of evolutionarily

diverse classes of cyanobacteria[36] : *Prochlorococcus, Synechococcus, Nostocales* and *Synechocystis*.

The enzymes selected were *P. marinus* MIT9313, *N. punctiformes,* PCC73102, *Synechococcus sp.* RS9917 and *Synechocystis sp.* PCC6803. An alignment of all four sequences, reveals these enzymes share 52% identity and 65% similarity with each other, with the *P. marinus* and *Synechocystis* enzyme being most closely related (68% identity and 82% similarity) and the *Synechococcus* being least similar (40% identity and 57% similarity to *P. marinus).* The enzymes were over expressed in *E.coli* from synthetic genes and purified by standard methods, as decribed in the experimental section. I note that the stability of *Synechococcus sp.* RS9917 cAD was not as good as the other three orthologs as this enzyme suffered from precipitation after purification by FPLC. Activities of these proteins under microaerobic conditions were compared with both octadecanal and heptanal as substrates. All the enzymes exhibited broadly similar activities, with the *P. marinus* and *N. Punctiformes* enzymes being somewhat more active (Figure 2.28). Interestingly, *in vitro* activity of *P. marinus* MIT9313 cAD and *N. Punctiformes* PCC73102 was very similar which is in contrast with their reported *in vivo* activity. *Synechocystis sp.* PCC6803 cAD shows similar activity with both long and short chain aldehyde whereas, *Synechococcus sp.* RS9917 seems to be somewhat more active with shorter chain aldehyde than longer chain aldehyde.

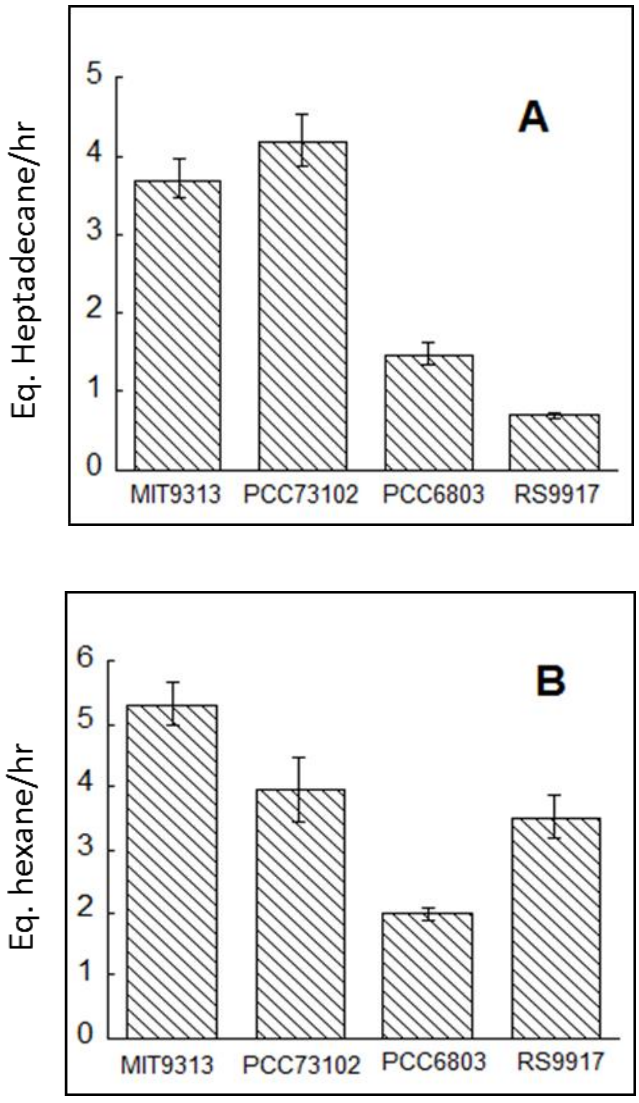

Figure 2.28. Comparison of activities of cAD enzymes from four different cyanobacterial classes: *P. marinus* MIT9313, *N. punctiformes* PCC73102, *Synechococcus sp.* RS9917, and *Synechocystis sp.*PCC6803. Both sets of experiments were performed with 10 µM holocAD 75 µM PMS, 1 mM NADH, and either 500 μM octadecanal (A) or 2 mM heptanal (B), for 1 h with shaking at 37 °C.

2.3.9 Oxygen Dependence of cAD-Catalytic Activity

In our original publications, cAD was characterized as being independent of oxygen (*Angewandte Chemie International Edition,* **2011**, 50 (31), 7148-7152 and in *Biochemistry* **2011**, 50 (49), 10743-10750). Evidence to support this view derives from the fact that the reaction

does not formally involve the oxidation of the substrate and that we observed a higher number of turnovers under anaerobic conditions (actually *micro-aerobic* condition) than in aerobic buffers. Further support came from $H_2{}^{18}O$ labeling experiments that indicated that the oxygen in formate was derived from water, rather than molecular oxygen, and the fact that the formation of alkanes did not appear to consume NADH, which would be necessary for an oxidative reaction. However, subsequent to publication, we performed further experiments that led us to conclude that we cannot exclude the possibility that the activity we observed was due to trace amounts of oxygen in the reaction buffer. The difficulties in establishing the dependence of the reaction on molecular oxygen stem, in part, from the very low activity of the enzyme under either aerobic or anaerobic conditions. Also, a Coy anaerobic chamber (Coy Laboratory Product Inc. Grass Lake, MI) was used for all the studies and it turns out that the chamber was not entirely inert and the error limit of oxygen detection is ~20 ppm. Further, even in the presence of routinely used oxygen scrubbing systems to scavenge oxygen from biochemical reactions, such as sodium dithionite, glucose oxidase/glucose, and protocatechuate dioxygenase/protocatechuate, high levels of activity was obtained using the assay conditions we describe. Although these observations were in accordance with our initial assertion that oxygen was not involved in the cAD-catalyzed reaction, when the assays were performed in an anaerobic chamber capable of maintaining oxygen concentrations at very low concentrations, i.e., <0.5 ppm (which was not available to us in our original investigations), almost no activity was obtained. Although the ^{18}O labeling experiment should have identified the involvement of molecular oxygen, analysis of the data was complicated by a background rate of nonenzymatic exchange of ^{18}O into the aldehyde substrate from $H_2{}^{18}O$. Appropriate

controls were performed to account for this background reaction, but if the enzyme itself significantly increased the rate of exchange of ^{18}O into the aldehyde prior to reaction, the conclusions drawn from the experiment may not be valid. Given this discrepancy, the involvement of molecular oxygen in the cAD-catalyzed reaction is very likely and subsequent reports from other laboratories provided evidence for the involvement of molecular oxygen in cAD-catalyzed reaction.[37]

2.4 Conclusions

In summary, cyanobacterial aldehyde decaebonylase (cAD) differs in several respects from the aldehyde decarbonylases (ADs) from higher organisms. Unlike plant, algal or insect AD enzymes, which were shown to be membrane associated proteins, cyanobacterial aldehyde decarbonylase was found to be a small soluble protein and was easily expressed and purified from *E. coli.* cAD was found to be a metallo-protein with the as-isolated protein having ~ 30% metal content with mostly iron. The enzyme could be de-metallated using various chelating agents and reconstituted with iron to almost the full occupancy. The iron (II) reconstituted enzyme was found to be inactive by itself and required an auxiliary reducing system for activity. A physiological reducing system comprised of ferredoxin/ferredoxin reductase/NADPH supported activity, although the rate of the reaction was extremely slow and not more than ~1 turnover was obtained. A chemical reducing system comprising of phenazine methosulphate (PMS)/NADH was found to support multiple turnovers at a much improved rate. PMS was found to bind the enzyme in equimolar ratio and played a catalytic role in the reaction.

Omission of PMS completely abolished the activity. NADH was required to reduce the oxidized PMS but could be substituted by other reducing agents such as ascorbate. cAD catalyzes the conversion of a long chain aldehyde octadecanal, to the corresponding alkane heptadecane. However, unlike other AD enzymes from higher organisms, which produce either CO or CO_2 as the co-product and aldehyde hydrogen usually retained in the product alkane, cAD produced formate and the aldehyde hydrogen was found to be retained in the formate. The enzyme was quite versatile and accepted aliphatic aldehydes with varying chain length (C18-C7) as substrates. Several kinetic parameters of this enzyme with both octadecanal and the more soluble substrate heptanal were also established. Octadecanal kinetics showed a burst phase of ~1 equivalent of product formation/cAD followed by a slow steady state rate indicating product release to be rate limiting. Heptanal kinetics did not show any burst phase under the same condition indicating chemistry to be rate limiting. α,β-unsaturated aldehydes did not work as substrates for cAD and played a role of competitive reversible inhibitor. Aldehyde decarbonylase enzymes from different cyanobacterial species were also expressed and their activities were evaluated. The results indicated *Prochlorococcus marinus* and *Nostoc punctoforme* cAD to be somewhat more active than other orthologs under our assay conditions.

2.5 References

1. Keasling, J. D. (2010) Manufacturing Molecules Through Metabolic Engineering, *Science 330*, 1355-1358.
2. Steen, E. J., Kang, Y. S., Bokinsky, G., Hu, Z. H., Schirmer, A., McClure, A., del Cardayre, S. B., and Keasling, J. D. (2010) Microbial production of fatty-acid-derived fuels and chemicals from plant biomass, *Nature 463*, 559-562.
3. Connor, M. R., and Atsumi, S. (2010) Synthetic Biology Guides Biofuel Production, *J. Biomed. Biotechnol.*, 1-9.
4. Schirmer, A., Rude, M. A., Li, X. Z., Popova, E., and del Cardayre, S. B. (2010) Microbial biosynthesis of alkanes, *Science 329*, 559–562.
5. Unpublished, structure solved by Joint Center of Structural Genomics (protein database entry PDB|2OC5|A).
6. Cheesbrough, T. M., and Kolattukudy, P. E. (1984) Alkane biosynthesis by decarbonylation of aldehydes catalyzed by a particulate preparation from *Pisum sativum*, *Proc. Natl. Acad. Sci. USA. 81*, 6613–6617.
7. Dennis, M., and Kolattukudy, P. E. (1992) A cobalt-porphyrin enzyme converts a fatty aldehyde to a hydrocarbon and CO, *Proc. Natl. Acad. Sci. USA. 89*, 5306–5310.
8. Yoder, J. A., Denlinger, D. L., Dennis, M. W., and Kolattukudy, P. E. (1992) Enhancement of diapausing flesh fly puparia with additional hydrocarbons and evidence for alkane biosynthesis by a decarbonylation mechanism, *Insect Biochem. Mol. Biol. 22*, 237–243.
9. Laemmli, U. K. (1970) Cleavage of structural proteins during the assembly of the head of bacteriophage T4, *Nature 227*, 680-685.
10. Sambrook, J. R. D. (2001) *Molecular Cloning: A Laboratory Manual*, Cold Spring Harbor Laboratory Press.
11. Bradford, M. M. (1976) A rapid and sensitive method for the quantitation of microgram quantities of protein utilizing the principle of protein-dye binding, *Anal. Biochem. 72*, 248-254.
12. Gill, S. C., and von Hippel, P. H. (1989) Calculation of protein extinction coefficients from amino acid sequence data, *Anal. Biochem. 182*, 319-326.
13. Jiang, W., Yun, D., Saleh, L., Barr, E. W., Xing, G., Hoffart, L. M., Maslak, M. A., Krebs, C., and Bollinger, J. M. (2007) A manganese(IV)/iron(III) cofactor in Chlamydia trachomatis ribonucleotide reductase, *Science 316*, 1188-1191.
14. Corey, E. J., and Schmidt, G. (1979) Useful Procedures for the Oxidation of Alcohols Involving Pyridinium Dichromate in Aprotic Media, *Tetrahedron Lett. 5*, 399-402.
15. Makris, T. M., Chakrabarti, M., Munck, E., and Lipscomb, J. D. (2010) A family of diiron monooxygenases catalyzing amino acid beta-hydroxylation in antibiotic biosynthesis, *Proc. Natl. Acad. Sci. USA. 107*, 15391-15396.
16. Fox, B. G., Shanklin, J., Somerville, C., and Munck, E. (1993) Stearoyl-acyl carrier protein delta 9 desaturase from Ricinus communis is a diiron-oxo protein, *Proc. Natl. Acad. Sci. USA. 90*, 2486-2890.
17. Stookey, L. L. (1970) Ferrozine - a New Spectrophotometric Reagent for Iron, *Anal. Chem. 42*, 779-781.

18. Sobrado, P., Lyle, K. S., Kaul, S. P., Turco, M. M., Arabshahi, I., Marwah, A., and Fox, B. G. (2006) Identification of the binding region of the [2Fe-2S] ferredoxin in stearoyl-acyl carrier protein desaturase: insight into the catalytic complex and mechanism of action, *Biochemistry 45*, 4848-4858.
19. Lyle, K. S., Haas, J. A., and Fox, B. G. (2003) Rapid-mix and chemical quench studies of ferredoxin-reduced stearoyl-acyl carrier protein desaturase, *Biochemistry 42*, 5857-5866.
20. Rhie, G., and Beale, S. I. (1995) Phycobilin biosynthesis: reductant requirements and product identification for heme oxygenase from Cyanidium caldarium, *Arch. Biochem. Biophys. 320*, 182-194.
21. Warui, D. M., Li, N., Norgaard, H., Krebs, C., Bollinger, J. M., and Booker, S. J. (2011) Detection of formate, rather than carbon monoxide, as the stoichiometric coproduct in conversion of fatty aldehydes to alkanes by a cyanobacterial aldehyde decarbonylase, *J. Am. Chem. Soc. 133*, 3316–3319.
22. Halaka, F. G., Babcock, G. T., and Dye, J. L. (1982) Propoerties of 5-methylphenazinium methyl sulfate - reaction of the oxidized form with NADH and of the reduced form with oxygen, *J. Biol. Chem. 257*, 1458-1461.
23. Zaugg, W. S. (1964) Spectroscopic Characteristics and Some Chemical Properties of N-Methylphenazinium Methyl Sulfate (Phenazine Methosulfate) and Pyocyanine at the Semiquidnoid Oxidation Level, *J. Biol. Chem. 239*, 3964-3970.
24. Kearney, E. B., and Singer, T. P. (1956) Studies on succinic dehydrogenase. I. Preparation and assay of the soluble dehydrogenase, *J. Biol. Chem. 219*, 963-975.
25. Jiang, W., Yun, D., Saleh, L., Bollinger, J. M., and Krebs, C. (2008) Formation and Function of the Manganese(IV)/Iron(III) Cofactor in Chlamydia trachomatis Ribonucleotide Reductase, *Biochemistry 47*, 13736-13744.
26. Wahlen, B. D., Oswald, W. S., Seefeldt, L. C., and Barney, B. M. (2009) Purification, Characterization, and Potential Bacterial Wax Production Role of an NADPH-Dependent Fatty Aldehyde Reductase from Marinobacter aquaeolei VT8, *Appl. Environ. Microbiol. 75*, 2758-2764.
27. Cahoon, E. B., Coughlan, S. J., and Shanklin, J. (1997) Characterization of a structurally and functionally diverged acyl-acyl carrier protein desaturase from milkweed seed, *Plant. Mol. Biol. 33*, 1105-1110.
28. Cahoon, E. B., Shah, S., Shanklin, J., and Browse, J. (1998) A determinant of substrate specificity predicted from the acyl-acyl carrier protein desaturase of developing cat's claw seed, *Plant Physiol. 117*, 593-598.
29. Wilks, A., and Ortiz de Montellano, P. R. (1992) Intramolecular translocation of the protein radical formed in the reaction of recombinant sperm whale myoglobin with H2O2, *J. Biol. Chem. 267*, 8827-8833.
30. Lipari, F., and Swarin, S. J. (1982) Determination of Formaldehyde and Other Aldehydes in Automobile Exhaust with an Improved 2,4-Dinitrophenylhydrazine Method., *J. Chromatogr. 247*, 297-306.
31. Quesenberry, M. S., and Lee, Y. C. (1995) A Rapid Formaldehyde Assay Using Purpald Reagent: Application under Periodation Conditions, *Anal. Biochem. 234*, 50-55.

32. Peters, R., Hellenbrand, J., Mengerink, Y., and Van der Wal, S. (2004) On-line determination of carboxylic acids, aldehydes and ketones by high-performance liquid chromatography-diode array detection-atmospheric pressure chemical ionisation mass spectrometry after derivatization with 2-nitrophenylhydrazine, *J. Chromatogr. A 1031*, 35-50.
33. Cheesbrough, T. M., and Kolattukudy, P. E. (1988) Microsomal preparation from an animal tissue catalyzes release of carbon monoxide from a fatty aldehyde to generate an alkane, *J. Biol. Chem. 263*, 2738–2743.
34. Wallar, B. J., and Lipscomb, J. D. (1996) Dioxygen activation by enzymes containing binuclear non-heme iron clusters, *Chem. Rev. 96*, 2625-2657.
35. Que, L. (2007) The road to non-heme oxoferryls and beyond, *Acc. Chem. Res. 40*, 493-500.
36. Hess, W. R. (2011) Cyanobacterial genomics for ecology and biotechnology, *Curr. Opin. Microbiol. 14*, 608-614.
37. Li, N., Chang, W.-C., Warui, D. M., Booker, S. J., Krebs, C., and Bollinger, J. M. (2012) Evidence for only oxygenative cleavage of aldehydes to alk(a/e)nes and formate by cyanobacterial aldehyde decarbonylases, *Biochemistry 51*, 7908–7916.

Chapter 3

Investigations of Ferredoxin-Dependent Cyanobacterial Aldehyde Decarbonylase Activity

3.1 Introduction

Aldehyde decarbonylase (AD)-catalyzes the conversion of aldehydes to alkanes, which is chemically a very challenging reaction. It appears that there are three distinct AD enzymes that catalyze different chemical reactions to effect removal of the aldehyde carbon. In higher plants and green algae the enzyme is a metal-dependent, integral membrane protein that converts the aldehyde carbon to carbon monoxide (CO).[1,2] These enzymes do not require any cofactor for activity and are inhibited in the presence of oxygen. In contrary, a recent report suggests involvement of CytB5 and NADPH as cofactors in the formation of very long chain alkanes by aldehyde decarbonylase from *Arabidopsis thaliana*.[3] In insects, AD appears to be a cytochrome p450 enzyme that oxidizes the aldehyde carbon to carbon dioxide (CO_2).[4,5] Unlike plant or algae enzyme, insect AD requires O_2 and NADPH for activity. In cyanobacteria AD (cAD) was recently found to be a small, soluble protein whose structure is closely related to the non-heme di-iron oxygenases.[6] Initial characterization of this enzyme revealed that cAD requires a reducing system made of ferredoxin (Fd)/ferredoxin reductase (FdR) and NADPH for activity. Omission of any one of these components completely abolished the activity. This requirement for a reducing system was later verified by several independent research groups.[7,8,9] For non-heme

di-iron enzymes an auxiliary reducing system usually serves to reduce the 'resting' di-ferric state of the enzyme to the active 'di-ferrous' state at the start of each turnover. Although the biological reducing system comprising Fd/FdR/NADPH supported the activity of cAD, no more than ~1 turnover could be obtained. Therefore, a chemical reducing system comprising phenazine methosulphate (PMS)/NADH was employed that supported ~100 times faster activity as well as multiple turnovers.[8] However, utilization of a physiological reducing system was considered to be essential to better understand the underlying properties of cAD. I therefore re-investigated the effectiveness of the biological reducing system comprising Fd/FdR/NADPH for supporting the activity of cAD. In particular my research has focused on ferredoxin, the protein that would presumably play the role of a direct binding partner with cAD to supply electrons to the di-iron active site of cAD.

Ferredoxins are small, soluble, acidic proteins found in all organisms but which play an especially important role in photosynthetic organisms such as plants, algae and cycnobacteria (Figure 3.1).[10,11] Ferredoxins work as the terminal electron acceptor from photosystem I. Reduced ferredoxins subsequently serve as electron donors for many ferredoxin dependent enzymes.[11] Feredoxin contains an iron-sulfur cluster in the active site that serves as one electron acceptor/donor. Plant, algal and cyanobacterial ferredoxins contain a 2Fe-2S cluster as the prosthetic group in which each iron center is coordinated to two inorganic sulfur atoms and two cysteinyl sulfur atoms. These ferredoxins have fairly low potential of -420 mV.[10] A very well characterized and extensively studied ferredoxin dependent enzyme is ferredoxin-NADP+ oxidoreductase (FdR) that reduces NADP+ to NADPH using electrons supplied from reduced Fd. FdR forms high affinity 1:1 complex with ferredoxin through electrostatic interactions and the

crystal structures of several Fd:FdR complexes are known (Figure 3.2).[12] A few other well characterized Fd-dependent enzymes are nitrite reductase, sulfite reductase and glutamate synthase. These enzymes play crucial roles in nitrogen, sulphur and carbon metabolism in different organisms.[10] Although ferredoxin is known to form a 1:1 complex with most of the ferredoxin-dependent enzymes through electrostatic interactions, electron transfer from ferredoxin to the partner protein takes place through a hydrophobic environment.[13]

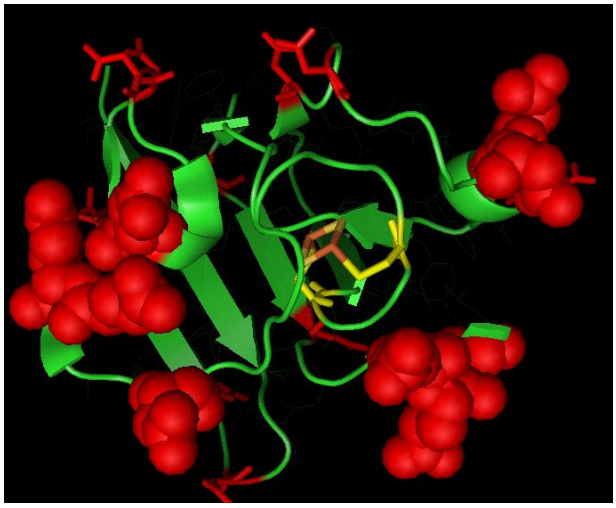

Figure 3.1. Crystal structure of Fd from *Synechocystis sp*. PCC6803 (PDB ID 1OFF). The negatively charged surface residues are shown in red. The residues shown in spheres participate in electrostatic interactions with FdR. The prosthetic group, 2Fe-2S cluster is also shown.

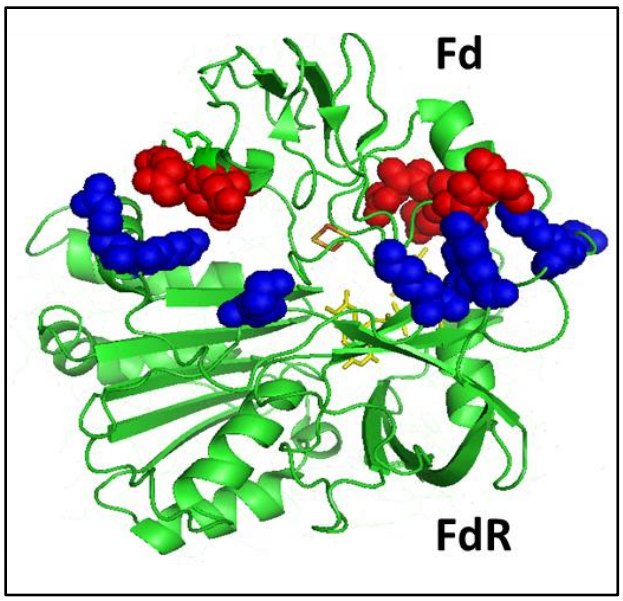

Figure 3.2. Crystal structure of 1:1 Fd:FdR complex from maize (PDB ID 1GAQ). The residues shown in red (in Fd) and blue spheres (in FdR) participate in electrostatic interactions. The 2Fe-2S cluster of Fd and flavin adenine dinucleotide cofactor of (FAD) of FdR are also shown.

Given that ferredoxin supported activity of cAD but only at the level of a single turnover, this led us to question the physiological relevance of Fd as a binding partner of cAD. The initially reported studies were all carried out using commercially available spinach ferredoxin with cyanobacterial aldehyde decarbonylase (except a recent report where cyanobacterial Fds were employed).[14] A possible reason for the sluggish activity of cAD might be the low efficiency in electron transfer between these two proteins from two different organisms. It might also be possible that the assay conditions have not yet been properly developed for the newly discovered cAD. With this premise, my goal was to establish the reason(s) for the sluggish activity of cAD in presence of ferredoxin. A also wanted to explore the interaction between Fd and cAD and develop a superior assay for cAD in which ferredoxin support multiple turnovers. Towards this goal, I investigated native cyanobacterial ferredoxins as cofactors of cAD.

3.2 Materials and Methods

Cyanobacterial aldehyde decarbonylase enzymes used for the studies reported in this chapter were from *Prochlorococcus marinus* MIT9313, *Synechocystis sp.* PCC6803 and *Nostoc punctiforme* PCC73102 species. *Pm* cAD and *Syn sp.* cAD were expressed and purified as described in Chapter 2. *Np* cAD was expressed and purified as described below. All the cAD proteins were expressed with N-terminal His-tags. Cyanobacterial ferredoxins used were also from the same species. Expression and purification procedure for *Pm* Fd and *Np* Fd are described below. *Pm* Fd was expressed without any tag attached to it whereas *Np* Fd was expressed with an N-terminal His-tag. While designing the *Np* cAD and *Np* Fd genes, a TEV-protease site was included in between the N-terminus His-tag and the protein so that the His-tag could be cleaved whenever required for the experiments. *Syn sp.* ferredoxin and maize ferredoxin NADP+ oxidoreductase were generous gifts from Dr. Guy. T. Hanke, Department of Plant Physiology, University of Osnabrück. Spinach ferredoxin was obtained from Sigma-Aldrich.

Ac-TEV protease utilized for cleaving N-terminus His-tag from proteins was obtained from Life Technologies.

The materials and instrumentation used for cloning the gene in the expression vector, transforming *E. coli* with the construct, cell growth, protein purification and characterization were all same and purchased from the same vendors as described in materials section of Chapter 2. Commercial reagents were reagent grade and used without further purifications.

Heterologous expression and purification of Nostoc punctiforme* PCC73102 *aldehyde decarbonylase (Np cAD). A synthetic gene, *Np* cAD PCC73102, (768 bp), encoding aldehyde

decarbonylase from cyanobacterium *Nostoc Punctiforme* PCC73102*,* was codon optimized for expression in *E. coli and* purchased from GenScript USA Inc. The gene was cloned into the expression vector pMCSG7 using the restriction enzymes BamHI and HindIII (New England BioLabs). The gene was cloned in such a way that allows expression of an N-terminus His-tag along with the expected protein. The transformation of *E. coli* BL21 (DE3) with the construct, growth of the single colonies on agar plate with 50 µg/mL ampicillin as antibiotics resistance, overnight growth of the culture and protein expression with IPTG were carried out in the similar way as described for *Pm* cAD in the Chapter 2. Protein purification and characterization were also carried out in a similar fashion. Protein expression and FPLC purification resulted in great yield (~80 mg/L culture) of the protein. The molar extinction coefficient 19.9 $mM^{-1}cm^{-1}$ was used to calculate the concentration of the protein.

Heterologous expression and purification of Prochlorococcus marinus* MIT9313 *ferredoxin (Pm Fd). Ferredoxins were purified in collaboration with Mr. Benjamin Levin. A synthetic gene, *Pm Fd*, (315 bp), encoding ferredoxin from cyanobacterium *Prochlorococcus marinus* MIT9313*,* was codon optimized for expression in *E. coli and* purchased from GenScript USA Inc. The gene was cloned into the expression vector pET-28b(+) using the restriction sites NcoI and BamHI. After cloning, the identity of the gene was confirmed by DNA sequencing by the DNA sequencing core facility at the University of Michigan. The gene was cloned in such a way that did not allow expression of the N-terminus His-tag along with the expected protein. After transformation of electro-competent *E.coli* BL21 (DE3) cells with this construct, cells were grown overnight on agar plates with kanamycin antibiotics resistance (50 µg/mL) to obtain single colonies. To express the protein, a single colony was grown overnight at 37 °C in 5 mL 2x-YT media

supplemented with kanamycin, transferred to 1 L of the same medium and grown at 37 °C to an optical density of 0.7 at 600 nm. To this culture, ferrous ammonium sulfate was added to a final conc. 50 µM to enhance the expression of ferredoxin. IPTG was added to a final concentration of 500 µM to induce protein expression. Cells were further grown for 10 h at the same temperature and then harvested by centrifugation at 4000 *g* at 4 °C for 25 min.

6 g (damp weight) of cells were resuspended in 30 mL 50 mM Tris-HCl buffer, pH 7.5, containing 200 mM NaCl, 5% glycerol, 0.1% β-mercaptoethanol, 0.5 mg/mL of lysozyme, 1/ 50 mL EDTA-free protease inhibitor tablet and 1 µL of DNAse and incubated for 45 min on ice and then lysed by sonication using a 550 Sonic Dismembrator with a micro-tip at maximum power using 2s pulses separated by 8s to prevent overheating for a total time of 30 min. The supernatant was separated from cell pellet by centrifugation at 14500 *g* at 4 °C for 30 min.

Purification of *Pm* Fd was achieved using FPLC (ActaPure, UPC10) by affinity chromatography using a Q-sepharose anion exchange column (70 mL). The column was equilibrated with buffer A: 50 mM Tris-HCl, pH 7.5, 50 mM NaCl. The supernatant from cell lysis was loaded onto the column using a 50 mL super-loop at a flow rate of 1mL/min and the column was washed with 140 mL of the same buffer at the same flow rate. Ferredoxin was found to bind to the column as a reddish-brown band could be observed on the column. Proteins were eluted from the column using a gradient flow of 0 - 40% buffer B (50 mM Tris-HCl, pH 7.5, 1M NaCl) over the course of two column volume. Fd started eluting out at 40% buffer B and the gradient was hold at the same concentration until the elution of Fd was complete (elution of Fd could be visualized by the reddish-brown color of the protein).

Fractions were collected using automatic fraction collector. The gradient was further increased to 100% over three column volume to wash out any other proteins bound to the column. The relatively pure fractions were combined and dialyzed against 150 mM Tris-HCl, pH 7.3 containing 100 mM NaCl and 10% glycerol. After dialysis, the protein was concentrated using Amicon Ultra-15 centrifugal filters. Concentration of the resulted ferredoxin was measured by using extinction coefficient of Fd of 9.68 $mM^{-1}cm^{-1}$ at 422 nm.

Heterologous expression and purification of Nostoc punctiforme* PCC73102 *ferredoxin (Np Fd).

A synthetic gene, *Np Fd*, (297 bp), encoding ferredoxin from cyanobacterium *Nostoc punctiforme* PCC73102*,* was codon optimized for expression in *E. coli and* purchased from GenScript USA Inc. The gene was cloned into the expression vector pMCSG7 using the restriction sites BamHI and HindIII. The gene was cloned in such a way that allows expression of an N-terminus His-tag along with the expected protein. The transformation of *E. coli* BL21 (DE3) with the construct, growth of the single colonies on agar plate with 50 µg/mL ampicillin as antibiotics resistance, overnight growth of the culture and protein expression with IPTG were carried out in the similar way as described for the expression of *Pm* Fd.

10 g (damp weight) of cells were resuspended in 60 mL of the same lysis buffer as described for the *Pm* Fd purification and sonicated in the same way. Purification of His-tagged *Np* Fd was achieved using FPLC (ActaPure, UPC10) by affinity chromatography using a Ni-affinity column (5 mL, HisTrap HP) and taking the advantage of expressed N-terminal His-tag. The column was equilibrated with buffer A: 50 mM Tris-HCl, pH 7.5, 500 mM NaCl, 20 mM imidazole, 5% glycerol. The supernatant from cell lysis was loaded onto the column using a 50

mL super-loop at a flow rate of 1mL/min and the column was washed with 25 mL of the same buffer at a flow rate of 2 mL/min. Non-specifically bound proteins were washed out of the column with 20 mL of buffer containing 50 mM Tris-HCl, pH 7.5, 500 mM NaCl, 50 mM imidazole, 5% glycerol at the same flow rate. Finally, *Np* Fd was eluted from the column with 10 mL of buffer B: 20 mM HEPES, pH 7.4, 500 mM NaCl, 250 mM imidazole, 5% glycerol at a flow rate of 2 mL/min. Ferredoxin was purified as a reddish-brown protein. The fractions were judged by SDS-PAGE gel for purity. The fractions containing pure protein were pooled and dialyzed using 3.5 kDa molecular wt. cutoff dialysis tubing at 4 °C against the final buffer: 150 mM Tris-HCl, pH 7.3 containing 100 mM NaCl and 10% glycerol. After dialysis, the protein was concentrated using Amicon Ultra-15 centrifugal filters. Concentration of the resulted ferredoxin was measured by using extinction coefficient of Fd of 9.68 $mM^{-1}cm^{-1}$ at 422 nm.

Enzyme assays. Typically, assays were performed in 100 mM HEPES buffer, pH 7.2 containing 100 mM KCl and 10% glycerol. The salt concentration was later varied to examine the effect of ionic strength on the activity of the enzyme. Assays were performed under complete aerobic condition. Aldehyde substrates were made up as stock solutions in DMSO. In general, enzymatic reactions contained 10 µM cAD, 20 µM ferrous ammonium sulfate, 500 µM octadecanal/2 mM heptanal in a total volume of 500 µL. The reducing system comprised of 10 µM ferredoxin, 20 nM ferredoxin oxidoreductase and 800 µM NADPH final. Assays were carried out with/without shaking at 37 °C. While assaying octadecanal as a substrate, assays were quenched with ethyl acetate and studied by GC. While heptanal was used as the substrate, the reaction headspace was studied by GC.

GC/GC-MS analysis. Analysis were performed using Agilent 6850 GC as described in Chapter 2.

3.3 Results and Discussion

3.3.1 Characterization of *Np* cAD

The identity of the purified *Np* cAD was confirmed by SDS-PAGE gel as well as by LC-MS studies. Calculated average mass (Mr) of *Np* cAD: 28910.62 Da matched really well with experimentally determined average mass (Mr) of *Np* cAD: 28910.85 Da (Figure 3.3).

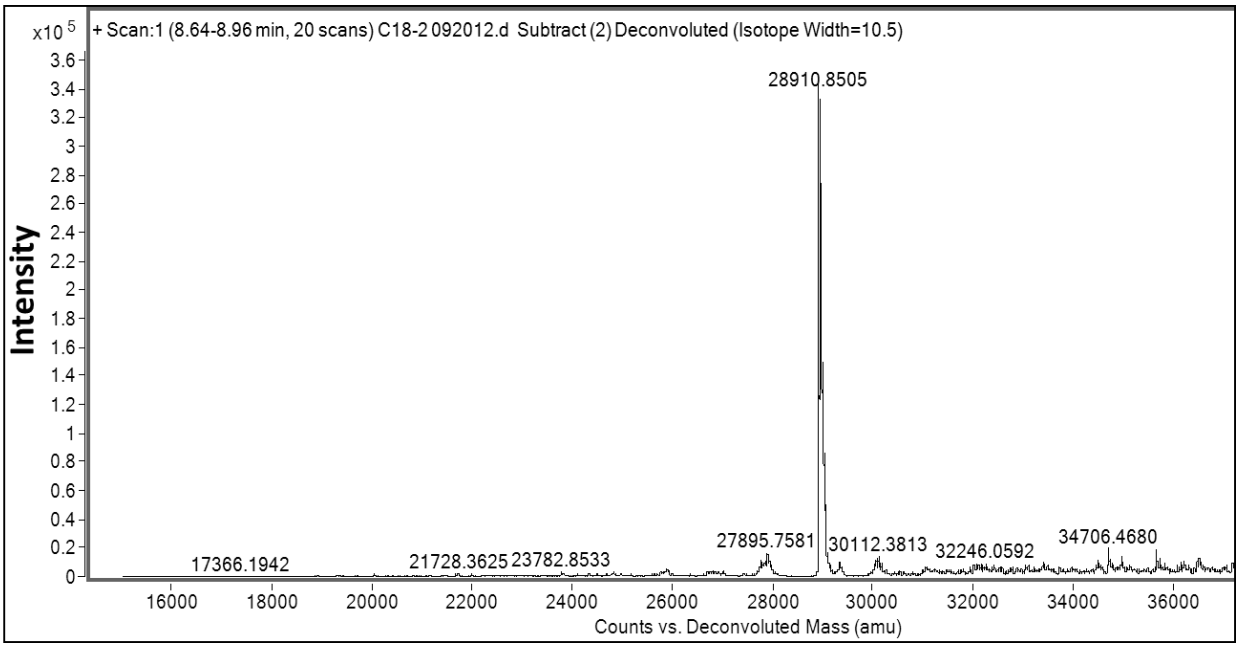

Figure 3.3. Mass spectrum of purified recombinant *Np* cAD depicting the deconvoluted average mass.

3.3.2 Characterization of Ferredoxin

The cyanobacterial ferredoxins were expressed as soluble stable proteins. No precipitation was noticed after purification of Fd by FPLC at room temperature. Very little

precipitation was observed during extensive dialysis at 4 °C for 24 h. Purified *Pm* Fd were judged to be more than 80% pure by SDS-PAGE gel (Figure 3.4).

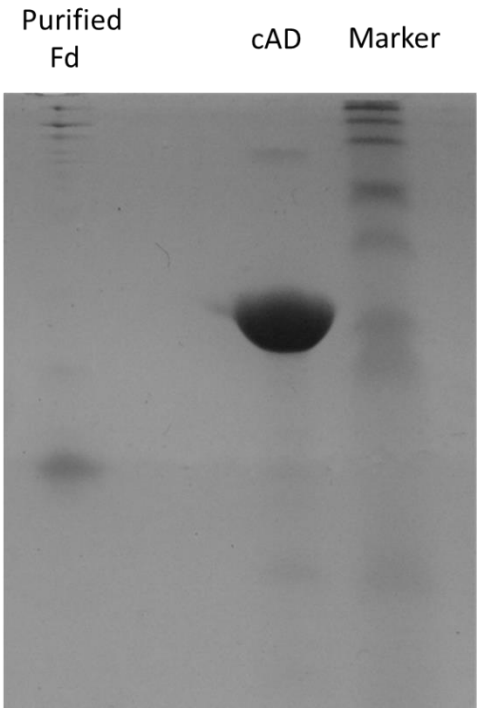

Figure 3.4. SDS-PAGE analysis of purified *Pm* Fd, a purified cAD standard and the molecular weight marker. Purified Fd was judged to be more than 80% pure.

3.3.3 Activity Assays of cAD in Presence of Ferredoxin

As mentioned earlier, spinach ferredoxin did not support more than one turnover with cAD using octadecanal as a substrate. Therefore, I wanted to examine whether the using cAD and Fd from same cyanobacterial species would enhance the activity.

Assays of Syn. sp. PCC6803 cAD with Syn. sp. PCC6803 Fd. Assays were performed using both cAD and ferredoxin from *Syn. sp.* PCC6803 cyanobacterium in 100 mM HEPES buffer, pH 7.2 containing 100 mM KCl and 10% glycerol. Both hepatnal and octadecanal were used as

substrates and at the end of an assay, formation of hexane or heptadecane was quantified. As shown in Figure 3.5, hexane formation slowly increased with time but unfortunately, did not reach a full turnover. After one h, only 0.65 turnovers (w.r.t cAD) of hexane could be obtained. Formation of heptadecane from octadecanal was even slower as only 0.35 equivalent of heptadecane was formed.

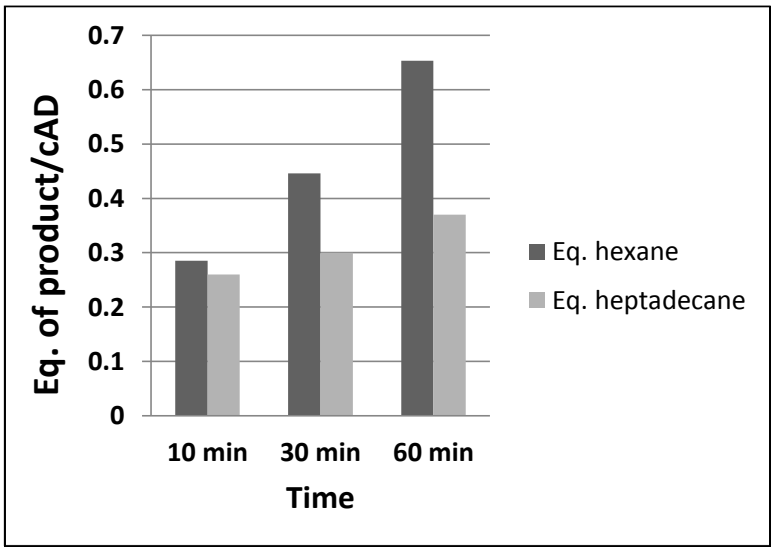

Figure 3.5. Formation of hexane and heptadecane from heptanal and octadecanal respectively from the assays containing *Syn. sp.* cAD and *Syn. sp.* PCC6803 Fd.

Next, *Pm* cAD was assayed with Fd using octadecanal as a substrate under identical assay conditions. As shown in Figure 3.6, the time course exhibits slightly better activity, with formation of 0.6 equivalent of heptadecane in 1 h. compared to 0.35 eq. of heptadecane in the same time with *Syn. sp.* cAD.

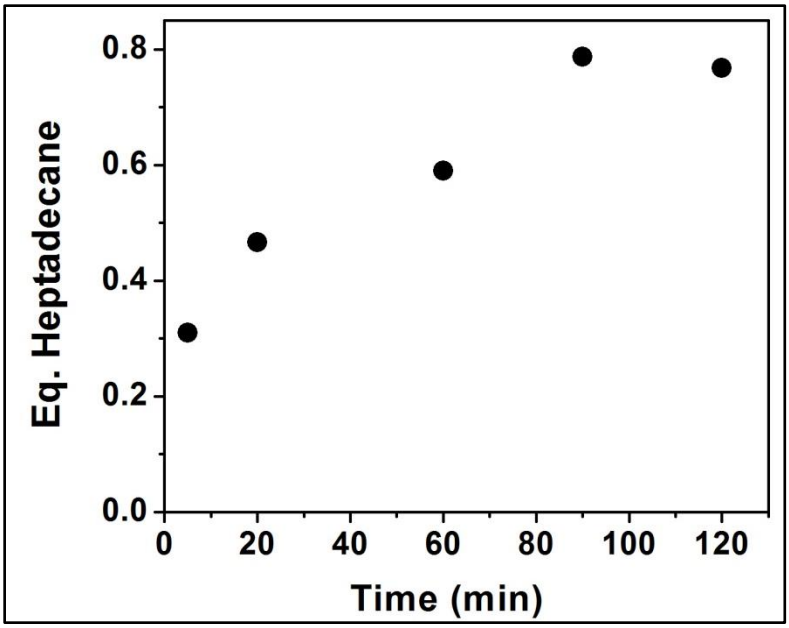

Figure 3.6. Formation of heptadecane from octadecanal from the reaction of *Pm* cAD with *Syn. sp.* PCC6803 Fd.

A possible reason for these sluggish activities could be the presence of '6-His-tag' at the N-terminus of cAD. The positively charged 6-His tag, could possibly interact with the negatively charged ferredoxin that would interfere with the necessary interaction between cAD and Fd. To check this possibility, heterologously expressed His-tagged *Np* cAD was treated with TEV protease. The protein was designed in such a way that a TEV cleavage site (ENLYFQG) was incorporated in between the 6-His-tag and the expressed protein. In addition, *Np* Fd was also designed similarly. Both the proteins were treated with TEV protease to remove the tag as described below.

Preparation of Np cAD without His-tag using TEV protease. 4.5 mg of purified *Np* cAD was treated with 300 U (30 µL) of Ac-TEV protease in presence of the 1 mM DTT and 1X Ac-TEV buffer (final) overnight at 4 °C in a total volume 4.5 mL. After digestion, the sample was diluted

with 4.5 mL of buffer A containing 20 mM HEPES, pH 7.4, 500 mM NaCl, 20 mM imidazole, 5% glycerol. The resulting sample was loaded onto the 5 mL HisTrap column using FPLC and eluted at a flow rate 0.5 mL/min using the same buffer. The TEV cleaved protein eluted with the flow through which was collected and dialyzed using 10-12 kDa molecular wt. cutoff dialysis tubing at 4 °C against the final assay buffer: 100 mM HEPES, pH 7.2 containing 100 mM KCl and 10% glycerol. The purified protein was > 95% pure as judged by SDS-PAGE gel. The activity of this preparation of *Np* cAD was measured using PMS/NADH reducing system following the procedure described in Chapter 2 and compared with the activity of His-tagged *Np* cAD. The data suggests that the *Np* cAD without the His-tag lost ~20% activity compared the His-tagged version of *Np* cAD (data not shown).

Preparation of Np Fd without His-tag using TEV protease. To obtain *Np* Fd without the His-tag, the His-tagged *Np* Fd was treated with Ac-TEV protease similarly as described for the *Np* cAD. After overnight proteolysis, the sample was diluted with the same volume of buffer containing 50 mM Tris-HCl, PH 7.5 containing 500 mM NaCl, 20 mM imidazole and 5% glycerol. This sample was purified using HisTrap column as described before. The protein was dialyzed using 3.5 kDa molecular wt. cutoff dialysis tubing at 4 °C against the final assay buffer: 150 mM Tris-HCl, pH 7.3 containing 100 mM NaCl and 10% glycerol. The purified protein was > 90% pure as judged by SDS-PAGE gel.

Activity of TEV cleaved Np Fd. The activity of this preparation of *Np* Fd was measured using cytochrome C (CytC). This activity was compared with the activity of *Synechocystis sp.* PCC6803

ferredoxin that was isolated from the cyanobacteriam *Synechocystis sp.* PCC6803. CytC accepts electrons from reduced ferredoxin and the reduced form of CytC has a strong absorbance at 550 nm (ε_{550} = 28 $mM^{-1}cm^{-1}$). The assay mixture contained 5 µM Fd, 100 µM NADPH, 80 µM CytC and 20 nM maize FdR in a final assay volume 500 µL. The increase in the absorption was followed at 550 nm using UV-Vis spectroscopy. As it can be seen from Figure 3.7, the activity of both TEV-cleaved *Np* Fd and the native *Syn. sp.* Fd were very similar.

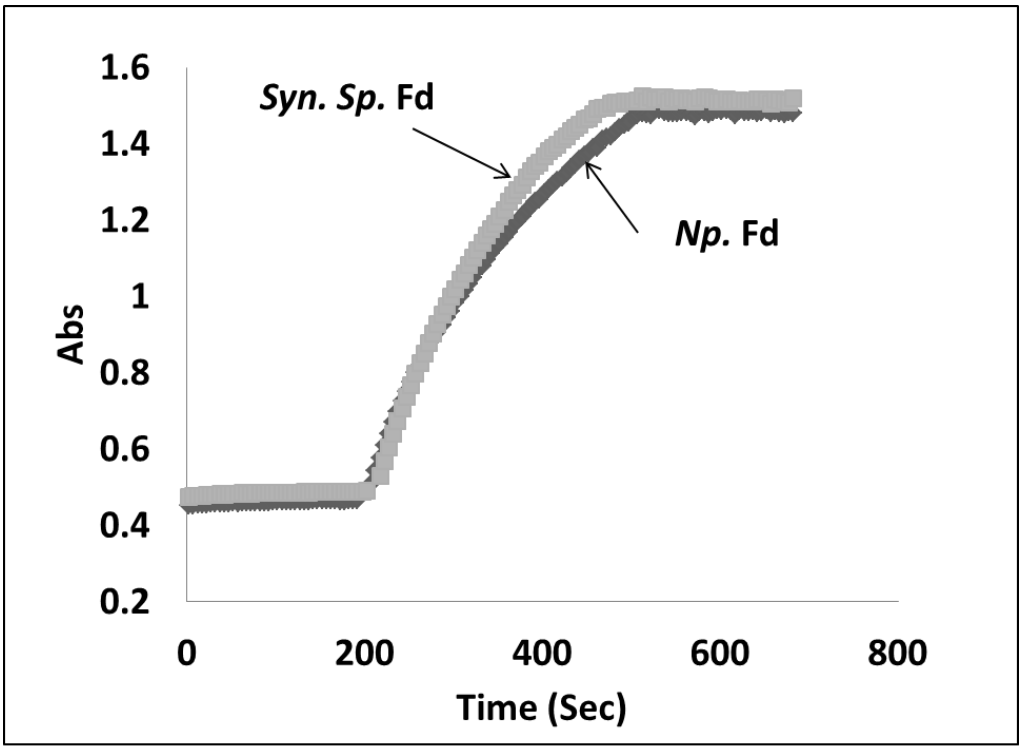

Figure 3.7. Comparison of activity of *Syn. sp*. Fd and *Np* Fd (without His tag) by following their effectiveness to reduce CytC. The formation of reduced CytC was followed at 550 nm.

Assays of TEV-cleaved Np cAD with TEV-cleaved Np Fd. After purification of *Np* cAD and *Np* Fd lacking His-tags, and verifying their individual activities, the decarbonylase activity combined the enzyme systems was examined. Assays were performed in 100 mM HEPES, pH 7.2

containing 100 mM KCl and 10% glycerol at 37 °C without any shaking as described before. Both heptanal and octadecanal were employed as substrate and the corresponding alkane products were quantified. From these assays 1 turnover of hexane and 0.5 turnover of heptadecane were obtained in 20 min. Note that when His-tagged *Np* cAD and His-tagged *Np* Fd were employed together and assayed in an identical way, only 0.3 equivalent of hexane could be obtained in 20 min. This suggests that removal of of His-tag from both the proteins enhanced the activity by ~ 3 times, although the activity is still extremely sluggish.

3.3.4 Effect of Salt Concentrations on the Fd-Dependent Activity of cAD

Most of ferredoxin-dependent proteins interact with ferredoxin through electrostatic interactions. These enzymes form complexes with ferredoxin at low ionic strength and as the ionic strength increases their interaction weakens. This suggests that electrostatics play critical role in their interactions.[15]

The effect of ionic strength on Fd-dependent cAD activity had never been explored. At low ionic strength, Fd might tightly bind to the cAD, which would result in very efficient electron transfer but the tight binding might also lead to the formation of an inhibitory complex and thus would not allow multiple turnovers. At high ionic strength, the proteins might not interact well with each other and thus would exhibit sluggish activity. Thus the effect of ionic strength on cAD activity needs to be studied.

In the crystal structure of Fd-FdR complex from maize (Figure 3.2, PDB ID 1GAQ), the negatively charged residues on Fd and the positively charged residues of FdR are geometrically positioned in such a way that facilitates the interaction between them. Therefore, the structure

of cyanobacterial AD (Figure 3.8) and cyanobacterial Fd were examined but no obvious complementary regions of opposite charges could be found. For the enzyme ferredoxin NADP+ oxidoreductase, the positively charged residues that interact with the negatively charged residues of ferredoxin are conserved. To examine whether the conserved positively charged residues of FdR are also conserved in cAD, co-alignment of the sequences of *Pm* cAD and maize FdR was carried out using CLUSTAL software. Unfortunately, the alignment could not detect the same conserved residues on cAD, instead, some other co-aligned positively charged residues were detected on both the proteins (Figure 3.9). Overall, whether Fd is capable of effectively binding to cAD could not be concluded from these analyses.

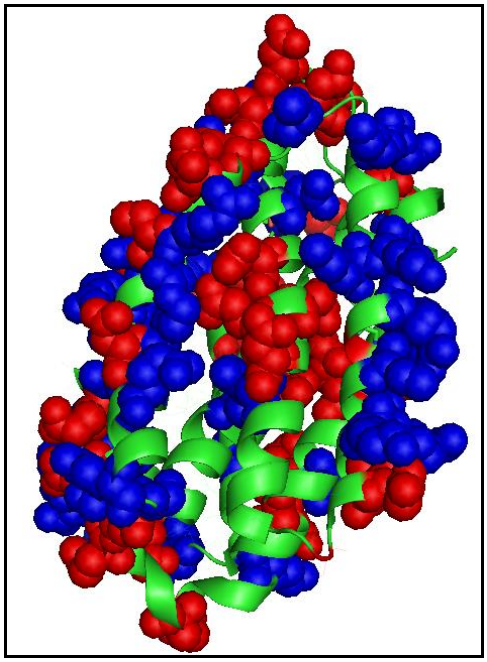

Figure 3.8. Charge distribution on *Pm* cAD (PDB ID 2OC5). The positively charged residues are shown in blue and the negatively charged residues are shown in red.

```
CLUSTAL format alignment by MAFFT (v6.901b)


FdR             IRAQASAVEAPATAKAKKESKKQEEGVVTNLYKPKEPYVGRCLLNTKITGDDAPGETWHM
cAD             M----PTLEMPVAA---------------------------VLDSTVGSSEA-------
                :    .::* *.:*                           :*::.: ..:*

FdR             VFSTEGKIPYREGQSIGVIADGVDKNGKPHKVRLYSIASSAIGDFGDSKTVSLCVKRLIY
cAD             ------------------------------------------------------------


FdR             TNDAGEIVKGVCSNFLCDLQPGDNVQITGPVGKEMLMPKDPNATIIMLATGTGIAPFRSF
cAD             ------------------------------------------------------------


FdR             LWKMFFEKHDDYKFNGLGWLFLGVPTSSSLLYKEEFGKMKERAPENFRVDYAVSREQTNA
cAD             ----------------------LPDFTSDRYKDAYS----------RINAIVIEGEQEA
                                      :*  :*  **: :.          *::  * . : :*

FdR             AGERMYIQTRMAEYKEELWELLKKDNTY---VYMCGLK-GMEKGID--------------
cAD             HDNYIAIGTLLPDHVEELKRLAKMEMRHKKGFTACGKNLGVEADMDFAREFFAPLRDNFQ
                 .: : * * :.:: *** .* * :  :   .  ** : *:* .:*

FdR             ------------DIMVSLAEKDGIDWF--------------------DYKKQLKRGDQW-
cAD             TALGQGKTPTCLLIQALLIEAFAISAYHTYIPVSDPFARKITEGVVKDEYTHLNYGEAWL
                             * . * *  .*. :                   *  .:*: *: *

FdR             --NVE-----------------------------------------------------
cAD             KANLESCREELLEANRENLPLIRRMLDQVAGDAAVLQMDKEDLIEDFLIAYQESLTEIGF
                  *:*

FdR             -------------VY
cAD             NTREITRMAAAALVS
                             *
```

Figure 3.9. CLUSTAL co-alignment of the sequences of maize FdR and of *Pm* cAD. In yellow, the conserved residues on FdR participate in electrostatic interaction with Fd. In pink, the positively charged co-aligned residues on FdR and cAD.

Effect of salt concentration on activity. Salt concentration has been shown to play significant role in assays containing Fd and Fd-dependent enzymes. It has been observed that activity of Fd-dependent nitrite reductase falls dramatically above ~ 50 mM salt in the assay.[15] This is due to diminishing electrostatic interactions beteen Fd and nitrite reductase at higher salt

concentrations. Therefore, an investigation on the effect of salt conentration on Fd- dependent cAD activity was initiated. A buffer containing 100 mM HEPES, pH 7.5 containing 40 mM NaCl (buffer 1) was used to perform assays. Note that in this buffer, salt concentration was reduced to 40 mM from the usual 100 mM salt in assay buffer. Assays were performed using heptanal as substrate without shaking as described before and the product hexane was quantified from the reaction headspace. *Np* cAD (with His-tag) and *Syn. sc.* Fd were employed for these assays. Reactions were carried out at 37 °C for 20 min without shaking. Interestingly, 2.4 turnovers (w.r.t cAD) were obtained from these assays. This result was exciting because, for the first time, multiple turnovers were obtained from Fd-dependent cAD assays. Notably, changing buffer concentration from 100 mM HEPES to 40 mM HEPES resulted ~20% decrease in activity (data not shown). This suggests that the effect of ionic strength due to the buffer and the salt concentration on the activity of cAD is not additive and specific ions (here Na^+ and Cl^-) might play significant role on the cAD activity. Further studies are necessary to explore the effect of different ions on the activity of cAD.

Effect of shaking the assay mixture on activity. The effect of agitation of the assay mixture on the activity was examined. Shaking was typically employed in cAD assays using the PMS/NADH as the reducing system. Because long chain aldehydes are very poorly water soluble, shaking presumably enhanced the diffusion of aldehyde molecules to the enzyme and thus enhanced the activity. cAD is quite stable and doesn't get inactivated by shaking (Chapter 2). Therefore, assays were performed with shaking at 200 rpm. All other assay conditions were kept identical except that assay time was reduced to 2 min (Shorter time points were preferred because of the possibility of inactivation of enzyme components involved in the assay at longer time). For

compaison, an identical assay was also performed without shaking for 2 min. As shown in Figure 3.10, Shaking enhances the activity ~2 fold and, more interestingly, a little more than one turnover was obtained in 2 min.

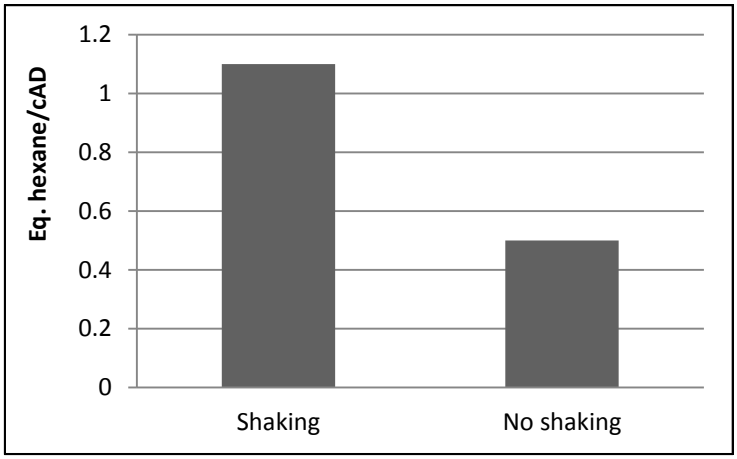

Figure 3.10. Effect of shaking on hexane formation from heptanal by cAD in presence of Fd.

These experiments resulted in improvement of the activity of cAD from ~1 turnover per h to ~1 turnover in 2 min. These results also implied that the salt concentration plays very crucial role for Fd supported cAD activity. To optimize the concentration of salt required in an assay to obtain the higheat activity, further assays were carried out with varying salt concentrations.

Along with Buffer 1: 100 mM HEPES, pH 7.5 containing 40 mM NaCl, two other buffers were made with varying salt concentration; 20 mM (buffer 2) and 2 mM (buffer 3) of NaCl respectively. Assays were performed for 2 min with shaking at 200 rpm at 37 °C. When assaying cAD using heptanal as a substrate, Buffer 1 and Buffer3 exhibited almost similar activity with

slightly improved activity for buffer 2 (Figure 3.11). So, the buffer 2 (100 mM HEPES, pH 7.5 containing 20 mM NaCl) was used for all subsequent assays of cAD in presence of Fd.

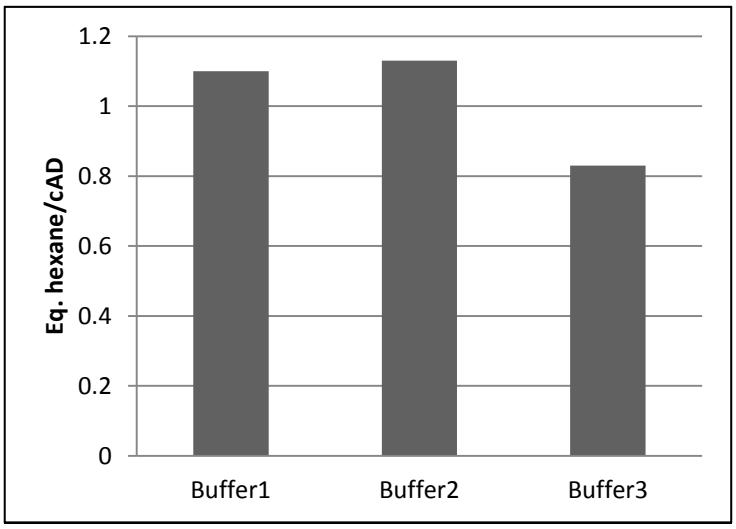

Figure 3.11. Effect of salt concentrations on cAD activity supported by Fd. Activity did not change significantly from 40 mM NaCl to 20 mM NaCl. 2 mM salt proved to be less effective.

Time course of hexane formation by cAD. To determine the progress of product formation, assays contained 10 µM *Np* cAD, 20 µM ferrous ammonium sulphate, 10 µM *Syn. sp.* PCC6803 ferredoxin, 20 nM ferredoxin oxidoreductase, 800 µM NADPH and 2 mM heptanal final. Assays were performed in buffer 2 at 37 °C with shaking at 200 rpm. Hexane production was quantified by sampling the headspace. The reactions exhibited an initial burst phase of an almost stoichiometric amount of hexane formation followed by a slower steady state rate (Figure 3.12). The data can be well fitted to burst phase kinetics with burst phase rate 0.59 ± 0.14 min^{-1} and a slower steady state rate of 0.013 ± 0.004 min^{-1}. However, the possibility that the kinetic profile may result from inactivation of one of the assay components with time leading the slower rate of turnover cannot be eliminated. It should be noted that the assay involves three

enzyme components and inactivation of one or more components with shaking is certainly possible.

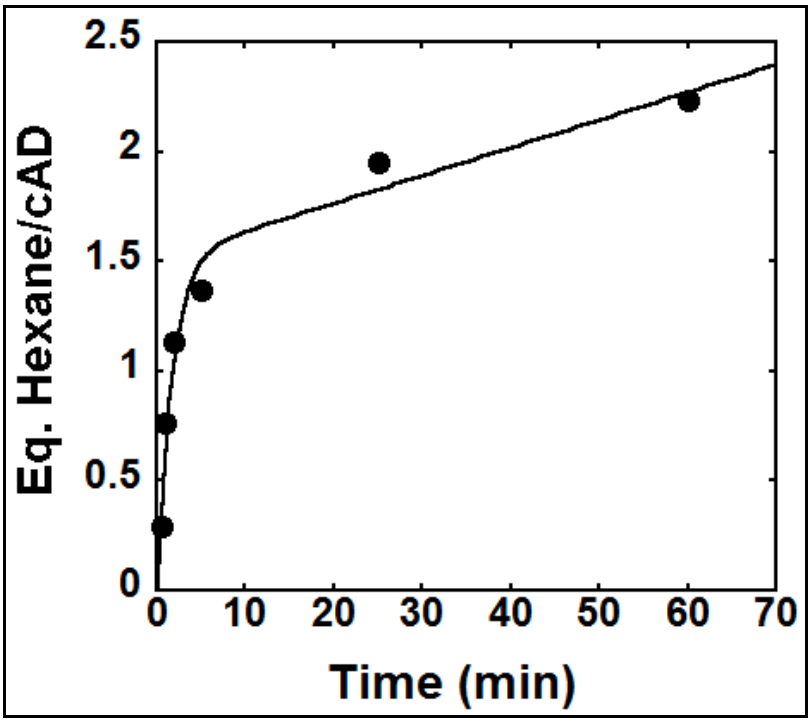

Figure 3.12. A time course of hexane formation by cAD in presence of Fd. The progress curve exhibits a burst phase of hexane formation at a rate of 0.59 min^{-1} which was followed by a slower steady state rate of 0.013 min^{-1}.

To compare the effectiveness of Fd and the chemical reducing system in supporting the activity of *Np* cAD, the time course of hexane formation was examined in presence of the chemical reducing system under completely aerobic conditions. Assays contain 10 µM Np cAD, 20 µM FeAS, 75 µM PMS, 1 mM NADH and 2 mM heptanal. Assays were shaken at 200 rpm at 37 °C. Hexane formation was quantified as before. The PMS/NADH system is not very stable under completely aerobic condition. In spite of having 1 mM NADH in the assay, it has been seen that the reduced PMS oxidizes in ~ 3-4 mins in air saturated buffer. In accordance with this observation, when PMS/NADH was employed with cAD under aerobic conditions, the activity of

cAD increased linearly for a short period of time and then reached a plateau. A comparison of the time courses of hexane formation using PMS/NADH system and Fd system is shown in Figure 3.13. From the initial time points (up to 3 min) the rate of hexane formation by cAD using PMS/NADH system (in red) was slightly faster than the Fd-supported activity (in black).

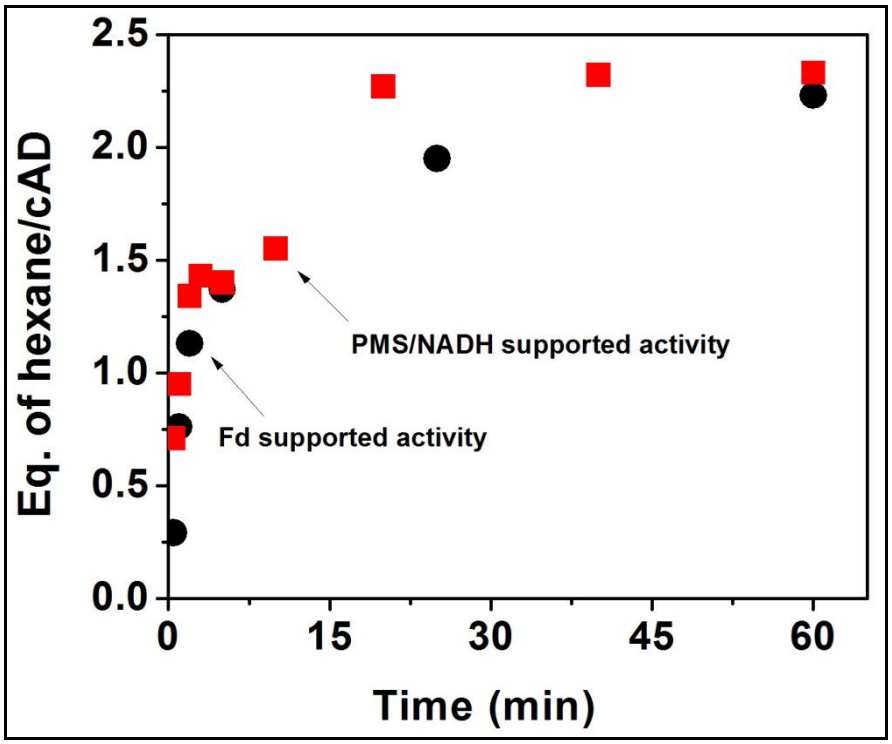

Figure 3.13. Comparison of the time courses of hexane formation by Fd-supported activity (in black) and PMS/NADH supported activity (in red) of cAD.

3.3.5 Comparison of Activity of Different cADs with Ferredoxins and PMS/NADH

Inspired by the improved activity of Fd-supported cAD, different cAD enzymes were tested against different Fds and the activity was compared with PMS/NADH-supported activity of cAD enzymes. Further, assays were also performed with spinach ferredoxin under the

optimized assay conditions to re-evaluate the potential of spinach ferredoxin as an auxiliary reducing system. All the assays were performed in 100 mM HEPES, 20 mM NaCl, pH 7.5. Assays were shaken for 2 min at 37°C at 200 rpm and 1 mL of headspace was analyzed by GC. Assay components were 10 µM cAD, 20 µM FeAS, 10 µM Fd, 40 nM Maize FdR, 2 mM NADPH, (or 75 µM PMS, 2 mM NADH) and 2 mM Heptanal. Initial rates of product formation were measured.

As it can be seen from Figure 3.14, in general, *Pm* cAD and *Np* cAD exhibit very similar activity with PMS/NADH (trace A and E). *Pm* cAD showed slightly better activity with its native Fd compared PMS/NADH (trace B and A). Interestingly, *Syn. sp.* Fd supported better activity of *Pm* cAD compared to its native Fd (trace C and B). With, *Syn. sp.* Fd, *Pm* cAD supported an initial rate of 1 turnover/min, the best activity of cAD obtained so far under the improved assay conditions. These observations indicate that cAD is not very specific to its native ferredoxin. Another interesting observation was that, under the optimized assay conditions, spinach ferredoxin also supported significant activity with both *Pm* cAD (initial rate = 0.5 turnover/min) and *Np* cAD (initial rate = 0.3 turnover/min).

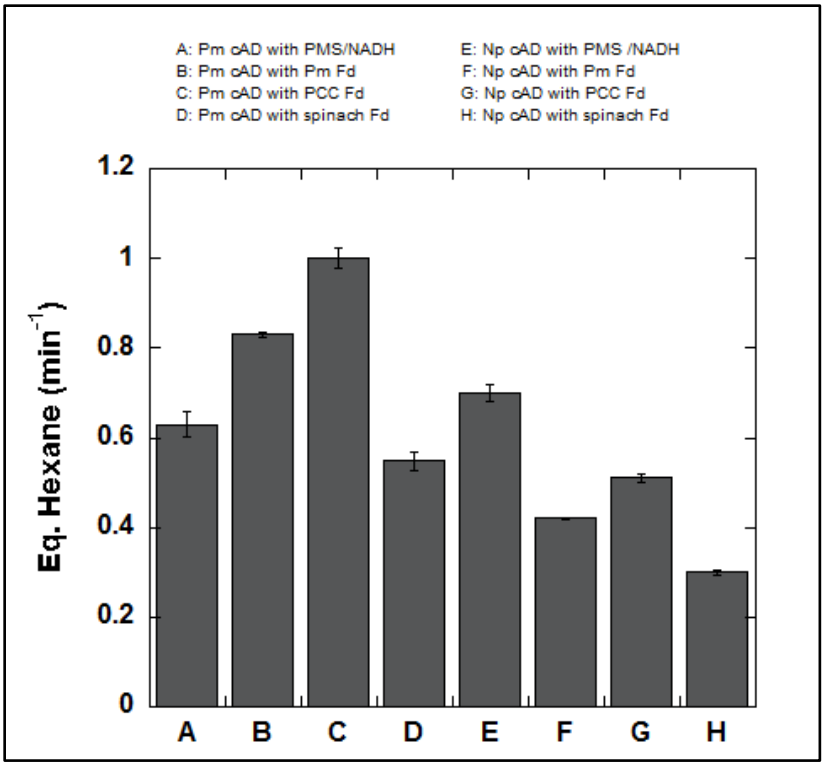

Figure 3.14. Comparison of activity of cAD in presence of different ferredoxins and PMS/NADH.

Overall, these experiments explored two important aspects of cAD. First, salt concentration plays a significant role in cAD activity where Fd system is used as the reducing system. Secondly, cAD is not highly specific towards its native ferredoxin. Although the activity of cAD is almost doubled with its native ferredoxin compared to spinach ferredoxin, the later supported significant activity.

3.3.6 Evidences of Electron Transfer from Reduced Fd to cAD

Direct electron transfer from reduced Fd to cAD. Electron transfer from reduced Fd to cAD is necessary for the later protein's activity. To obtain direct evidence of electron transfer, UV-Vis spectrophotometric studies were initiated.

Ferredoxin is reddish-brown in color due to the presence of an iron-sulfur cluster as the prosthetic group. Plant and cyanobacterial ferredoxins have a characteristic absorption spectra with absorption maxima at 275, 330, 422 and 465 nm and absorption minima at 315, 398 nm.[16] Reduction of Fd can be followed by the decrease in absorbance at 422 nm. Ferredoxins can be chemically reduced by sodium dithionite.[16,17]

All the experiments were carried out anaerobically using an anaerobic cuvette. Sodium dithionite solution was standardized by titration with methyl viologen using an extinction coefficient of ε_{730} = 2.4 mM^{-1} cm^{-1} methyl viologen. A standard solution of dithionite was used to reduce the ferredoxin completely. Reduction of ferredoxin was monitored by following the change in absorbance at 422 nm of ferredoxin and as the ratio A_{398}/A_{422} reached > 1.2, Fd was believed to be completely reduced.[18] The color of the solution changed from dark reddish-brown to light brown during this process.

The spectrum of 100 µM as-isolated (oxidized) Fd (Figure 3.15) showed an absorption maximum at 422 nm and an absorption minimum at 398 nm. This ferredoxin was reduced by addition of standard dithionite solution (Step 2). Then as a control, 18 µL of anaerobic assay buffer was added to 300 µL of assay solution to quantify the extent of background oxidation. Partial oxidation of reduced ferredoxin occurred (~20%) as seen from the partial appearance of the 422 nm peak (Step 3). This observation suggests that the anaerobic buffer is contaminated with some oxygen. The partially oxidized ferredoxin was further re-reduced with sodium dithionite (Step 4). Then, as the final step, 18 µL of cAD (final conc. 100 µM) was added in the assay solution. Immediately, oxidation of ferredoxin occurred (step 5). This indicates very rapid

electron transfer from ferredoxin to cAD. To determine the rate of electron transfer from Fd to cAD, stop-flow experiments need to be performed.

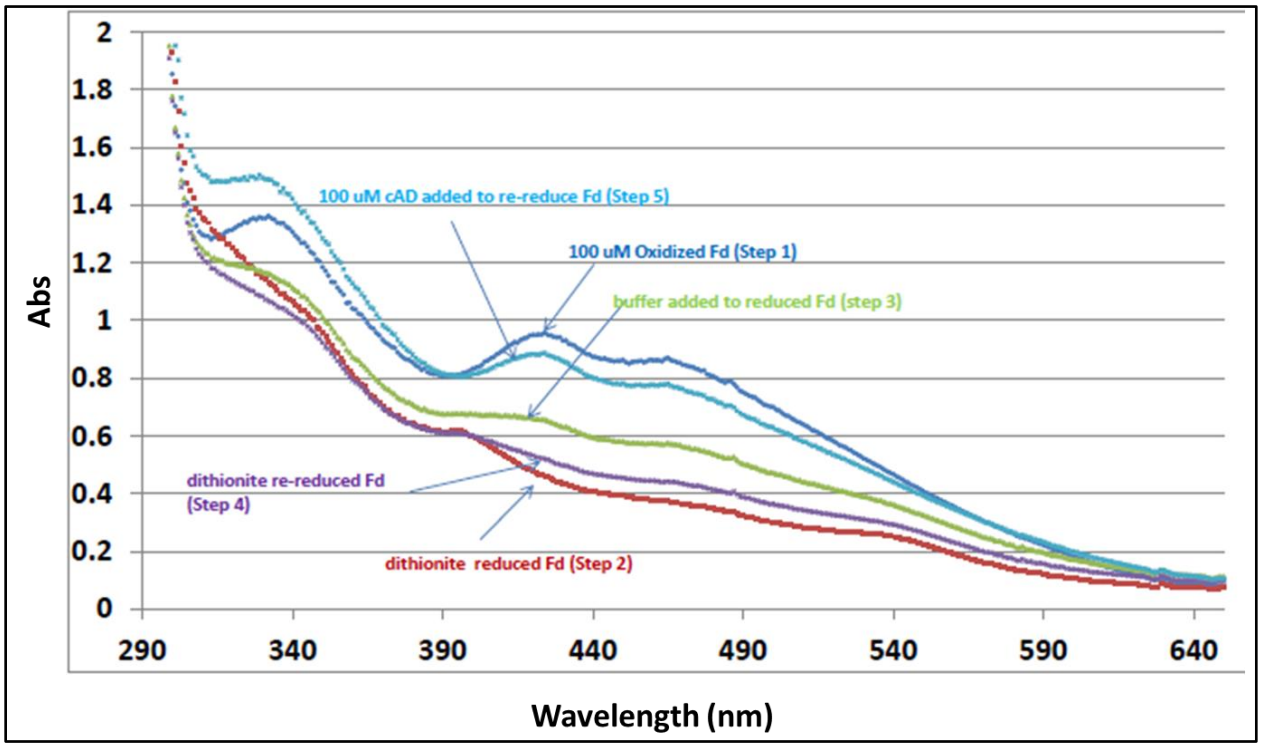

Figure 3.15. UV-Vis spectra of oxidized Fd (Step1), dithionite reduced Fd (Step 2) and cAD treated reduced-Fd (Step 5). As a control, reduced Fd also treated with anaerobic buffer (Step 3) to measure the extent of background oxidation.

Evidence of electron transfer from NADPH to cAD through FdR and Fd. UV-Vis spectroscopic studies were carried out using an anaerobic cuvette. For these experiments, 100 µM of NADPH and 1 µM of Fd was added to the buffer followed by addition of with 40 nM of FdR in a total volume 500 µL. Finally, cAD was added to the resulting mixture. Changes in the absorbance of NADPH at each step of addition of different components were followed at 340 nm (Figure 3.16). As control experiments, assays were also performed where Fd was omitted from the assays (Figure 3.17).

Measurements were taken every 5 seconds. After addition of NADPH and Fd to the buffer, measurements were taken for 3 min in order to estimate the rate of background oxidation of NADPH, then 40 nM FNR was added. The volume change was negligible due to this addition. The solution was monitored for another 7 min. No significant change in the absorbance of NADPH was observed. To the resulting solution, 30 µL of as-isolated *Np* cAD was added to make the final conc. of cAD 60 µM. Immediately after addition of the enzyme to the mixture, the absorbance of NADPH started decreasing and continued for the next 10 min until the rate of decrease became similar to the rate of background oxidation of NADPH. The net decrease in absorbance is almost equivalent to 14 µM NAHPH corresponding to reduction of 28 µM of total iron in cAD. It should be noted that the enzyme was ~30% loaded with iron, corresponding to ~36 µM iron in total. This observation implies the indirect electron transfer from NADPH to cAD through FdR and Fd. Interestingly, the depletion of NADPH seems to follow two different rates and each segment of depletion corresponds to ~7 µM of NADPH. This observation might suggest that the two iron centers in the di-iron center of cAD accept electron at a slightly different rate from ferredoxin. The NADPH depletion curve could also be fit with a first order kinetics. Control experiments, where Fd was omitted from the assay, did not lead to any net depletion of NADPH (Figure 3.17). This observation is also consistent with the Fd to be the mediator of electron transport from NADPH to cAD through FdR. Similar behavior was observed while assays were performed with holo-cAD and ratio of cAD:Fd was kept as 1:1.

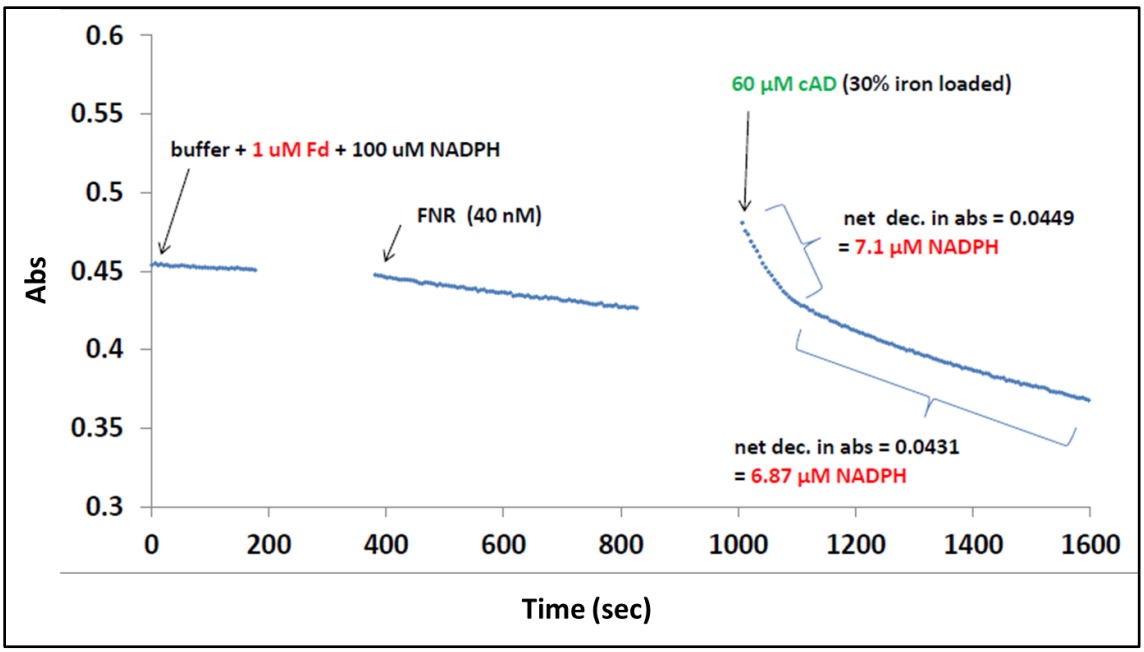

Figure 3.16. Evidence of electron transfer from NADPH to cAD through FdR and Fd. The electron transfer was monitored by measuring the depletion of NADPH at 340 nm.

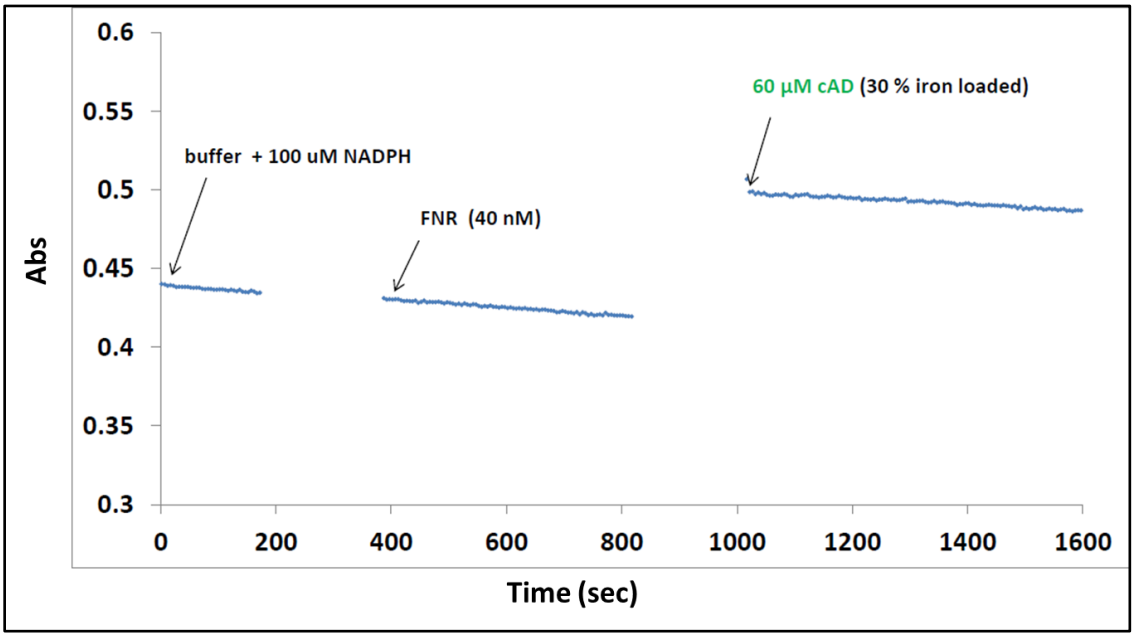

Figure 3.17. A control experiment where Fd was omitted from the assay did not show decrease in the absorbance of NADPH implying Fd works as a direct electron transfer mediator to cAD.

Further investigations were carried out to measure the activity of cAD indirectly by the following the consumption of NADPH. To test this, after reduction of cAD to the diferrous form using Fd and FdR, the reaction mixture was opened to air and an aerobic solution of substrate heptanal (500 µM final) was added. NADPH depletion could be observed from the subsequent time points but this decrease was almost identical with the decrease where aerobic buffer was substituted for heptanal in an otherwise identical assay (Figure 3.18). This suggests uncoupling of the reducing power of NADPH. Since the depletion of NADPH takes place after addition of aerobic buffer, most likely the reducing system reacts with molecular oxygen at a much faster rate rather than with cAD leading to uncoupling.

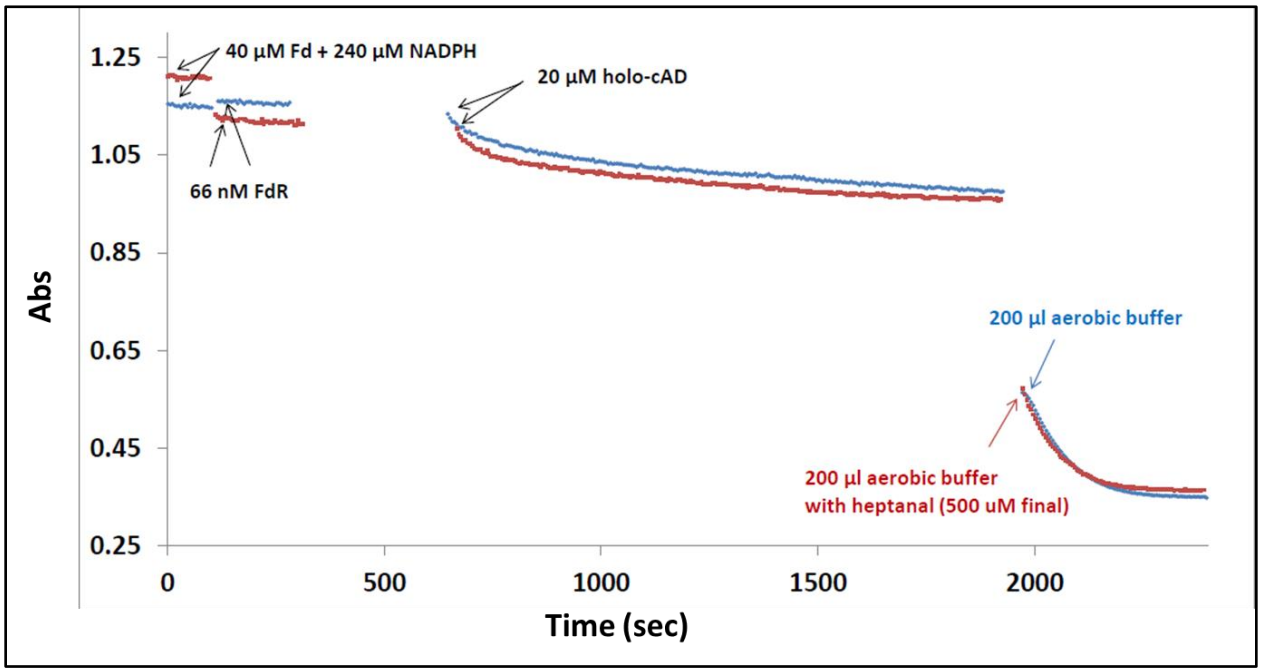

Figure 3.18. Comparison of assays where cAD was first reduced anaerobically by ferredoxin in presence of NADPH and FdR and then either aerobic solution of heptanal (in grey) or aerobic buffer (in blue) was added to the reaction mixture. No net depletion of NADPH could be observed due to the addition of substrate to the reaction mixture indicating a faster uncoupling of the reducing power of NADPH compared to electron transfer to cAD.

3.3.7 Cross-Linking of cAD with Fd

It has been shown in the literature that Fd can be cross linked with ferredoxin dependent enzymes and the coupled enzyme exhibit activity without the addition of free ferredoxin.[19] Therefore, crosslinking experiments of Fd with cAD was initiated using EDC (N-ethyl-3-(3-dimethylaminopropyl) carbodiimide) as the crosslinking agent.

The two proteins were mixed together in buffer made of 25 mM HEPES, pH 7. The ratio of Fd to cAD in the solution was 5:1. EDC was freshly made in the same buffer and added to the protein solution to a final concentration of 5 mM. The resulting mixture was mixed well, taken to the anaerobic chamber and incubated for 2 h at room temperature. The reaction was terminated by adding 0.1 M ammonium sulfate (final concentration). The resulting solution was concentrated using 3K amicon filter. The recovered protein was judged by SDS-PAGE gel. As can be seen from the gel (Figure 3.19), the crosslinking experiment resulted in the formation of a major band that was slightly higher in molecular weight compared to cAD. The size of the band matches with the expected size of 1:1 cAD-Fd complex (40 kDa). Some other higher molecular weight complexes were also be observed, which might have formed due to non-specific coupling by EDC. Since excess ferredoxin was employed during cross linking, some unreacted Fd was also observed. A control experiment, where Fd was omitted did not show any crosslinking.

Attempts to purify the cAD-Fd covalent complex were also made. The recovered product mixture from the cross linking experiment was passed through size exclusion superose 6 column using FPLC. A buffer of 50 mM Tris-HCl, pH 7.5 containing 200 mM KCl was used for elution. The flow rate was kept constant at 0.1 mL/min. Two peaks were obtained on the chromatogram. The peaks were collected separately and both of fractions had reddish-brown

color indicating both of them contain ferredoxin. Presumably the first peak from the size exclusion column would be the cAD-Fd complex and the second peak would be Fd. The first peak was judged by SDS-PAGE gel. A faint band which might be the cross-linked complex was detected from the gel (Figure 3.20).

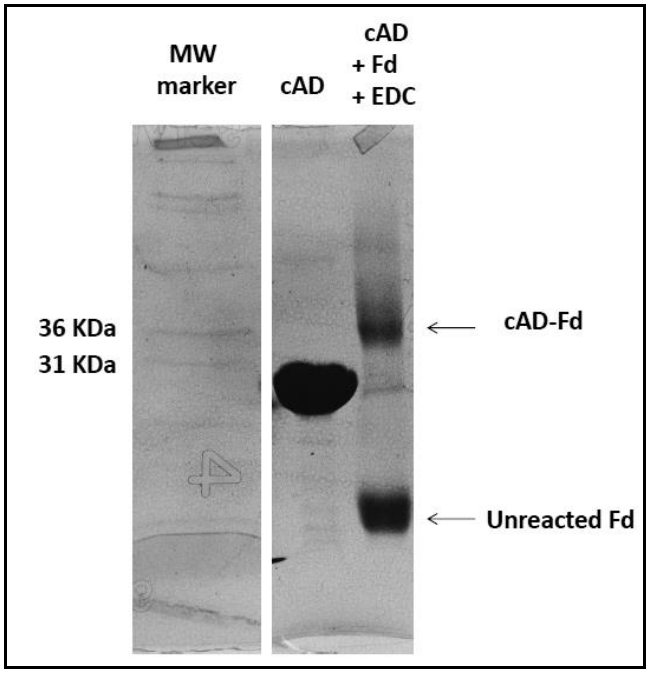

Figure 3.19. SDS-PAGE analysis of molecular wt. standards, a purified cAD and the 1:1 cAD-Fd. The cAD-Fd complex was obtained from the reaction of cAD with Fd in presence of EDC.

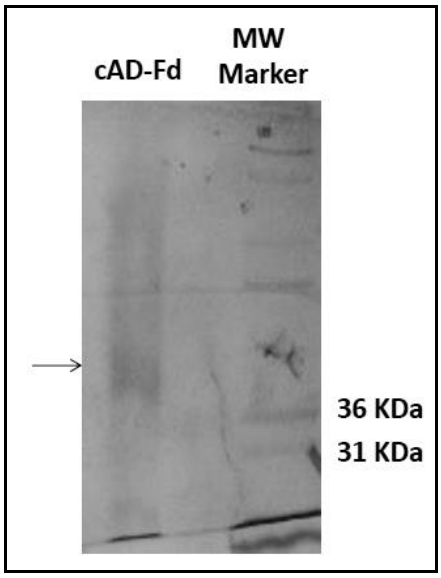

Figure 3.20. SDS-PAGE analysis showing purified fraction (a faint band) from cAD-Fd cross linking experiment and the molecular wt. marker.

Attempts to measure the activity of cAD-Fd cross-linked complex. After cross-linking cAD with Fd, and purifying the likely complex using size exclusion chromatography, attempts were made to examine whether the complex is active under optimized assay conditions. Assays were performed in 100 mM HEPES, pH 7.5 containing 20 mM NaCl in presence of 20 nM FdR, 1 mM NADPH and 2 mM heptanal with shaking at 37 °C for 5 min but unfortunately, no hexane formation was detected. Assays were also performed in buffers with different salt concentrations with longer assay time but no improvements could be made.

The inability of the cAD-Fd complex to exhibit any activity could be explained by the formation of non-specific complex between the two proteins by the action of EDC which is a non-specific coupling agent. Although apparently a 1:1 covalent complex was formed between Fd and cAD, the residues involved in the cross-linking are unknown. It might be possible that the surface residues on Fd that involve in the interaction with FdR participate in the crosslinking thus hindering the supply of electrons from NADPH to Fd. It would also be reasonable to

assume that the cross-linking would reduce the flexibility necessary for cAD to perform its catalysis. It might also be possible that the cross-linking with Fd blocks the substrate access channel of cAD therefore, inhibiting the activity. More studies need to be performed to verify these possibilities.

3.4 Conclusions

In summary, the role of biological electron carrier ferredoxins in the cycnobacterial aldehyde decarbonylase-catalyzed conversion of aldehydes to alkanes has been explored. It was verified that a reducing system made of Fd/FdR/NADPH supports the activity of cAD, although the activity is very sluggish (max ~1 turnover in one h). Therefore, investigations of the factors that might be responsible for the very poor activity of cAD in presence of Fd/FdR/NADPH were performed. First, native cyanobacterial ferredoxins were used as cofactors of cAD. Unfortunately, these experiments did not result in improved activity. To verify whether the expressed N-terminus His-tag on the proteins inhibited the interaction between cAD and Fd, the tag was removed from both the proteins and then assays were performed. Although this resulted in three fold improved activity, the activity was still quite poor. Therefore, the effect of salt concentration in the activity was carried out. Interestingly, lowering the salt concentrations in the buffer to 20 mM resulted in significant improvement in activity of cAD (~ 60 times, from ~1 turnover/h to ~1 turnover/min). This activity was very similar to the activity exhibited by cAD in presence of PMS/NADH reducing system in air saturated buffer. This suggests salt concentration (and possibly individual ions) plays a significant role for the activity of cAD in presence of Fd. Under improved assay conditions, spinach ferredoxin, which

supported very poor activity (~1 turnover in overnight - ~1 turnover/h), supported much improved activity (0.5 turnover/min) which is almost half of the activity supported by the native cyanobacterial ferredoxins. This suggests that cAD is not very specific for the native ferredoxin. After exploring enhanced activity of cAD in presence of ferredoxin, the interaction between the two proteins was examined. Transfer of electrons from Fd to cAD was followed in two ways. First, dithionite-reduced Fd was found to be oxidized immediately when incubated with cAD. Second, when cAD was added to the reaction mixture containing Fd, FdR and NADPH, depletion of NADPH was monitored: the extent of depletion of NADPH approximately matched the iron content in cAD. These experiments confirm the direct interaction between the two proteins, although the strength of the interaction could not be determined. Using EDC, cross linking experiments were performed. A 1:1 cross-linked complex of Fd and cAD was obtained. Unfortunately, the cross-linked complex was found to be inactive.

3.5 References

1. Cheesbrough, T. M., and Kolattukudy, P. E. (1984) Alkane biosynthesis by decarbonylation of aldehydes catalyzed by a particulate preparation from *Pisum sativum*, *Proc. Natl. Acad. Sci. USA. 81*, 6613–6617.
2. Dennis, M., and Kolattukudy, P. E. (1992) A cobalt-porphyrin enzyme converts a fatty aldehyde to a hydrocarbon and CO, *Proc. Natl. Acad. Sci. USA. 89*, 5306–5310.
3. Bernard, A., Domergue, F., Pascal, S., Jetter, R., Renne, C., Faure, J. D., Haslam, R. P., Napier, J. A., Lessire, R., and Joubes, J. (2012) Reconstitution of plant alkane biosynthesis in yeast demonstrates that Arabidopsis ECERIFERUM1 and ECERIFERUM3 are core components of a very-long-chain alkane synthesis complex, *Plant Cell 24*, 3106-3118.
4. Reed, J. R., Vanderwel, D., Choi, S. W., Pomonis, J. G., Reitz, R. C., and Blomquist, G. J. (1994) Unusual mechanism of hydrocarbon formation in the housefly: cytochrome-P450 converts aldehyde to the sex-pheromone component (Z)-9-tricosene and CO_2, *Proc. Natl. Acad. Sci. USA. 91*, 10000–10004.

5. Qui, Y., Tittiger, C., Wicker-Thomas, C., Le Goff, G., Young, S., Wajnberg, E., Fricaux, T., Taquet, N., Blomquist, G. J., and Feyereisen, R. (2012) An insect-specific P450 oxidative decarbonylase for cuticular hydrocarbon biosynthesis, *Proc. Natl. Acad. Sci. USA. 109*, 14858–14863.
6. Schirmer, A., Rude, M. A., Li, X. Z., Popova, E., and del Cardayre, S. B. (2010) Microbial biosynthesis of alkanes, *Science 329*, 559–562.
7. Warui, D. M., Li, N., Norgaard, H., Krebs, C., Bollinger, J. M., and Booker, S. J. (2011) Detection of formate, rather than carbon monoxide, as the stoichiometric coproduct in conversion of fatty aldehydes to alkanes by a cyanobacterial aldehyde decarbonylase, *J. Am. Chem. Soc. 133*, 3316–3319.
8. Das, D., Eser, B. E., Han, J., Sciore, A., and Marsh, E. N. G. (2011) Oxygen-independent decarbonylation of aldehydes by cyanobacterial aldehyde decarbonylase: a new reaction of di-iron enzymes, *Angew. Chem. Int. Ed. 50*, 7148–7152.
9. Andre, C., Kim, S. W., Yu, X. H., and Shanklin, J. (2013) Fusing catalase to an alkane-producing enzyme maintains enzymatic activity by converting the inhibitory byproduct H_2O_2 to the cosubstrate O_2, *Proc. Natl. Acad. Sci. USA. 110*, 3191–3196.
10. Knaff, D., B. (2004) Ferredoxin and Ferredoxin-Dependent Enzymes, *Advances in Photosynthesis and Respiration 4*, 333-361.
11. Hanke, G. T., Satomi, Y., Shinmura, K., Takao, T., and Hase, T. (2011) A screen for potential ferredoxin electron transfer partners uncovers new, redox dependent interections, *Biochim. Biophys. Acta 1814*, 366-374.
12. Kurisu, G., Kusunoki, M., Katoh, E., Yamazaki, T., Teshima, K., Onda, Y., Kimata-Ariga, Y., and Hase, T. (2001) Structure of the electron transfer complex between ferredoxin and ferredoxin-NADP(+) reductase, *Nat. Struct. Biol. 8*, 117-121.
13. Kimata-Ariga, Y., Sakakibara, Y., Ikegami, T., and Hase, T. (2010) Electron transfer of site-specifically cross-linked complexes between ferredoxin and ferredoxin-NADP(+) reductase, *Biochemistry 49*, 10013-10023.
14. Zhang, J., Lu, X., and Li, J. J. (2013) Conversion of fatty aldehydes into alk (a/e)nes by in vitro reconstituted cyanobacterial aldehydedeformylating oxygenase with the cognate electron transfer system, *Biotechnol. Biofuels 6*, 86.
15. Hirasawa, M., Rubio, L. M., Griffin, J. L., Flores, E., Herrero, A., Li, J., Kim, S. K., Hurley, J. K., Tollin, G., and Knaff, D. B. (2004) Complex formation between ferredoxin and Synechococcus ferredoxin: nitrate oxidoreductase, *Biochim. Biophys. Acta 1608*, 155-162.
16. Mayhew, S. G., Petering, D., Palmer, G., and Foust, G. P. (1969) Spectrophotometric titration of ferredoxins and Chromatium high potential iron protein with sodium dithionite, *J. Biol. Chem. 244*, 2830-2834.
17. Boll, M., and Fuchs, G. (1998) Identification and characterization of the natural electron donor ferredoxin and of FAD as a possible prosthetic group of benzoyl-CoA reductase (dearomatizing), a key enzyme of anaerobic aromatic metabolism, *Eur. J. Biochem. 251*, 946-954.
18. Lyle, K. S., Haas, J. A., and Fox, B. G. (2003) Rapid-mix and chemical quench studies of ferredoxin-reduced stearoyl-acyl carrier protein desaturase, *Biochemistry 42*, 5857-5866.

19. Sobrado, P., Lyle, K. S., Kaul, S. P., Turco, M. M., Arabshahi, I., Marwah, A., and Fox, B. G. (2006) Identification of the binding region of the [2Fe-2S] ferredoxin in stearoyl-acyl carrier protein desaturase: insight into the catalytic complex and mechanism of action, *Biochemistry 45*, 4848-4858.

Chapter 4

Probing the Mechanism of Cyanobacterial Aldehyde Decarbonylase using a Cyclopropyl Aldehyde

4.1 Introduction

The conversion of aldehydes to completely un-functionalized alkanes by aldehyde decarbonylase is a rare and a very poorly understood biological reaction.[1] Although the enzyme has been known for almost three decades,[2] its mechanism of action is not well-understood. The lack of information is partly due to the difficulties associated with isolation from the native organisms in sufficient quantities as the enzymes are membrane-associated proteins[2,3,4] and are not expressed in great quantities. Attempts at heterologous expression of these proteins have not been successful enough to allow purifying them to homogeneity and dissecting the mechanism of this unusual reaction.[5,4] But the recent discovery of a soluble version of aldehyde decarbonylase (cAD) from cyanobacteria,[6] has facilitated invstigation of the mechanism of this reaction. As it has been already described in Chapter 2, heterologous expression this enzyme in *E. coli* and purification resulted in high yields and allowed the reaction to be partially characterized. A central mechanics question that remains to be answered is how the bond between aldehyde carbon (C1) and α-carbon (C2) is cleaved. One plausible mechanism is proposed by Li et. al.[7] as shown in Scheme 4.1. This involves initial formation of a reactive iron-peroxo species due to the binding of molecular oxygen to the di-iron center of the enzyme

followed by attack at the aldehyde carbon. A one electron reduction leads to the formation of a hemiacetal radical, which is followed by scission of the C1-C2 bond. A subsequent proton-coupled electron transfer step reduces the alkyl radical to the alkane. A following two electron reduction of the di-ferric center results in the regeneration of the di-ferrous active site for the subsequent turnover. Although the mechanism is proposed based on the prior knowledge on di-iron chemistry with molecular oxygen in methane monoxygenase or ribonucleotide reductase, no evidence was shown to support the proposed steps until very recently, the di-iron peroxo intermediate was characterized in presence of the aldehyde substrate.[8]

Scheme 4.1. Proposed mechanism of action of cAD

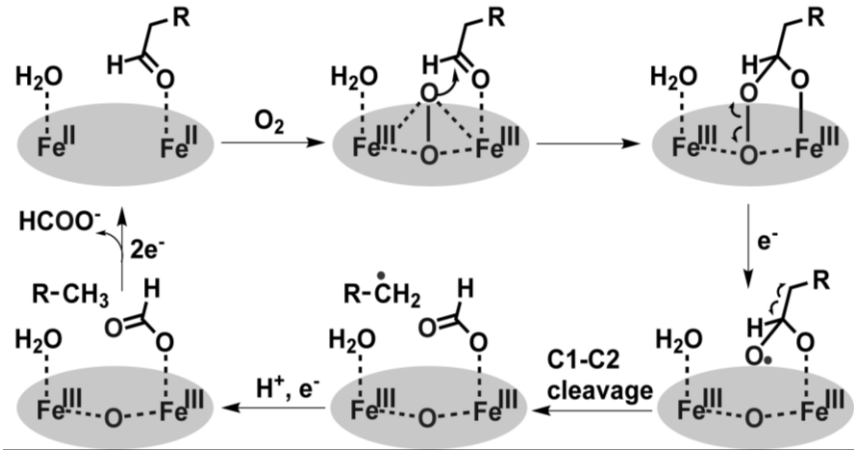

To obtain more insight into the mechanistic details, an investigation was initiated on the interaction of the substrate aldehyde with the di-iron active site of the enzyme using EPR spectroscopy. Furthermore, the mechanism of the C1-C2 bond scission step was examined by employing a substrate that incorporates a strategically placed cyclopropyl group that can act as a 'radical clock'.

The work described in this chapter was carried out in collaboration with Dr. Jaehong Han, Dr. Bekir Eser, Dr. Bishwajit Paul and Mr. Benjamin Ellington. Dr. Jaehong Han recorded and analyzed the EPR spectra. Dr. Bishwajit Paul synthesized the cyclopropyl analog of octadecanal and authentic product standards. Kinetic studies were performed by Mr. Benjamin Ellington. The work has been published in part in the *Angewandte Chemie International Edition,* **2011**, *50* (31), 7148-7152 and the *Journal of the American Chemical Society* **2013**, *135* (14), 5234-5237.

4.2 Materials and Methods

The EPR studies described in this chapter were performed with *Pm* cAD that was expressed and purified as described in Chapter 2. All the other studies were performed using cyanobacterial aldehyde decarbonylase from *Nostoc Punctiforme* PCC73012. Expression and purification of this enzyme is described in Chapter 3. This selection was solely based on the availability of the protein stock.

The materials and instrumentation used for cloning the gene in an expression vector, transforming *E. coli* with this construct, cell growth, protein purification and characterization were all the same as described in materials and methods section in Chapter 2. Commercial reagents were reagent grade and used without further purifications. 1-octadecene, pentadecanal, tetradecane were obtained from Sigma-Aldrich. For EPR analysis, quartz EPR tubes (4 mm OD, 707-SQ-250M) were obtained from Wilmad, Buena, NJ. The liquid helium tanks were obtained from Linde Cryogenics, USA. For LC-MS analysis, desalting was performed

using Zeba Spin Desalting column (2 mL, Thermo Scientific) following the manufacture's protocol. For MALDI-TOF and LTQ mass analysis, sequence grade trypsin and Glu-C were obtained from Promega (USA).

EPR experiments. EPR samples were prepared in an anaerobic glove box (Coy laboratory, MI) as described in Chapter 2 (the box had ~ 10-20 ppm O_2); all reagents used were deoxygenated and stored in the glove box for several hours. For a typical EPR sample, 425 μM (all concentrations are final) cAD was mixed with ferrous ammonium sulfate (800 μM) inside the glove box and incubated for ~10 min. Afterwards, substrate (600 μM) were added. The samples were allowed to incubate for periods varying between 5 and 30 min, depending upon the experiment. For spin-trap experiments, apo-cAD solution was incubated with ferrous ammonium sulfate before addition of the spin trap reagent α-phenyl-N-tert-butyl-nitrone (PBN) to a final concentration of 50 mM. ~250 μL of the sample was transferred to a quartz EPR tube and frozen in liquid nitrogen inside glove box. EPR spectra were recorded using a Bruker EMX EPR spectrometer equipped with a liquid nitrogen or liquid helium Dewar system. The data were analyzed using the Bruker Win-EPR data manipulation program. Spectra were recorded at 77 K (using liquid nitrogen) and 6 K (using liquid helium).

Synthesis of 2-(2-tetradecylcyclopropyl)-acetaldehyde. A potential 'radical clock', the cyclopropyl analogue of octadecanal, 2-(2-tetradecylcyclopropyl)-acetaldehyde (**1**) was synthesized by Dr. Bishwajit Paul. In the cyclopropyl aldehyde, cyclopropyl group was positioned at the β, γ-carbons to the carbonyl group. The detailed procedure of synthesis and the characterization of the compounds **1** are described in appendix A.

Enzyme assays. Assays were performed in 100 mM HEPES buffer, pH 7.2, containing 100 mM KCl and 10% glycerol as described previously.[9,10] Aldehydes substrates were made up as a stock solution in DMSO. A typical assay contained 10 µM cAD, 20 µM ferrous ammonium sulfate, 400 µM aldehyde substrate, 100 µM phenazine methosulfate (PMS) and 1 mM NADH in a total volume of 500 µL. Assays were shaken for 1 h at 37 °C at 200 rpm. Reactions were quenched by addition of 500 µL ethyl acetate and vortexed well to extract alkane products and un-reacted substrate. The ethyl acetate layer was separated and 8 µL sample of the ethyl acetate layer was injected into GC-MS for analysis.

GC-MS analysis. Gas chromatography-mass spectrometry analysis was performed using a Shimadzu QP-2010S GC-MS instrument equipped a quadrupole mass detector. A DB-5 column (Restek, 30m x 0.25 mm x 0.25 µm) was used for elution. The flow rate of the helium carrier gas was kept constant at 1 mL/min and the inlet temperature was maintained at 200 °C. The interface temperature was maintained at 250 °C. Injections were made in splitless mode. Oven temperature was held initially at 70 °C for 2 min and then gradually increased to 300 °C at 20 °C/min and finally maintained at 300 °C for 5 min. Data analysis was performed by GC-MS PostRun analysis software.

Formate assays. Fromate detection was carried out by Dr. Bishwajit Paul using 2-nitrophenylhydrazine (2-NPH) as a derivatizing agent as described in Chapter 2 with the following modifications: For derivatization, 40 µL of 120 mM 2-NPH solution (aqueous solution in 0.25 M HCl) and 40 µL of EDC working solution (300 mM EDC in 1:1 pyridine:HCl) was added to 400 µL the enzyme reaction and for elution using HPLC, the Nucleosil C18 RP HPLC column

(250 mm x 4 mm, 5 μM, 120 Å) column was equilibrated in 50 % water, (acidified with 0.05% AcOH) and 50 % methanol (acidified with 0.05% AcOH) and compounds were eluted with a gradient of 30% methanol to 90% methanol over 45 min at 0.7 mL/min.

LC-ESI-MS analysis. Inactivated cAD was analyzed by LC-ESI-MS using an Agilent 6520 LC - accurate-mass Q-TOF MS system. Assays were performed as described before. After 1 h of incubation of cAD with either cyclopropyl analogue of octadecanal or with octadecanal, 500 μL assay mixtures were directly applied to a desalting column (2 mL, Zeba spin desalting column) and centrifuged according to the manufacture's protocol to recover protein. The desalted samples were concentrated using Amicon Ultra 0.5 mL centrifugal filters (Millipore) to 100 μL final volume. 25 μL of a sample was reconstituted with the same volume of MiliQ water containing 0.1% formic acid. 5 μL of the sample was injected into a Poroshell 300SB-C8 column equilibrated with 0.1% formic acid and 5% acetonitrile. Proteins were eluted for 5 min with 95% water: 5% acetonitrile at 0.5 mL/min followed by an increase in gradient to 95% acetonitrile over 7 min at a constant flow rate of 0.5 mL/min. Eluting proteins were detected at 280 nm; cAD eluted with a retention time of 8.6 - 9.5 min. Mass data were obtained using intact protein mode and analyzed using Agilent MassHunter Qualitative Analysis software. The raw data was deconvoluted with respect to maximum entropy.

MALDI-TOF analysis. To perform this analysis, proteins were denatured with 8 M urea and reduced with 10 mM DTT followed by alkylation of the cysteine residues using 50 mM iodoacetamide. The resulting alkylated protein was diluted to lower the urea concentration to 1.5 M and treated with sequencing grade modified trypsin and Glu-C separately overnight at 37

°C. The proteolytic fragments were analyzed by Micromass TofSpec-2E MALDI-TOF mass spectrometry using reflectron mode. α-cyano-4-hydroxycinnamic acid (CHCA) was used as a matrix. The instrument was calibrated using an external reference of five standard peptide of known mass. Data were collected by Dr. Benjamin Buer.

LC-Tandem mass analysis. Analysis was performed by ion-trap mass spectrometer (LTQ-XL, ThermoFisher). Protein samples were digested as described for MALDI-TOF analysis. Digests were acidified with trifluoroacetic acid and peptides were purified using SepPak C18 cartridge (Waters). The resulting sample was injected into a C18 reverse phase column (Aquasil) equilibrated with 5% acetonitrile/1% acetic acid and peptides eluted with a linear gradient of increasing acetonitrile from 5 % to 60% over 40 min at a flow rate of 300 nL/min. The eluting peptides were directly introduced into ion-trap mass spectrometer (LTQ-XL) equipped with a nano-spray source. A full MS scan (m/z 400-2000) was acquired and the most abundant 6 ions were studied by MS/MS mode (relative collision energy ~ 35%). Raw files were searched against an *E. coli* database appended with the *Np* cAD sequence and a decoy database using X!Tandem (www.thegpm.org). The modification of phenylalanine, tyrosine, histidine, or glutamic acid, by a mass increment of 250.4 Da, together with methionine oxidation (+16 Da) and carbamidomethylation of cysteine (+ 57 Da) were considered as variables. The mass tolerance limit was set at 1 Da for precursor peptides and 0.5 Da for fragmented peptides. Results were further analyzed by Trans-Proteomic Pipeline (TPP) analysis, including PeptideProphet and ProteinProphet.[11]

4.3 Results and Discussion

4.3.1 EPR Experiments to Explore the Interaction of cAD with Substrate Aldehyde

To understand the nature of interaction of the substrate aldehyde with the enzme, EPR experiments were performed. We wanted to know whether the reaction involves any radical intermediate(s). The samples for the experiments were prepared by Dr. Bekir Eser. The samples were run by Prof. Jaehong Han who also processed the data.

Experiments were conducted in the absence of reducing system (PMS/NADH) to prevent turnover. Assays were performed with 425 µM holo cAD (prepared by adding Fe(II) to apo-cAD as described before). At 77 K the enzyme was EPR-silent, as expected for a di-ferrous iron center,[12] however, at 6 K, a broad peak appeared at g = 13 that is characteristic of diferrous center. Addition of substrate heptanal, 600 µM, to holo-cAD resulted in the appearance of a signal at g = 4.3 characteristic of a high-spin ferric ion. Heptanal, rather than octadecanal, was used in this experiment due to its higher solubility. This observation suggests partial oxidation of Fe(II) to Fe(III), which should also be accompanied by an organic radical either substrate or protein derived. However, the expected organic radical could not be directly detected. Support for the generation of an organic radical came from experiments in which the spin-trapping agent *N*-*tert*-Butyl-α-phenylnitrone (phenyl-N-t-butylnitrone, PBN), which has been used to trap radical intermediates in other enzyme reactions,[13] was included in the reaction. The ferric signal is now accompanied by a characteristic signal for the PBN nitroxide radical-adduct at g = 2 (Figure 4.1). The hyperfine structure of the nitroxide radical is broadened, indicating that it results from PBN intercalated within the protein,[13] rather than free in solution. This is

consistent with PBN reacting with the substrate radical, or possibly a protein-based radical. (Scheme 4.2). Addition of PBN in the absence of heptanal (Figure 4.1, spectrum d) appears to result in some oxidation of Fe(II), but very little radical-adduct is observed.

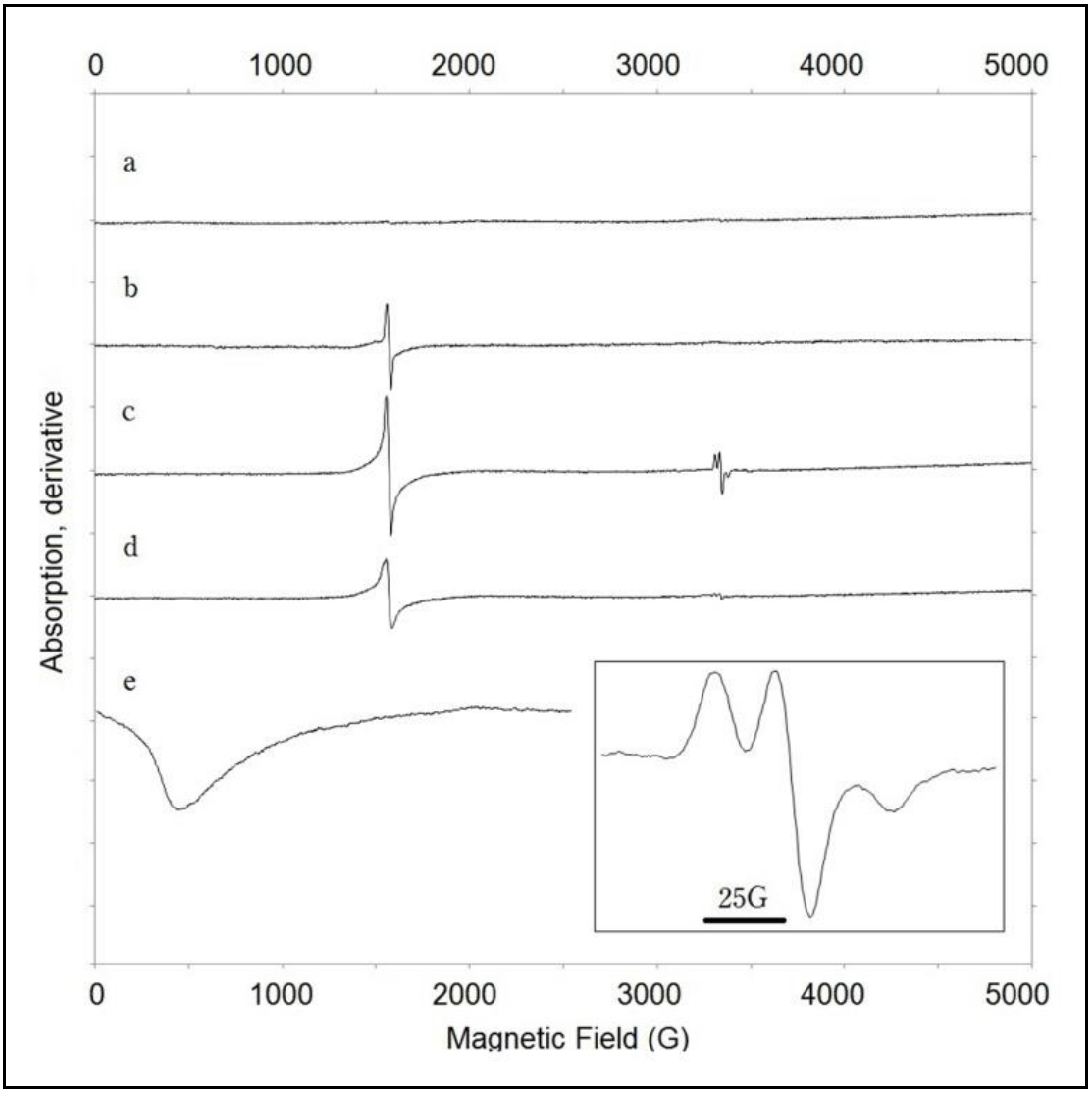

Figure 4.1. EPR spectra of cAD prepared under anaerobic conditions: a) apo-cAD reconstituted with Fe(II) to form di-ferrous enzyme; b) addition of heptanal to di-ferrous cAD; c) addition of heptanal and spin trapping reagent PBN to di-ferrous cAD. inset: expansion of g = 2 region of this spectrum showing PBN radical-adduct; d) addition of PBN only to di-ferrous cAD resulted in some oxidation of Fe(II), which might be due to oxygen contamination or transfer of electron from Fe(II) to PBN. e) spectrum of di-ferrous enzyme ion at 6 K (20 mW microwave power). All spectra except e) were recorded at 9.395 GHz; microwave power, 2 mW; modulation amplitude, 16 G; temperature, 77 K, and are plotted on the same scale.

Further experiments need to be performed to quantify the radical generated due to the interaction of the substrate with cAD. Power-dependence experiments also need to be carried out since the existing experiments were performed using a high microwave power.

Scheme 4.2. PBN reacts with organic radicals to generate a relatively stable PBN nitroxide radical-adduct

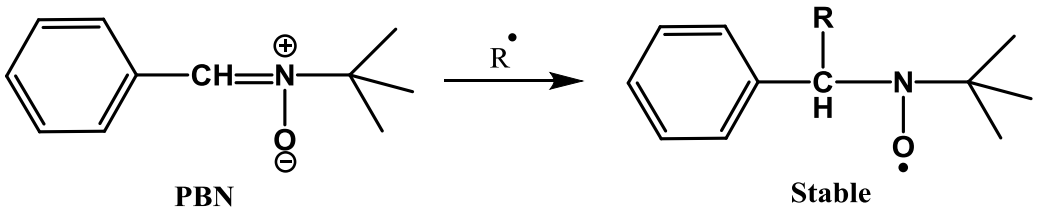

4.3.2 Cyclopropyl Analog of Octadecanal as a Substrate of cAD

'Radical clock' substrates are excellent tools to indirectly measure the lifetime of radical intermediates. In a radical clock substrate, a cyclopropyl group is placed adjacent to the carbon atom where the proposed radical might generate. Cyclopropylcarbinyl radicals, once formed, undergo rapid and very well characterized ring-opening reactions.[14] Cyclopropyl compounds have been extensively employed to investigate the mechanisms of cytochrome P450 enzymes[14, 15] and non-heme iron enzymes including methane monooxygenase,[16] isopenicillin N synthase[17] and, most recently, HppE ((S)-2-Hydroxypropylphosphonic acid epoxidase) enzyme that catalyzes epoxide formation in the biosynthesis of fosfomycin.[18] Depending upon the lifetime of the postulated alkyl radical intermediate, one would expect to observe either retention of the cyclopropyl ring in the product, if either the radical is very short lived or the reaction is concerted, or ring-opening if the radical intermediate is relatively long-lived.

To investigate the mechanism of cAD, the radical clock substrate, cyclopropyl analog of octadecanal (Scheme 4.3) was synthesized by Dr. Bishwajit Paul. Most of the kinetic assays were performed by Mr. Benjamin Ellington.

Scheme 4.3. Structure of 2-(2-tetradecylcyclopropyl)-acetaldehyde (**1**) used in these studies

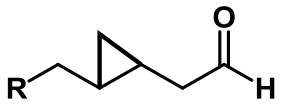

(R = -$C_{13}H_{27}$)

Formation of 1-octadecene as the rearranged product. When *Np* cAD was incubated with the cyclopropyl aldehyde in assay buffer containing 100 mM HEPES buffer, pH 7.2, containing 100 mM KCl and 10% glycerol, the product formed was not the deformylated alkane as observed for linear aliphatic aldehydes. The retention time of the product formed from the enzyme reaction on gas chromatography and the mass spectrum did not match an authentic standard of 1-ethyl-2-tetradecylcyclopropane, the deformylated cyclopropyl aldehyde. Rather, the mass spectra of the product matched with 1-octadecene and an authentic 1-octadecene standard co-eluted with the product. Formation of 1-octadecene was dependent on the enzyme, the reducing system and molecular oxygen. Omission of any one of these reaction components completely abolished the activity. These results confirm the formation of 1-octadecene as the enzymatic product. This observation also supports the generation of a radical intermediate at the adjacent carbon to the cyclopropyl group due to cleavage of the aldehyde C1-C2 bond. The rate constant of rearrangement of cyclopropylcarbinyl radical is k = 8.6 X 10^7 s^{-1} at 298 K.[15] Accordingly, formation of the rearranged product 1-octadecene also indicates that the lifetime of the

intermediate radical formed is ≥ 10 ns so that the radical has time to undergo rearrangement via cyclopropyl ring opening (Scheme 4.4).

Scheme 4.4. Enzymatic conversion of cyclopropyl aldehyde to 1-octadecene through a radical intermediate with lifetime ≥ 10 ns

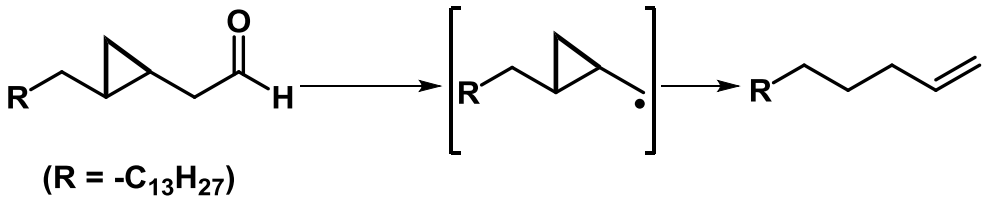

(R = -$C_{13}H_{27}$)

Identification of formate as co-product in reaction of 1 with cAD. Formate was shown to be the co-product of cAD-catalyzed reaction of octadecanal. The cleavage of octadecanal produced a ~1:1 ratio of heptadecane and formate. Therefore, formate seemed a reasonable candidate as a co-product of 1-octadecene from cyclopropyl aldehyde. Assays were performed and the resulting reaction mixture was treated with 2-NPH as described in the material and methods section. The hydrazide derivative of formate was eluted at ~28 min and detected at 230 nm (Figure 4.2). Formate was produced at equimolar ratio with 1-octadecene.

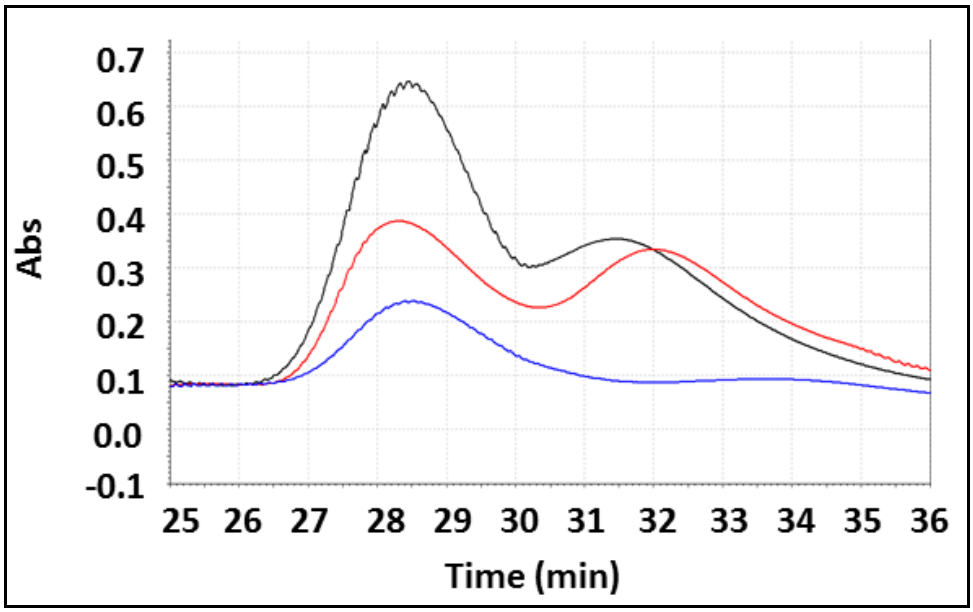

Figure 4.2. Overlaid HPLC traces of 2-NPH derivatives of authentic formate (in blue), *Np* cAD reaction product with cyclopropyl compound **1** (red) and *Np* cAD reaction product with octadecanal (black) at 230 nm. 2NPH-formate derivative elutes at retention time of ~28 min. Fractions were collected and studied by ESI-MS (negative mode). Identity of each formate derivative was confirmed by obtained mass of *m/z* = 180.1.

Inhibition of cAD by cyclopropyl aldehyde. Unlike the octadecanal that underwent multiple turnovers, the cyclopropyl aldehyde did not show more than one equivalent of product formation (w.r.t cAD) under identical assay conditions. Formation of equivalent of product is appeared to be a coincidence. A time course of 1-octadecene formation revealed a first order rate of product formation up to 1 turnover followed by a plateau region of no further increase in the product formation (Figure 4.3).

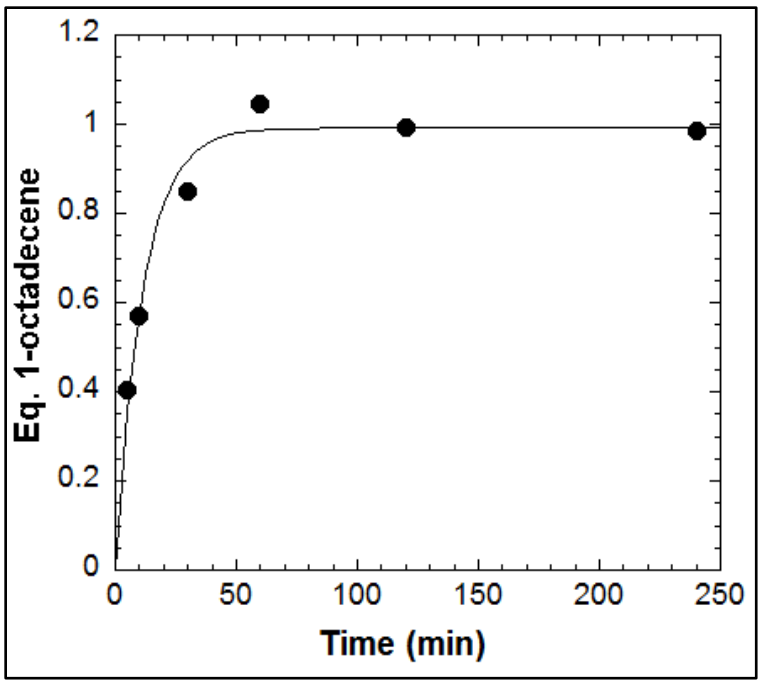

Figure 4.3. Time course of 1-octedecene formation from cyclopropyl aldehyde **1,** by cAD.

This observation was interesting as it deviated from the normal behavior of cAD and indicated that there is a possibility of inhibition of cAD by the cyclopropyl substrate. To determine whether the enzyme was inactivated, cAD was incubated with **1,** 400 µM, in presence of Fe^{2+}, PMS, NADH and O_2. The reaction mixture was shaken for 1 h at 37 °C and then the authentic substrate, octadecanal, 400 µM, was added. The assay mixture was shaken for an additional 1 h, alkanes extracted with ethyl acetate and product formation was quantified by GC-MS. ~1-equivalent (w.r.t cAD) of 1-octadecene was formed whereas less than 0.1 equivalents of heptadecane were formed (Figure 4.4 I). As a control experiment, cAD was similarly incubated with the alternative substrate pentadecanal, 400 µM, for 1 h and then assayed with octadecanal for an additional 1 h ~6.5 equivalents of tetradecane and ~4 equivalents of heptadecane were

formed (Figure 4.4 II), demonstrating that the inactivation of cAD was not due to non-specific loss of activity during turnover. These experiments indicate irreversible inactivation of cAD by the cyclopropyl aldehyde.

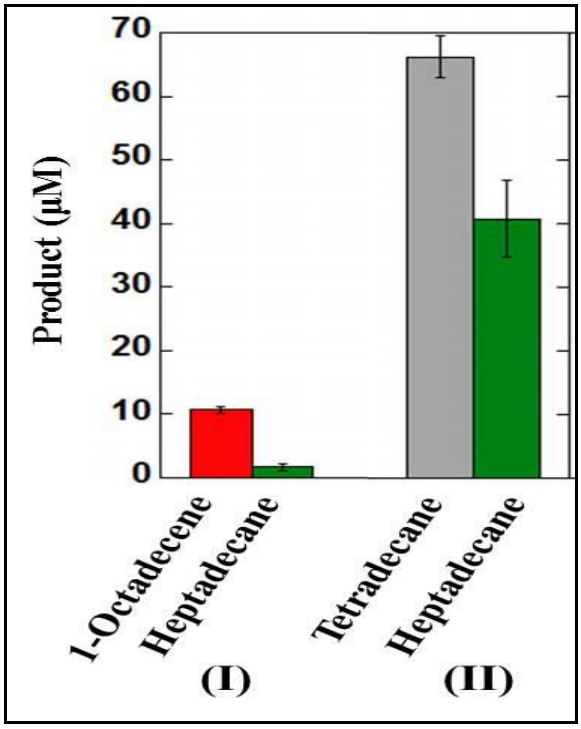

Figure 4.4. (I) Incubation of cAD with **1** for 1 h followed by octadecanal for 1 more h resulted in formation of 1 equivalent of 1-octadecene and almost no heptadecane; (II) Incubation of cAD with an alternate substrate pentadecanal for 1 h followed by octadecanal for 1 more h redulted in formation of ~6.5 eq. of tetradecane and ~4 eq. of heptadecane.

4.3.3 Covalent Modification of cAD by Cyclopropyl Aldehyde

To gain further insight into the mechanism of inactivation, the inactivated cAD was investigated by LC-ESI-MS. As a control experiment, cAD was also incubated with octadecanal under the same conditions and examined. The goal was to identify if there was covalent modification of the protein that could lead to inactivation.

Identification of covalent modification on inactivated cAD. The mass of cAD prior to reaction with **1** was determined as 28911 ± 0.5 Da (Figure 4.5), in excellent agreement with the calculated molecular weight. The mass of cAD incubated with octadecanal was also 28911 ± 0.5 Da (Figure 4.6) that was identical to the mass of as-isolated cAD. However, incubation of cAD with **1** resulted in ~60 - 80 % of the recovered enzyme eluting from the column as a modified species characterized by a slightly longer retention time and a molecular weight of 29162 ± 0.5 Da (Figure 4.7). The increase in molecular weight of 251 ± 0.5 Da was consistent with the formation of a covalent adduct between decarbonylated **1** and cAD that leads to enzyme inactivation.

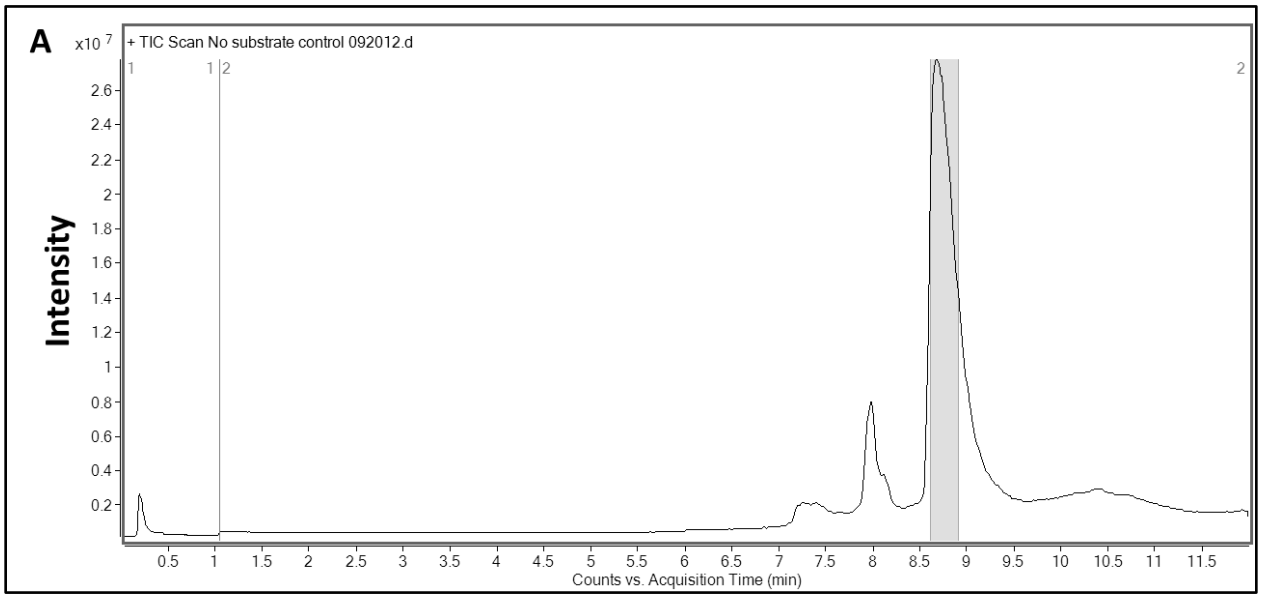

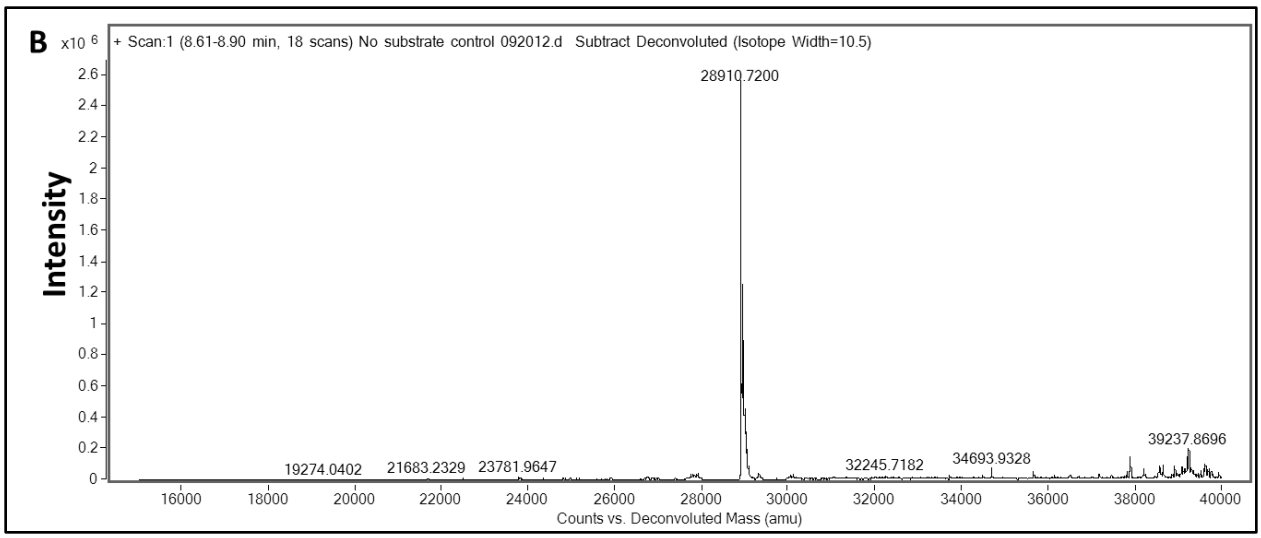

Figure 4.5. Reverse phase liquid chromatogram and mass spectral analysis of *Np* cAD. A. Total ion chromatogram (TIC) B. Deconvoluted mass spectrum of as-isolated *Np* cAD. Highlighted region of A was extracted for mass spectral analysis. *Np* cAD elutes as a single peak with retention time 8.6 to 9.2 min. Mass of *Np* cAD is 28911 ± 0.5 Da.

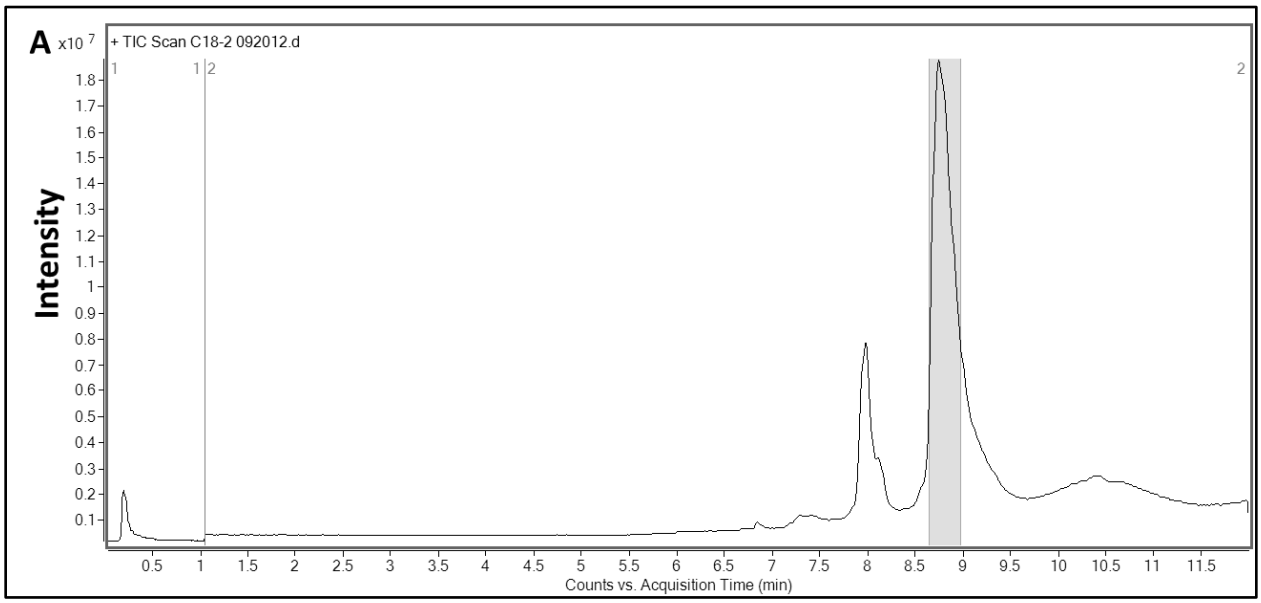

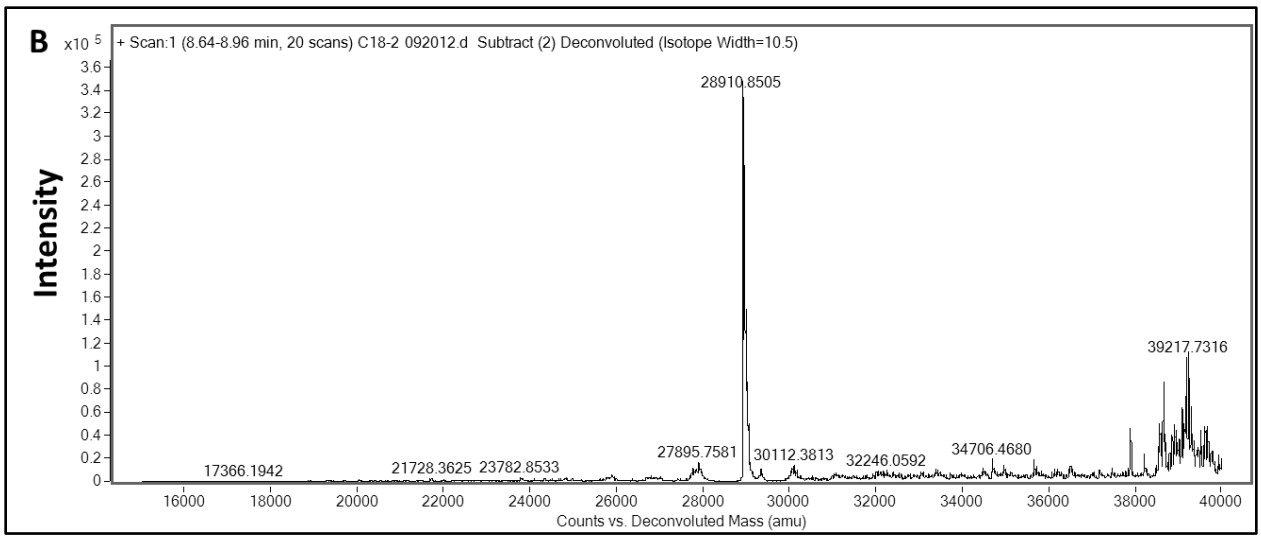

Figure 4.6. Reverse phase liquid chromatogram and mass spectral analysis of *Np* cAD reacted with 1-octadecanal. A. Total ion chromatogram (TIC) B. Deconvoluted mass spectrum of 1-octadecanal-reacted *Np* cAD. Highlighted region of A was extracted for mass spectral analysis. Octadecanal-reacted *Np* cAD elutes as a single peak with retention time 8.6 to 9.2 min. The M_r of octadecanal-reacted *Np* cAD was 28911 ± 0.5 Da which was indistinguishable from as-isolated *Np* cAD.

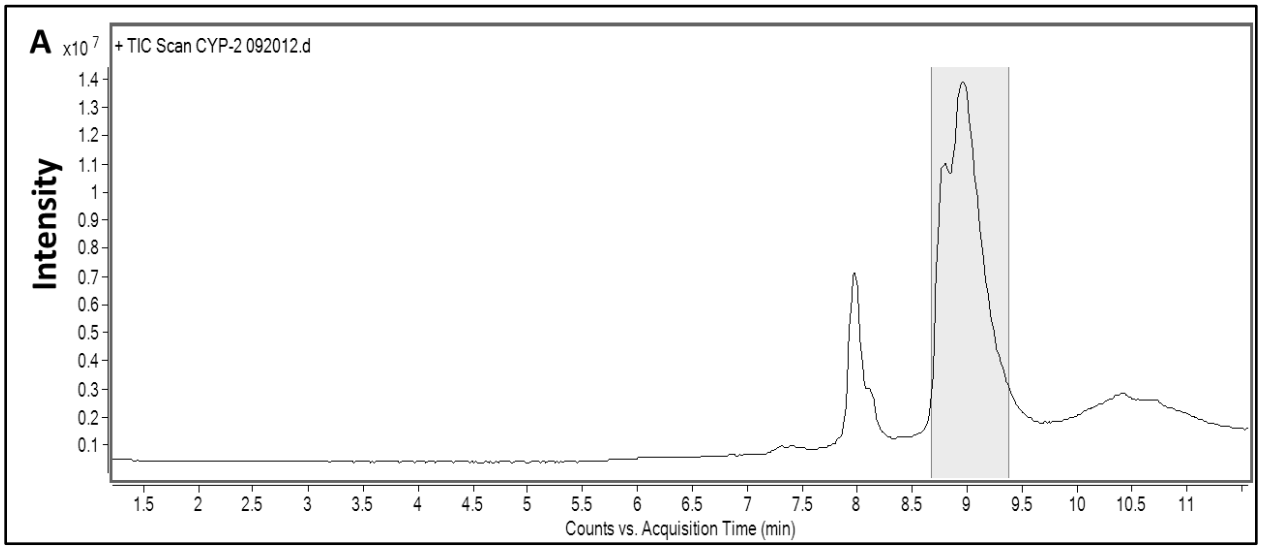

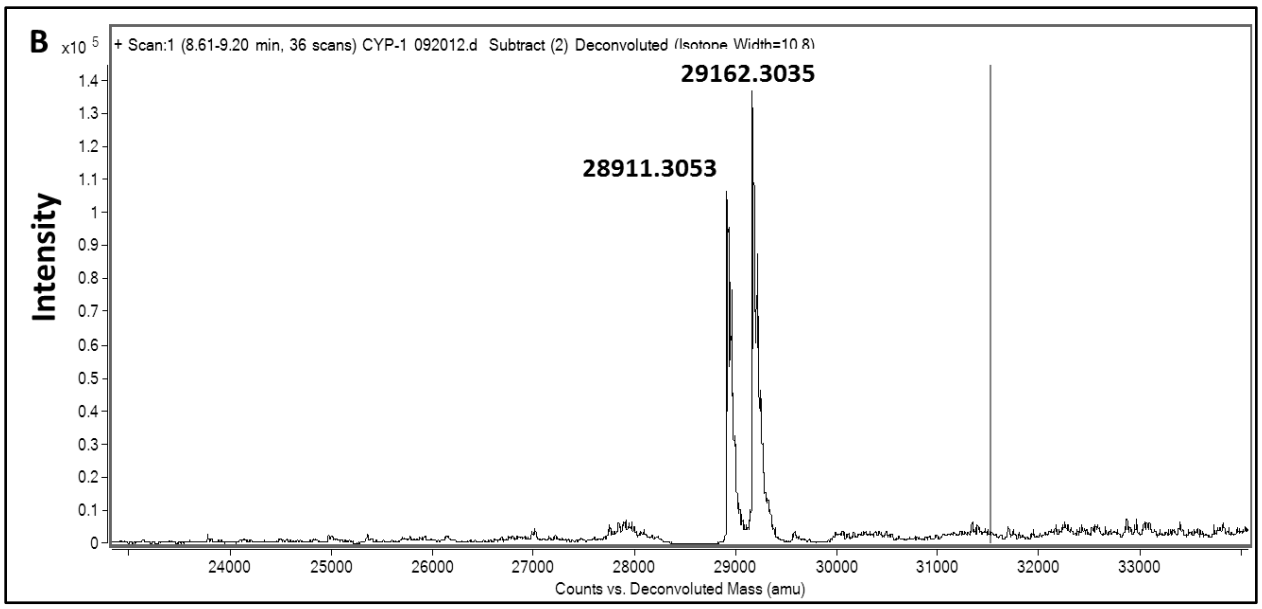

Figure 4.7. Reverse phase liquid chromatogram and mass spectral analysis of *Np* cAD incubated with cyclopropyl substrate **1.** A. Total ion chromatogram (TIC) showing both unmodified and modified protein. B. Deconvoluted mass spectrum of *Np* cAD reacted with **1**. Highlighted region of A was extracted for mass spectral analysis. *Np* cAD reacted with **1** shows two peaks; one peak with the same retention time as unmodified *Np* cAD and another peak with slightly higher retention time with a higher M_r of 29162 ± 0.5 Da. The increase in molecular weight of 251 ± 0.5 Da is consistent with the formation of a covalent adduct between decarbonylated **1** and cAD.

4.3.4 Determination of the Location of Covalent Modification

To further investigate the pathway and the location of the covalent modification, MALDI-TOF and LC-tandem mass analysis were carried out. For this purpose, samples of the inactivated and unmodified enzyme were digested using trypsin (a serine protease that cleaves after lysine and arginine) and Glu-C (a serine protease that cleaves after glutamates and aspartates) and the proteolytic digests were investigated.

Amino acid sequence of His-tagged *Np* cAD:

MHHHHHHSSGVDLGTENLYFQSNAQQLTDQSKELDFKSETYKDAYSRINAIVIEGEQEAHENYITLAQLLPES
HDELIRLSKMESRHKKGFEACGRNLAVTPDLQFAKEFFSGLHQNFQTAAAEGKVVTCLLIQSLIIECFAIAAYNI
YIPVADDFARKITEGVVKEEYSHLNFGEVWLKEHFAESKAELELANRQNLPIVWKMLNQVEGDAHTMAMEK
DALVEDFMIQYGEALSNIGFSTRDIMRLSAYGLIGA

MALDI-TOF data analysis. To determine the location of the covalent modification, spectra of the modified and unmodified enzyme digests were compared using MALDI-TOF spectroscopy. Analysis of the spectra of unmodified enzyme identified two peptides, one Glu-C-derived (Figure 4.8), the other trypsin-derived (Figure 4.9), which were absent from the spectra of the covalently modified enzyme. Significantly, the peptides overlapped in sequence and encompassed a 20-residue segment, CFAIAAYNIYIPVADDFARK that forms part of the hydrophobic substrate-binding channel of cAD.

Unfortunately, direct detection of the alkylated peptides by MALDI-TOF mass spectrometry was not possible. However, it is commonly observed that hydrophobic peptides are under-represented or absent in "bottom up" proteomic analyses of proteins.[19] This may be attributed to loss of hydrophobic peptides during sample preparation steps prior to MS analysis; there is also the potential for the modification to interfere with the proteolytic digestion of the peptide, and/or adversely affect its ability to ionize in the mass spectrometer.

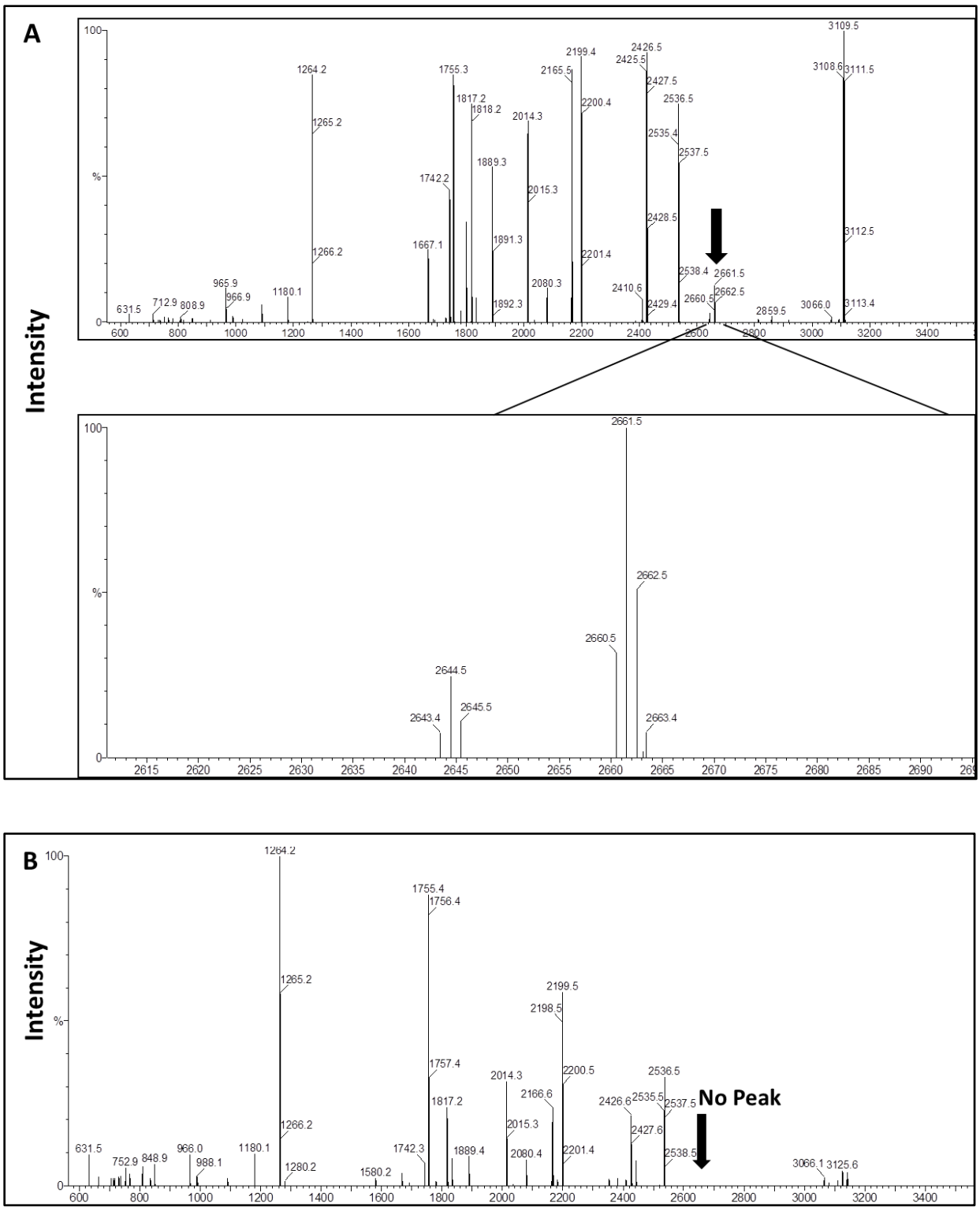

Figure 4.8. MALDI spectrum of GluC digests of *Np* cAD (A) and **1** treated *Np* cAD (B). Black arrow on spectrum **A** shows the peak of interest with mass 2661.5 Da that represents

carbamidomethylated CFAIAAYNIYIPVADDFARKIT peptide fragment that is absent in spectrum **B**.

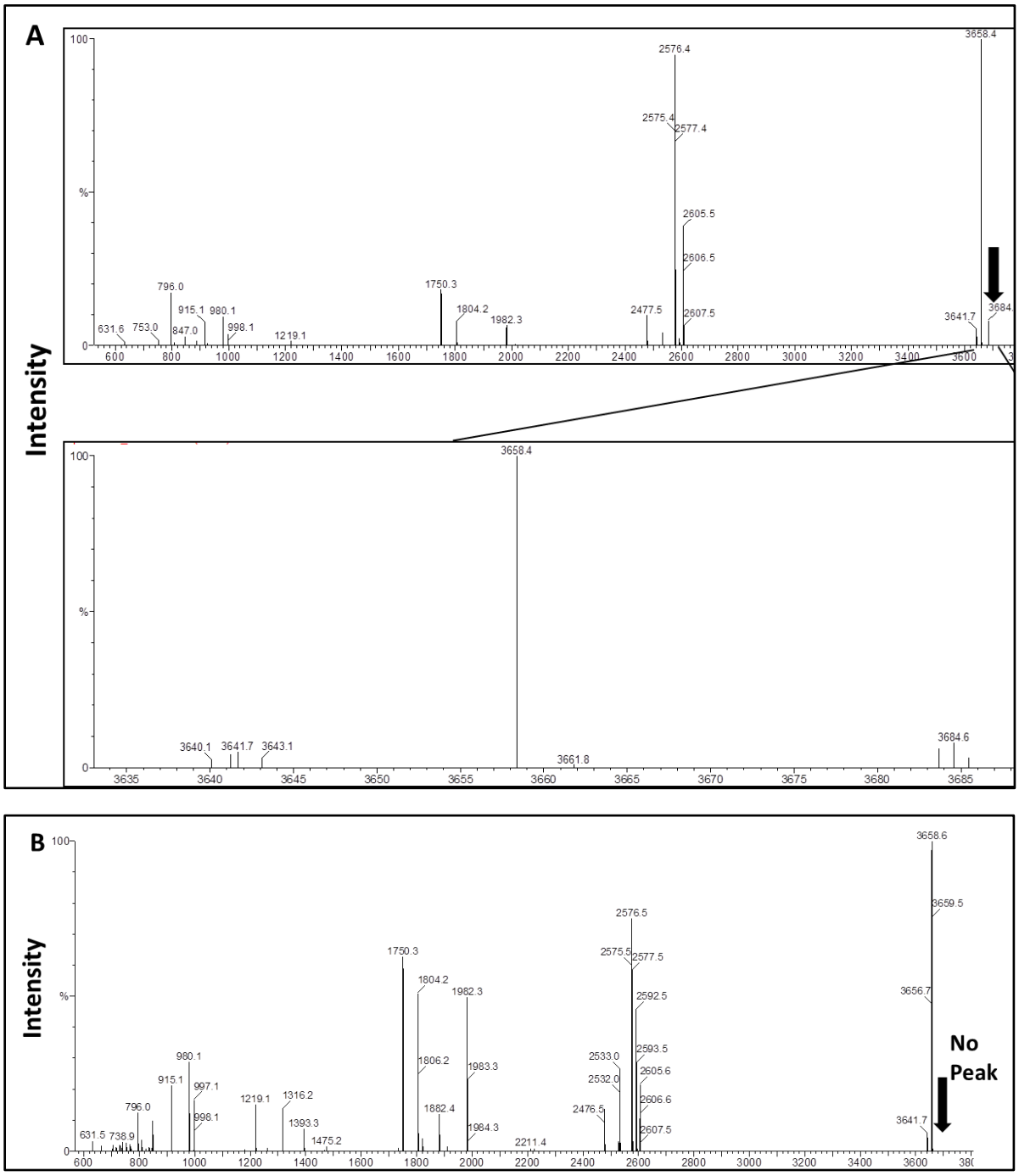

Figure 4.9. MALDI spectrum of trypsin digests of *Np* cAD (A) and 1 treated *Np* cAD (B). Black arrow on spectrum A shows the peak of interest with mass 3684.6 Da that represents VVTCLLIQSLIIECFAIAAYNIYIPVADDFARK peptide fragment that is absent in spectrum B.

LC-Tandem mass analysis. To directly identify the location of covalent modification, extensive LC-Tandem mass analysis was carried out in collaboration with Dr. V. Basrur at the University of Michigan Proteomics Facility. The digested peptides (prepared as described before for MALDI-TOF analysis) were examined by tandem mass spectrophotometer (ES-MS/MS).

These analyses succeeded in identifying one covalently modified peptide IECFAIAAYNIYIPVAADDFAR, which was present in low-abundance in the tryptic digest. The mass of the peptide was 557.8 Da more than the calculated mass. In this peptide, the highlighted Glu105, Cys106 and Phe107 residues were found to be potentially modified. The cysteine residue was modified with a mass of 57 Da that arose due to carbamidomethylation as a result of treatment of the sample with iodoacetamide during sample preparation. The phenylalanine and glutamate residues were modified with an additional mass of 251 Da. This data suggests that the deformylated species (mass = 251 Da) generated from the cyclopropyl aldehyde undergoes covalent attachment to the phenylalanine and/or glutamate. However, the presence of $b5^{++}$ (in blue, 561.6836 Da) and $y19^{+++}$ (in red, 814.2336 Da) ions in the secondary mass spectrum was more consistent with Phe107 being modified by an additional mass of 251 Da (Figure 4.10). The grey lines indicate the expected mass peaks.

IECFAIAAYNIYIPVAADDFAR, MH+ 2933.2853

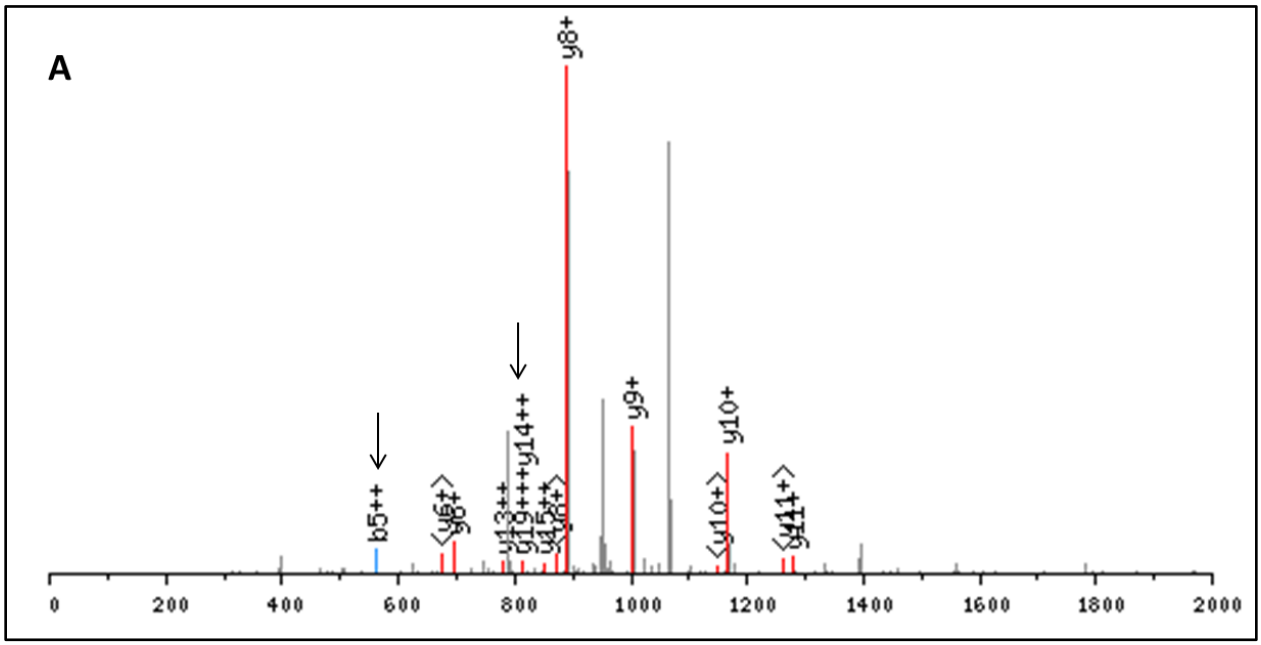

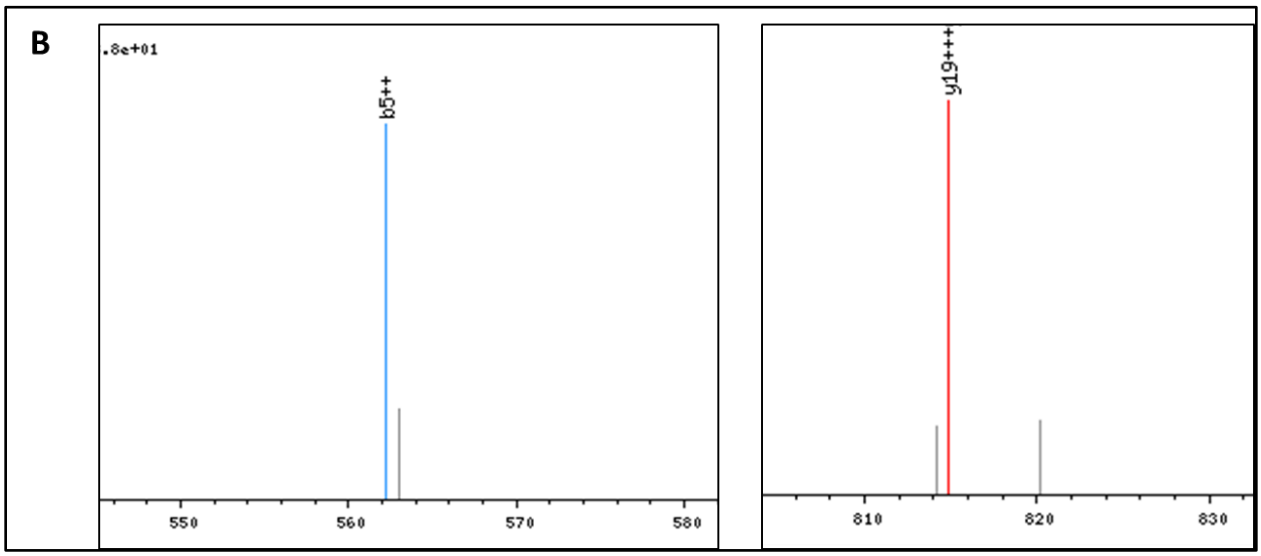

C

b^+	b^{2+}	#	AA	#	y^+	y^{2+}	y^{3+}
114.0913	57.5496	1	I	21			
493.6068	247.3073	2	E	20	2820.2007	1410.6043	940.7388
653.7456	327.3767	3	C	19	2440.6852	1220.8465	**814.2336**
1051.3222	526.1650	4	F	18	2280.5464	1140.7771	760.8540
1122.3594	**561.6836**	5	A	17	1882.9698	941.9888	628.3285
1235.4434	618.2256	6	I	16	1811.9327	906.4702	604.6494
1306.4805	653.7442	7	A	15	1698.8486	**849.9282**	566.9547
1377.5176	689.2627	8	A	14	1627.8115	**814.4097**	543.2757
1540.5810	770.7944	9	Y	13	1556.7744	**778.8911**	519.5967
1654.6239	827.8159	10	N	12	1393.7110	697.3594	465.2422
1767.7080	884.3579	11	I	11	**1279.6681**	640.3380	427.2279
1930.7713	965.8896	12	Y	10	**1166.5841**	583.7959	389.5332
2043.8554	1022.4316	13	I	9	**1003.5207**	502.2643	335.1788
2140.9081	1070.9580	14	P	8	**890.4367**	445.7222	297.4841
2239.9765	1120.4922	15	V	7	793.3839	397.1959	265.1332
2311.0137	1156.0107	16	A	6	**694.3155**	347.6617	232.1104
2426.0406	1213.5242	17	D	5	623.2784	312.1431	208.4313
2541.0675	1271.0377	18	D	4	508.2514	254.6296	170.0890
2688.1360	1344.5719	19	F	3	393.2245	197.1162	131.7467
2759.1731	1380.0904	20	A	2	246.1561	123.5819	82.7239
		21	R	1	175.1190	88.0634	59.0449

Figure 4.10. *Linear trap quadrupole (LTQ)* mass spectral analysis of trypsin digests of *Np* cAD after reaction with **1**. **A**. Mass spectrum of the peptide fragment IECFAIAAYNIYIPVADDFAR. **B**. Presence of b5++ and y19+++ ions is consistent with F107 residue of *Np* cAD modified with the alkane chain. **C.** Expected (in grey) and observed (in blue and pink) peptide ions from the tryptic peptide fragment with different charges.

Additional support for this claim came from the crystal structure of cAD. The crystal structure of *Np* cAD has not been solved, however, the structure of cAD from *Prochlorococcus marinus* MIT9313 (*Pm* cAD, PDB ID 2OC5A) has been solved as part of a structural proteomics project.[20] An alignment of the sequences of these two proteins revealed 62% sequence identity and 79% sequence similarity, indicating a high degree of structural similarity. Phe107 in *Np* cAD is conserved in *Pm* cAD (Phe130) and in all other known cAD sequences. Based on the structure of *Pm* cAD (Figure 4.11), Phe107 forms part of the hydrophobic substrate binding channel. The residue would be within ~5 Å of the putative alkyl radical formed by the opening of the cyclopropyl ring of **1.** These results suggested that the reaction of the product alkyl radical with the phenylalanine ring resulted in the covalent attachment of the alkyl fragment to the protein, thereby inactivating the enzyme.

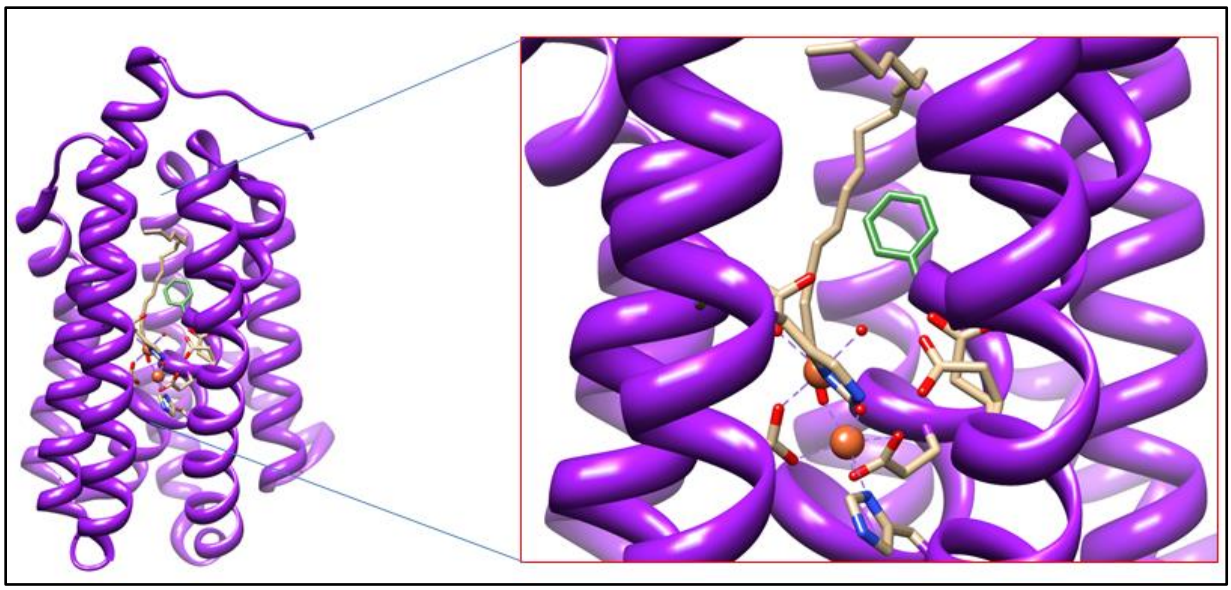

Figure 4.11. Crystal structure of cAD from *Prochlorococcus marinus* MIT9313 (PDB ID 2OC5A) showing di-iron active site and co-crystalized long chain fatty acid. The phenylalanine residue, shown in green, most likely undergoes covalent modification after incubation of cAD with cyclopropyl aldehyde **1**.

Another possible mechanism of inactivation. Covalent modification of cAD by cyclopropyl aldehyde did not lead to 100% covalently modified protein. Rather, a significant portion of protein (20-40%) escaped modification as seen from LC-chromatogram of cyclopropyl aldehyde-treated cAD. This suggested possibility of another mechanism of inactivation. Evidence of an alternate mechanism of inactivation of cAD came from isotope labeling experiments. These experiments were performed by Mr. Benjamin Ellington.

It has been established that in the cAD-catalyzed conversion of octadecanal to heptadecane, the proton in newly formed methyl group of heptadecane came from solvent or solvent exchangeable group of amino acids (Chapter 2). However, the reaction of cyclopropyl

aldehyde with cAD generated a cyclopropylcarbinyl radical that would rearrange to octadecenyl radical where the radical would be placed at the C4 carbon of the species (Scheme 4.5).

Scheme 4.5. Reaction of cyclopropyl aldehyde with *Np* cAD depicting the possible radical intermediates

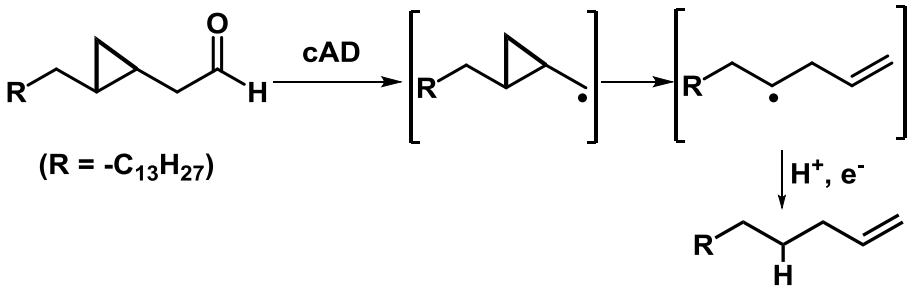

Given that usually the radcal is generated at the C1 carbon of the product and then quenched by proton coupled electron transfer, it became interesting to explore the source of the new proton in the rearranged product 1-octadecene. Assays were performed in D_2O (99.9%) using the standard assay protocol. The final conc. of H_2O did not exceed more than 2%. The products were extracted by ethyl acetate and analyzed by GC-MS. As expected, 1-octadecene obtained from this assay had molecular ion peak with *m/z* = 253 indicating the source of proton was solvent or solvent exchangeable group (1-octadecene has a molecular ion peak with *m/z* = 252). The 253 peak was also accompanied by less intense peaks with *m/z* = 254 and 255 presumably due to aldehyde α-hydrogen exchange with the solvent during the course of the assay (Figure 4.12). Interestingly, a significant peak with *m/z* = 252 was also observed on the spectrum. This peak corresponds to the non-deuterated product. Obviously, the presence of 2% H_2O in the assay could not account for the intensity of 252 peak.

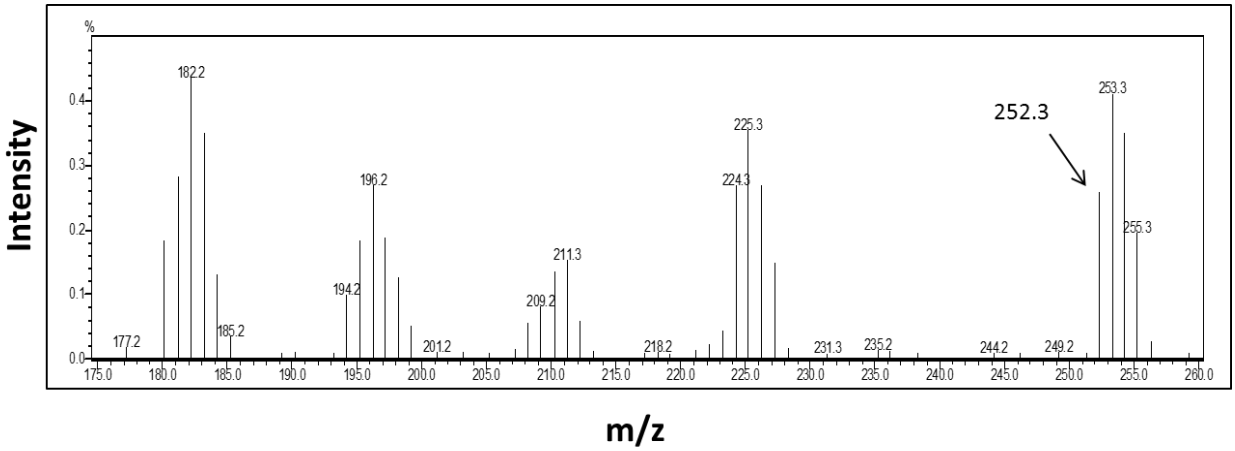

Figure 4.12. A section of the mass spectrum of 1-octadecene formed from cyclopropyl aldehyde in D_2O buffer.

To avoid complications that could arise due to exchange of aldehyde α-protons with the solvent during assay, di-deuterated cyclopropyl aldehyde (Scheme 4.6) was made. When assaying this substrate with cAD in D_2O, tri-deuterated 1-octadecene with the molecular ion peak of 255 was the major peak, as expected, but a significant peak of mass 254 Da was also observed. This peak corresponds to the di-deuterated product (Figure 4.13). The assay contained a maximum of 2% H_2O and this amount of H_2O could not account for the intensity of 254 peak. These experiments suggest that along with abstracting hydrogen from solvent, the rearranged radical also abstract hydrogen from non-exchangeable side chains of the protein leading to oxidative damage and inactivation of the protein.

Scheme 4.6. Chemical strucrure of di-deuterated **1**

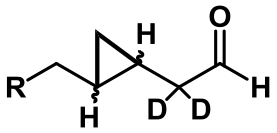

(R = -$C_{13}H_{27}$)

Di-deuterated 1

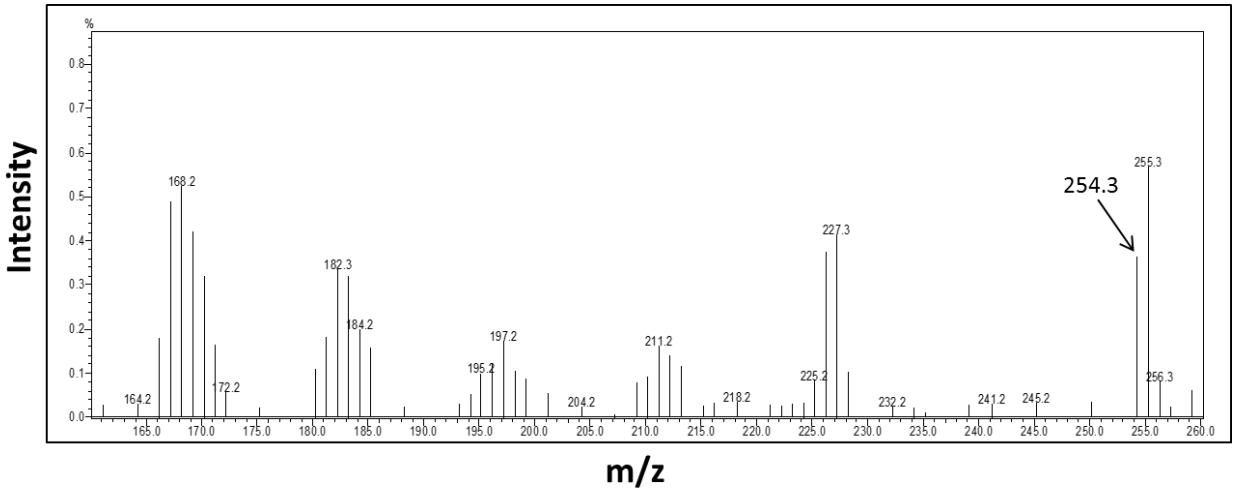

Figure 4.13. A section of the mass spectrum of 1-octadecene formed from di-deutereated cyclopropyl aldehyde in D_2O buffer by cAD.

4.4 Conclusions

In summary, in the family of aldehyde decarbonylases (ADs), cAD is the only soluble enzyme that can easily be expressed and purified from *E. coli*. This gives a unique opportunity to study the mechanism of action of the very unusual conversion of an aldehyde to alkane catalyzed by cAD.

Two different approaches to dissect the mechanism of cAD were taken. First, EPR spectroscopy was employed to investigate the interaction of substrate aldehyde with cAD. Upon incubation of heptanal with Fe(II) reconstituted cAD, generation of an organic radical was detected using a spin trapping agent PBN. This radical adduct was characterized by g = 2 signal. The radical adduct was most likely bound to the protein as indicated by the hyperfine splitting of the species. Further EPR experiments need to be performed to quantify the radical adduct.

In a second approach, a mechanistic probe was employed to investigate the C1-C2 bond scission of aldehyde. A cyclopropyl analogue of octadecanal was synthesized where the cyclopropyl group was strategically placed to the β, γ-carbon of the aldehyde. After incubation of the aldehyde with cAD, the product was characterized as 1-octadecene, a rearranged product. This suggested a homolytic cleavage of the C1-C2 bond that led to the generation of a cyclopropylcarbinyl radical that underwent ring-opening rearrangement to form the octadecenyl radical leading to the production of 1-octadecene. Interestingly no more than one turnover was obtained under multiple turnover conditions. Further, incubation of the cyclopropyl aldehyde treated cAD with octadecanal did not result any heptadecane formation, suggested inactivation of cAD by cyclopropyl aldehyde.

The mechanism of inactivation of cAD by cylopropyl aldehyde was further investigated by using LC-MS, MALDI-TOF and ES-MS/MS spectroscopy. LC-MS studies identified that the protein was covalently modified (60-80%) with the deformylated cyclopropyl aldehyde. To detect the location of modification, the modified and as-isolated enzymes were digested with trypsin and Glu-C. The digests were studied by MALDI-TOF and compared. The peptide fragment carrying the modification could not be directly detected but a peptide fragment was identified that was missing from both the digests of the modified peptide. The fragment was a part of the hydrophobic substrate binding channel.

To directly identify the modified amino acid, the tryptic and Glu-C digests were further examined by tandem mass spectrophotometer. This study identified a fragment, present in less

abundance in the tryptic digest, and an amino acid therein, Phe107, to be covalently attached with decerbonylated cyclopropyl aldehyde.

Further evidence for inactivation mechanism came from isotope labeling experiments where the di-deutreated cyclopropyl aldehyde reacted to produce mainly tri-deuterated alkene in deuterated buffer. However, a significant amount of di-deuterated product was also present. This observation suggests that in an alternate pathway, the intermediate rearranged radical abstracts hydrogen from non-exchangeable sites on the protein. This leads to inactivation of the enzyme by oxidative damage. These observations are summarized in Scheme 4.7.

Scheme 4.7. Alternate pathways of reaction of cyclopropyl aldehyde with cAD

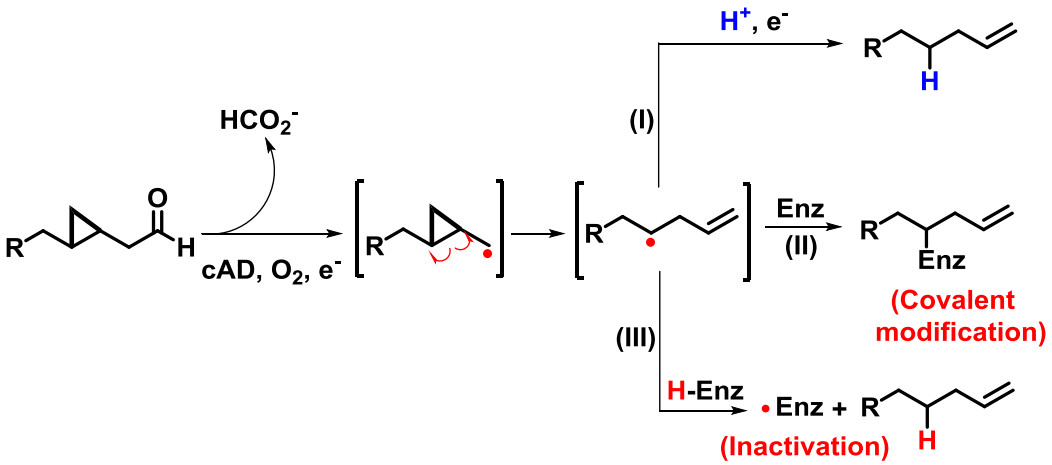

4.5 References

1. Buist, P. H., and Adeney, R. A. (1991) Synthesis of a new family of chiral fluorinated synthons - (R)-4-fluoro-1-alkynes and (S)-4-fluoro-1-alkynes, *J. Org. Chem. 56*, 3449-3452.
2. Cheesbrough, T. M., and Kolattukudy, P. E. (1984) Alkane biosynthesis by decarbonylation of aldehydes catalyzed by a particulate preparation from *Pisum sativum*, *Proc. Natl. Acad. Sci. USA. 81*, 6613–6617.
3. Qui, Y., Tittiger, C., Wicker-Thomas, C., Le Goff, G., Young, S., Wajnberg, E., Fricaux, T., Taquet, N., Blomquist, G. J., and Feyereisen, R. (2012) An insect-specific P450 oxidative decarbonylase for cuticular hydrocarbon biosynthesis, *Proc. Natl. Acad. Sci. USA. 109*, 14858–14863.
4. Bernard, A., Domergue, F., Pascal, S., Jetter, R., Renne, C., Faure, J. D., Haslam, R. P., Napier, J. A., Lessire, R., and Joubes, J. (2012) Reconstitution of plant alkane biosynthesis in yeast demonstrates that Arabidopsis ECERIFERUM1 and ECERIFERUM3 are core components of a very-long-chain alkane synthesis complex, *Plant Cell 24*, 3106-3118.
5. Bourdenx, B., Bernard, A., Domergue, F., Pascal, S., Leger, A., Roby, D., Pervent, M., Vile, D., Haslam, R. P., Napier, J. A., Lessire, R., and Joubes, J. (2011) Overexpression of Arabidopsis ECERIFERUM1 promotes wax very-long-chain alkane biosynthesis and influences plant response to biotic and abiotic stresses, *Plant Physiol. 156*, 29–45.
6. Schirmer, A., Rude, M. A., Li, X. Z., Popova, E., and del Cardayre, S. B. (2010) Microbial biosynthesis of alkanes, *Science 329*, 559–562.
7. Li, N., Norgaard, H., Warui, D. M., Booker, S. J., Krebs, C., and Bollinger, J. M. (2011) Conversion of fatty aldehydes to alka(e)nes and foramte by a cyanobacterial aldehyde decarbonylase: crypric redox by an unusual dimetal oxygenase, *J. Am. Chem. Soc. 133*, 7148–7152.
8. Pandelia, M. E., Li, N., Norgaard, H., Warui, D. M., Rajakovich, L. J., Chang, W. C., Booker, S. J., Krebs, C., and Bollinger, J. M. (2013) Substrate-triggered addition of dioxygen to the diferrous cofactor of aldehyde-deformylating oxygenase to form a diferric-peroxide intermediate, *J. Am. Chem. Soc. 135*, 15801–15812.
9. Das, D., Eser, B. E., Han, J., Sciore, A., and Marsh, E. N. G. (2011) Oxygen-independent decarbonylation of aldehydes by cyanobacterial aldehyde decarbonylase: a new reaction of di-iron enzymes, *Angew. Chem. Int. Ed. 50*, 7148–7152.
10. Eser, B. E., Das, D., Han, J., Jones, P. R., and Marsh, E. N. G. (2011) Oxygen-independent alkane formation by non-heme iron-dependent cyanobacterial aldehyde decarbonylase: investigation of kinetics and requirement for an external electron donor, *Biochemistry 50*, 10743–10750.
11. Cao, F., Chen, Y., Cierpicki, T., Liu, Y., Basrur, V., Lei, M., and Dou, Y. (2010) An Ash2L/RbBP5 heterodimer stimulates the MLL1 methyltransferase activity through coordinated substrate interactions with the MLL1 SET domain, *PLoS One 5*, e14102.
12. Hendrick, M. P., Munck, E., Fox, B. G., and Lipscomb, J. D. (1990) Integer-Spin EPR Studies of the Fully Reduced Methane Monooxygenase Hydroxylase Component, *J. Am. Chem. Soc. 112*, 5861-5865.

13. Kolberg, M., Bleifuss, G., Sjoberg, B. M., Graslund, A., Lubitz, W., Lendzian, F., and Lassmann, G. (2002) Generation and electron paramagnetic resonance spin trapping detection of thiyl radicals in model proteins and in the R1 subunit of Escherichia coli ribonucleotide reductase, *Arch. Biochem. Biophys. 397*, 57-68.
14. Newcomb, M., and Toy, P. H. (2000) Hypersensitive radical probes and the mechanisms of cytochrome P450-catalyzed hydroxylation reactions, *Acc. Chem. Res. 33*, 449-455.
15. Bowry, V. W., and Ingold, K. U. (1991) A Radical Clock Investigation of Microsomal Cytochrome-P-450 Hydroxylation of Hydrocarbons - Rate of Oxygen Rebound, *J. Am. Chem. Soc. 113*, 5699-5707.
16. Valentine, A. M., LeTadic-Biadatti, M. H., Toy, P. H., Newcomb, M., and Lippard, S. J. (1999) Oxidation of ultrafast radical clock substrate probes by the soluble methane monooxygenase from Methylococcus capsulatus (Bath), *J. Biol. Chem. 274*, 10771-10776.
17. Baldwin, J. E., Adlington, R. M., Domaynehayman, B. P., Knight, G., and Ting, H. H. (1987) Use of the cyclopropylcarbinyl test to detect a radical-like intermediate in penicillin biosynthesis, *J. Chem. Soc., Chem. Commun.*, 1661-1663.
18. Huang, H., Chang, W.-C., Pai, P. J., Romo, A., Mansoorabadi, S. O., Russell, D. H., and Liu, H.-W. (2012) Evidence for Radical-Mediated Catalysis by HppE: A Study Using Cyclopropyl and Methylenecyclopropyl Substrate Analogues, *J. Am. Chem. Soc. 134*, 16171-16174.
19. Souda, P., Ryan, C. M., Cramer, W. A., and Whitelegge, J. (2011) Profiling of integral membrane proteins and their post translational modifications using high-resolution mass spectrometry, *Methods 55*, 330-336.
20. Unpublished, structure solved by Joint Center of Structural Genomics (protein database entry PDB|2OC5|A).

Chapter 5

Mechanistic Insights from Reaction of α-Oxiranyl-Aldehydes with Cyanobacterial Aldehyde Decarbonylase

5.1 Introduction

Cyanobacterial aldehyde decarbonylase (cAD)-catalyzed conversion of aldehydes to alkanes involves an unusual cleavage of the C1-C2 bond of aldehydes. The bond possesses high energy (85 kcal/mol) and both the carbon atoms are attached to other atoms that make the environment around the C1-C2 bond sterically difficult to access.[1,2] This makes the cleavage of the C1-C2 bond particularly challenging. In order to dissect the mechanism of the cleavage of the C1-C2 bond of the aldehydes by cAD, a β, γ-cyclopropyl analog of octadecanal was employed and extensive investigations were carried out as described in Chapter 4. Experiments suggested that the cleavage of the C1-C2 bond takes place in a homolytic fashion and radical intermediates are involved in the catalysis. Although the experiments suggested a radical pathway, the evidence is indirect since there is no direct spectroscopic observation of the radical intermediate(s) derived from the cyclopropyl aldehyde. We have not investigated the reaction of the cyclopropyl aldehyde with cAD by EPR spectroscopy because most likely, insufficient concentrations of radical intermediates would form to allow detection by EPR spectroscopy.

Due to the challenges associated with the direct detection of the intermediate(s), further investigations were performed on cAD using different substrate analogs. The goal was to strengthen the evidence for the involvement of radical intermediates in the cAD-catalyzed reaction. In particular, I was interested in the mechanism of the cleavage of C1-C2 bond in the aldehyde. For this purpose, the synthesis of α, β-epoxide (oxiranyl) aldehydes were carried out. Compounds that generate oxiranyl radicals can also be used as radical clocks as oxiranyl radicals, although not extensively studied, also undergo ring-opening rearrangements, but at a much slower rates (~10^3-10^4 sec^{-1}) that allow them to be used as slow radical clocks. Rearrangements of oxiranyl radicals are established reactions documented in the literature.[3,4] The hypothesis was that, if the cleavage takes place homolytically, an oxiranyl radical would be generated. Depending on the lifetime of the radical, it can either be quenched to produce oxirane or be rearranged to an α-keto radical that might yield the corresponding aldehyde as a product. Since the rate constant of the rearrangement of oxiranyl radical is slow, there is a possibility to obtain both rearranged and non-rearranged products. The ratio of these two product and the known rate constant of the rearrangement of oxiranyl radical would allow us to determine the rate constant of the proton-coupled electron transfer in the following step. In this Chapter, I discuss our findings on the reaction of oxiranyl aldehydes with cyanobacterial aldehyde decarbonylase.

The work described in this chapter was carried out in collaboration with Dr. Bishwajit Paul and Mr. Benjamin Ellington. Dr. Paul synthesized the oxiranyl aldehydes and the oxirane standards. Mr. Ellington performed the NMR studies.

5.2 Materials and Methods

All assays described in this chapter were performed using *Np* cAD. The enzyme was expressed and purified as described in the Chapter 3. The materials and instrumentation used to perform the experiments described in this chapter were identical to Chapter 4.

Synthesis of oxirane aldehydes. α-oxiranyl aldehydes, 3-pentadecyloxirane-2-carbaldehyde (**1**) and 3-nonyloxirane-2-carbaldehyde (**2**) used as substrates of cAD were synthesized by Dr. Bishwajit Paul. 2-pentadecyloxirane (**3**) and 2-nonyloxirane (**4**) were also synthesized as authentic standards in order to verify the production of these compounds from the enzyme reaction. The detailed procedure of synthesis of the compounds is described in appendix B.

Enzyme assay. Under fully aerobic conditions very little activity was observed. Therefore assays were carried out under micro-aerobic environment keeping O_2 conc. ~20 ppm. I note that, although this concentration of oxygen is too low (dissolved O_2 concentration is ~0.025 μM) to support significant activity of the enzyme, asays were shaken continuously in GC-vials that might not be entirely gas tight. This appears to allow slow diffusion of O_2 to the reaction mixture. The buffer used was 100 mM HEPES, pH 7.2, containing 100 mM KCl and 10% glycerol as described previously.[5,6] Aldehyde substrates were made up as a 10 mM stock solution in DMSO. A typical assay contained 10 μM cAD, 20 μM ferrous ammonium sulfate, 300 μM aldehyde substrate, 100 μM phenazine methosulfate (PMS) and 2 mM NADH in a total volume of 500 μL. Assays were shaken at 37 °C at 200 rpm. Reactions were quenched by addition of 500 μL ethyl acetate. Mixtures were vortexed well followed by centrifugation at 14000 rpm for 30 min to separate the organic phase. The ethyl acetate layer was collected and 8 μL of sample was injected into

GC-MS for analysis. Product formation was quantified using calibration plots of authentic product standards.

GC-MS analysis. Gas chromatography analysis was performed using a Shimadzu QP-2010S GC-MS instrument equipped with a DB-5 column (Restek, 30m x 0.25 mm x 0.25 μm) and a quadrupole mass detector and as described previously.[5] The flow rate of the helium carrier gas was kept constant at 1 mL/min and the inlet temperature was maintained at 200 °C. The interface temperature kept constant at 250 °C. Injections were made in splitless mode. Unless specified, oven temperature was held initially at 70 °C for 2 min and then gradually increased to 300 °C at 20 °C/min and finally maintained at 300 °C for 5 min.

Formate assay. 2-Nitrophenylhydrazine (2-NPH) was used to detect formate as the co-product of cAD-catalyzed reaction as described previously.[5,7] Assays were carried out for 2 h. A 500 μL of the reaction was mixed with 40 μL of 40 mM 2-NPH solution (aqueous solution with 0.2 M HCl and 50% ethanol) and 100 μL of EDC working solution (125 mM EDC with 1.5% pyridine in 50% ethanol). The mixture was vortexed for 30s and incubated at 65 °C for 1 h. The samples were then cooled to room temperature and centrifuged at 14000 rpm for 30 min to remove any precipitate. The supernatant was subjected to HPLC (Shimadzu LC-20AT coupled to SPD-M20A diode array detector) using a Phenomenex C18 RP HPLC column (25 mm x 4 mm, 5 μm, 120 Å). The column was equilibrated with 90% water, 10% MeOH with 0.05% Acetic acid and the sample was run isocratically at 1mL/min using the same solvent.

Deuterium incorporation experiments. To investigate deuterium incorporation into alkane products, assays were performed in 100 mM HEPES buffer containing 100 mM KCl in 99.9%

D_2O, pD 7.2. Substrates were made up as 10 mM stock solutions in 99.9% DMSO-d6. cAD was added as a concentrated stock solution in non-deuterated buffer such that the final H_2O concentration did not exceed 3%. The enzyme was incubated in the buffer for 1 h prior to initiating the reaction by addition of substrate. Assays were shaken at 37 °C for 2 h at 200 rpm. Products were extracted and analyzed as described above.

Preparation of samples for NMR assays. These experiments were performed by Mr. Benjamin Ellington. The experiments were performed as described above except that phosphate buffer was substituted for HEPES buffer which otherwise interfered with the NMR spectra. Assays were carried out either in 10 mM potassium phosphate, pH 7.2, containing 50 mM KCl in H_2O or 10 mM potassium phosphate, pD 7.2, containing 50 mM KCl in D_2O (99.9%). Aldehyde solutions were made up as a stock solution in DMSO or DMSO-d6 for the respective experiments. A typical assay contained 40 µM *Np* cAD, 80 µM ferrous ammonium sulfate, 100 µM PMS, 2 mM NADH and 400 µM substrate in a total volume of 500 µL. For assays performed in deuterated buffer, the final H_2O concentration was ~5% after adding all the assay components. Ten identical 500 µL reactions were set up in each buffer and shaken at 37 °C at 200 rpm for 2 h. The reaction mixtures were sequentially extracted with a total volume of 1 mL $CDCl_3$ (99.9%). The $CDCl_3$ layers were washed with D_2O, dried over sodium sulfate and filtered before analysis by ^1H NMR.

5.3 Results and Discussion

5.3.1 Chemical Structures of Oxiranyl Aldehydes

Chemical structures of the 3-pentadecyloxirane-2-carbaldehyde (**1**), 3-nonyloxirane 2-carbaldehyde (**2**), 2-pentadecyloxirane (**3**) and 2-nonyloxirane (**4**) are shown in Scheme 5.1 and 5.2. The detailed procedure of synthesis of the compounds is described in appendix B.

Scheme 5.1. Structures of pentadecanyloxirane-2-carbaldehyde (**1**), and *trans*-3-nonyloxirane-2-carbaldehyde, (**2**) used in these studies

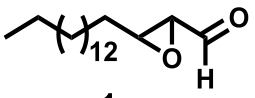

1

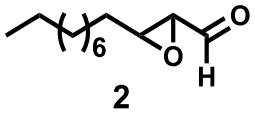

2

Scheme 5.2. Structures of 2-pentadecyloxirane (**3**) and 2-nonyloxirane (**4**)

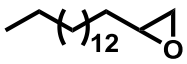

3

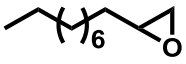

4

5.3.2 3-Pentadecyloxiran-2-Carbaldehyde (1), as a Substrate of cAD

It has been shown that the cyanobacterial aldehyde decarbonylase (cAD) was active with both a long-chain aldehyde, octadecanal and a short-chain aldehyde, heptanal (Chapter 2). It has also been demonstrated that the enzyme reacted with a cyclopropyl analog of octadecanal to yield a rearranged product (Chapter 4). Although the β, γ-cyclopropyl analog of octadecanal yielded 1-octadecene, the reaction did not proceed beyond one turnover and the enzyme became inactivated by the substrate. All these observations suggest that cAD is quite promiscuous. With this premise, I became interested in exploring the reaction of cAD with a different type of aldehyde, **1**, containing an epoxide ring adjacent to the carbonyl carbon.

Formation of 2-pentadecyloxirane (3) as the major product. *Np* cAD was incubated with **1,** in presence of reducing system; the reaction mixture was extracted with ethyl acetate and analyzed by GC-MS. Several new peaks appeared in the chromatogram. Among these peaks, the major peak at 10.5 min (Figure 5.1) had the same retention time and mass spectrum of the authentic 2-pentadecyloxirane (**3**). This identifies the major peak as 2-pentadecyloxirane (**3**), the non-rearranged product.

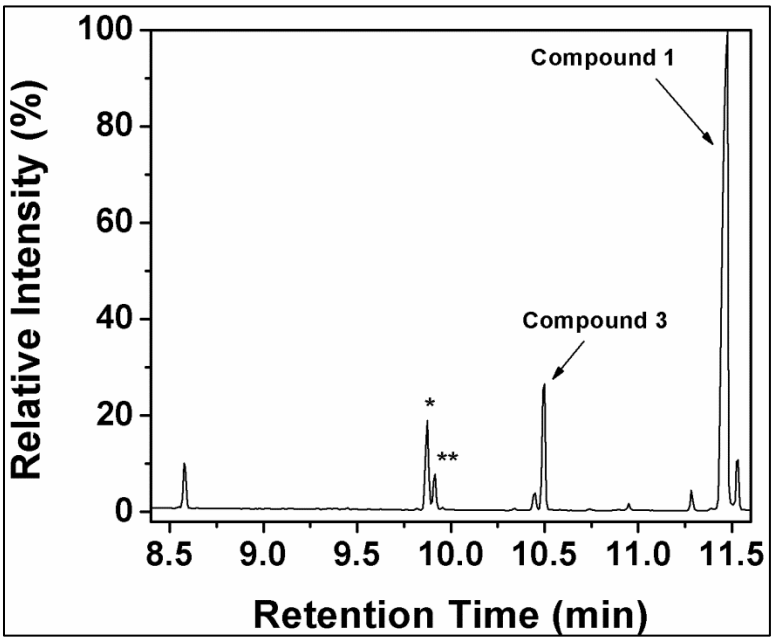

Figure 5.1. A gas-chromatogram depicting the conversion of **1** to 2-pentadecyloxirane (**3**) by *Np* cAD. The peak identified by * is PMS and the peak identified by ** is hexadecanal impurity.

Formation of 2-pentadecyloxirane from **1** was absolutely dependent on the presence of the enzyme and the reducing system, PMS/NADH. Omission of one of these components totally abolished the activity (Figure 5.2). Formation of **3** increased linearly up to ~2 h (Figure 5.3). The initial rate of formation of **3** was 0.029 ± 0.001 min^{-1} from these data points. This rate is ~4 times slower than the rate of the reaction with octadecanal[7] and ~6 times slower than that of

heptanal.[6] Although compound **1** behaved like a true substrate, the consistent appearance of peaks other than 2-pentadecyloxirane led us to investigate their identity and origin. For this purpose, several control assays were performed either by omitting the enzyme or the reducing system from the assay. When assays were performed in the absence of PMS, the peak at 9.87 min disappeared, suggested the peak was arising due to PMS (PMS is partial soluble in ethyl acetate). The peak at 9.95 min is present in equal amount in both the enzyme assays as well as in control assays where the enzyme or the reducing system was omitted. This peak matched very well with the retention time and the mass spectrum of standard hexadecanal (TCI America) suggested that the starting material, hexadecanal, for the synthesis of compound **1,** was carried along with the later steps of synthesis. In fact, conversion of hexadecanal to pentadecane by cAD could also be seen on the gas chromatogram (data not shown). To confirm the presence of hexadecanal in compound **1**, a standard solution of compound **1** in ethyl acetate was judged by GC-MS. 2% of hexadecanal (w.r.t compound **1**) was seen to be present in the sample as impurity that escaped detecetion by NMR. When incubated with **1**, cAD also produced some pentadecane by deformylation of hexadecanal (data not shown).

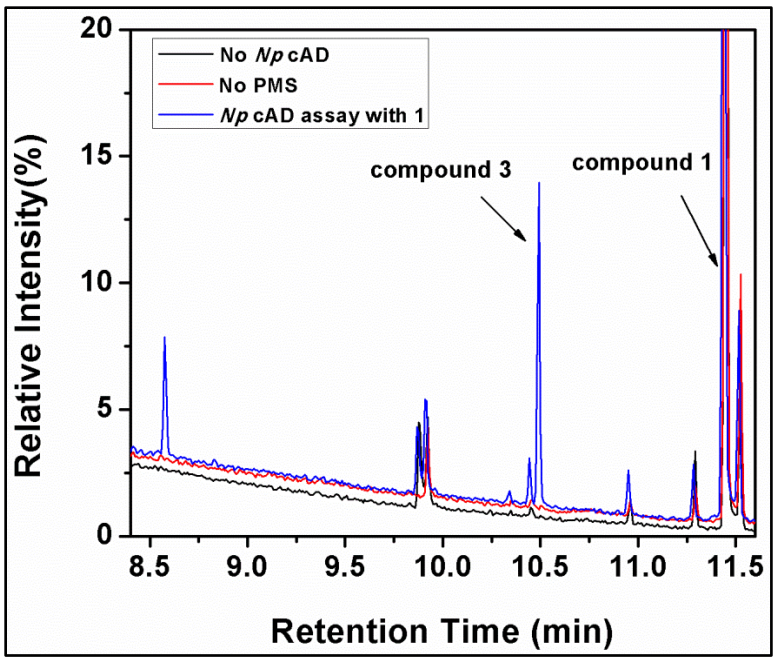

Figure 5.2. Overlaid gas-chromatographs of conversion of **1** to 2-pentadecyloxirane (**3**) by *Np* cAD and the control experiments where cAD or PMS were omitted.

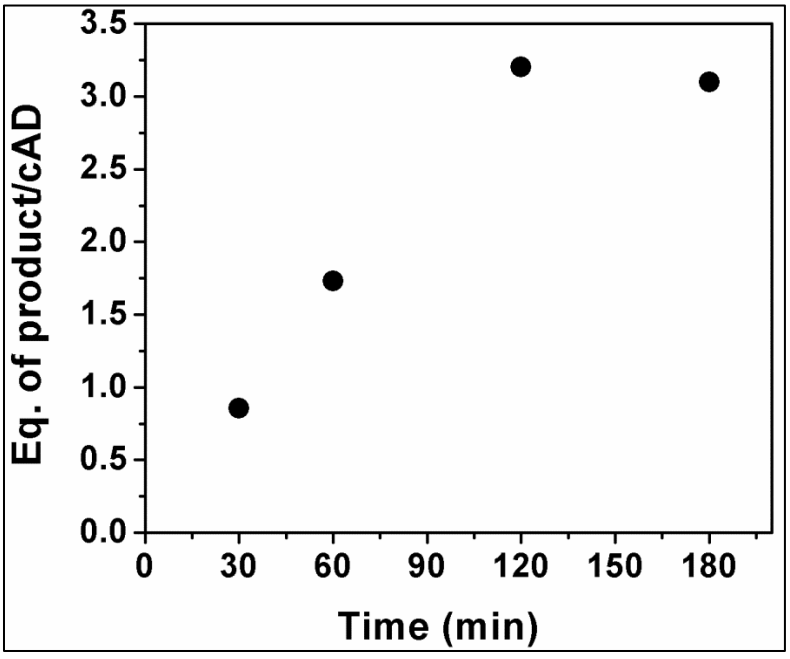

Figure 5.3. Time course of formation of compound **3** from compound **1** by *Np* cAD depicting multiple turnovers and linear increase in the product formation up to 2 h.

Formation of hexadecane from 3-pentadecyloxirane-2-carbaldehyde (1) by Np cAD. The investigation of 3-pentadecyloxirane-2-carbaldehyde **(1)** as a substrate for cAD led us to detect an additional product apart from **3** on the GC chromatogram. The peaks at 9.87 min and 9.95 min were identified as PMS and hexadecanal respectively using control experiments and authentic standards. Interestingly one more peak appeared at at 8.58 min. The intensity of the peak was significant. The appearance of the peak was found to be dependent on the enzyme. This peak was absent from the control experiments and only appeared when all the assay components were included in the assay (Figure 5.2). Analysis of the mass spectrum of this peak showed a standard hydrocarbon fragmentation pattern along with a molecular ion peak 226 that corresponds to hexadecane. To confirm the identity of this peak as hexadecane, a standard hexadecane sample was chromtographed and retention times and mass spectra were compared. Both the retention time (Figure 5.3 & Figure 5.5 *vide infra*) and the mass spectrum were identical to the peak at 8.58 min. These results confirmed the identity of the peak as hexadecane. This observation was interesting and implied that a **1** was converted to a completely un-functionalized product, an alkane with 16 carbons (Scheme 5.3) by the action of cAD. Hexadecane produced from these assays was quantified using a standard calibration plot of authentic hexadecane. Hexadecane production increased linearly up to almost 3 h. The rate of production of hexadecane was ~10 times lower compared to the rate of production of **3**, the major product. An apparent k_{cat} = 0.003 ± 0.0004 min^{-1} for hexadecane formation could be calculated for the reacton of **1** with *Np* cAD (Figure 5.4).

Scheme 5.3. Conversion of compound **1** to compound **3** and hexadecane by *Np* cAD

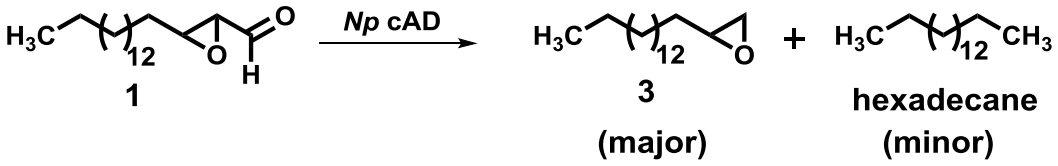

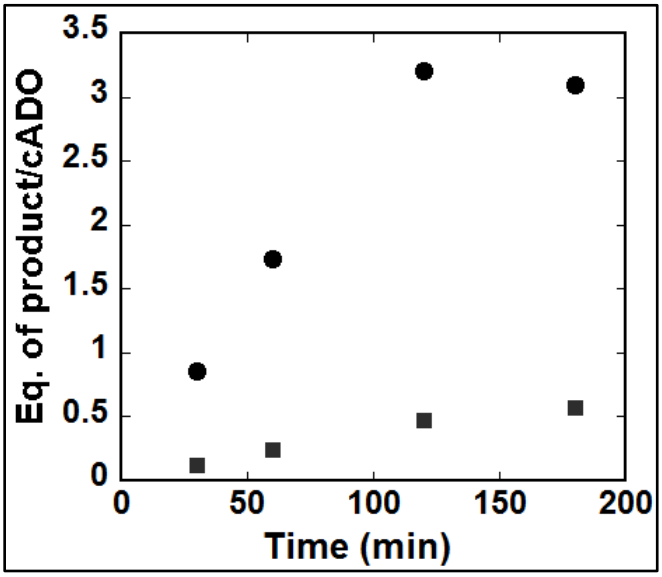

Figure 5.4. Comparison in the time course of production of compound **3** (●, major product) and hexadecane (■, minor product) from compound **1**.

Precursor of hexadecane. The production of C_{n-2} un-functionalized alkane, hexadecane, from compound **1** was unexpected. But according to the mechanistic hypothesis, homolytic cleavage of the C1-C2 bond would generate an oxiranyl radical and depending on the lifetime of the radical, rearrangement of the oxyranyl radical to an α-aldehyde radical could occur leading to formation of heptadecanal.

Re-analysis of the GC-MS chromatogram for conversion of compound **1** to **3** and hexadecane was carried out. Careful examination showed a small new peak eluted at 10.46 min, just before the elution time of compound **3**. The peak was present in negligible amount in

the control reactions but stood out when both the enzyme and the reducing system were included in the reaction. The mass fragmentation pattern of this peak indicated it to be a long chain aldehyde.

Although the molecular ion for this peak could not be detected in the mass spectrum due to insufficient intensity of the peak, an authentic heptadecanal standard co-eluted with this small peak confirming its identity as heptadecanal (Figure 5.5). This suggests that heptadecanal serves as an intermediate that is subsequently converted to hexadecane. The rate of formation of heptadecanal must have been slightly faster than the rate of disappearance as an apparent linear increase in accumulation of heptadecanal was evident from the time course (Figure 5.6).

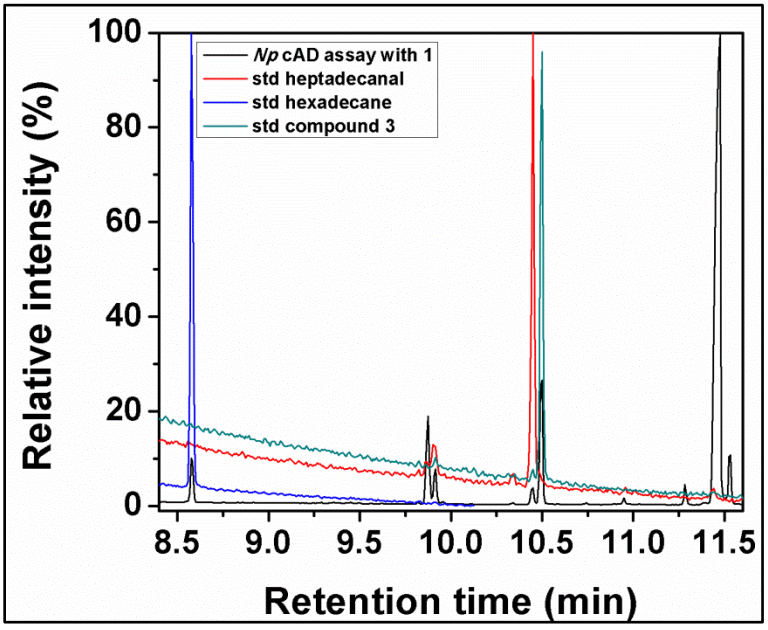

Figure 5.5. Overlaid gas-chromatographs of reaction of **1** with *Np* cAD and standard samples of heptadecanal, hexadecane and compound **3**.

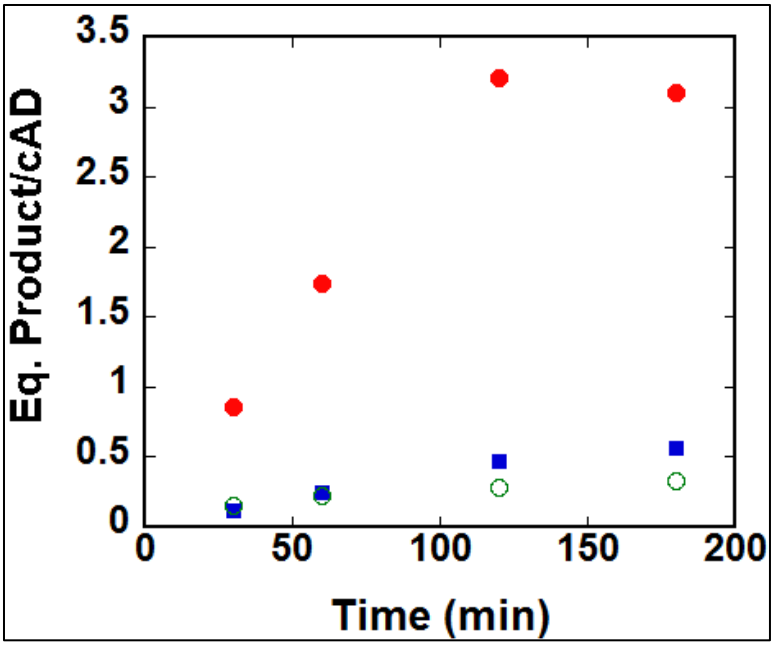

Figure 5.6. Comparison in the time course of production of compound **3** (●) and hexadecane (■) and heptadecanal (○) from compound **1**. Heptadecanal production slowly increases with time.

5.3.3 Identification of Formate as the Co-Product

Due to the unusual nature of the reaction of **1** with cAD, the identity of the co-product was investigated. It has already been established that formate is the co-product for the conversion of octadecanal to heptadecane (Chapter 2) as well as for the conversion of β, γ-cyclopropyl analogue of octadecanal to 1-octadecene (Chapter 4). In the case of the reaction of pentadecyloxirane-2-carbaldehyde (**1**) with cAD, formate seemed a reasonable candidate. Assays were carried out as described in the materials and methods section. Resulting products were derivatized using 2-NPH. The formate hydrazide derivative was detected at 230 nm at ~17 min (Figure 5.7) and its identity was confirmed by comparing it with an authentic standard and by UV-Vis spectrum.

Using 10 µM cAD, from a 2 h assay, ~30 ± 5 µM of formate was obtained as quantified using formate-NPH authentic standards. The amount of formate formed was very similar to the total amount of 2-pentadecyloxirane (**3,** the major product, ~30 ± 3 µM) and hexadecane (the minor product, ~5 ± 0.5 µM) obtained from the assay. This confirmed that the conversion of compound **1** to compound **3** was also an example of deformylation reaction. The formate quantification should include the amount of formate formed from the conversion of heptadecanal to hexadecane. The amount of hexadecane formed is ~5 µM from 10 µM cAD in 2 h and an identical amount of formate would have been formed. To distinguish between the formate formed from deformylation of compound **1** and from heptadecanal, employment of isotopically labeled substrates would be necessary.

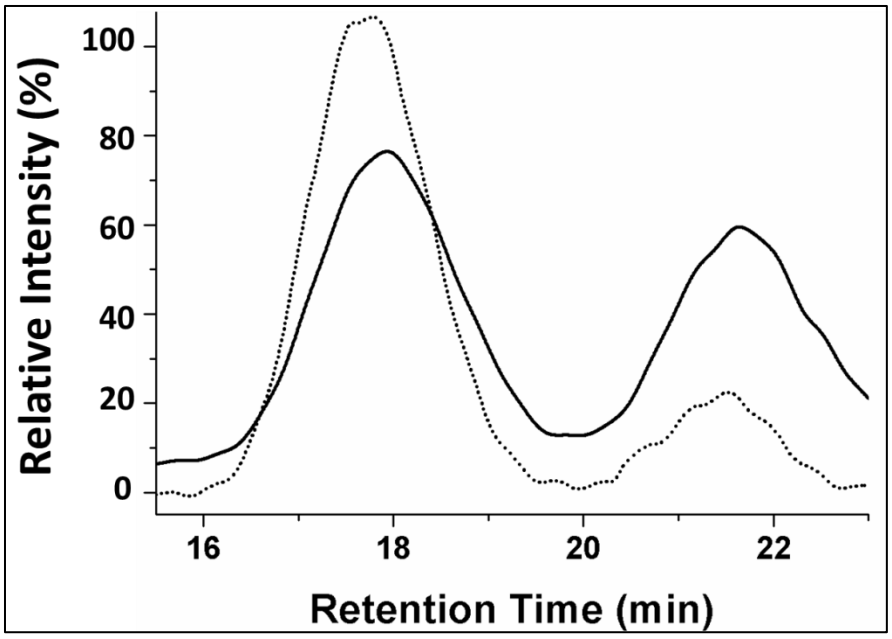

Figure 5.7. Overlaid HPLC traces of formate NPH-derivative from 50 µM standard formate (dotted line) and the formate-NPH obtained from the formate produced by the enzymatic reaction of **1** with *Np* cAD (solid line).

5.3.4 Elucidation on the Mechanism of the Reaction of 1 with cAD

Immediate Precursor of heptadecanal. It was considered that heptadecanal could form in two ways. One possibility is that the major product, 2-pentadecyloxirane, could undergo a ring-opening rearrangement under the assay conditions to produce heptadecanal. The second possibility is that the intermediate species formed after cleaving the C1-C2 bond of **1** could undergo rearrangement to produce heptadecanal. To distinguish between these two alternatives, cAD was incubated with authentic 2-pentadecyloxirane (**3**) in presence and absence of the reducing system. As a further control, 2-pentadecyloxirane was incubated with all the assay components except the enzyme. Investigation of all these conditions indicated that compound **3** was stable under the assay conditions and did not undergo any transformation to produce heptadecanal. A direct comparison of an assay where compound **3** was treated as a substrate and an actual assay where compound **1** was used as a substrate under identical conditions is shown in Figure 5.8.

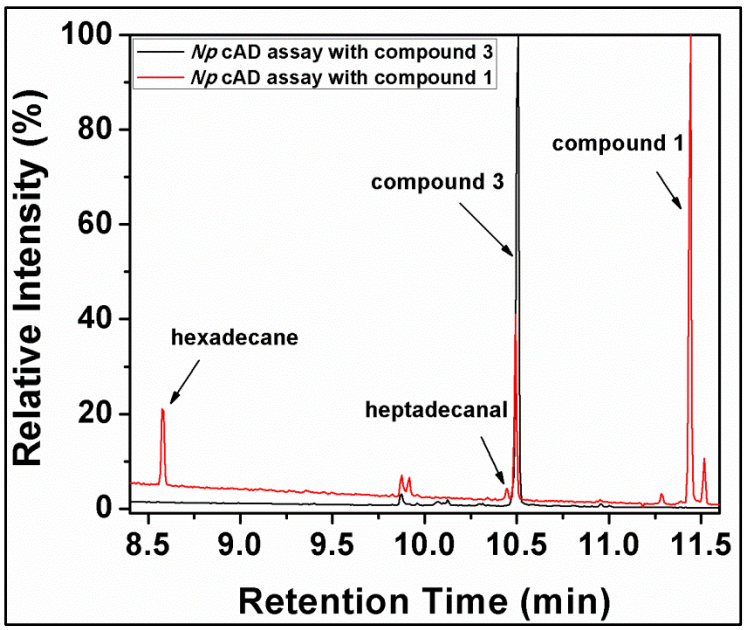

Figure 5.8. Overlaid chromatographs of *Np* cAD assay with compound **1** (in red) and *Np* cAD assay with compound **3** (in black).

Assays containing 2-pentadecyloxirane failed to produce any heptadecanal. This suggested that the precursor of heptadecanal must be the intermediate species generated by the C1-C2 bond cleavage of aldehyde **1** as shown in the Scheme 5.4.

Nature of the C1-C2 bond cleavage. Although it appears that the intermediate species generated by the C1-C2 bond cleavage of aldehyde **1** is responsible for the production of heptadecanal, the nature of the species could not be directly identified from the experimental data. Our hypothesis was that the intermediate species would be a radical. As mentioned above, rearrangements of oxiranyl (epoxide) radicals are known from the literature. It has been shown that alkyl substituted epoxide radicals undergo rearrangement to α-keto alkyl radicals by ring opening.[3,4] By employing EPR spectroscopy, the rate of the ring-opening rearrangement of alkyl substituted epoxide radical has also been measured to be on the order of 10^3 sec^{-1} at > 0

°C.[3] It has also been shown that the rate of the rearrangement increases with the number of alkyl substituents. In another example, 2,3-*trans*-diphenyl-2,3-epoxypropanal has been shown to undergo decarbonylation to produce an oxiranyl radical that undergoes ring opening rearrangement to yield an α-keto radical, although in this case the radical was stabilized by resonance with an adjacent phenyl group.[4] Based on these data, the rate constant of rearrangement of 2-pentadecyloxiranyl radical to the corresponding α-keto heptadecyl radical would be on the order of 10^3 sec^{-1}. The ratio of 2-pentadecyloxirane and hexadecane formed in the cAD-catalyzed reaction of **1** is ~10:1. Based on these, a rate constant for the step that involves proton-coupled electron transfer to produce 2-pentadecyloxiranyl can be calculated to be ~10^4 sec^{-1}. This also suggests that the lifetime of the radical, generated due to cleavage of the C1-C2 bond of an aldehyde by cAD, is ~0.1 ms. This is a significantly long-life for a radical. This is in accordance with our previous findings on the lifetime of cyclopropylcarbinyl radical, generated through the cleavage of C1-C2 bond of the β, γ-cyclopropyl analog of octadecanal by cAD. The cyclopropylcarbinyl radical has a known rate constant for rearrangement which is on the order of 10^8 sec^{-1}.[8] While incubated with cAD, the cyclopropyl aldehyde rearranged to produce 1-octadecene as the exclusive product. This suggested that the cyclopropyl carbonyl radical had a lifetime ≥ 10 ns.[5] Our current finding of the lifetime of the intermediate radical suggests formation of a relatively long lived radical due to cleavage of C1-C2 bond of an aldehyde by cAD.

Although radical intermediate is most likely, we could not completely rule out the possibility of carbanion/carbocation generated due to the heterolytic cleavahe of the C-C bond (Scheme 5.4). There are a few examples in the literature, where oxiranyl carbanions, formed by

the employment of strong and hinderd bases, have been shown to undergo ring-opening rearrangements to the corresponding keto species.[9,10] However, this seems to be unlikely under enzymatic conditions that lacks any strong base. Formation of carbacationic intermediate (Scheme 5.4) would be quite unlikely as once rearranged, it would place a carbocation adjacent to the carbonyl group which is energetically very unlikely. Furthermore, the carbocation would require a source of hydride to be quenched to produce the corresponding aldehyde, which would seem unlikely. Therefore, the mechanism that involves the homolytic cleavage of the C1-C2 bond is currently favored.

Scheme 5.4. Possible intermediates that could form due to the cleavage of C1-C2 bond of compound **1** by cAD. Formation of the radical intermediate is most likely

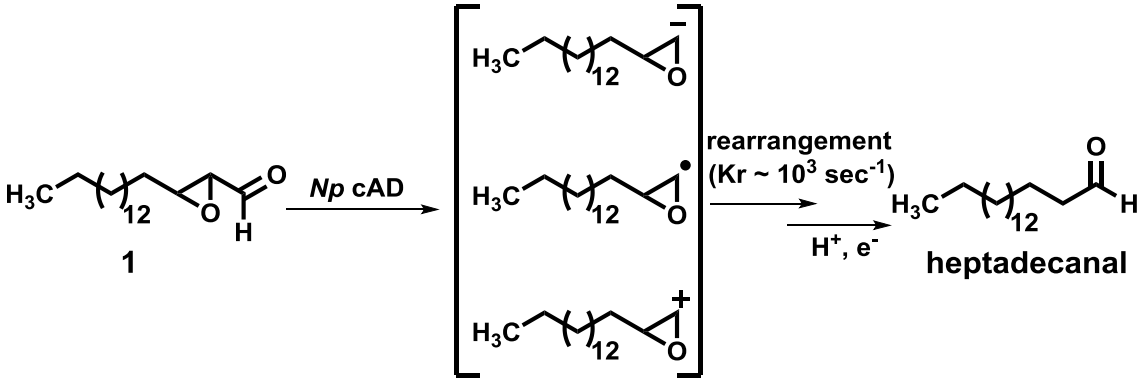

Source of protons in hexadecane. In the cAD-catalyzed conversion of octadecanal to heptadecane, the hydrogen in the newly formed methyl group of heptadecane was found to be derived from solvent or solvent exchangeable group on the protein. But hexadecane production from compound **1** was quite unusual because compound **1** underwent elimination of two carbons to produce hexadecane. It was therefore important to establish the source and number of incorporated new hydrogen(s) into hexadecane. To address that, assays were performed in D_2O buffer. Hexadecane has a molecular ion peak with *m/z* = 226. When assays were

performed in H_2O buffer, this peak could easily be detected as shown in Figure 5.9 A. However, when assays were performed in D_2O buffer, the recovered hexadecane had a molecular ion peak of 228 (Figure 5.9 B). This suggested the incorporation of two deuterium atoms into hexadecane. No apparent difference in the amount of hexadecane formation in proteated and deuterated buffer could be detected. This might be because the absolute amount of hexadecane formation (~5 μM in 2 h using 10 μM cAD) was not high enough to reliably measure the difference. A plausible mechanism for hexadecane formation that accommodates these findings is depicted in Scheme 5.5.

Compound **1** undergoes *Np* cAD-catalyzed C1-C2 bond cleavage to produce an oxiranyl radical and formate. The intermediate oxiranyl radical then partitions between two paths. In one pathway, the radical intermediate undergoes a proton-coupled electron transfer to produce the compound **3** as the major product. In the other pathway, the oxiranyl radical undergoes ring-opening rearrangement to produce an α-keto heptadecanyl radical as an intermediate. This α-keto heptadecanyl radical plausibly undergoes a proton-coupled electron transfer to produce heptadecanal. This would account for one deuterium incorporation into heptadecanal that is the immediate precursor of hexadecane. The mono-deuterated heptadecanal would then undergo a C1-C2 bond cleavage in presence of *Np* cAD followed by proton-coupled electron transfer to produce hexadecane and formate. Incorporation of a proton from solvent in the conversion of long-chain aldehyde to the corresponding alkane is an established feature of the cAD-catalyzed reaction.

It should be noted that the peak with *m/z* = 228 was accompanied by a minor peak with *m/z* = 227 that corresponds to mono-deuterated hexadecane. The appearance of the peak with *m/z* = 227 could partially be attributed to the presence of 3% H_2O in D_2O buffer. The possible involvement of solvent kinetic isotope effect that will discriminate against deuterium might also play role for the appearance of the peak with *m/z* = 227. Abstraction of non-exchangeable hydrogen from an amino acid side chain of the protein by the intermediate α-keto heptadecanyl radical might also account for the appearance of the peak with *m/z* = 227, although this would lead to enzyme inactivation by oxidative damage.

Theoretically, by prforming the reactions in H_2O buffer and D_2O buffer and quantifying the ratio of respective proteated and deuteratedhexadecane products, a solvent isotope effect can be calculated. However, the absolute amount of hexadecane formed from a 3 h assay of **1** with cAD is very low (~3 μM). This impedes reliable determination of solvent isotope effect.

Unlike the β, γ-cyclopropyl analog of octadecanal that partially inactivated the enzyme by covalent modification, no covalent modification of the enzyme by 3-pentadecyloxirane-2-carbaldehyde (**1**) could be detected when the enzyme was examined by LC-MS following the method as described in Chapter 4. As-isolated *Np* cAD has an isotope averaged molecular wt. (Mr) = 28911 ± 0.5 Da.[5] The observed average mass of compound **1** treated *Np* cAD (Figure 5.10) is identical with the calculated mass of the *Np* cAD. This is consistent with the enzyme exhibiting multiple turnovers when incubated with **1**.

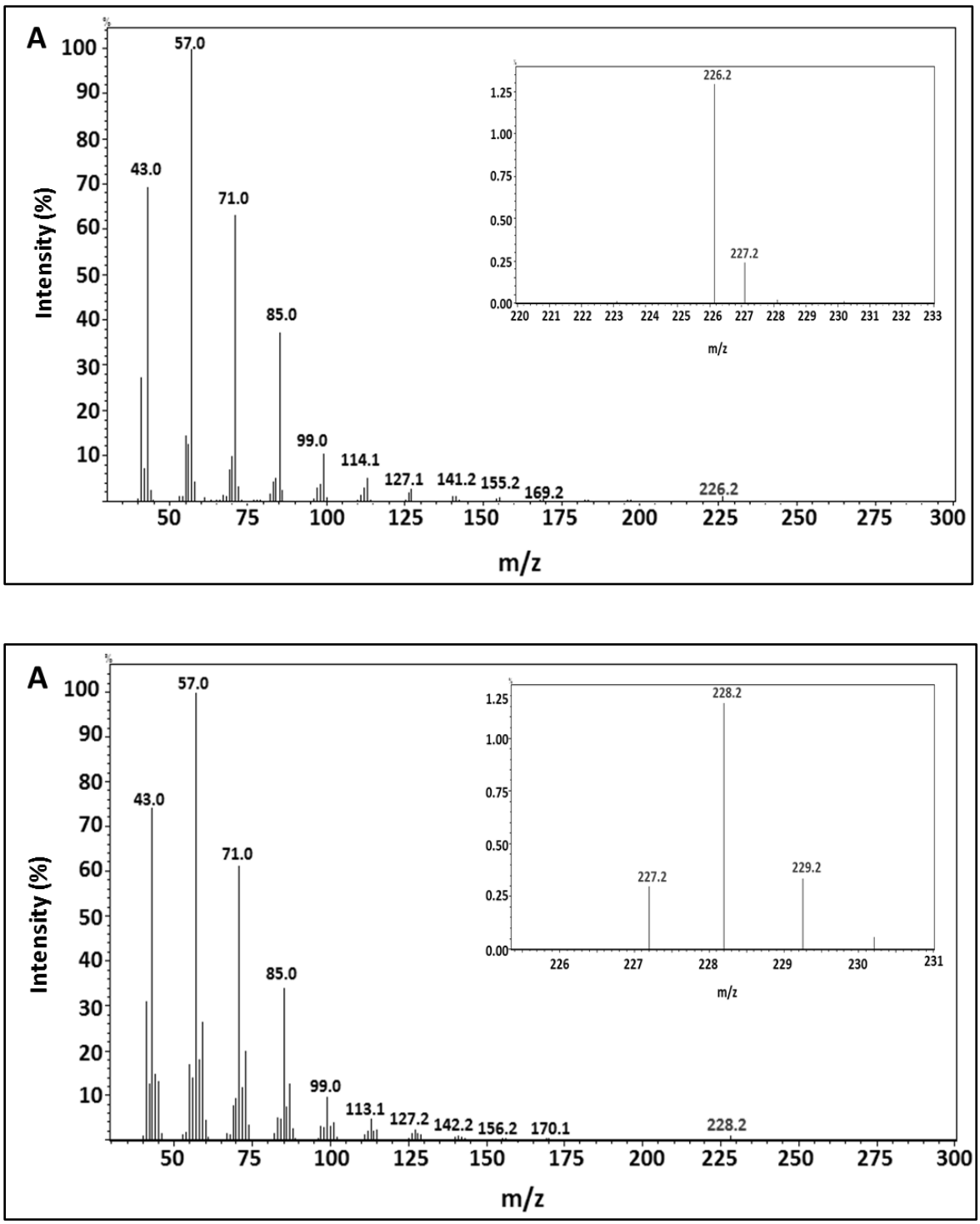

Figure 5.9. Mass spectrum of hexadecane produced from **1** in H_2O buffer **(A)** and D_2O buffer **(B)**. Zoomed in view of the molecular ion peaks of hexadecane were shown in the insets.

Scheme 5.5. Plausible mechanism of conversion of compound **1** to compound **3** and hexadecane

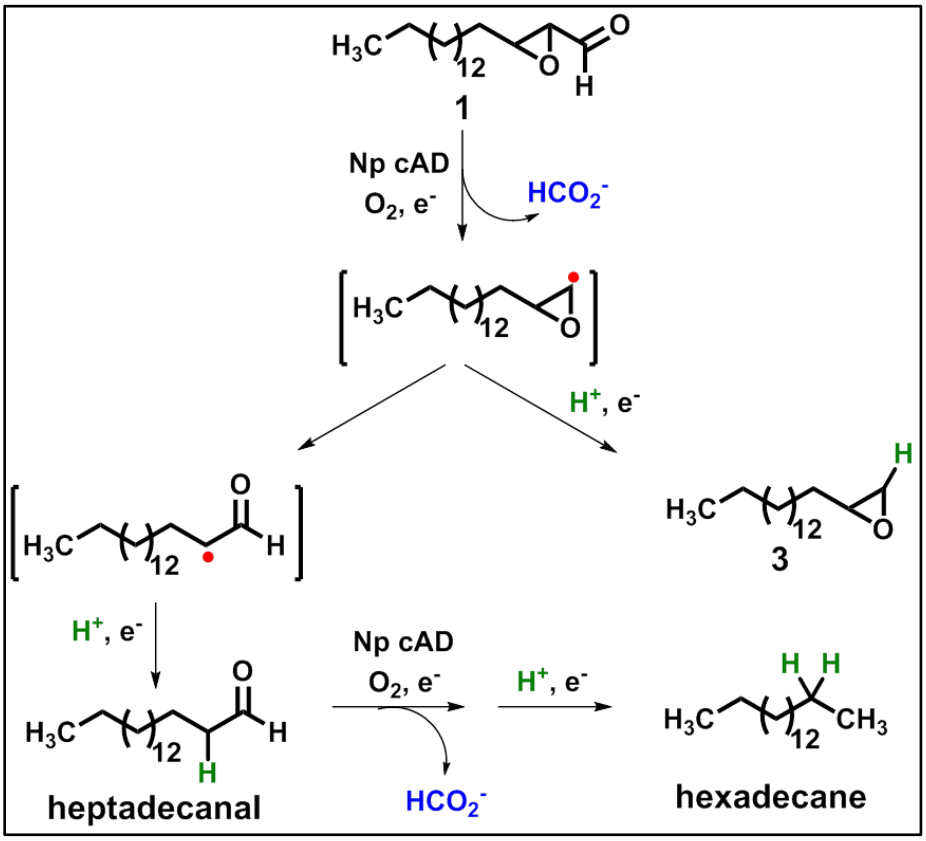

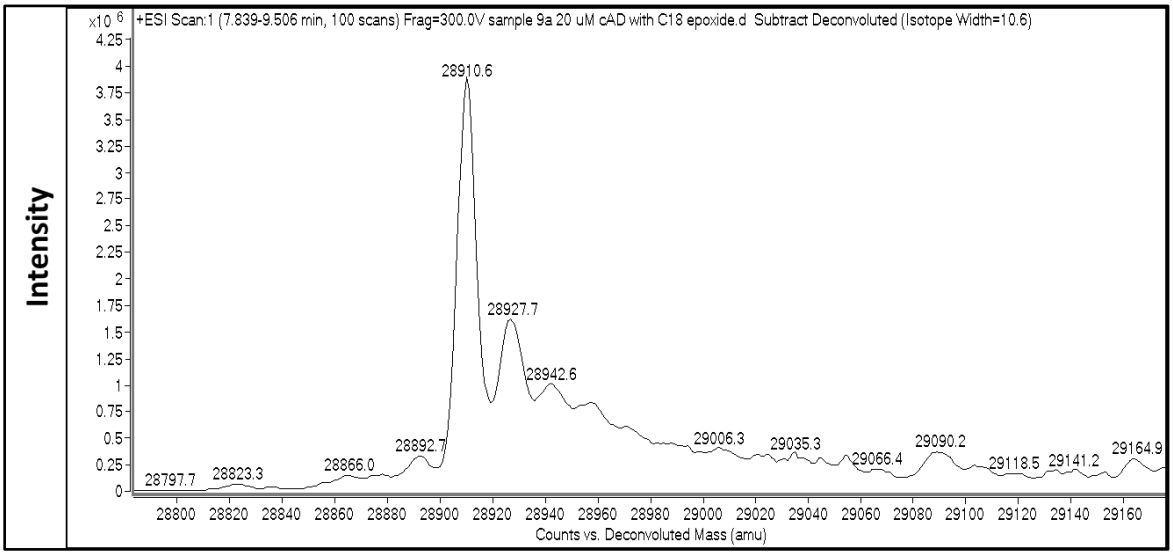

Figure 5.10. Deconvoluted mass spectrum of compound **1** treated *Np* cAD.

It should also be noted that, although the mass spectrum of heptadecanal produced from D_2O assays was carefully investigated, the molecular ion peak to directly identify the deuterium incorporation in heptadecanal could not be detected. This is due to the lack of material in the reaction mixture.

5.3.5 3-Nonyloxirane-2-Carbaldehyde (2) as a Substrate of cAD

Reaction of 3-pentadecyloxirane-2-carbaldehyde **(1)** with *Np* cAD resulted in the formation of 2-pentadecyloxirane (**3**) as the major product and hexadecane as the minor product. In this respect, it was interesting to learn whether reaction of shorter chain 3-nonyloxirane-2-carbaldehyde **(1)** with *Np* cAD would result in the formation of 2-nonyloxirane **(4)** and the C_{n-2} alkane, decane. Compound **2** was incubated with *Np* cAD in presence of PMS/NADH. Assays were performed as described before and after completion, assays were extracted with ethyl acetate and analyzed by GC-MS. Similar to the results of the reaction compound **1** with cAD, compound **2** resulted in the production of 2-nonyloxirane as the major product (eluted at 6.79 min) and decane as the minor product (eluted at 4.10 min) (Figure 5.11).

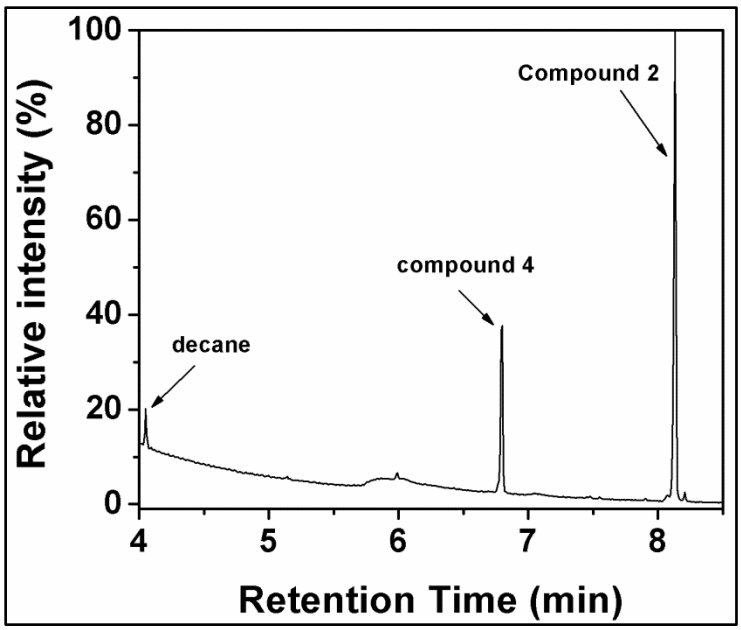

Figure 5.11. Conversion of **2** to 2-nonyloxirane (**4**) and decane by *Np* cAD.

Formation of 2-nonyloxirane (**4**) and decane were confirmed by using authentic standards (Figure 5.12). Formation of decane was also confirmed by the molecular ion peak of 142 (Figure 5.13). Control experiments were also performed to confirm enzymatic production of 2-nonyloxirane and decane. Neither 2-nonyloxirane nor decane was produced when one of the assay components were omitted from the assay (Figure 5.14).

Formation of 2-nonyloxirane was linear with time and a rate constant for formation = 0.016 ± 0.001 min^{-1} could be calculated from the time course (Figure 5.15). This is comparable with the rate of formation of undecane (0.01 ± 0.001 min^{-1}) from dodecanal by *Np* cAD (Figure 5.16) under identical assay conditions.

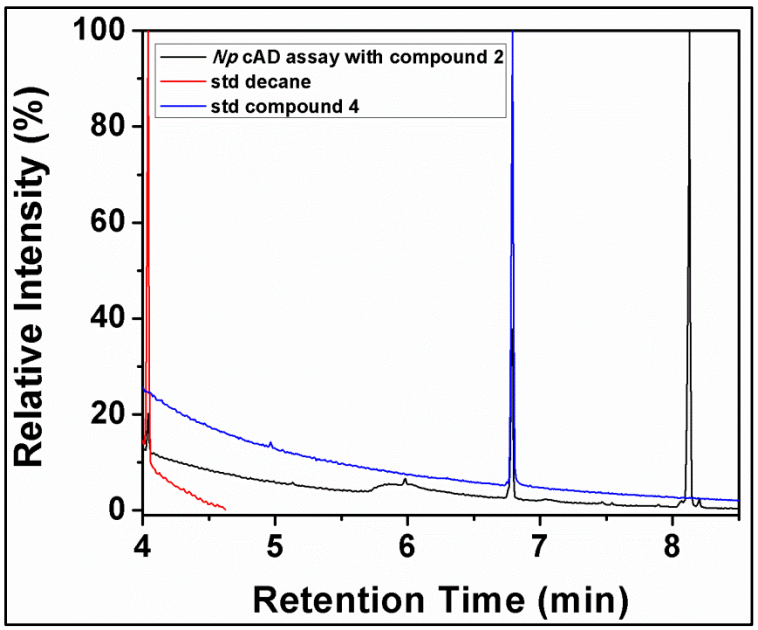

Figure 5.12. Overlaid chromatographs of the reaction of **2** with *Np* cAD with standard samples of decane and compound **4**.

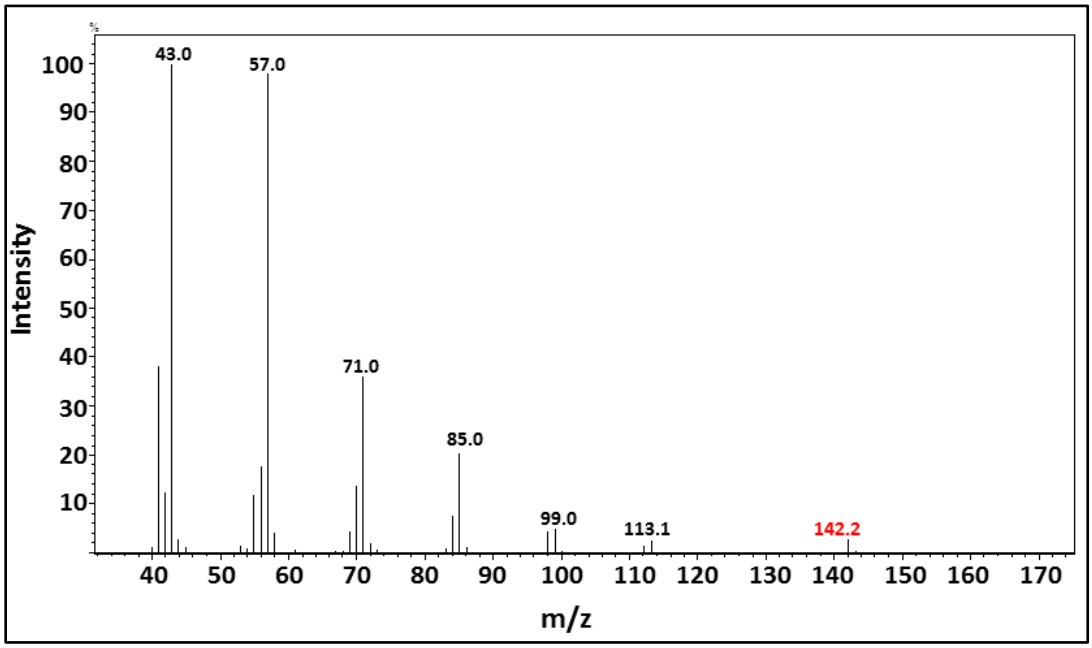

Figure 5.13. Mass spectrum of the decane peak eluted at 4.10 min showing molecular ion at 142.2 Da.

Undecanal as the precursor of decane. After identifying decane as the minor product of *Np* cAD-catalyzed reaction of **2**, the GC-MS trace was examined for undecanal that would be the obvious precursor for decane. Unfortunately, undecanal could not be clearly resolved on the GC-MS chromatogram. However, a narrow shoulder was noticed on the peak that corresponds to 2-nonyloxirane at 6.79 min. It was suspected that the undecanal peak might have been masked by this predominant peak on the chromatogram. To verify this, the GC-MS method was modified to a slightly different one that includes slower increase in the column temperature.

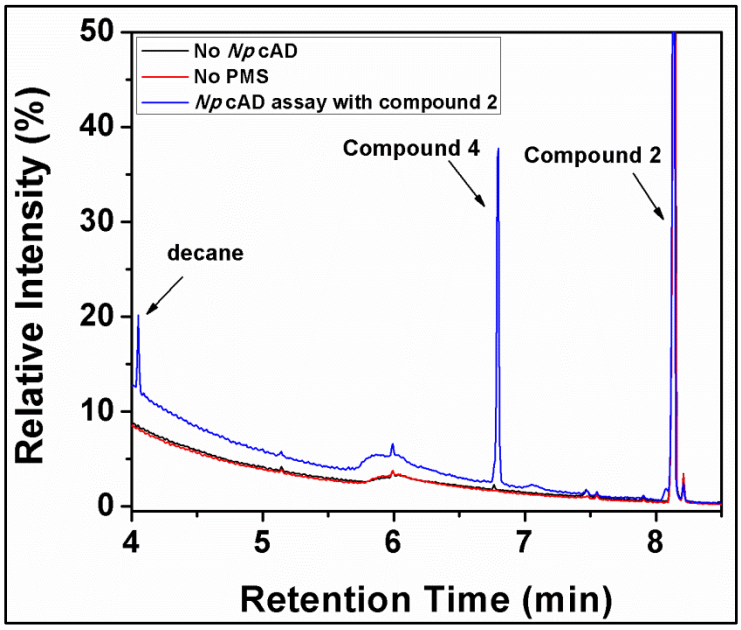

Figure 5.14. Overlaid chromatographs of conversion of **2** to 2-nonyloxirane (**4**) by *Np* cAD and the control experiments where cAD or PMS were omitted.

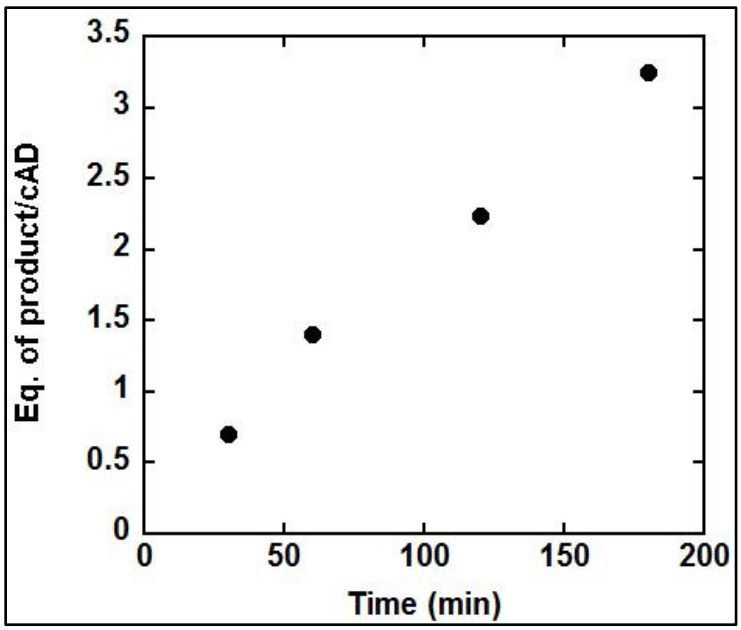

Figure 5.15. A time course of *Np* cAD-catalyzed formation of 2-nonyloxirane (**4**) from compound **2.**

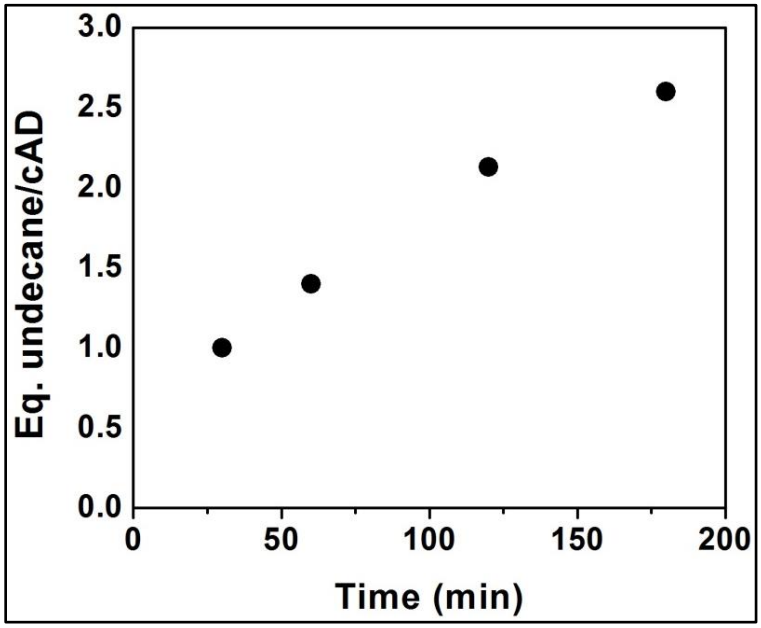

Figure 5.16. A time course of undecane formation from dodecanal by *Np* cAD.

Modified GC-MS method gave better separation of the components of the assay. The oven temperature was held initially at 70 °C for 2 min and then gradually increased to 120 °C at 20 °C/min and finally increased to 160 °C at 5 °C/min. This allowed the peak that originally eluted at 6.79 min be resolved into two separate peaks and eluting at 7.80 min and 7.87 min. As expected the peak at 7.80 min overlaid well with an authentic standard of undecanal (Figure 5.17).

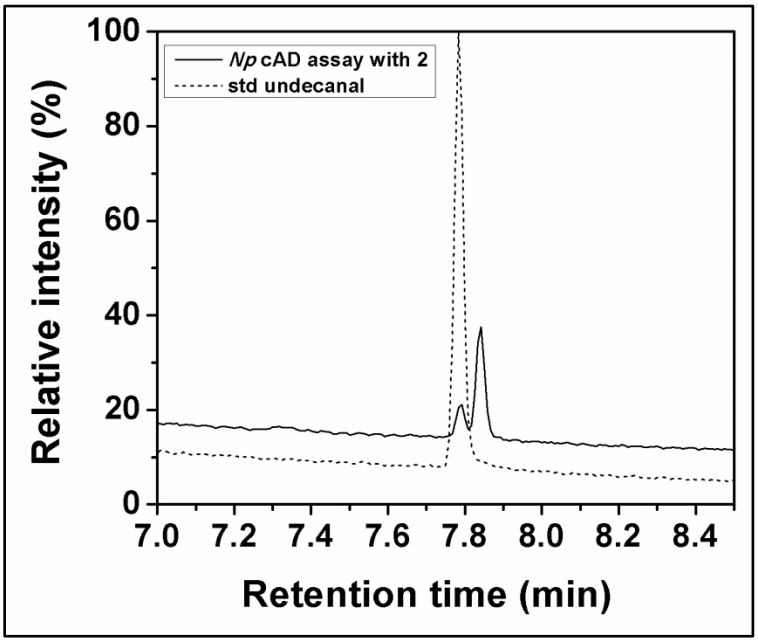

Figure 5.17. Overlaid chromatographs of *Np* cAD assays with compound **2** and standard undecanal.

Facial selectivity of proton transfer. Previous studies have established that the proton in the product alkane derives from the solvent in the cAD-catalyzed reaction;[7,11] this is in contrast to the decarbonylation reactions catalyzed by the insect and plant enzymes in which the aldehyde hydrogen is transferred to the alkane.[12,13] However, the facial selectivity of proton transfer of this step has not been determined for any of these enzymes. Taking advantage of the distinct

chemical shifts of oxirane-ring protons, we investigated the facial selectivity of proton addtition to the oxiranyl radical. The experiments were performed by Mr. Benjamin Ellington. Reactions were set up containing 40 µM cAD, 80 µM ferrous ammonium sulfate, 400 µM **2**, 2 mM NADH and 100 µM PMS in 10 mM potassium phosphate buffer, pH/pD 7.2 in either H_2O or D_2O. After 2 h incubation at 37 °C the products of the reaction, together with unreacted substrate, were extracted with $CDCl_3$, dried and their ^1H NMR spectra recorded.

The oxirane protons (Figure 5.18A) are clearly separated from other resonances and comprise a broad multiple due to H_a, δ = 2.89 ppm, (J_1 = 3.22, J_2 = 5.83 Hz) and overlapping doublet-of-doublets due to H_b, δ = 2.73 ppm, (J_1 = 3.90, J_2 = 5.08 Hz) and a doublet-of-doublets due to H_c, δ = 2.45 ppm, (J_1 = 2.75 Hz; J_2 = 5.07 Hz). For the reaction performed in H_2O, integration of H_a, H_b and H_c reveals, as expected, equal intensities for all 3 protons (Figure 5.18B). For the reaction performed in D_2O, however, both H_b and H_c are almost equally reduced in intensity to 0.67 and 0.74 respectively relative to H_a (Figure 5.18C), indicating that the deuteron can be transferred with equal probability to either face of the oxirane ring. It is evident that the intensities of H_b and H_c are not reduced to the theoretical value of 0.50. We attribute this to residual protons in the D_2O buffer, which are estimated to comprise ~5 % of the solvent. Proton incorporation is enhanced by a solvent kinetic isotope effect, which is currently under investigation. Nevertheless, considering the percentage of residual proton in D_2O buffer and based on the intensities of peak H_b and H_c that are originated from assays performed in D_2O buffer, an approximate solvent kinetic isotope effect ~3.4-4.8 can be calculated for the proton transfer step that leads to the product formation.

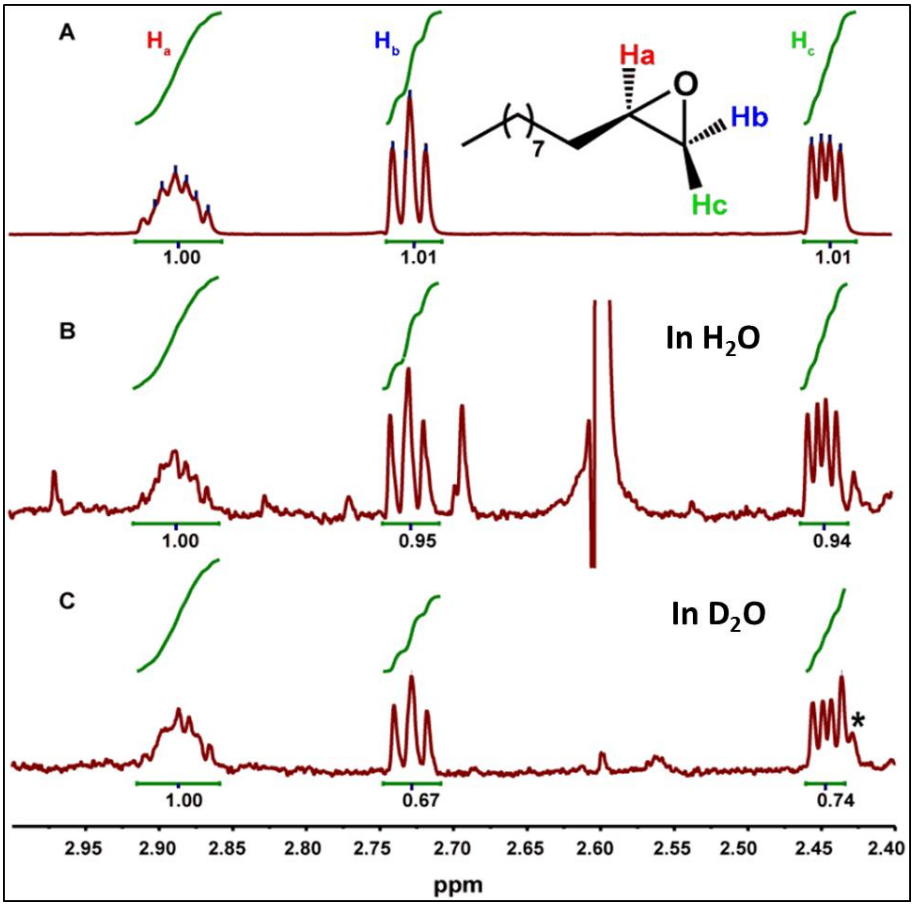

Figure 5.18. Facial selectivity of proton addition to 2-nonyloxirane. ^{1}H-NMR spectra of the oxirane ring protons H_a, H_b and H_c are shown. **A**: an authentic standard of racemic 2-nonyloxirane (for clarity the structure of the (R)-enantiomer is drawn, although it's currently not known which isomer serves as the substrate of the enzyme); **B**: products of the reaction of **2** with cAD in H_2O; **C**: products of the reaction of **2** with cAD in D_2O. In each case integrations are relative to H_a. Peak identified by * on **C** is contaminant. Peak at 2.60 and 2.68 ppm on **B** is derived from HEPES buffer used in the assay.

Formation of an unidentified new compound. 3-nonyloxirane-2-carbaldehyde **(2)** showed similar behavior with cAD as 3-pentadecanyloxirane-2-carbaldehyde **(1)**. When incubated with cAD, the compound **2** produced 2-nonyloxirane (**4**) as the major product and decane as the minor product. Interestingly, another new and slightly broad peak appeared at 7.98 min on the GC-chromatogram. Although the intensity of this peak was low on the chromatogram, the peak

was absent from the control experiments where either the enzyme or the reducing system were omitted. These confirmed the enzymatic production of the new compound that was eluted at 7.98 min (Figure 5.19). The mass spectrum of the peak showed standard hydrocarbon fragmentation pattern with an auxiliary peak at 155 Da (Figure 5.20). At this moment, the identity of this peak is not known but very recently it has been shown that, along with producing C_{n-1} alkanes from C_n aldehydes, cAD also produces some C_{n-1} alcohols and C_{n-1} aldehyde as the other co-products.[14] In this respect, the unidentified compound might possibly be an α-hydroxy aldehyde formed from the radical intermediate generated due to cleavage of the C1-C2 bond of 3-nonyloxirane-2-carbaldehyde.

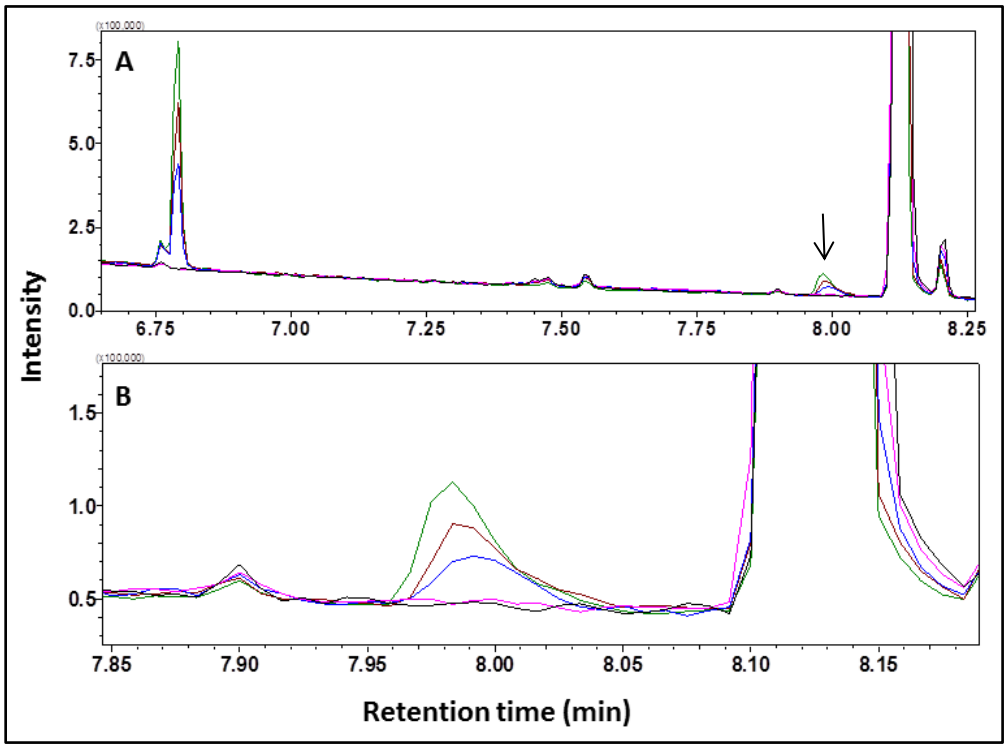

Figure 5.19. A new compound eluted at 7.98 min when compound **2** was incubated with *Np* cAD. A. Overlaid chromatographs of control experiments and time course assays. B. Zoomed in view of the peak at 7.98 min; control experiments (black: no cAD, pink: no PMS); time course assays (blue: 30 min, grey: 1 h, green: 2 h assay).

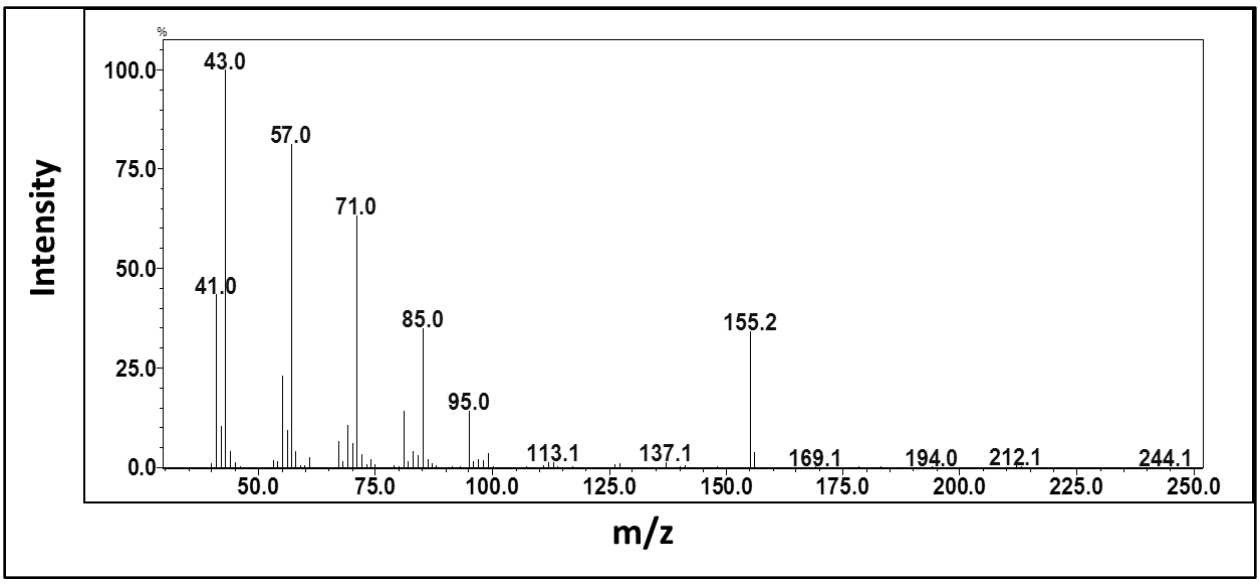

Figure 5.20. Mass spectrum of the unidentified peak eluted at 7.98 min.

5.4 Conclusions

In summary, the α, β-epoxide (oxiranyl) analogs of octadecanal and dodecanal were employed as substrates of cAD in order to investigate the nature of C1-C2 bond cleavage of an aldehyde. The hypothesis was that homolytic cleavage of C1-C2 bond would generate an oxiranyl radical that could potentially rearrange. The oxiranyl radical would either be quenched if the lifetime of the radical is less than the rate of rearrangement; or be rearranged to an α-keto radical if the lifetime of the radical is more than the rate of the rearrangement. Treatment of 3-pentadecyloxirane-2-carbaldehyde (**1**), with *Np* cAD resulted in the production of 2-pentadecyloxirane (**3**), as the non-rearranged product and surprisingly, hexadecane, a C_{n-2} alkane, as a minor product. Unlike β, γ-cyclopropyl aldehyde analog of octadecanal, the oxiranyl aldehyde exhibited multiple turnovers. Based on the prior knowledge of the reaction catalyzed by cAD that converts a C_n aldehyde to C_{n-1} alkane, it was reasoned that the immediate precursor

for hexadecane would be heptadecanal. Careful investigations of the GC-MS traces lead us to detect a small but significant peak that co-eluted with standard heptadecanal. Control experiments established that heptadecanal formation is an enzymatic reaction. Thus, it was confirmed that heptadecanal was produced in the reaction and served as an intermediate in the conversion compound **1** to hexadecane. Formation of heptadecanal was in accordance with our hypothesis of homolytic cleavage of the C1-C2 bond of the substrate. These findings consolidate our previous findings that a radical mechanism is more likely in cAD-catalyzed reaction. From the ratio of 2-pentadecyloxirane and hexadecane produced from **1** and the known rate constant of rearrangement of oxiranyl radicals, the rate constant of the proton-coupled electron transfer step in the mechanism was estimated to be ~10^4 sec^{-1}. Formate was also identified as the co-product of the reaction which is similar to the true substrates reacting with cAD. An almost equimolar ratio of formate and compound **3** was measured as a result of deformylation of **1** by cAD. The conversion of **1** to hexadecane could be attributed as an example of a tandem deformylation reaction which is unique among known reactions of cAD. Isotope labeling experiments showed incorporation of two solvent hydrogens in the resulting hexadecane which is in accordance with the proposed mechanism. Similar studies have also been carried out with shorter chain aldehyde, 3-nonyloxirane-2-carbaldehyde (**2**), the α, β-epoxide analog of dodecanal. Investigations using this substrate suggested that it also behaved in the similar fashion as **1** and produced 2-nonyloxirane (**4**) as a non-rearranged major product and decane as the minor product. Undecanal has also been identified as an intermediate of conversion of compound **2** to decane. Performing the reaction in D_2O allowed the facial selectivity of proton addition to be examined by 1H-NMR spectroscopy. The proton is delivered

with equal probability to either face of the oxirane ring, indicating the formation of an oxiranyl radical intermediate that is free to rotate during the reaction. Interestingly, the reaction of cAD with **2** resulted in the formation of a new compound, the identity of which is yet to be explored.

5.5 References

1. Ito, Y., and Murakami, M. (1999) Cleavage of Carbon–Carbon Single Bonds by Transition Metals, *Top. Organomet. Chem. 3*, 97-129.
2. Jun, C. H. (2004) Transition metal-catalyzed carbon-carbon bond activation, *Chem. Soc. Rev. 33*, 610-618.
3. Itzel, H., and Fischer, H. (1976) Electron spin resonance of oxiranyl radicals in solution: configurational stabilities and rearrangement reactions, *Helv. Chim. Acta 59*, 880–901.
4. Padwa, A., and Das, N. C. (1969) Oxirane radicals. The thermal decomposition of *t*-butyl *cis*- and *trans*-α,β-6-diphenylperglycidates, *J. Org. Chem. 34*, 816–821.
5. Paul, B., Das, D., Ellington, B., and Marsh, E. N. G. (2013) Probing the mechanism of cyanobacterial aldehyde decarbonylase using a cyclopropyl aldehyde, *J. Am. Chem. Soc. 135*, 5234–5237.
6. Eser, B. E., Das, D., Han, J., Jones, P. R., and Marsh, E. N. G. (2011) Oxygen-independent alkane formation by non-heme iron-dependent cyanobacterial aldehyde decarbonylase: investigation of kinetics and requirement for an external electron donor, *Biochemistry 50*, 10743–10750.
7. Das, D., Eser, B. E., Han, J., Sciore, A., and Marsh, E. N. G. (2011) Oxygen-independent decarbonylation of aldehydes by cyanobacterial aldehyde decarbonylase: a new reaction of di-iron enzymes, *Angew. Chem. Int. Ed. 50*, 7148–7152.
8. Bowry, V. W., and Ingold, K. U. (1991) A Radical Clock Investigation of Microsomal Cytochrome-P-450 Hydroxylation of Hydrocarbons - Rate of Oxygen Rebound, *J. Am. Chem. Soc. 113*, 5699-5707.
9. Yanagisawa, A., Yasue, K., and Yamamoto, H. (1994) Selective lsomerization of 1,2-Epoxyalkanes to Aldehydes with Lithium Dialkylamides, *J. Chem. Soc., Chem. Commun.*, 2013-2014.
10. Satoh, T. (1996) Oxiranyl Anions and Aziridinyl Anions, *Chem. Rev. 96*, 3303-3325.
11. Warui, D. M., Li, N., Norgaard, H., Krebs, C., Bollinger, J. M., and Booker, S. J. (2011) Detection of formate, rather than carbon monoxide, as the stoichiometric coproduct in conversion of fatty aldehydes to alkanes by a cyanobacterial aldehyde decarbonylase, *J. Am. Chem. Soc. 133*, 3316–3319.
12. Cheesbrough, T. M., and Kolattukudy, P. E. (1984) Alkane biosynthesis by decarbonylation of aldehydes catalyzed by a particulate preparation from *Pisum sativum*, *Proc. Natl. Acad. Sci. USA. 81*, 6613–6617.

13. Reed, J. R., Quilici, D. R., Blomquist, G. J., and Reitz, R. C. (1995) Proposed mechanism for the cytochrome P450-catalyzed conversion of aldehydes to hydrocarbons in the house fly, Musca domestica, *Biochemistry 34*, 16221–16227.
14. Aukema, K. G., Makris, T. M., Stoian, S. A., Richman, J. E., Münck, E., Lipscomb, J. D., and Wackett, L. P. (2013) Cyanobacterial aldehyde deformylase oxygenation of aldehydes yields *n*-1 aldehydes and alcohols in addition to alkanes, *ACS catal. 3*, 2228–2238.

Chapter 6

Conclusions and Future Directions

6.1 Conclusions

The work described in this thesis characterized a recently discovered enzyme, cyanobacterial aldehyde decarbonylase (cAD) that plays a crucial role in alkane biosynthesis in cyanobacteria.[1] This enzyme gained attention because of its potential for future biofuel applications as well as the unusual nature of the conversion of aldehydes to alka(e)nes that is very poorly understood.

In the original discovery of the enzyme,[1] cyanobacterial aldehyde decarbonylase was shown to be a small protein that produces long chain alka(e)nes from the corresponding aldehydes both *in vivo* (in *E. coli*) and *in vitro*. The discovery was intriguing as it identified the first soluble aldehyde decarbonylase. All other known aldehyde decarbonylase enzymes are membrane proteins that have resisted characterization and mechanistic studies due to the difficulties associated with extraction from the native organisms and heterologous expression. Based on a previously known crystal structure,[2] cAD was shown to be a member of non-heme di-iron oxygenase family of enzymes that comprise methane monoxygenase, class 1 ribonucleotide reductase and ferritin. However, the metal requirement for the enzyme was not established. The kinetic parameters of the enzyme, mechanistic details of the unusual conversion of aldehyde to alkane and the nature of the C1 co-product were not determined.

My work began with the heterologous expression and purification of the enzyme. This resulted in a high yield of the pure protein that appeared to be quite stable at room temperature. The brown color of the as-isolated protein indicated the presence of iron-oxo charge transfer band in the UV-Vis spectrum. Investigation of the as-isolated protein by ICP-MS indicated that only ~30% of the enzyme was bound to metals in which ~20% was iron. Further evidence that iron is the required metal for cAD came from the activity studies, in which only iron was found to support activity of the enzyme. In the original report, the *in vitro* activity was found to be dependent on a reducing system made of ferredoxin/ferredoxin reductase/NADPH but the resulted activity was shown to be extremely sluggish and not more than ~1 turnover was obtained. This poor activity of cAD created a barrier for further investigation on the mechanism of action of the enzyme. To improve activity, various chemical reducing systems were employed and the reducing system made of phenazine methosulfate (PMS)/NADH supported multiple turnovers of the enzyme and enhanced the activity by ~100 folds. Furthermore, a broad range of aldehydes were tested as substrates for cAD and it was found that cAD was able to convert aliphatic C18-C7 aldehydes to the corresponding alkanes. The improvement in activity of the enzyme enabled us to explore the kinetic parameters of cAD with octadecanal as well as with a shorter, relatively soluble substrate heptanal. These experiments provided fundamental understanding of the properties and the activity of the enzyme.[3,4]

After characterization of cAD and improving the activity of the enzyme using PMS/NADH as a chemical reducing system, the more physiologically relevant reducing system composed of Fd/FdR/NADPH was re-examined for activity of cAD. For this purpose, cyanobacterial

ferredoxins were expressed and purified. When employed with cAD in a buffer containing low salt concentrations (20-40 mM), multiple turnovers were obtained and the activity was improved by ~60 times compared to the originally reported activity. This suggests that the salt concentrations plays crucial role in the interaction of cAD with Fd. Furthermore, electron transfer from Fd to cAD was examined to confirm that electrons from NADPH are transported to cAD via FdR and Fd.

To investigate the interaction of the enzyme with substrate, EPR spectroscopy was employed. Upon introduction of heptanal to cAD, an organic radical was generated that was probed by using a radical trap. Further, the enzyme was found to effect removal of the C1 carbon of the aldehyde as formate rather than CO (which is the co-product of plant and algal AD reactions) or CO_2 (which is the co-product of insect AD reaction) and the aldehyde hydrogen was found to be incorporated into formate whereas the new proton on the product alkane was derived from the solvent as evaluated by isotope labeling experiments.[3] One important question that was unanswered for decades was the mechanism of cleavage of the C1-C2 bond of aldehydes by AD enzymes. Employing a β, γ-'radical clock' cyclopropyl analog of octadecanal as a substrate, the mechanism of the C1-C2 bond scission was investigated. The cyclopropyl aldehyde underwent rearrangement to produce alkene as the only product. Based on the known chemistry of the rearrangement of 'radical clock' cyclopropyl compounds, a homolytic cleavage of the C1-C2 bond of aldehyde was inferred. The lifetime of the radical intermediate generated due to the scission of the C1-C2 bond was also estimated to be ≥ 10 ns.[5] Further evidence for the involvement of radical intermediate(s) in the cAD-catalyzed reaction came from the use of α, β-oxiranyl aldehydes as substrates for cAD. Oxiranyl compounds are known

to undergo radical-mediated rearrangements and thus could function as slow 'radical clocks'. Reaction of cAD with an oxiranyl aldehyde furnished an oxirane one carbon shorter as the major product and unexpectedly, an alkane two carbons shorter as the minor product. From the ratio of oxirane and alkane products, the rate constant for the proton coupled electron transfer was estimated to be ~10^4 sec^{-1}. This also suggests that the lifetime of the oxiranyl radical is significantly long, ~0.1 ms. Careful investigation of the reaction products also identified an aldehyde one carbon shorter than the starting oxiranyl aldehyde suggesting rearrangement of the oxiranyl radical intermediate to the shorter aldehyde provided the immediate precursor for the alkane produced in the reaction.

Interestingly, while studying the cyclopropyl aldehyde, the enzyme exhibited only one turnover and in the end of the reaction, the enzyme was found to be completely inactivated by this substrate in an unproductive pathway. Another interesting observation while using this cyclopropyl aldehyde was that the enzyme was found to be covalently modified by deformylated substrate. By various mass spectroscopic analyses it was shown that a phenylalanine residue, in the hydrophobic substrate binding channel of the enzyme, most likely underwent covalent modification.

Unlike the cyclopropyl aldehyde, the oxiranyl aldehydes underwent multiple turnovers and the enzyme was not inactivated by the substrate. Examination of the oxirane produced by reaction in D_2O buffer allowed the facial selectivity of proton addition in the last step of the cAD-catalyzed reaction to be determined. The deuterion was found to deliver to either face of

the oxirane ring with equal probability indicating formation of an oxiranyl radical intermediate that is free to rotate during the reaction.

These observations provide the necessary framework to design further experiments to strengthen our understanding on this fascinating enzyme.

6.2 Future Directions

X-ray crystal crystallography. This is a powerful tool to obtain information on the molecular level interactions of an enzyme. The crystal structure of cAD was originally determined as a part of a structural proteomics project and it was found that the enzyme binds to a long chain fatty acid in a narrow hydrophobic channel that extends to the di-iron metal center.[2] The carboxylate group of the fatty acid coordinates to the metal center. To understand the interaction of substrate with the metals in the active site and the active site residues, several attempts were made to co-crystalize the enzyme with aldehyde substrates of varying chain lengths, however, the crystalized enzyme has always been found to retain the long chain fatty acid (unpublished data) most likely originated from the host strain. Recently, cAD was strategically engineered by site-directed mutagenesis to specifically block the access of long chain fatty acids into the hydrophobic pocket of the enzyme. The resulting proteins were found not to bind long chain fatty acids. Furthermore, the proteins were shown to be active and selectivity was shifted towards shorter chain aldehydes.[6] Although efforts to crystallize these variants with short chain aldehydes were unsuccessful, crystallization occurred in the presence of hexanoic acid that was found to bind in the hydrophobic channel of the enzyme and chelate the iron atoms.[6] These

observations suggested that the enzyme invariably requires fatty acids for crystallization. Hydrophobic interactions of alkyl part of the fatty acid with the hydrophobic channel residues and chelation by the carboxylate group of the fatty acid to the di-ferric center appear to be necessary to obtain crystal structure of the protein. To crystalize the wild type cAD with substrate aldehyde, a different approach would be necessary. Our hypothesis is that incubation of the wild type cAD with excess short chain soluble aldehyde (e.g. heptanal) would displace the long chain fatty acid from the active site. This preparation of cAD could be co-crystallized with a fatty aldehyde. Examination of the structure of cAD revealed that the enzyme can accommodate aldehydes with a cyclopropyl group adjacent to the aldehyde carbon with minimal perturbation of the structure. Activity study with α, β-cyclopropyl aldehyde substrate reveals that it behaves as a very slow substrate of cAD (unpublished data). This aldehyde might work as a suitable candidate for the crystallization purpose. However, it will be necessary to perform the crystallization under anoxic conditions to prevent aerobic oxidation of the substrate aldehyde which has been shown to occur easily.

Solvent kinetic isotope effects. Kinetic isotope effects provide information about the rate limiting step of a reaction. In the cAD-catalyzed conversion of aldehydes to alkanes, a chemically challenging cleavage of the C1-C2 bond of aldehyde takes place. To determine whether this step is rate limiting measurement of the ^{13}C kinetic isotope effect would be necessary. However, such measurements are extremely challenging because of the slow rate of cAD-catalyzed reaction and the low theoretical maximum of ^{13}C isotope effect (1.04). The reaction also involves a subsequent proton-coupled electron transfer to generate the alkane. To investigate whether this step is rate limiting, reactions were performed in buffers made of H_2O

and D_2O but no conclusion could be made as the slow rate of the reaction impeded comparison of the reaction rates. However, preliminary data on the solvent kinetic isotope effect was obtained by varying the mole fraction of D_2O in the assay buffer and analyzing the ratio of protium and deuterium incorporation into the product alkane using GC-MS (unpublished data). The data indicates that the solvent has some isotope effect on the rate limiting step of the reaction. However, accurate analysis of the mass spectrum of the product alkane using a high resolution mass spectrometer would be necessary to obtain reliable results. The high resolution data would allow the contribution of ^{13}C isotope on the solvent kinetic isotope effect to be deconvoluted. Precise determination of the solvent kinetic isotope effect would also be useful for proton inventory analysis that will provide information on the number of protons involved in the rate limiting step.

Binding partner of cAD. Many unanswered questions related to cAD could be addressed by improving the activity of the enzyme. In fact, enhancement of activity is absolutely necessary for its proposed future biofuel applications. Currently, it's not known whether the low activity of the enzyme is inherent to the enzyme. It's also unclear whether the low activity of the enzyme is due to improper *in vitro* reconstitution of the enzyme reaction that might be lacking the right cofactors or activating factors.[7] Furthermore, the fact that, unlike all other known membrane-associated aldehyde decarbonylases, cAD is a soluble protein that uses insoluble fatty aldehydes as substrate to make highly insoluble alka(e)ne products raises the possibility of involvement of membrane-associated binding partner(s) of cAD. Recently it has been shown that the AD enzyme from plant requires a similar membrane associated partner protein for activity.[8] It has also been shown that this enzyme requires a cytochrome-based membrane

bound cofactor for enhanced activity. These observations suggest possible involvement of one or more cofactor(s) for cAD.

In the original discovery of cAD, an acyl-CoA/acyl-ACP reductase (cACR) was shown to produce the aldehyde substrates for cAD.[1] It might also be possible that along with providing the required substrates for cAD, the reductase functions as an activator for cAD. Recently, we have expressed the reductase (a soluble protein) and examined its activity but it appears that the activity is extremely low and comparable to that of cAD. Some other reductases that catalyze similar reactions 3 to 4 orders of magnitude faster.[9] cAD activity was tested in presence of cACR and acyl-coA but unfortunately, no significant improvement in activity was noticed. This was not totally unexpected as the sluggish activity of cACR would not generate high enough concentrations of aldehyde for cAD to work on. One alternate approach to counter these challenges would be to cross link the cACR and cAD using a suitable linker and then employ either acyl-CoA or more suitable substrate Acyl-ACP in the reaction. The cross-linking might be useful for directing the flux of the intermediate aldehyde produced by cACR to cAD. To perform these experiments, a well-designed linker would be necessary. In addition, preparation of acyl-ACP would also be necessary that would need expression and purification of ACP protein as well as acyl-ACP synthase enzyme.

A bioinformatics approach might also be useful to identify potential binding protein(s) of cAD. Use of cyanobacterial ferredoxins as an electron mediator resulted in improved activity of cAD, but the final activity was very similar to the activity supported by the chemical electron mediator PMS. This indicates that ferredoxins are probably not the physiological co-factors of

cAD. A recent study shows substrate-mediated formation of di-iron peroxo/peroxyhemiacetal intermediate by the reaction of cAD with molecular oxygen. The intermediate has significantly long lifetime ($t_{1/2}$ ~400s at 5 °C) in the absence of reductants, however, decays very rapidly ($t_{1/2}$ ~0.14s) upon addition of electrons from the reducing system and produced ~0.5 eq. of formate/cAD.[10] This observation also suggests that electron transfer could be the rate limiting (or partially rate limiting) step of the reaction. If this is the case, investigation and employment of the correct reducing system would be crucial to enhance the activity of the enzyme. There might well be other, yet unidentified, binding protein(s) of cAD that needs to be reinvestigated using bioinformatics tools.

Further mechanistic studies on the cAD-catalyzed reaction. As mentioned earlier, di-iron peroxo/peroxyhemiacetal intermediate has recently been characterized in the cAD-catalyzed reaction.[10] Triggering of the reduced enzyme with linear aldehyde in presence of O_2 was necessary to generate the intermediate. There are several other proposed intermediates associated with the mechanism, which need to be characterized. Our studies using 'radical clock' aldehyde substrates (Chapter 4 and 5) provide evidences of formation of a radical intermediate due to the C1-C2 bond cleavage of aldehyde substrate. Nonetheless, we don't have direct spectroscopic evidence of this intermediate. Given that the reaction of oxiranyl aldehyde with cAD generated a relatively long-lived oxiranyl radical (lifetime ~10^{-4}-10^{-5} sec), it might be possible to directly detect this radical by EPR spectroscopy. To pursue that, single turnover experiments need to be perfomed. High concentration of enzyme could be treated with oxiranyl aldehyde in presence of the reducing system under single turnover conditions;

reactions could be freeze-quenched at different time points; and the resulted samples could be studied by EPR spectroscopy to detect the radical intermediate.

Furthe insights on the rate-limiting step could be obtained from single turnover experiments. According the proposed mechanism (Chapter 4), formate and alkane are generated in two consequitive steps. To determine whether one of these two steps is slow, asays could be performed under single turnover conditions. Reactions could be chemically quenched and formation of formate and alkane could be measured. Comparison of the rate of formation of these two products under single turnover conditions would provide an insight whether one of these two steps is slow. In adition, comparison of the rate of formation of formate and alkane under single turnover conditions with that of under multiple turnover conditions would provide an insight whether these steps are involved in the slow step of the cAD-catalyzed reaction.

6.3 References

1. Schirmer, A., Rude, M. A., Li, X. Z., Popova, E., and del Cardayre, S. B. (2010) Microbial biosynthesis of alkanes, *Science 329*, 559–562.
2. Unpublished, structure solved by Joint Center of Structural Genomics (protein database entry PDB|2OC5|A).
3. Das, D., Eser, B. E., Han, J., Sciore, A., and Marsh, E. N. G. (2011) Oxygen-independent decarbonylation of aldehydes by cyanobacterial aldehyde decarbonylase: a new reaction of di-iron enzymes, *Angew. Chem. Int. Ed. 50*, 7148–7152.
4. Eser, B. E., Das, D., Han, J., Jones, P. R., and Marsh, E. N. G. (2011) Oxygen-independent alkane formation by non-heme iron-dependent cyanobacterial aldehyde decarbonylase: investigation of kinetics and requirement for an external electron donor, *Biochemistry 50*, 10743–10750.

5. Paul, B., Das, D., Ellington, B., and Marsh, E. N. G. (2013) Probing the mechanism of cyanobacterial aldehyde decarbonylase using a cyclopropyl aldehyde, *J. Am. Chem. Soc. 135*, 5234–5237.
6. Khara, B., Menon, N., Levy, C., Mansell, D., Das, D., Marsh, E. N. G., Leys, D., and Scrutton, N. S. (2013) Production of propane and other short-chain alkanes by structure-based engineering of ligand specificity in aldehyde-deformylating oxygenase, *ChemBioChem 14*, 1204–1208.
7. Marsh, E. N. G., and Waugh, M. (2013) Aldehyde decarbonylases: enigmatic enzymes of hydrocarbon biosynthesis, *ACS catal. 3*, 2515–2521.
8. Bernard, A., and Joubes, J. (2013) Arabidopsis cuticular waxes: advances in synthesis, export and regulation, *Prog. Lipid Res. 52*, 110–129.
9. Kockelkorn, D., and Fuchs, G. (2009) Malonic semialdehyde reductase, succinic semialdehyde reductase, and succinyl-coenzyme A reductase from Metallosphaera sedula: enzymes of the autotrophic 3-hydroxypropionate/4 hydroxybutyrate cycle in Sulfolobales., *J. Bacteriol. 191*, 6352-6362.
10. Pandelia, M. E., Li, N., Norgaard, H., Warui, D. M., Rajakovich, L. J., Chang, W. C., Booker, S. J., Krebs, C., and Bollinger, J. M. (2013) Substrate-triggered addition of dioxygen to the diferrous cofactor of aldehyde-deformylating oxygenase to form a diferric-peroxide intermediate, *J. Am. Chem. Soc. 135*, 15801–15812.

Appendices

Appendix A

Synthesis of 2-(2-tetradecylcyclopropyl)acetaldehyde (1)

Synthesis of β, γ-cyclopropyl analog of octadecanal was carried out by Dr. Bishwajit Paul as shown in Scheme A.1. A Wittig reaction was carried out between pentadecanal (**I**) and 3-hydroxypropyl-triphenylphosphonium bromide to synthesized octadec-3-ene-1-ol, **II**, as the (*E*) stereoisomer. After protection of the alcohol as its *tert*-Butyl-dimethylsilyl (TBDMS) silyl ether, **III**, the double bond was converted to a cyclopropyl group using diethylzinc and diiodomethane, to give the *trans* stereoisomer, **IV**, as major product.[1,2] Finally, deprotection of TBDMS group by tetrabytylammonium fluoride (TBAF), followed by oxidation of the alcohol with TEMPO yielded the cyclopropyl aldehyde, **1**.[3]

Scheme A.1. Synthesis route to 2-(2-tetradecylcyclopropyl)-acetaldehyde (**1**)

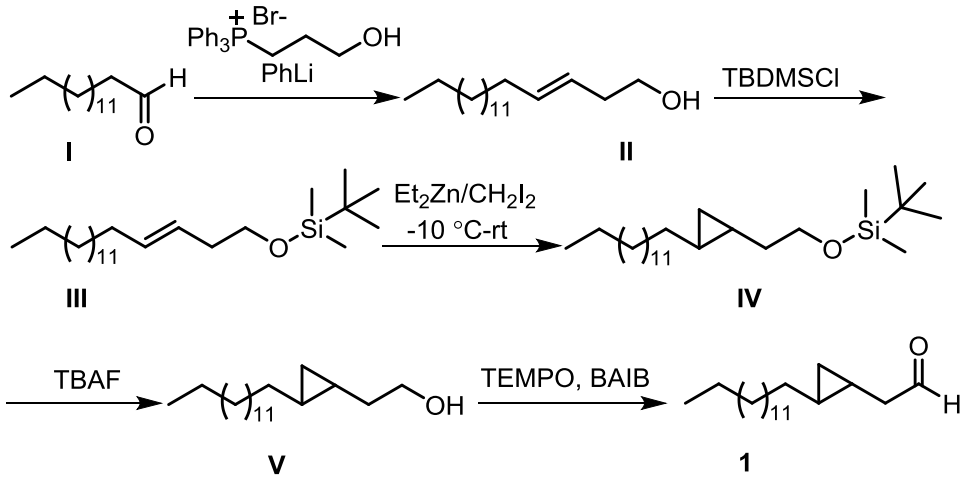

The cyclopropyl aldehyde was pure as judged by NMR (Figure A.1) and TLC. The overall yield was 10%. The identity of the compound was confirmed by high resolution electron-impact MS (*m/z*): calculated 280.2760; observed 280.2766. GC-MS analysis of **1** indicated that the compound was a mixture of ~ 70:30 *trans*- to *cis*-stereoisomers. ^{1}H NMR (400 MHz, $CDCl_3$) of **1** (major stereoisomer) δ 9.76 (t, *J* = 7 Hz, 1H), 2.30-2.26 (m, 2H), 1.39-1.24 (m, 22H), 0.86 (t, *J* = 6.8 Hz, 3H), 0.70-0.66 (m, 1H), 0.55-0.50 (m, 1H), 0.41-0.30 (m, 2H); ^{13}C NMR (100 MHz, $CDCl_3$) δ 202.52, 48.20, 47.30, 43.22, 33.87, 32.69, 31.89, 29.80, 29.67, 29.65, 29.63, 29.53, 29.45, 29.39, 29.33, 29.13, 28.95, 22.66, 18.54, 15.04, 14.09, 11.70, 11.51, 10.74, 8.95.

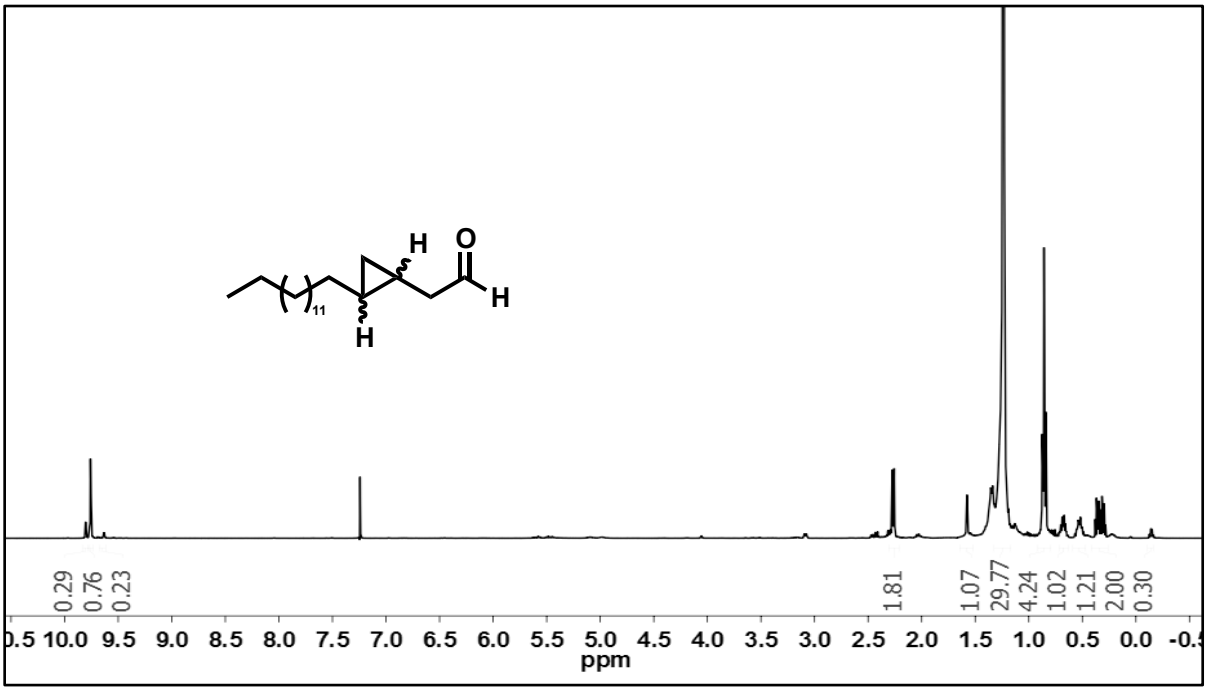

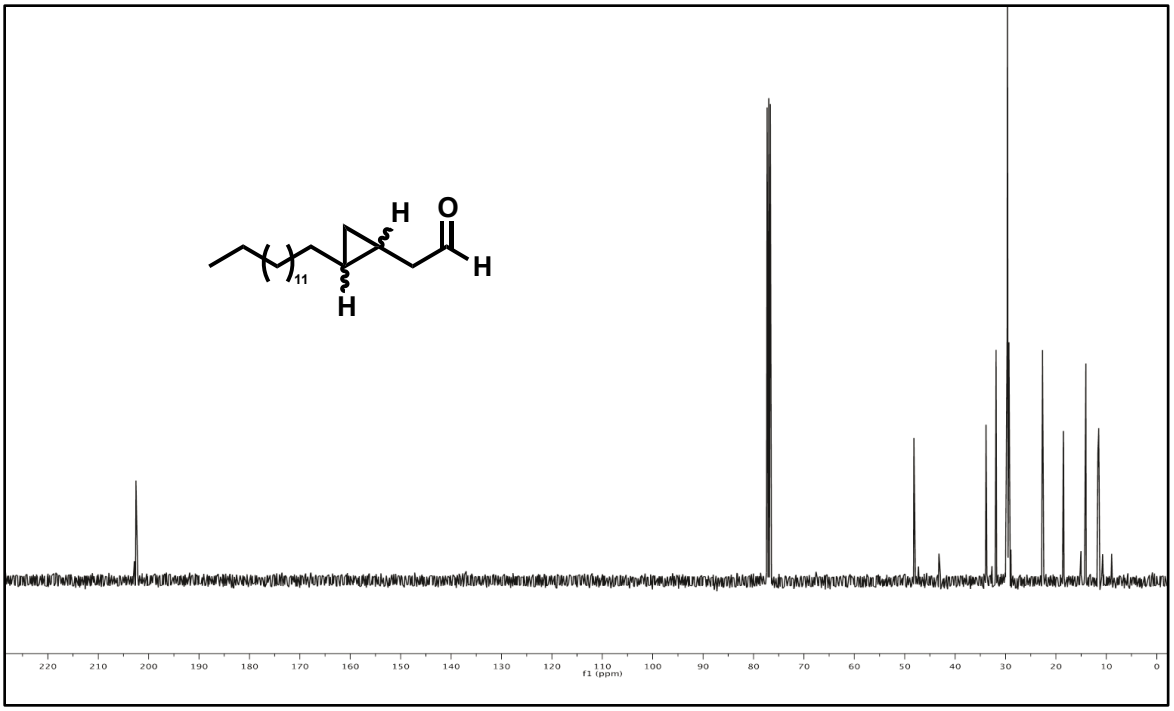

Figure A.1. ^{1}H and ^{13}C-NMR of cyclopropyl compound **1**.

References

1. Furukawa, J., Kawabata, N., and Nishimura, J. (1968) Synthesis of Cyclopropanes by the Reaction of Olefins with Dialkylzinc and Methylene Iodide, *Tetrahedron 24*, 53-58.
2. Lebel, H. l. n., Marcoux, J.-F. o., Molinaro, C., and Charette, A. B. (2008) Stereoselective Cyclopropanation Reactions, *Chem. Rev. 103*, 977-1050.
3. De Mico, A., Margarita, R., Parlanti, L., Vescovi, A., and Piancatelli, G. (1997) A Versatile and Highly Selective Hypervalent Iodine (III)/2,2,6,6-Tetramethyl-1-piperidinyloxyl-Mediated Oxidation of Alcohols to Carbonyl Compounds, *J. Org. Chem. 62*, 6974-6977.

Appendix B

Synthesis of Oxirane Aldehydes 3-Pentadecyloxirane-2-Carbaldehyde (1) and 3-Nonyloxirane-2-Carbaldehyde (2)

The synthesis of compound **1** and **2** was performed by Dr. Bishwajit Paul as outlined in Scheme B.1 and B.2.

Scheme B.1. Synthesis route to of 3-pentadecyloxirane-2-carbaldehyde **(1)**

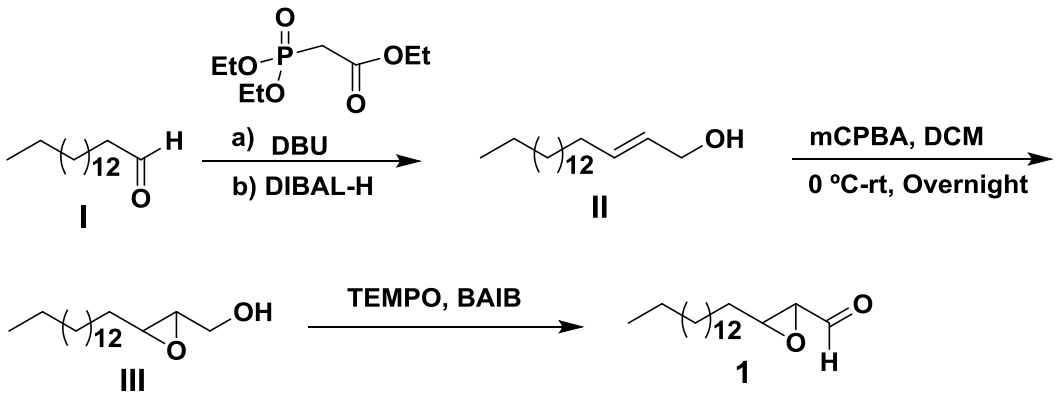

A Horner-Wittig reaction was carried out between hexadecanal, **I**, and ethyl-2-(diethoxylphosphoryl) acetate to synthesize (*E*)-Octadec-2-ene-1-ol (**II**).[1] The oxidation of (*E*)-Octadec-2-ene-1-ol (**II**) to (3-pentadecyloxiran-2-yl)methanol **(III)** was performed using standard perbenzoic acid strategy using metachloroperbenzoic acid.[1] Finally, the oxidation of **III** using TEMPO produced the oxiranyl aldehyde **1** in 27% yield.[2]

The compound was pure as judged by NMR (Figure B.1) and TLC. The identity of the compound was confirmed by high resolution electron-impact MS (*m/z*): calculated 282.2559; observed 282.2561. GC-MS analysis of **1** indicated that the compound was a mixture of ~ 90:10 *trans*- to *cis*-stereoisomers. ^{1}H NMR (400 MHz, $CDCl_3$) of **1** (major stereoisomer) δ 9.01-8.99 (d,

1H),3.23-3.19 (m, 1H),3.13-3.10 (m, 1H),1.66-1.62 (m, 2H), 1.46-1.44 (m, 2H), 1.34-1.24 (m, 24H) 0.88-0.86 (t, 3H),^{13}C NMR (100 MHz, $CDCl_3$) δ198.49, 59.15, 56.78, 31.90, 31.18, 29.67, 29.66, 29.64, 29.63, 29.61, 29.57, 29.46, 29.40, 29.33, 29.20, 25.75, 22.67, 14.10.

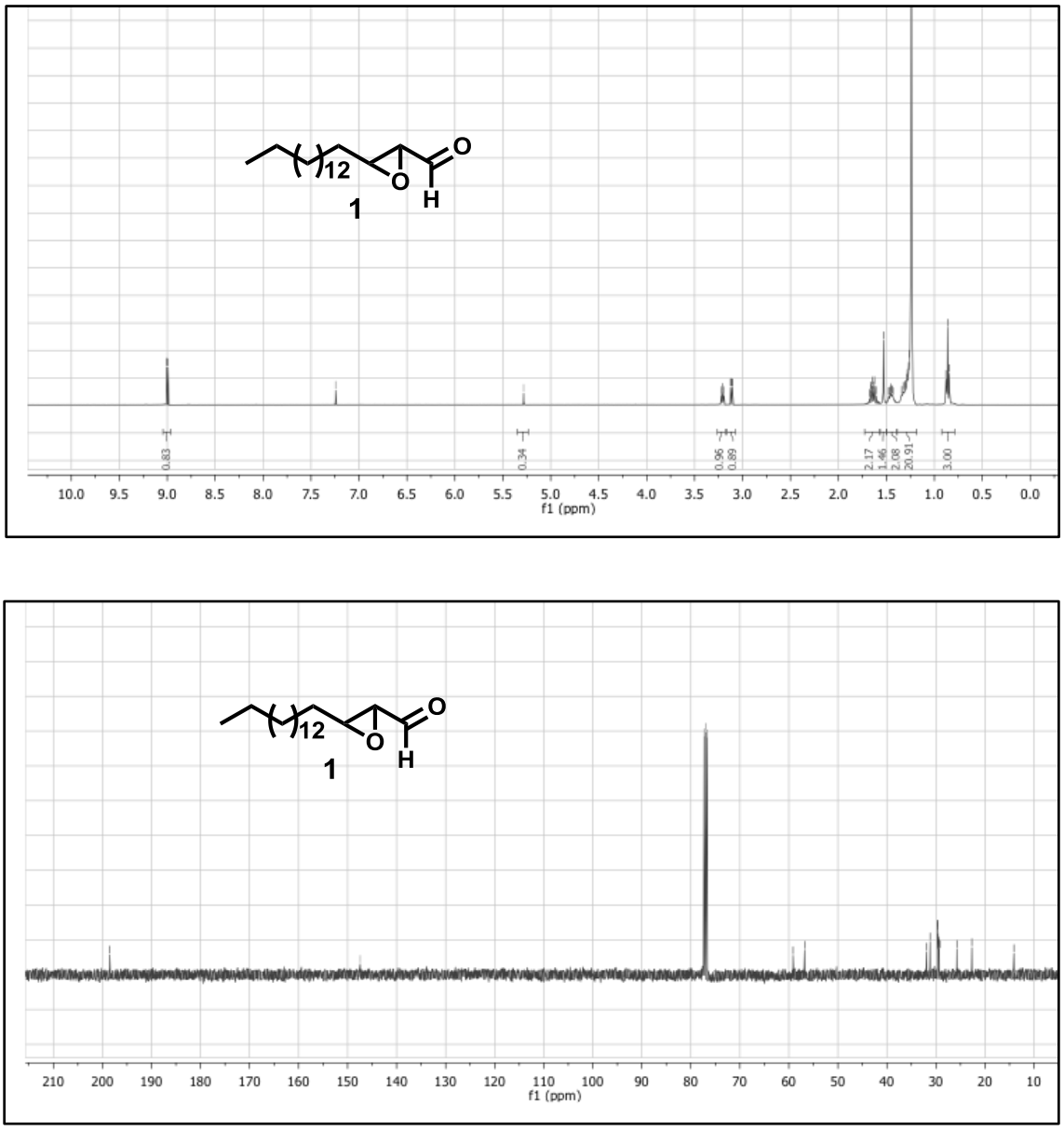

Figure B.1. ^{1}H and ^{13}C-NMR of 3-pentadecyloxiran-2-carbaldehyde (**1**)**.**

Scheme B.2. Synthesis route to 3-nonyloxirane-2-carbaldehyde (**2**)

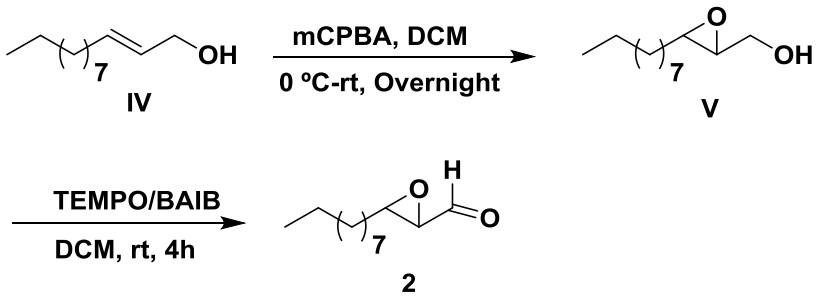

Oxidation of (*E*)-Dodec-2-ene-1-ol **(IV)** to (3-nonyloxiran-2-yl)methanol **(V)** was performed using standard perbenzoic acid strategy.[1] Finally, the oxidation of **V** using TEMPO produced the oxiranyl aldehyde **2** in 29% yields.

The compound was pure as judged by NMR (Figure B.2) and TLC. The identity of the compound was confirmed by high resolution electron-impactMS (*m/z*): calculated 198.1620; observed 198.1617. GC-MS analysis of **2** indicated that the compound was a mixture of ~ 98:2 *trans*- to *cis*-stereoisomers. ^{1}H NMR (400 MHz, $CDCl_3$),8.97-8.95 (d, 1H), 3.20-3.16 (m, 1H), 3.09-3.07 (m, H), 1.65-1.56 (m, 2H), 1.47-1.40 (m, 2H),1.39-1.22 (m, 12H), 0.85-0.81 (t, 3H),^{13}C NMR (400 MHz, $CDCl_3$) δ198.4, 59.09, 56.71, 31.79, 31.15, 29.38, 29.37, 29.34, 29.20, 29.16, 28.08, 25.71, 22.60, 14.03.

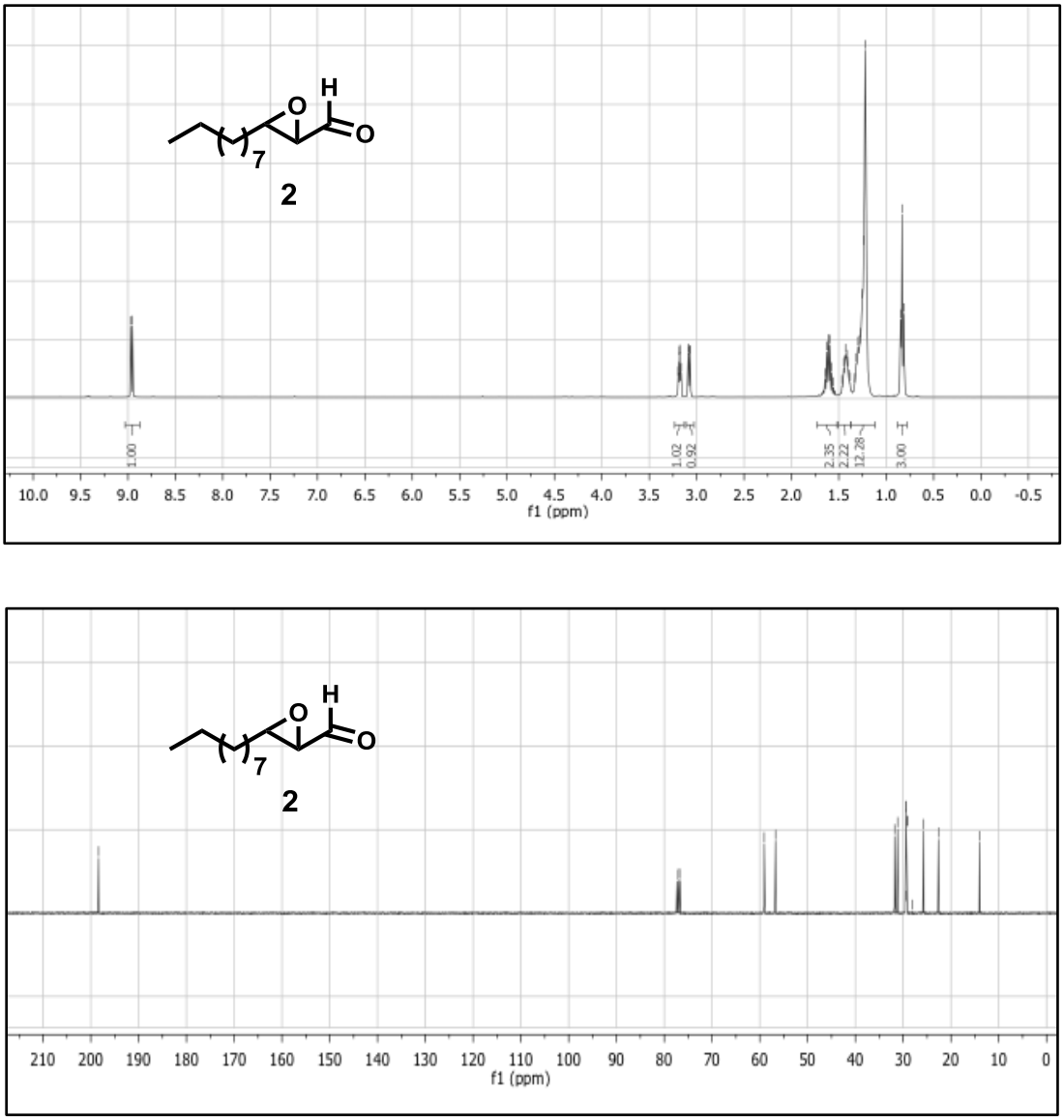

Figure B.2. ^{1}H and ^{13}C NMR Spectrum of compound **2**.

Synthesis of 2-pentadecyloxirane (3) and 2-nonyloxirane (4)

The synthesis of compound **3** and **4** was performed by Dr. Bishwajit Paul as outlined in Scheme B.3 and B.4.

Scheme B.3. Synthesis route to 2-pentadecyloxirane **(3)**

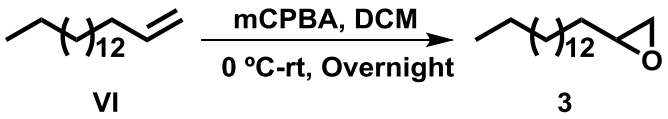

VI 3

The oxidation of heptadec-1-ene (**VI**) to 2-pentadecyloxirane **(3)** was performed using standard perbenzoic acid strategy.[1] The compound was pure as judged by NMR (Figure B.3) and TLC. The yield of the product was 75%. ^{1}H NMR (400 MHz, $CDCl_3$) δ 2.91-2.89 (m, 1H),2.76-2.73 (t, 1H),2.47-2.45 (m, 1H)1.53-1.50 (m, 2H),1.47-1.41 (m, 2H),1.33-1.25 (m, 24H), 0.89-0.86 (t, 3H).^{13}C NMR (100MHz, $CDCl_3$), 52.42, 47.15,32.49, 31.92, 29.69, 29.66, 29.63, 29.55, 29.45, 29.36, 25.97, 22.69, 14.13.

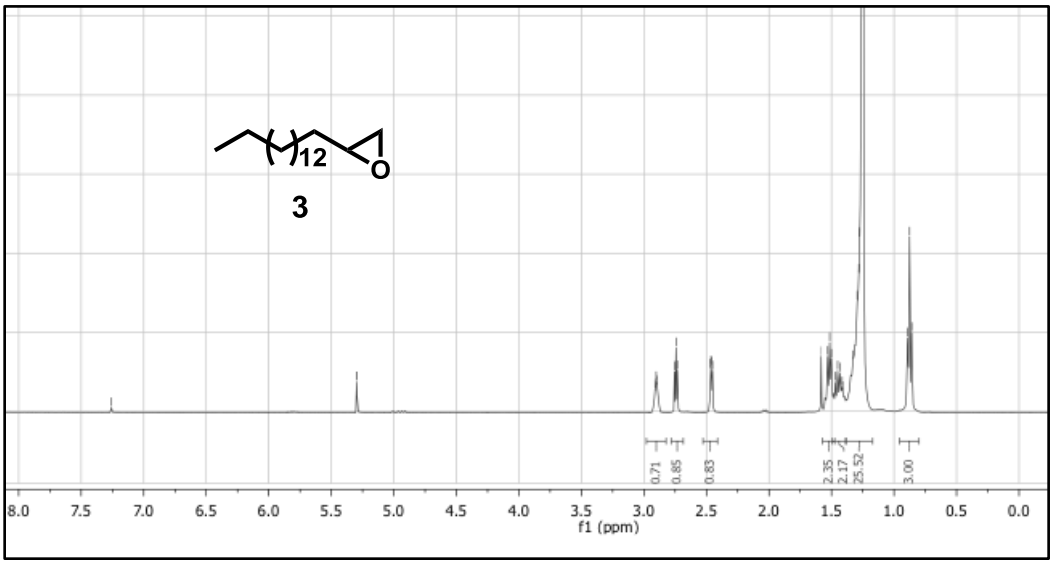

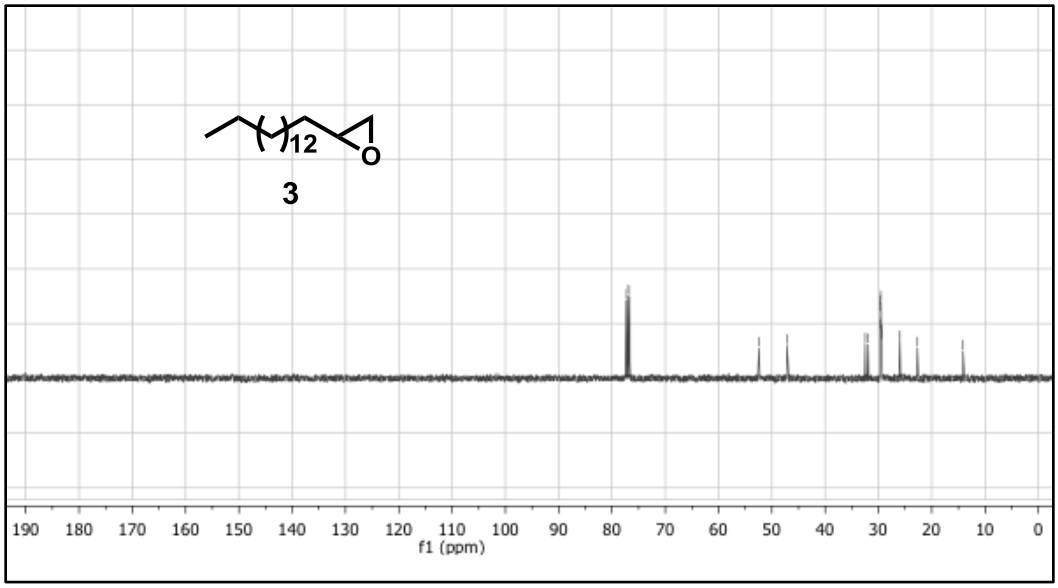

Figure B.3. ^{1}H and ^{13}C-NMR of 2-pentadecyloxirane **(3).**

Scheme B.4. Synthesis route to 2-nonyloxirane (**4**)

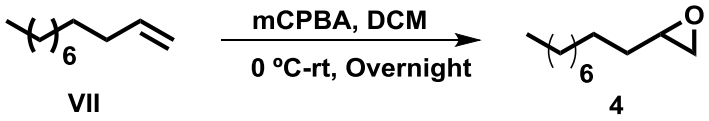

The oxidation of dodec-1-ene (**VII**) to 2-nonyloxirane **(4)** was performed using standard perbenzoic acid strategy.[1] The compound was pure as judged by NMR (Figure B.4).^{1}H NMR (400 MHz, $CDCl_3$) δ 2.91-2.85 (m, 1H), 2.75-2.73 (t, 1H), 2.46-2.43 (dd, 1H), 1.55-1.50 (m, 2H), 1.48-1.43 (m, 2H), 1.35-1.27 (m, 12H), 0.89-0.86 (t, 3H). ^{13}C NMR (100 MHz, $CDCl_3$), 52.29, 47.10, 32.50, 31.88, 29.56, 29.51, 29.45, 29.30, 25.98, 22.67, 14.09.

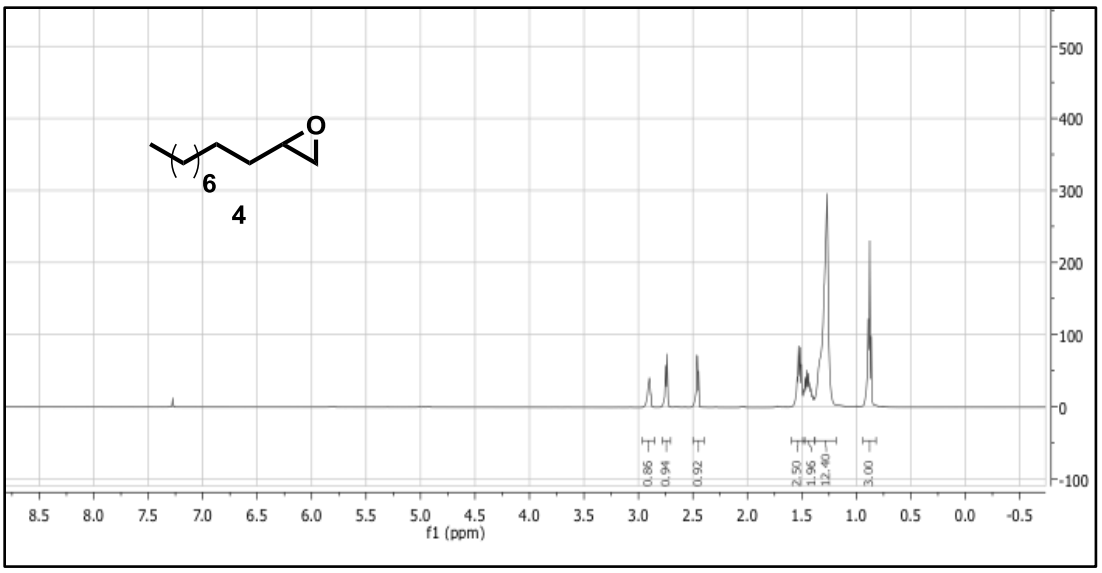

Figure B.4. ^{1}H NMR Spectrum of compound **4**.

References

1. Barret, A. G. M., Head, J., Smith, M. L., Stock, N. S., White, A. J. P., and Williams, D. J. (1999) Fleming-Tamao oxidation and masked hydroxyl functionality: total synthesis of (+)-pramanicin and structural elucidation of the antifungal natural product (-)-pramanicin, *J. Org. Chem. 64*, 6005–6018.
2. Paul, B., Das, D., Ellington, B., and Marsh, E. N. G. (2013) Probing the mechanism of cyanobacterial aldehyde decarbonylase using a cyclopropyl aldehyde, *J. Am. Chem. Soc. 135*, 5234–5237.